

Analyses multidisciplinaires des sédiments laminés de trois lacs profonds de la Côte-Nord du Québec pour reconstituer les variations paléoenvironnementales

Par

Obinna Peter Nzekwe

Thèse présentée pour l'obtention du grade de Philosophiae Doctor, Ph.D.

Doctorat en sciences de la terre

Programme géré conjointement par l'INRS et l'Université Laval

Jury d'évaluation

Présidente du jury et
Examinateuse interne

Isabelle Lavoie
Centre - Eau Terre Environnement
Institut National de la Recherche Scientifique

Examinateur externe

Mathew Peros
Department of Environment and Geography
Université Bishop's

Examinateur externe

Dermot Antoniades
Département de Géographie
Université Laval

Directeur de recherche

Pierre Francus
Centre - Eau Terre Environnement
Institute National de le Recherche Scienfique

Codirecteur de recherche

Guillaume St-Onge
Institut des sciences de la mer (ISMER)
Université de Québec à Rimouski

Codirecteur de recherche

Patrick Lajeunesse,
Département de Géographie,
Université Laval

REMERCIEMENTS

Cette thèse a duré six ans, j'ai donc beaucoup de gens à remercier. Je tiens à exprimer, en tout premier lieu, à monsieur le Professeur Pierre Francus, mon directeur, ma profonde gratitude et mes remerciements les plus sincères pour son encadrement infaillible, pour ses conseils académiques et également pour la confiance et la patience qu'il m'a apportées. Je souhaite également remercier mes deux co-directeurs de recherche, messieurs les Professeurs Guillaume St-Onge et Patrick Lajeunesse, de m'avoir accompagné tout au long de ce projet, pour leur disponibilité et leurs conseils avisés. Encore merci à vous trois de m'avoir intégré dans vos équipes pour ce grand projet sur la Côte-Nord et pour la chance d'avoir appris le français rapidement. Merci aux membres du jury qui ont accepté d'évaluer cette thèse.

Je remercie tous les membres des laboratoires de Pierre Francus : le laboratoire de géochimie, imagerie et radiographie des sédiments (GIRAS) et le laboratoire multidisciplinaire de tomodensitométrie. Particulièrement, je voudrais remercier Arnaud De Coninck de m'avoir appris à utiliser tous les équipements. Merci à François Lapointe, Antoine-Gagnon-Poiré, David Fortin, Thibault Labarre, Louis-Frédéric Daigle, Mathieu Des Roches et Jean-Philippe Jenny pour leur assistance au laboratoire. Dans l'équipe de Guillaume St-Onge à l'Institut de sciences de la mer de Rimouski (ISMER), et dans l'équipe de Patrick Lajeunesse au centre d'études Nordiques et département de Géographie à l'Université Laval, je voudrais remercier, Alexandre Normandeau, Léo Chassiot, Quentin Beauvais, Édouard Philippe, Annie-Pier Trottier et Marie-Pierre St-Onge, pour leur assistance au laboratoire et / ou au terrain.

Je remercie toutes les sources de bourses et de prix. Celles-ci incluent : le Conseil de recherche en sciences naturelles et en génie du Canada (CRSNG-EnviroNord) et le centre de recherche Geotop, pour leur bourse des études. L'INRS pour le prix de la 1ère place, présentation orale «Thèse de 3 minutes» en 2016. À cet égard, merci à monsieur Philippe-Edwin Bélanger et le Service des études supérieures et postdoctorales de l'INRS pour la bourse afin de représenter l'INRS à la finale régionale, Est du Canada de «Thèse de 3 minutes» au Memorial University, Terre-Neuve. Merci au Symposium Québec-Ontario de paléolimnologie pour le prix de la meilleure affiche en 2016. La journée des sciences de la terre et de l'environnement (JSTE), Université Laval, pour le prix de la 2e présentation orale, session géologie sédimentaire et géochimie environnementale en 2015.

En ce qui concerne les engagements volontaires, merci aux collègues du comité d'organisation des congrès étudiant INRS-ETE de l'année 2015 intitulé «Passé, Présent, Futur». Merci à l'INRS-ETE de m'avoir choisi comme ambassadeur étudiant et pour la bourse d'excellence soulignant l'implication étudiante pour l'année 2016-2017. Merci à Mitacs Globalink de m'avoir choisi comme mentor pour les

stagiaires internationaux pour l'été de 2017. Aux membres du chapitre étudiant de la “*Society of Exploration Geophysicists*” de l’INRS dont j’ai été secrétaire pendant presque quatre ans. Merci pour la nomination pour le prix de “*Chevron Student Leadership Symposium Grant*” qui m’a permis d’aller en Nouvelle-Orléans, États-Unis en 2016. Merci aux messieurs les Prof. Erwan Gloaguen et Prof. Bernard Giroux, nos sponsors académiques.

Mes remerciements s’adressent également aux employés de l’INRS-ETE, qui m’ont aidé dans mes démarches administratives. Un remerciement particulier s’adresse à mesdames Linda Aubert, Mélanie Laverdière, Suzanne Dussault, Céline Bélanger, Mathilde Renaud et Patricia Munoz pour leur aide administrative. Merci à Jean-Daniel Bourgault pour le service de bibliothèque et à Lisa Rancourt et Philippe Girard pour leur aide analytique.

Je voudrais remercier tous mes amis de l’INRS-ETE : Angus Calderhead, Dany Roy, Cecelia Dip, Imad Touahar, Maher Nasr, Sophie Costis, Mehdi Zolfaghari Moutiy El Houssaine, Josue Jautzy et Margherita Martini. Merci à mes amis de Communauté Allemand Québec : Melanie Beimann, Richard Barham, Catherine Béland et Niklas Rusche. Merci aussi à la communauté de l’Université Laval : Jean Abud, etc. Merci à mes amis de communautaire sportif à la piscine Lucerne-Borne à Québec. Merci à tous ceux dont je n’ai pas mentionné les noms.

Enfin, je remercie du fond du cœur ma mère, pour son soutien infaillible et grâce à qui j’ai pu me rendre jusqu’ici. Merci également à mon jumeau et à ma sœur qui ont toujours été présents malgré la distance et qui ont su m’encourager pendant toutes ces années de ma vie. Vous avez toujours été là pour moi!

AVANT-PROPOS

Cette thèse est composée de deux parties principales : la synthèse (Chapitre 1) et les articles scientifiques (Chapitres 2 à 4). La première partie (Chapitre 1) présente le contexte scientifique de cette étude sur des sédiments (annuellement) laminés dans trois lacs profonds de type fjord (lacs Pentecôte, Walker et Pasteur) sur la Côte-Nord du Québec, ainsi qu'une brève description des objectifs, hypothèses, méthodologies et principaux résultats de cette recherche. La deuxième partie de cette thèse comprend trois articles scientifiques. Le premier article (Chapitre 2) examine si les sédiments récents étudiés dans les lacs étudiés sont effectivement annuellement laminés. Le deuxième article (Chapitre 3) expose le premier enregistrement de sédiments varvés de l'Holocène supérieur établi à partir d'une analyse détaillée d'images en haute résolution de lames minces. Le troisième article (Chapitre 4) est consacré à la reconstitution environnementale de la zone d'étude sur la base des dépôts successifs allant du dernier maximum glaciaire (~ 21 ka) à l'Holocène supérieur. Il s'agit d'une analyse multi-paramètres comprenant granulométrie, palynologie, paléomagnétisme et modélisation hydraulique. Enfin, le Chapitre 5 présente les principaux résultats de cette recherche et quelques perspectives.

RÉSUMÉ

Cette thèse a pour objectif de reconstituer les contextes environnementaux passés à partir de l'étude de sédiments (annuellement) laminés de trois lacs de fjord profonds (les lacs Pentecôte, Walker et Pasteur) sur la Côte-Nord, Québec, dans l'Est du Canada. L'analyse des faciès à l'aide de tomodensitogrammes et de lames minces de 42 carottes de sédiments prélevées le long de transects révèle que les lacs Pentecôte, Walker et Pasteur contiennent des sédiments bioturbés, partiellement laminés et bien laminés. Il a été établi que le lac Walker est caractérisé par des facteurs morphologiques (tels qu'une profondeur relative plus élevée, une profondeur moyenne, une profondeur maximale, une limite critique et une exposition topographique) qui favorisent la préservation de la structure laminée des sédiments. La comparaison du nombre de couplets annuels avec les modèles chronologiques du ^{210}Pb d'une carotte courte, WA14-06-R (43 cm de long), indique que les sédiments laminés récents de ce lac sont probablement des varves. Ces résultats ont motivé les analyses multi-échelles d'une séquence composite de ~4,0 m de long, WA15-08-U, afin de reconstituer un enregistrement varvé de l'Holocène Supérieur de ce lac.

Une nouvelle chronologie varvée de ~ 900 ans du lac Walker a été établie sur la base de l'analyse d'image de 16 lames minces. Le comptage des varves est ancré par quatre datations au radiocarbone. Celle-ci fournit le premier enregistrement annuellement laminé dans une région où des enregistrements similaires sont actuellement inexistant. Par conséquent, l'enregistrement du Lac Walker entre 2340 et 3200 ± 20 cal BP offre un fort potentiel pour reconstituer les conditions hydro-climatiques dans cette région. Ce lac contient principalement des varves clastiques; l'épaisseur moyenne des varves est de 0,86 mm.

Des analyses multi-paramètres incluant les propriétés sédimentologiques, géochimiques, paléomagnétiques et palynologiques des sédiments des lacs de fjord Pentecôte et Walker ont été utilisées pour reconstituer les changements paléoenvironnementaux survenus lors de la transition d'un environnement glaciaire à postglaciaire. Deux principaux faciès sédimentaires ont été identifiés : les faciès argileux et lamines déposés dans un environnement proglaciaire et les sédiments laminés déposés dans un environnement paraglaciaire / postglaciaire. La transition entre ces deux environnements est caractérisée par de brusques changements des propriétés texturales et géochimiques. Au même titre, des changements abrupts de l'inclinaison magnétique et d'une augmentation de la diversité des palynomorphes caractérisent cette transition. Sur la base de la datation au radiocarbone, il apparaît qu'une interruption (hiatus) de la sédimentation dans les lacs Pentecôte et Walker est survenue entre ~ 22 et 8 ka cal BP et entre ~ 18 et 8 ka cal BP, respectivement.

ABSTRACT

This thesis aims to reconstruct past depositional environments based on laminated sediments from three deep fjord-lakes (lakes Pentecôte, Walker and Pasteur) on the Québec North Shore, eastern Canada. Facies analysis using CT-scan images and thin-sections of 42 short sediment cores sampled along transects reveals that lakes Pentecôte, Walker and Pasteur contain bioturbated, partially laminated and well laminated sediments. It has been established that Lake Walker is characterized by morphological factors (such as higher relative depth, mean depth, maximum depth, critical boundary and topographic exposure) that favour the preservation of sediment laminae. Comparison of laminae couplets counts to ^{210}Pb chronology models of a short core, WA14-06-R (43 cm long) indicates that the laminated upper sediments from that lake are likely varves. This evidence formed the basis for multi-scale analyses of a ~4.0 m long composite sequence, WA15-08-U from Lake Walker in order to reconstruct a late Holocene varve record from that Lake.

A new ~900-year varve chronology from Lake Walker was established based on image analysis of 16 thin-sections supported by radiocarbon dating. The varve counts are anchored on four radiocarbon dates. The varve chronology from Lake Walker provides the first varve record in a region where similar records are presently non-existent. Moreover, there is a high potential to establish longer and high-resolution records of past climate in the region based on these findings. Lake Walker contains mainly clastic varves; mean varve thickness is 0.86 mm.

Multi-proxy analyses including sedimentological, geochemical, paleomagnetic and palynological properties of sediments from fjord-lakes Pentecôte and Walker were used to reconstruct paleoenvironmental changes that occurred during the transition from glacial to postglacial environments. Two principal sediment facies were identified: rhythmically laminated clay facies deposited in a proglacial environment, and laminated sediments deposited in paraglacial/postglacial environment. The transition from the former to the latter is characterized by abrupt changes in textural and geochemical properties and paleomagnetic inclinations, as well as increase in palynomorph diversity. Based on radiocarbon dating, age and/or sedimentation hiatus is inferred in lakes Pentecôte and Walker between ~22 and 8 ka cal BP and between ~18 and 8 ka cal BP, respectively.

TABLE DES MATIÈRES

| | |
|--|-----------|
| 1 INTRODUCTION GÉNÉRALE | 3 |
| 1.1 Introduction | 3 |
| 1.2 Contexte scientifique des études sur la Côte-Nord | 6 |
| 1.3 Terminologies relatives aux sédiments laminés | 7 |
| 1.4 Formation et conservation des sédiments (annuellement) laminés | 8 |
| 1.5 Composition des sédiments (annuellement) laminés | 9 |
| 1.6 Une brève revue de l'origine des études des sédiments varvés | 11 |
| 1.7 Une brève revue des études sur les varves au Québec | 11 |
| 1.8 Objectifs de la thèse | 15 |
| 1.9 Hypothèses de recherche | 16 |
| 1.9.1 Hypothèse 1 | 16 |
| 1.9.2 Hypothèse 2 | 19 |
| 1.9.3 Hypothèse 3 | 21 |
| 1.9.4 Hypothèse 4 | 23 |
| 1.10 Cadre régional | 27 |
| 1.10.1 Zone d'étude | 27 |
| 1.10.2 Géomorphologie et géologie | 27 |
| 1.11 Déglaciation du Québec | 30 |
| 1.11.1 La déglaciation au Québec du Wisconsinien supérieur à l'Holocène | 30 |
| 1.11.2 Déglaciation de la Côte-Nord du Québec | 32 |
| 1.12 Les travaux de terrain réalisés durant cette étude | 34 |
| 2 RECENT SEDIMENTATION IN THREE ADJACENT FJORD-LAKES ON THE QUÉBEC NORTH SHORE (EASTERN CANADA): FACIES ANALYSIS, LAMINAES PRESERVATION AND POTENTIAL FOR VARVE FORMATION | 45 |
| 2.1 Abstract | 48 |
| 2.2 Introduction | 49 |
| 2.3 Regional setting | 50 |
| 2.4 Methods and materials | 51 |
| 2.4.1 Fieldwork and sediment coring | 51 |
| 2.4.2 Computed tomography and digital photography | 54 |
| 2.4.3 Facies- and image analysis | 54 |
| 2.4.4 Sediment dating | 55 |

| | | |
|------------|---|-----------|
| 2.4.5 | Loss on ignition | 56 |
| 2.5 | Results..... | 56 |
| 2.5.1 | Physical limnology | 56 |
| 2.5.2 | Sedimentary facies..... | 59 |
| 2.5.2.1 | Laminated sediments (LS) | 59 |
| 2.5.2.2 | Partially laminated sediments (PLS)..... | 59 |
| 2.5.2.3 | Bioturbated sediment (BS)..... | 60 |
| 2.5.2.4 | Massive sediments (MS)..... | 60 |
| 2.5.2.5 | Rapidly deposited layers (RDLs)..... | 60 |
| 2.5.2.6 | Turbidites..... | 63 |
| 2.5.3 | Thin section image analysis..... | 63 |
| 2.5.4 | Age-depth models and sedimentation rates | 67 |
| 2.5.4.1 | ^{210}Pb and ^{137}Cs age models | 67 |
| 2.5.4.2 | Radiocarbon age | 67 |
| 2.5.5 | Comparison of laminae counts to radiometric dating..... | 69 |
| 2.6 | Discussion..... | 69 |
| 2.6.1 | Catchment and local controls over sediment deposition | 69 |
| 2.6.2 | Relating the presence of laminations to lake morphometry using empirical assumptions | 70 |
| 2.6.3 | Laminated vs possibly varved sediments in the three deep fjord-lakes..... | 72 |
| 2.7 | Summary and conclusions | 73 |
| 2.8 | Acknowledgement..... | 73 |
| 3 | THIN-SECTION ANALYSIS AND DATING OF A NEW ~900-YEAR (LATE HOLOCENE) VARVED RECORD IN LAKE WALKER, QUÉBEC NORTH SHORE, EASTERN CANADA | 77 |
| 3.1 | Abstract | 80 |
| 3.2 | Introduction | 81 |
| 3.3 | Site description..... | 82 |
| 3.4 | Methods and materials | 82 |
| 3.4.1 | Sediment coring and construction of the composite sequence | 82 |
| 3.4.2 | Computed tomography | 83 |
| 3.4.3 | X-ray microfluorescence and X-radiography | 85 |
| 3.4.4 | Stratigraphy, chronology and radiocarbon dating..... | 85 |
| 3.4.5 | Lamination and varve counting | 85 |
| 3.4.5.1 | Manual counting using PeakCounter | 85 |
| 3.4.5.2 | Thin-section and grain size analyses..... | 86 |
| 3.4.6 | Statistical analysis of proxy data | 87 |

| | |
|--|------------|
| 3.5 Results..... | 87 |
| 3.5.1 Stratigraphy, chronology and radiocarbon dating..... | 87 |
| 3.5.2 Laminae visibility and counting | 88 |
| 3.5.2.1 Manual counting of laminae couplets using PeakCounter | 91 |
| 3.5.2.2 Laminae couplet counts using thin-section and image analysis..... | 93 |
| 3.5.3 Statistical analysis of particle size proxies | 95 |
| 3.6 Discussion | 95 |
| 3.6.1 Classification of laminae couples “varves” from Lake Walker..... | 95 |
| 3.6.2 Comparison of varve counting methods and error estimates..... | 95 |
| 3.6.3 Chronology and radiometric dating | 96 |
| 3.6.4 Hypotheses on laminae formation and varve preservation..... | 98 |
| 3.6.5 Lake Walker varve record: prospects and challenges..... | 99 |
| 3.7 Summary and Conclusion..... | 100 |
| 4. GLACIAL TO PARAGLACIAL/POSTGLACIAL DEPOSITIONAL TRANSITION IN FJORD-LAKES PENTECÔTE AND WALKER, QUÉBEC (EASTERN CANADA) SINCE THE LAST GLACIATION: A MULTI-PROXY APPROACH..... | 105 |
| 4.1 Abstract | 108 |
| 4.2 Introduction | 109 |
| 4.3 Studied lakes | 110 |
| 4.4 Methods and materials | 112 |
| 4.4.1 Fieldwork and sediment coring | 112 |
| 4.4.2 Core scanning and logging | 112 |
| 4.4.3 Chronology and radiocarbon dating | 114 |
| 4.4.4 Grain size analysis | 114 |
| 4.4.5 Sediment description | 115 |
| 4.4.6 Palynological analysis | 115 |
| 4.4.7 Evaluation of hydraulic potential model..... | 115 |
| 4.5 Results..... | 116 |
| 4.5.1 ^{14}C age-depth models and sedimentation rates | 116 |
| 4.5.1.1 Core PC15-02C-P, Lake Pentecôte (Figure 4.3)..... | 116 |
| 4.5.1.2 Core PC15-04B-P, Lake Pentecôte (Figure 4.4)..... | 118 |
| 4.5.1.3 Composite core WA15-08-U, Lake Walker (Figure 4.7)..... | 118 |
| 4.5.2 Lithostratigraphy and sedimentary facies | 120 |
| 4.5.2.1 Core PC15-02C-P, Lake Pentecôte | 120 |

| | | |
|------------|--|------------|
| 4.5.2.2 | Core PC15-04B-P, Lake Pentecôte | 121 |
| 4.5.2.3 | Composite core WA15-08-U, Lake Walker..... | 124 |
| 4.5.3 | Palynological analysis | 127 |
| 4.5.4 | Evaluation of Hydraulic potential model..... | 130 |
| 4.6 | Discussion | 131 |
| 4.6.1 | Environmental interpretation of the sedimentary facies | 131 |
| 4.6.1.1 | Proglacial environment | 131 |
| 4.6.1.2 | Glacial-deglacial transition phase | 132 |
| 4.6.1.3 | Paraglacial to postglacial transitional environment | 132 |
| 4.6.1.4 | Postglacial environment..... | 133 |
| 4.6.2 | Chronological challenges and/or local controls..... | 133 |
| 4.6.3 | Inference from paleomagnetic reconstruction | 134 |
| 4.6.4 | Last glacial maximum (LGM), deglaciation and transitional phases | 134 |
| 4.7 | Conclusion | 137 |
| 4.8 | Acknowledgement..... | 138 |
| 5 | PRINCIPAUX RÉSULTATS ET CONTRIBUTIONS | 143 |
| 5.1 | Résultats du premier article | 143 |
| 5.2 | Résultats du second article..... | 143 |
| 5.3 | Résultats du troisième article | 144 |
| 5.4 | Originalité et forces de la recherche | 144 |
| 5.4.1 | Étude pionnière en limnologie des lacs étudiés | 144 |
| 5.4.2 | Nouvel enregistrement varvé du lac Walker..... | 145 |
| 5.4.3 | Amélioration des modèles antérieurs portant sur la déglaciation sur la Côte-nord, Québec | 146 |
| 5.5 | Limites et défis de la recherche | 146 |
| 5.5.1 | Logistique et instrumentation | 146 |
| 5.5.2 | Fabrication de lames minces..... | 146 |
| 5.5.3 | Déploiement de pièges à sédiments | 147 |
| 5.5.4 | Datation radiocarbone sur sédiment total | 147 |
| 5.5.5 | Contraintes de temps | 148 |
| 5.6 | Discussion générale et conclusions | 148 |
| 5.7 | Bibliographie intégrée | 151 |
| 6 | ANNEXE I : Informations complémentaires Chapitre 1..... | 167 |
| 7 | ANNEXE II : Supplementary information Chapter 2 (Article 1)..... | 169 |

| | |
|--|------------|
| 8 ANNEXE III: Supplementary information Chapter 3 (Article 2) | 172 |
| 9 ANNEXE IV : Supplementary information Chapter 4 (Article 3)..... | 182 |
| 10 ANNEXE V: Informations complémentaires Chapitre 5 | 188 |
| 10.1 Insights on natural modes of climate variability during the Late Holocene inferred from particle size analysis of ~900-year varved record in Lake Walker, Québec North Shore (eastern Canada)..... | 188 |
| 10.2 Deployment of sediment traps in Lake Walker, Québec North Shore, eastern Canada.... | 199 |

LISTE DES FIGURES

| | |
|---|----|
| Figure 1.1 : Carte illustrant les proxies de données utilisées pour la reconstruction du paléoclimat à l'échelle continentale. Les diagrammes à secteurs représentent la fraction de chaque type de paramètre utilisé pour les reconstructions régionales (tiré de Pages 2K Network 2013). | 3 |
| Figure 1.2 : Distribution mondiale de 143 enregistrements de sédiments varvés lacustres (Holocène et Pléistocène) d'après la revue par Zolitschka et al. (2015). La localisation de la Côte-Nord québécoise est indiquée (zone orange, cette étude), ce qui suggère qu'il n'existe aucune trace publiée de varves non glaciaires dans cette région. | 4 |
| Figure 1.3 : A) Les secteurs considérés dans le projet ARCHIVES pour des reconstitutions hydroclimatiques et spatiotemporelle du climat au Québec. (Ci-dessous) L'illustration des deux principaux paramètres pris en compte dans le projet ARCHIVES : B) la dendrochronologie (études précédents), et C) la sédimentologie (cette étude). L'image illustrant les lacs où les sédiments varvés pourraient être trouvés d'après Fortin et al. (2012) (modifié de ARCHIVES.INRS (2009))...... | 5 |
| Figure 1.4 : Illustration des facteurs et processus qui influent sur la formation et la conservation des sédiments lacustres varvés (adapté de Zolitschka et al. 2015). | 8 |
| Figure 1.5 : Modèles simplifiés pour les dépôts d'une varve organique calcaire (mixte) et d'une varve clastique (adapté de Zolitschka et al. 2015). | 9 |
| Figure 1.6 : Exemples de types de varves. (1.6-1) Varves clastiques-biogènes (mixtes) d'Alimmainen Savijarvi en Finlande (Ojala et al. 2000); (1.6-2) Varves biogéniques d'holocène moyen du lac Holzmaar, Allemagne (Zolitschka et al. 2000); (1.6-3) Varves calciques-biogènes de Sacrower See, Allemagne (Bluszcz et al. 2009; Lüder et al. 2006); (1.6-4) Varves endogènes (évaporitiques) (A) de la paleo Mer Morte du Pléistocène tardif (formation de Lisa) et (B) à 105,8 m au-dessous du fond du lac (projet de forage profond ICDP Dead Sea, Israël) (adapté de Zolitschka et al. 2015). | 10 |
| Figure 1.7 : Carte générale montrant les sites de sédiments varves du lac glaciaire Ojibway d'après les études d'Antev (1925, 1928), Hughes (1959, 1965), Paulen 2011 et Breckenridge et al 2012 (indiqués comme "cette étude" sur la carte). Les caractéristiques de la carte sont affichées (détaillées dans Breckenridge et al. 2012). | 12 |
| Figure 1.8 : Images sélectionnées de varves du lac Ojibway, Québec-Ontario, basées sur des études de Breckenridge et al. 2012. Les lignes verticales indiquent les couplets de laminae (varves) (tiré de Breckenridge et al. 2012). | 13 |
| Figure 1.9 : Rides de courant dans les rythmites du Saint-Maurice : A) aux Vieilles-Forges et B) à Sainte-Anne-de-la-Pérade, et C) Les rythmites des Leclercville (tiré de Besré et Occhietti 1990). | 14 |

| | |
|---|----|
| Figure 1.10 : Rythmites décrites dans les réserves fauniques du Lac Jacques-Cartier et des Laurentides, au Québec: A) sous un régime nival ; B) en tant que varves glaciolacustres (adapté de Philibert 2012)..... | 15 |
| Figure 1.11 : (A) Carte bathymétrique montrant la localisation des carottes sédimentaires extraites du lac Walker lors d'étude de reconnaissance par Fortin et al. (2012). B) Image tomodensitométrique d'un carotte montrant les lames régulières du sédiments (tiré de Fortin et al. 2012)..... | 17 |
| Figure 1.12 : Illustration de l'étendue latérale et des conditions générales de la distribution des sédiments varvés dans le lac Suminko (Tylmann et al. 2012). La stratification du lac est décrite comme suit : (1) mixolimnion, 2) chemocline, 3) monimolimnium (adapté de Zolitschka et al. 2015)..... | 18 |
| Figure 1.13 : Capture d'écran illustrant une approche multi-paramètres avec le logiciel PeakCounter pour le comptage des lames / varves sur les sédiments du lac Suigetsu au Japon. Épaisseur moyenne de couche: 0,8 - 1 mm, résolution minimale: 60 µm (adapté de Marshall et al. 2012)..... | 20 |
| Figure 1.14 : Structure des sédiments varvés dans le lac Szurpily, en Pologne (modifié de Kinder et al. 2013). La composition de varve est similaire à toutes les profondeurs dans le lac, respectivement. Des barres grises et blanches délimitent les couplets de varve. Les profondeurs centrales et l'âge des images sont marqués. La diminution notable de la variabilité avec l'augmentation de la profondeur des taux d'accumulation de sédiments au cours de l'Holocène et, dans une moindre mesure, en raison du compactage (adapté Zolitschka et al. 2015)..... | 21 |
| Figure 1.15 : Données de sismo-stratigraphie montrant une topographie de vallée à l'intérieur d'une vallée avec des bancs rocheux supérieurs et un profil en forme de V inférieur au lac Walker. Cela prouve que la vallée transversale en forme de V est plus ancienne que la dernière déglaciation (adapté de Lajeunesse 2014)..... | 23 |
| Figure 1.16 : Profils acoustiques de sous-surface dans (A) Lake Pentecôte et (B) Lake Walker montrant un mince drap sédimentaire (U3 : sédiments laminés rythmiquement et U4 : sédiments paraglaciaires et postglaciaires) sur la morphologie ondulante reposant sur le socle acoustique U1 (Gagnon-Poiré et al. 2019). La vallée en forme de V est remplie de sédiments supposés s'être déposés avant les dernières glaciations (tirés de Gagnon-Poiré et al. 2019)..... | 24 |
| Figure 1.17 : Les sept étapes d'une avance sur glace et d'une retraite qui affectera ou contribueront à la sédimentation sur un plateau continental (Svytski et Praeg 1989). | 25 |
| Figure 1.18 : Sélection des données d'étalonnage pour la modélisation glaciologique (tiré de Tarasov et al. 2012). Les données de cette étude ont été utilisées pour la modélisation hydraulique des lacs étudiés sur la Côte-Nord du Québec par Gagnon-Poiré et al. (2016). | 25 |
| Figure 1.19 : Modèle conceptuel de sédimentation dans le lac CF8 (l'île de Baffin, Canada) au cours du cycle glaciaire complet, montrant la formation et la préservation des unités interglaciaires, le hiatus de | |

| | |
|---|----|
| sédimentation pendant les intervalles glaciaires et les sédiments minéraux sédimentaires glaciaires (tiré de Briner et al. 2007) | 26 |
| Figure 1.20 : Vues panoramiques des lacs étudiés: (A) Lac Pentecôte, (B) Lac Walker et (C) Lac Pasteur, qui illustrent une série de longues vallées glaciaires orientées nord-sud (> 60 km)..... | 28 |
| Figure 1.21 : Localisation des lacs Pentecôte, Walker et Pasteur et leur bassin versant (ligne noir pointillée) sur la Côte-Nord, Québec (Est du Québec). B-C: Baie-Comeau; P-D-M: Pointe-Des-Monts; B-T: Baie-Trinité; R-P: Rivière-Pentecôte; P-C: Port-Cartier; S-I : Sept-Îles (tiré de Gagnon-Poiré 2016).. | 29 |
| Figure 1.22 : Carte géologique du Québec (tire de Ministère des Ressources naturelles et de la Faune du Québec 1997)..... | 30 |
| Figure 1.23 : (A) Le modèle de changements des températures pendant la glaciation Wisconsienne extraite de la carotte GRIP $\delta^{18}\text{O}$ du Groenland (Johnsen et al. 2001), (B) la courbe $\delta^{18}\text{O}$ des derniers 25,000 ans (Thompson et al. 2003); et (C) les changements climatiques majeurs extraite de la carotte GISP2 du Groenland par $\delta^{18}\text{O}$ (Stuiver et al. 1995) (Graphique tiré de Gagnon-Poiré 2016)..... | 31 |
| Figure 1.24 : Marge glacée et configuration de retrait de l’Inlandis laurentidien à : (A) étendue maximale de glace, (B) 20 ka, (C) 18 ka, (D) 16 ka, (E) 14 ka, (F), 13 ka (tiré de Shaw et al. 2006). | 33 |
| Figure 1.25 : Modèle du retrait de l’Inlandsis laurentidien au Québec entre 13,5 et 6 cal. ka BP, proposé par Occhietti et al. (2011). | 34 |
| Figure 1.26 : Illustration schématique sur le terrain des carottes longues (tableau 1.4) recueillies dans le lac Walker en 2015, qui ont été utilisées pour reconstruire la carotte composite (WA15-08-U) (pas à l'échelle). | 38 |
| Figure 1.27 : Illustration de la séquence composite WA15-08-U (0 – 740 cm cd) basée sur la corrélation des carottes en utilisant des marqueurs (par exemple des laminations) et le redimensionnement des photos pour représenter les longueurs réelles de chacun carottes. La légende est montrée dans la figure 1.28. Liste des laminations / marqueurs utilisées pour la corrélation est fourni en tableau 1.5. L'insert (boîte rouge, gauche) montre un exemple de lamination / marqueur à haute fiabilité pour la corrélation entre des carottes..... | 39 |
| Figure 1.28 : Illustration de la révision de la séquence composite basée sur la corrélation des carottes en utilisant des marqueurs (par exemple des laminations) et le redimensionnement des photos pour représenter les longueurs réelles de chacun carottes. Des lithofaciès sont également décrits. | 40 |

Figure 2.1: (A) Geographic location of the Québec North Shore region in Eastern Canada. The insert (B) shows the location of lakes Pentecôte (PC), Walker (WA) and Pasteur (PA) (shown in blue background)

| | |
|---|----|
| and the extent of their respective watersheds (marked by dark lines). Major river inflows in the northern area of each lake are also shown..... | 50 |
| Figure 2.2: Maps showing bathymetry, location of sediment cores and the sediment facies described in (A) Lake Pentecôte, (B) Lake Walker and (C) Lake Pasteur. Core names are abbreviated as serial numbers e.g. WA14-06-R written as 6 (Table 1). W5 refers to the reconnaissance core, WA11-W5-R from Lake Walker (see text). Also shown is the deployment location of Onset temperature sensors in Lake Walker, labelled as T. Schematic subbottom profiles along marked transects are shown in Fig. 3. Core names along transect c-c', Lake Pasteur, are clearer in Figure 2.4D. | 57 |
| Figure 2.3: Measurement of physical parameters: (A) Temperature variations in the water column of Lake Walker at 35 and 170 m depths below water level measured using Onset Hobo temperature sensors over a 2-year period (June 2014 - August 2016). Deployment location of sensors is marked as T in the Figure 2.2 (B and C) Profiles of temperature and salinity measured in lakes Pentecôte and Walker, respectively using an S4 current meter on September 24 2014 (sampling points are described in Table 2.3). | 58 |
| Figure 2.4: Schematic subbottom profiles along the transects shown in Fig. 2. (A) a – a', Lake Pentecôte; (B) (b – b', bb – bb', Lake Walker) and (C) c – c', Lake Pasteur. The location of cores retrieved and the sediment facies encountered are shown (see full legend in Figure 2.2). Core names are abbreviated as serial numbers (see Table 1). RF indicates the reference core for each lake. Thermal stratification zones are inferred from temperature measurements (see text). Also shown are the empirical depths of the critical boundary (Zm_1) described for each lake (See text and Table 2.1). | 61 |
| Figure 2.5: Digital photo (Ph), ITRAX line scan images (L) and CT-scan frontal view (CT) showing example images of the sedimentary facies described in lakes Pentecôte, Walker and Pasteur. Rapidly deposited layers (RDLs) and turbidites (TB) represent isolated events. The LLS (?) represents Late Quaternary glacial facies that was encountered (below the BS facies, 2.5B) but not discussed in detail in this study (see core PC15-04-P-CD; Gagnon-Poiré et al. 2019). Note that corresponding images may appear slightly different because they were taken along different slices/views of the respective sediment cores. | 62 |
| Figure 2.6: Profiles with the digital photo (Ph), ITRAX line scan image (L) and CT-scan frontal view (CT), and results of sedimentological analysis: laminae visibility index (LVI) and laminae counting error estimate for the reference cores (A) PC14-04-R, (B) WA14-06-R and (C) PA14-16-R from lakes Pentecôte, Walker and Pasteur, respectively. LVI index: 0 - none, 1- faint, 2 - visible, 3 - clear, 4 - distinct. Thin-sections from the lower part (marked “TS” on the digital photos) are shown in Figure. 2.7. | 64 |
| Figure 2.7: Image observation of laminae structure in lower intervals of the reference cores: (A) PC14-04-R, (B) WA14-06-R and (C) PA14-16-R using thin-sections viewed in plane (left) and cross polarized | |

light (right). Scale is 1 cm. Blue backgrounds in the cross-polarized light are due to the embedding resin. In the WA14-06-R and PA14-16-R, visible-distinct laminae couplets comprising a silty lamina and a clayey lamina with sharp contact with the overlying laminae can be seen.....66
 Figure 2.8: Recent chronology (^{210}Pb and ^{137}Cs) for the reference cores from (A) Lake Pentecôte, (B) Lake Walker and (C) Lake Pasteur, respectively: (A-1, B-1, and C-1) Total (measured) and supported (from ^{226}Ra decay) ^{210}Pb activity and ^{137}CS activity; (A-2, B-2, and C-2) Chronology models based on the constant rate of supply (CRS), the constant initial concentration (CIC) and constant flux-constant sedimentation (CF-CS); (B-3, and C-3) Comparison of applicable age models (CIC/CRS) to lamina couplet counts in the upper sediments of lakes Walker and Pasteur.....68

Figure 3.1: (A) Regional setting and geographic location of Lake Walker situated on the Québec North Shore (A') in southeastern Canada, as shown in the insert (B). (C) Panoramic view of Lake Walker (N-S direction). As illustrated, coring in Lake Walker posed technical challenges due to its remote location and geomorphology.83
 Figure 3.2: A) Showing the northern part of Lake Walker that was cored. B) Multi-beam bathymetry of the cored area (modified from Gagnon-Poiré et al. 2019). Also shown are the location of two cores: core WA14-06-R previously analysed (Nzekwe et al. 2018), and the composite core WA15-08-U (this study); C) shows a photo of the UWITEC piston corer that was used to retrieve cores WA15-08B-G, WA15-08C-U and WA15-08D-U (Table 1) over lake ice cover.....84
 Figure 3.3: (A) Age-depth model of the composite core WA15-08-U (~ 50–350 cm cd) from Lake Walker based on radiocarbon dating. The model is constrained by ten dates, with three other dates as outliers (sampled at 176, 207 and 350 cm cd and derived from bulk sediment; Table 3.2). The insert (B) shows the age-depth model of the section of core WA15-08-U (~175–263 cm cd) that was analyzed for varve occurrence.....89
 Figure 3.4: Illustration of multi-scale image analyses of the composite core WA15-08-U (Lake Walker) to select a laminated interval and establish a varve record: a) CT-scan of the upper ~4 m part of the core to delineate laminated intervals (black arrows indicate depths sampled for ^{14}C dating; b) Line-scan image of a selected interval with regular laminations; c) Thin-section from the selected interval showing laminae with clear-distinct boundaries; d) Image analysis of varve counts and selection of regions of interests for particle size analysis using SEM.....90
 Figure 3.5: XRF data for the composite core WA15-08-U showing CT-scan frontal view (CT) and vertical profiles of selected elements along the core. The number of counts for each element in a spectrum acquired for a specific depth interval was normalized by the total number of counts of that spectrum

| | |
|--|----|
| (expressed in counts per second, cps). Elemental variations are relatively more regular in the lower part of the core compared to the upper part, where they show general upward reduction. For preliminary attempts to establish a varve chronology, the middle part of the core (~175–263 cm cd) was selected for analysis using PeakCounter software (compare with Marshall et al. 2012; see Figure 1.13)..... | 91 |
| Figure 3.6: Illustration of the multi-parameter approach using the PeakCounter Software (Marshall et al. 2012) for lamina/varve counts on core WA15-08-U (Lake Walker). Parameters include: Radiograph (top) and optical image (below) of the core section (~175–263 cm cd, Table 3.1). (Middle) for an active window (see radiograph), grey scale and XRF elements (Fe, K, Ti, Si, inc/coh ratio) are overlapped, where vertical marked lines represent laminations labelled based on varve quality index (see levels 1 to 4 colours/marks, as shown in table 3.3)..... | 92 |
| Figure 3.7: Illustration of typical varve structure from Lake Walker, interpreted as clastic varves: A) Flatbed thin-section image showing (B) two main layers: clay-rich laminae (denoted as “c”) deposited during winter and silt-rich laminae (denoted as “s”) deposited between spring melt and autumn. Black horizontal bars indicate varve boundaries while numbers indicate varve counts (not in years). Regions of interest (ROIs) are shown at the right side lettered squares. (C) SEM images related to ROIs (as shown in B). SEM images show relatively clear contrast between clayey and silty laminae (letters and yellow squares indicate ROI boundaries, while black horizontal lines indicate varve boundaries) | 94 |
| Figure 3.8: Comparison of age-depth models for the laminated interval of core WA15-08-U (~175–263 cm cd) based on AMS ^{14}C dating, semi-automatic counting using PeakCounter software (Marshall et al 2012); two individual varve counts based on thin-sections in this study (O.P.N and F.L); and the mean varve count by the two researchers..... | 97 |

| | |
|--|-----|
| Figure 4.1: (A) Geographic location of the Québec North Shore region, eastern Canada. (A') indicates the location of lakes Pentecôte (PC) and Walker (WA) (shown within yellow rectangles). Also shown are images of multibeam bathymetry of (B) Lake Pentecôte (1-m resolution) and (C) Lake Walker (3-m resolution). The inserts (B', C') indicate the cored area in the both lakes and the location of analysed cores (Table 4.1) (adapted from Gagnon-Poiré et al. 2019) | 111 |
| Figure 4.2: Age-depth models based on radiocarbon dating from: A) core PC15-02C-P and B) core PC15-04B-P (Lake Pentecôte) and composite core WA15-08-U (Lake Walker). In B and C, the model shows an age gap between the lower unit (Unit I) and the upper unit (II) of the cores, which suggests an age/sedimentation hiatus, indicated as “H” | 117 |
| Figure 4.3: Multi-proxy analysis of core core PC15-2C-P (Lake Pentecôte). (From left to right, L-R): Digital photo (Ph), CT-scan image (CT), laminae counts on the CT-scan compared to age model based on | |

radiocarbon dating (dated intervals are marked by yellow star). The laminations are non-annual. Also shown are XRF data for selected elements. Values are given in peak area integrals normalized by the total counts per second of each spectrum (cps = counts per second). Comparison of elemental variation is rather difficult due to laminae disturbance. However, elemental peaks show strong correlation with laminae structure: Si, K, Sr are higher within light gray laminae, while inc/coh ratio and Fe/Ca are higher within the dark gray laminae..... 121

Figure 4.4: (A) Grain size analysis for core PC15-04B-P, Lake Pentecôte. (L-R): Digital photo (Ph), line scan image (L), CT-scan frontal view (CT) and CT number (HU), grain size statistical parameters (clay content, mean grain size, sorting, skewness and kurtosis) calculated by the GRADISTAT 4.0 software (Blott and Pye, 2001) using the Folks and Ward 1957 method. The lettering (A, B, C) on the digital photo indicates depths that were sampled for smear slide analysis, shown in Figure 4.5. Sediment facies are RLC rhythmically laminated clay sediments; LS-O laminated organic-rich silty clay and clay sediments; and LS - laminated sediments..... 122

Figure 4.5: (A1 – C1) Sediment core image and smear slide images from core PC15-04B-P at selected depths, as seen in plane- and crossed-polarized light: (A) RLC facies, 110 cm; (B2-B3) LS-O facies, 94 cm; (C2-C3) LS facies. Identifiable minerals include: Q - quart, F - feldspar, C - carbonates (calcite), M - muscovite, Ma - mafics, V - vivianite, Cl - clay minerals, OM - organic matter. Sediment facies are RLC rhythmically laminated clay sediments; LS-O laminated organic-rich silty clay and clay sediments; and LS - laminated sediments..... 123

Figure 4.6: XRF data for core PC15-4B-P showing digital photo (Ph), line scan image (L) and CT-scan frontal view (CT), and vertical profiles of selected elements along the core. Values are given in peak area integrals normalized by the total counts per second of each spectrum (cps = counts per second). Sediment facies are RLC rhythmically laminated clay sediments; LS-O laminated organic-rich silty clay and clay sediments; and LS - laminated sediments..... 124

Figure 4.7: Grain size analysis for the composite core, WA15-08-U from Lake Walker, showing: digital photo (Ph), line scan image (L), CT-scan frontal view (CT) and CT number (HU), grain size statistical parameters (clay content, mean grain size, sorting, skewness and kurtosis) calculated by the GRADISTAT 4.0 software (Blott and Pye, 2001) using the Folks and Ward 1957 method. The letterings A, B, C, D, E on the digital photo indicate depths that were sampled for smear slide analysis, shown in Appendix IV, Figure S4. Sediment facies are RLC rhythmically laminated clay sediments, and LS - laminated sediments..... 126

Figure 4.8: XRF data for core WA15-08-U from Lake Walker showing digital photo (Ph), line scan image (L), CT-scan frontal view, CT number (HU) and vertical profiles of selected elements along the core. Values are given in peak area integrals normalized by the total counts per second of each spectrum (cps =

| | |
|--|-----|
| counts per second). Sediment facies are RLC rhythmically laminated clay sediments, and LS - laminated sediments | 126 |
| Figure 4.9: Paleomagnetic secular variation records (PSV) for the lower part of the composite section, WA15-08-U from Lake Walker, showing Inclination (inc), Declinations (dec), Maximum angular deviation (MAD), and Natural Remnant Magnetization (NRM) and Anhysteretic Remnant Magnetization (ARM) ratio. Each profile consists of segments that correspond to individual cores comprising the composite..... | 127 |
| Figure 4.10: Optical images of selected palynomorphs observed in cores from lakes Pentecôte and Walker: (a) Betula Pollen, (b) Pinus Pollen, (c) Pteridophyte spores (d) Sphagnum, (e) Thecamoebian (Testate amoebae), (f) Radiosperma, (g) Stomata (h) Arthropoda segment. Scale bar (in white colour) in images a–h is 10 μm , except for image b where it is 20 μm | 128 |
| Figure 4.11: Simplified palynostratigraphy of selected cores showing palynomorph counts against depths and calibrated years BP. (A) PC15-02B-P and (B) PC15-04B-P from Lake Pentecôte, and (C) WA15-08-U from Lake Walker..... | 129 |
| Figure 4.12: Hydraulic potential for the Lake Pentecôte basin at the Last Glacial Maximum (LGM: 20-21 ka) following a southeastern ice flow direction (shown by black arrows; Dredge, 1983), considering a 1650 m ice thickness (Tarasov et al. 2012) and an ice sheet surface slope of 0.17. (A) Lake Pentecôte subglacial lake depth (m); (B) Geometry along longitudinal profile of the subglacial lake basin. The current lake shoreline is represented by the black dashline (Modified from Gagnon-Poiré 2016)..... | 130 |
| Figure 4.13: Hydraulic potential for the Lake Walker basin at the Last Glacial Maximum (LGM: 20 ka) following a south-eastern ice flow direction (shown by white arrows; Dredge, 1983), considering a 1650 m ice thickness (Tarasov et al. 2012) and an ice sheet surface slope of 0.17. (A) Hydraulic head (m) for Lake Walker; (B) Lake Walker subglacial lake depth (m); (C) Geometry along longitudinal profile of the subglacial lake basin (illustrated by white dashed line in B). The current lake shoreline is represented by the black dashline (Modified from Gagnon-Poiré 2016)..... | 131 |
| Figure 4.14: Conceptual hydraulic potential model for the evolution of the Lake Walker basin from the Last Glacial Maximum (LGM: 20 Ka) to the Late Holocene following a south-eastern ice flow direction considering a 1650 m ice thickness (Tarasov et al. 2012) and an ice sheet surface slope of 0.17. (A) at 20-21 ka BP, (B) 15 ka BP, (C) 12.5 ka BP, and (D) 10 ka BP..... | 135 |

LISTE DES TABLEAUX

| | |
|--|-----|
| Tableau 1.1 : Liste des carottes sédimentaires récupérées du lac Walker lors d'étude de reconnaissance in 2011. | 17 |
| Tableau 1.2 : Liste des carottes courtes de sédiments échantillonnées dans les trois lacs étudiés..... | 36 |
| Tableau 1.3 : Liste des carottes longues récupérées du lac Pentecôte en 2015..... | 37 |
| Tableau 1.4 : Liste des carottes longues récupérées du lac Walker en 2015. | 37 |
| Tableau 1.5 : Liste des laminations utilisées pour corréler des carottes pour construire la séquence composite WA15-08-U (Lac Walker)..... | 41 |
| | |
| Table 2.1: Characteristics of the studied lakes and empirical parameters relating laminated sediments to lake morphometry. | 52 |
| Table 2.2: List of short sediment cores sampled from the three studied lakes. | 53 |
| Table 2.3: List of sampling points for measurement of physico-chemical parameters in lakes Pentecôte and Walker. | 57 |
| Table 2.4: AMS ^{14}C age of the dated materials from lakes Pentecôte and Walker..... | 65 |
| Table 2.5: Comparison of sedimentation- rates and fluxes derived from sediment dating from surface cores from lakes Pentecôte, Walker and Pasteur. | 69 |
| | |
| Table 3.1: List of sediment cores used to reconstruct the (~4 m upper part of) composite core WA15-08-U (Lake Walker). | 84 |
| Table 3.2: AMS ^{14}C age of dated materials from the composite core WA15-08-U (Lake Walker). | 88 |
| Table 3.3: Summary data of varve counts on a section of the composite core WA15-08-U (~175–263 cm cd) using the PeakCounter software (Marshall et al. 2012). Level 1, 2, 3, 4 represent the varve quality indices used. | 93 |
| Table 3.4: Univariate statistics of the physical parameters analysed using PAST software from the composite core WA15-08-U (~175–263 cm cd) Lake Walker..... | 94 |
| Table 3.5: Spearman's rank correlation of varve thickness and grain size parameters from the composite core WA15-08-U (175 – 262.5 cm cd), Lake Walker..... | 95 |
| | |
| Table 4.1: List of sediment cores analysed from the Lake Pentecôte. | 112 |
| Table 4.2: List of sediment cores that were used to reconstruct composite core, WA15-08-U (~488-740 cm cd) from Lake Walker. | 112 |

| | |
|---|-----|
| Table 4.3: AMS ^{14}C age of the dated materials from Lake Pentecôte | 117 |
| Table 4.4: AMS ^{14}C age of the dated materials from the composite core, WA15-08-U (~488-740 cm cd) Lake Walker..... | 118 |
| Table 4.5: Summary of multi-proxy analyses and their environmental interpretation | 119 |

CHAPITRE 1

INTRODUCTION GÉNÉRALE

1 INTRODUCTION GÉNÉRALE

1.1 Introduction

Le Groupe Intergouvernemental sur l'évolution climatique (GIEC) affirme qu'étudier le climat du passé implique de reconstituer le «changement climatique», c'est-à-dire un changement dû à la variabilité naturelle et / ou aux activités anthropiques qui dure sur des décennies ou plus (IPCC 2014). La reconstitution du passé climatique nécessite la plus grande précision temporelle possible (Veiga-Pires and St-Onge 2008; Zolitschka et al. 2015). Cela incite donc à rechercher des enregistrements à haute-résolution temporelle des conditions climatiques passées tels que les cernes des arbres, les carottes glaciaires et les sédiments annuellement laminés d'origine lacustre ou marine (Francus et al. 2013a; O'Sullivan 1983; Veiga-Pires and St-Onge 2008). Le Programme international sur les changements globaux passés (PAGES) recommande des reconstitutions paléoclimatiques quantifiées, c'est-à-dire un lien mesuré avec certains paramètres climatiques (IPCC 2013). D'après le rapport de synthèse du GIEC (IPCC 2007), il a été observé une hausse globale des températures au cours des dernières décennies. Cette hausse a entraîné des modifications des systèmes hydrologiques, entre autres le réchauffement des lacs et / ou les débits de pointe du printemps.

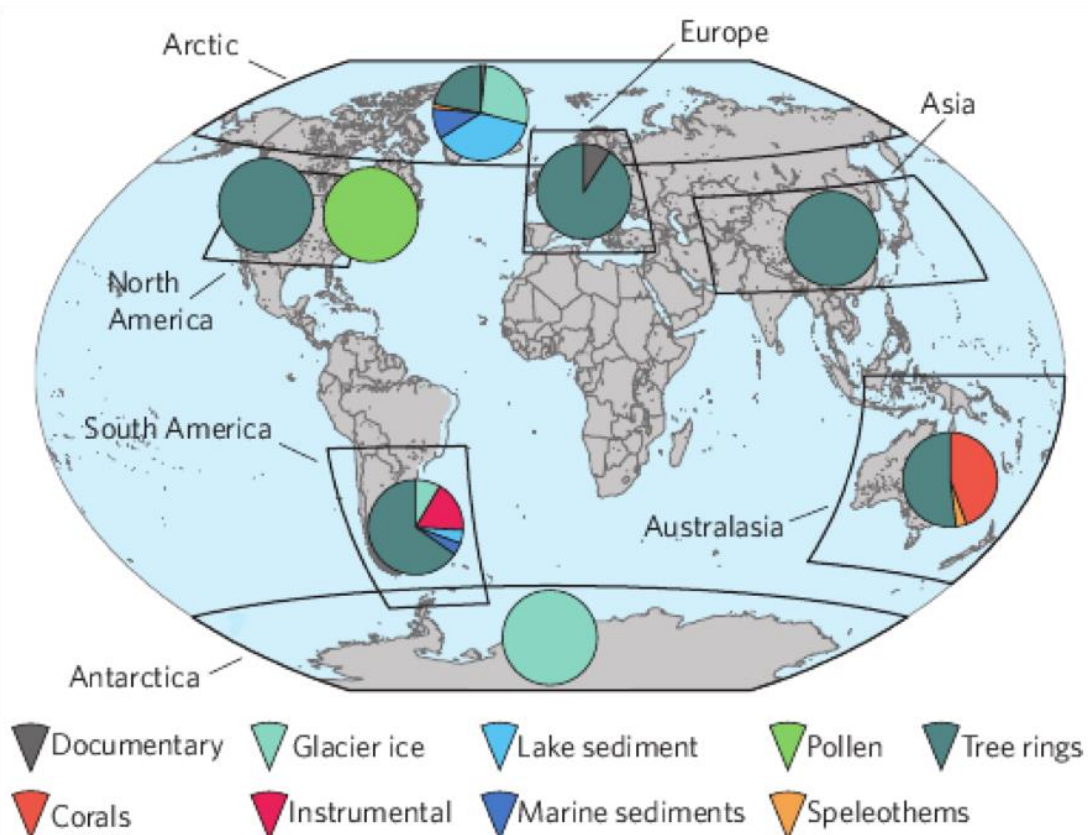


Figure 1.1 : Carte illustrant les proxies de données utilisées pour la reconstruction du paléoclimat à l'échelle continentale. Les diagrammes à secteurs représentent la fraction de chaque type de paramètre utilisé pour les reconstructions régionales (tiré de Pages 2K Network 2013).

La figure 1.1 présente différentes données indirectes qui ont été utilisées pour reconstituer les variations de la température mondiale au cours des deux derniers millénaires sur la base d'une étude réalisée par le Groupe PAGES 2k (PAGES 2k Network 2013). Cette étude a indiqué que les reconstructions en Amérique du Nord étaient principalement basées sur des cernes et du pollen, sauf dans le nord du Canada où les glaciers et les sédiments lacustres ont également été utilisés. Ici, les sédiments lacustres font référence à des sédiments annuellement laminés (varves) (Figure 1.1). Comme l'illustre la figure 1.2, la majorité des enregistrements de varves publiés ont été découverts dans trois régions principales : l'Amérique du Nord (Canada arctique et nord des États-Unis), l'Europe du Nord et centrale et l'Afrique orientale et centrale (O'Sullivan 1983; Zolitschka et al. 2015).

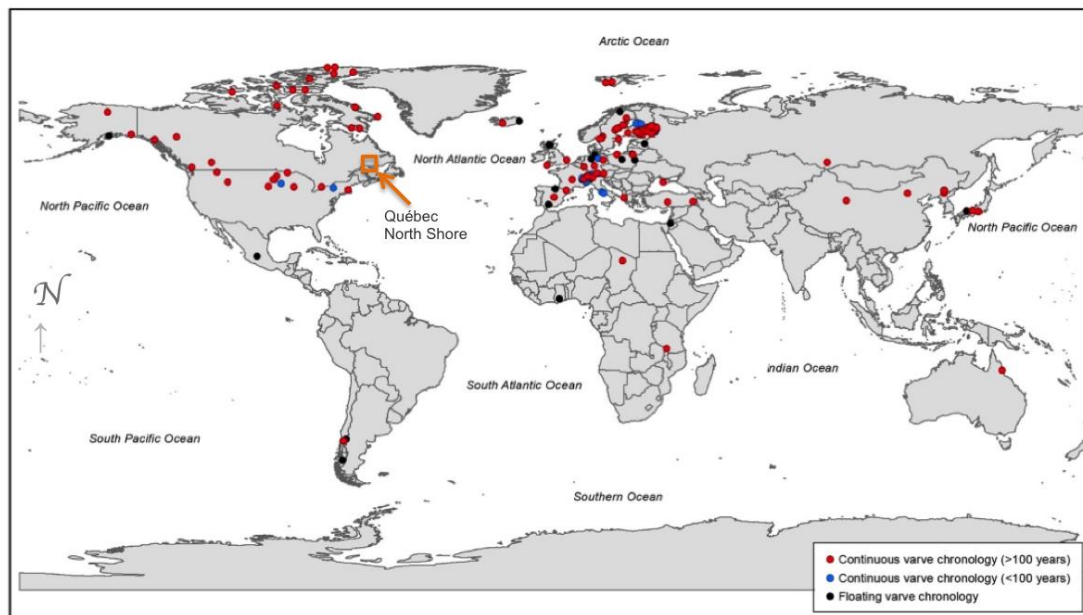
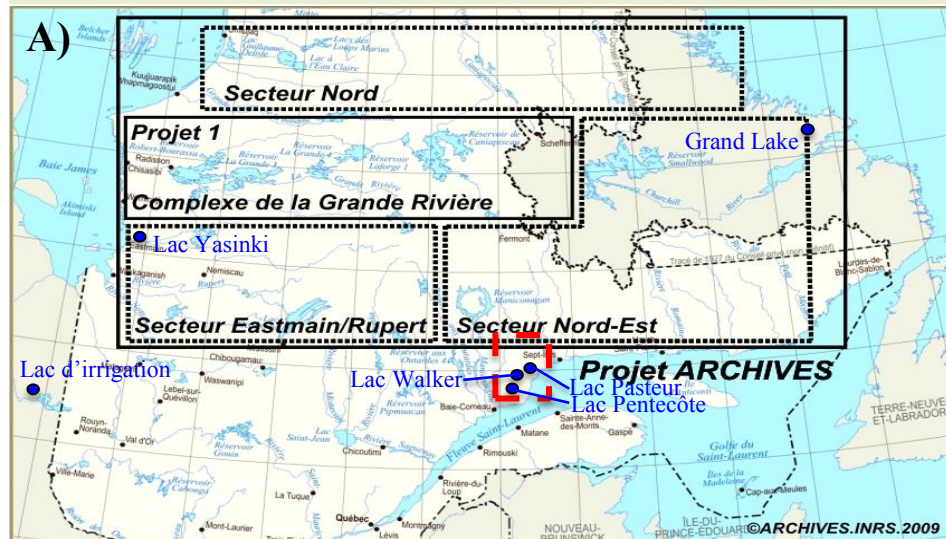
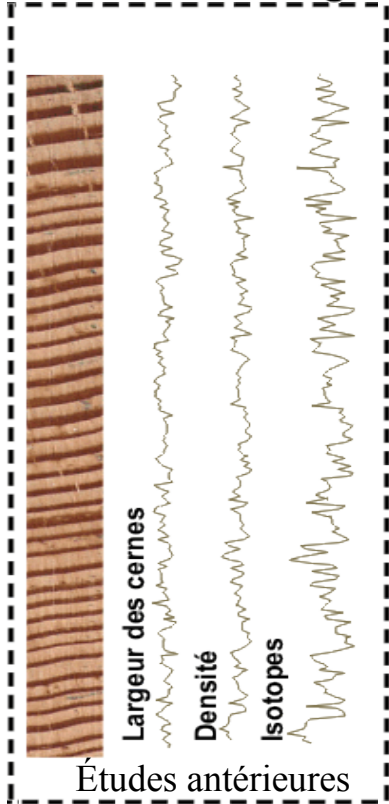


Figure 1.2 : Distribution mondiale de 143 enregistrements de sédiments varvés lacustres (Holocène et Pléistocène) d'après la revue par Zolitschka et al. (2015). La localisation de la Côte-Nord québécoise est indiquée (zone orange, cette étude), ce qui suggère qu'il n'existe aucune trace publiée de varves non glaciaires dans cette région.

Dans la province du Québec et dans l'est du Canada, il n'existe aucun enregistrement varvé non-glaciaire publié selon la base de données mondiale sur les varves (Ojala et al. 2013; Zolitschka et al. 2015). À ce jour, il existe dans le nord du Québec principalement des données instrumentales et des reconstitutions paléoclimatiques à partir de cernes et d'isotopes stables de cernes d'arbres, couvrant une période allant de 200 ans au dernier millénaire (Arseneault et al. 2013; Naulier et al. 2014; Nicault et al. 2014). Les sédiments annuellement laminés sont rares dans cette région. L'identification éventuelle de ce type d'archive dans les lacs profonds offre la possibilité d'explorer ces enregistrements environnementaux afin de reconstituer les conditions hydro-climatiques annuelles. Ce projet de recherche propose donc d'explorer les propriétés annuelles et texturales des sédiments varvés de trois lacs profonds (lacs Pentecôte, Walker et Pasteur) sur la Côte-Nord du Québec.



B) Dendrochronologie



C) Séimentologie

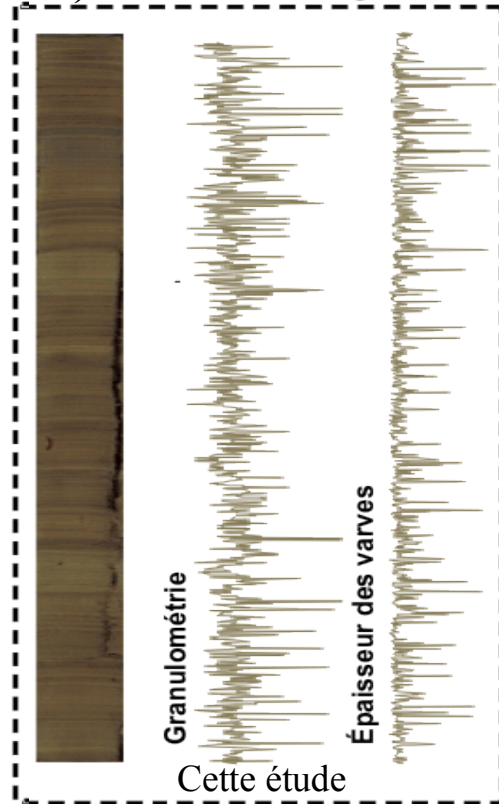


Figure 1.3 : A) Les secteurs considérés dans le projet ARCHIVES pour des reconstitutions hydroclimatiques et spatiotemporelle du climat au Québec. (Ci-dessous) L'illustration des deux principaux paramètres pris en compte dans le projet ARCHIVES : B) la dendrochronologie (études précédentes), et C) la séimentologie (cette étude). L'image illustrant les lacs où les sédiments varvés pourraient être trouvés d'après Fortin et al. (2012) (modifié de ARCHIVES.INRS (2009)).

Les trois lacs étudiés ont été sélectionnés sur la base d'études antérieures du projet ARCHIVES, soit un projet pluridisciplinaire associant plusieurs universités « INRS-ETE, UQAM, UQAR, Université de Liège (Belgique), CEREGE (France) et des partenaires industriels / agences Hydro-Québec, Ouranos, la Commission géologique de Canada-Québec », ayant comme mandat d'étudier les changements climatiques des 1000 dernières années dans le nord du Québec en se basant sur les cernes d'arbres et les sédiments lacustres (Fortin et al. 2012) (Figure 1.3). Bien que plusieurs reconstructions de cernes d'arbres aient été publiées (comme indiqué ci-dessus), des études de reconnaissance sur le terrain (de 2009 à 2012) suggéraient que les propriétés sédimentaires de Grand Lac (Labrador) étaient fortement liées à la décharge de la rivière Naskaupi. Trois autres lacs (les lacs Pentecôte, Walker et Pasteur) sur la Côte-Nord ont également retenu l'attention pour leur grand potentiel de contenir des sédiments annuellement laminés (Fortin et al. 2012) (Figure 1.3A). Le couplage spatio-temporel des cernes d'arbre avec les sédiments varvés serait bénéfique non seulement pour la comparaison avec les données instrumentales (derniers 50 ans dans la région), mais également pour l'extraction du signal température de celui des précipitations. En effet, les cernes d'arbres offrent souvent les deux paramètres (température et précipitation) qui peuvent être difficiles à différencier, alors que les sédiments varvés sont beaucoup plus sensibles et liés aux précipitations (fonte nivale et pluies pour nos sites). En raison de la rareté des enregistrements de cernes d'arbres qui dépassent la fin du millénaire (Bradley 1999; Zolitschka et al. 2015), les enregistrements de sédiments varvés des lacs étudiés (cette thèse) pourraient s'étendre au-delà des enregistrements de cernes d'arbres, c'est-à-dire +1000 ans, et même jusqu'à la fin de la période glaciaire. En plus de fournir des plus longs enregistrements paléoclimatiques, ces séquences sédimentaires avec des chronologies robustes seraient fort utiles pour calibrer la chronologie d'autres enregistrements à l'aide des mesures paléomagnétiques (Zolitschka et al. 2015) et / ou pour corrélérer les modèles paléoenvironnementaux (Gagnon-Poiré et al. 2019; Syvitski 1991; Syvitski and Praeg 1989) de la région de la Côte-Nord du Québec.

1.2 Contexte scientifique des études sur la Côte-Nord

À la suite du projet ARCHIVES (2009-2012), la recherche de sédiments varvés sur la Côte-Nord du Québec a finalement abouti à un projet financé par le Fonds de Recherche du Québec : Nature et Technologies (FRQNT) sur le thème «Lacs profonds de la Côte-Nord : exploration d'archives paléoenvironnementales uniques», sous la direction de Pierre Francus (INRS-ETE), Guillaume St-Onge (UQAR-ISMER) et Patrick Lajeunesse (Université Laval). Les principaux objectifs du projet étaient « d'analyser la variabilité interannuelle du climat dans la région de la Côte-Nord en fonction des sédiments (annuellement) laminés et de la géomorphologie glaciaire» du bassin versant de trois lacs profonds (les lacs Pentecôte, Walker et Pasteur). Ce projet est divisé en trois approches de recherche principales: la limnologie et les structures sédimentaires fines (cette étude, menée à l'INRS-

ETE); la sédimentologie et le paléomagnétisme (UQAR-ISMER); et la géomorphologie (Université Laval).

Cette thèse de doctorat a pour objet la recherche, la découverte et l'analyse des sédiments laminés pour étudier leurs propriétés afin d'en déduire les environnements passés depuis la dernière glaciation. Le grand intérêt porté sur les sédiments annuellement laminés découle de leurs caractéristiques uniques, notamment : leur rareté, leur potentiel pour déceler les changements (abruptes) environnementaux du passé grâce à leur haute résolution temporelle (jusqu'à l'échelle saisonnière). Ils peuvent être corrélés avec d'autres chronologies (Francus et al. 2013a; Lapointe et al. 2019; Ojala et al. 2012; Ojala et al. 2013). Toutefois, afin d'exploiter pleinement le potentiel des sédiments varvés pour la reconstitution paléoclimatique, des études préliminaires sont impératives (Schnurrenberger et al. 2003). Celles-ci comprennent une compréhension complète des processus de dépôt qui ont donné lieu à la formation des varves, des mécanismes de sédimentation et de la composition de chacune des lames intra-annuelles (Francus et al. 2013a; Larsen and MacDonald 1993; Larsen et al. 1998; Ojala et al. 2012; Schnurrenberger et al. 2003; Zolitschka 2007).

Afin d'améliorer la précision des chronologies varvées, il est nécessaire de combiner au moins deux techniques à haute résolution, telles que la tomographie axiale par ordinateur aux rayons X (CT-scan), la microfluorescence aux rayons X (μ -XRF) et le plus important, l'analyse détaillée à partir de lames minces (Ojala et al. 2013). De plus, des études récentes (Francus et al. 2013b; Lapointe et al. 2012; Ojala et al. 2012; Ojala et al. 2013; Schimmelmann et al. 2016; Zolitschka et al. 2015) confirment l'intérêt de coupler l'analyse des varves récentes avec le suivi de terrain (bassin versant, limnologie, etc). Ces approches multidisciplinaires ont donc été utilisées dans cette recherche doctorale.

1.3 Terminologies relatives aux sédiments laminés

Plusieurs termes ont été utilisés pour décrire les sédiments laminés, notamment les lits (Schnurrenberger et al. 2003), les lamination (Saarnisto et al. 1977), les rythmites saisonnières (Ludlam 1969), et les varves (Renberg 1981). Les lits ont généralement une épaisseur supérieure à 1 cm (Schnurrenberger et al. 2003), tandis qu'une lamination fait référence à une fine couche de sédiment, généralement inférieure ou égale à 1 cm (parfois plus épaisse) (Blatt et al. 2006; Boggs 1995; Schnurrenberger et al. 2003).

Les rythmites font référence à des sédiments caractérisés par des couches alternées qui ne suivent pas un schéma annuel (Besré and Occhietti 1990; O'Sullivan 1983; Quigley 1983). Certains articles introduisent un terme, sédiments partiellement laminés, pour décrire des sédiments qui ne suivent pas un schéma régulier (Larsen et al. 1998; Nzekwe et al. 2018). Par ailleurs, les couches annuelles, appelées varves, font généralement référence à deux lames saisonnières ou plus qui reflètent un

cycle annuel ou saisonnier (Francus et al. 2013a; Schnurrenberger et al. 2003; Zolitschka et al. 2015). Plus de détails sont fournis ci-dessous.

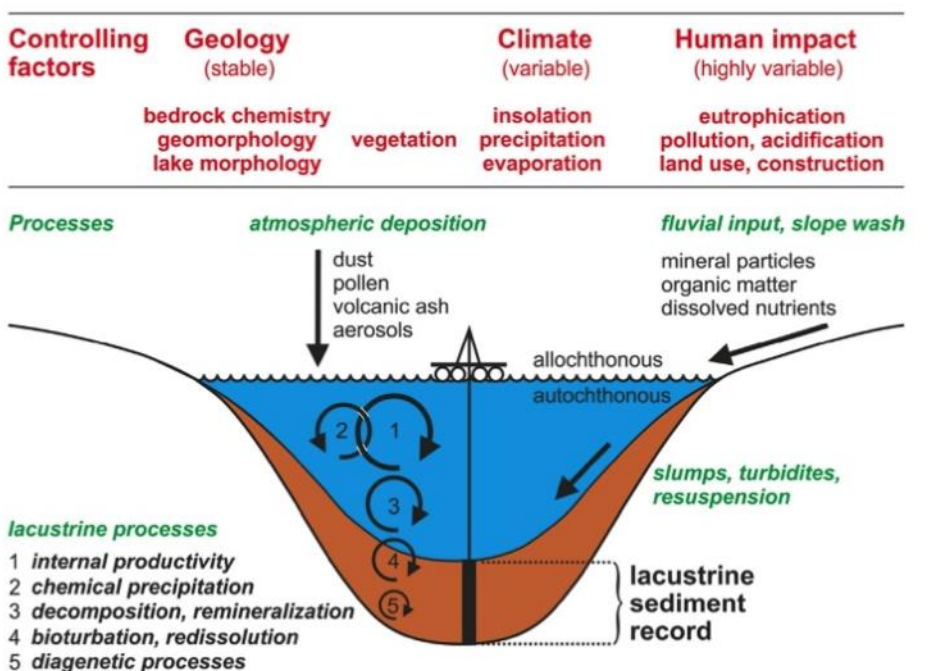


Figure 1.4 : Illustration des facteurs et processus qui influent sur la formation et la conservation des sédiments lacustres varvés (adapté de Zolitschka et al. 2015).

1.4 Formation et conservation des sédiments (annuellement) laminés

La figure 1.4 donne un aperçu des facteurs qui contrôlent la formation de sédiments varvés : climat, géologie, morphologie des lacs, végétation et impact humain (Larsen and MacDonald 1993; Larsen et al. 1998; Nzekwe et al. 2018; Tylmann et al. 2012; Tylmann et al. 2013; Valpola and Ojala 2006; Zolitschka 2007; Zolitschka et al. 2015). L'influence de facteurs climatiques tels que l'insolation et les précipitations reflètent les changements saisonniers qui sont donc généralement plus distincts dans les régions tempérées que dans les tropiques (Zolitschka et al. 2015). Les facteurs géologiques sont liés aux roches basales sous-jacentes du bassin lacustre et sont généralement stables, sauf dans les lacs affectés par les mouvements isostatiques postglaciaires (Schnurrenberger et al. 2003; Zolitschka et al. 2015). La formation et la préservation des lames dépendent de la présence de conditions favorables telles qu'un bassin relativement profond, une anoxie saisonnière ou permanente favorisant l'absence de bioturbation et donc une activité biologique réduite des organismes benthiques, ainsi qu'une sédimentation contrastée selon les saisons (Jenny et al. 2013; Larsen and MacDonald 1993; Larsen et al. 1998; O'Sullivan 1983; Schnurrenberger et al. 2003; Tylmann et al. 2012; Tylmann et al. 2013; Valpola and Ojala 2006; Wetzel and Likens 1991; Zolitschka 2007; Zolitschka et al. 2015). Dans certaines zones, des activités anthropiques telles que le déversement d'éléments nutritifs dans les

bassins lacustres peuvent également entraîner une hypoxie (Jenny et al. 2013; Jenny et al. 2016), favorisant ainsi la préservation des sédiments récents (Zolitschka et al. 2015).

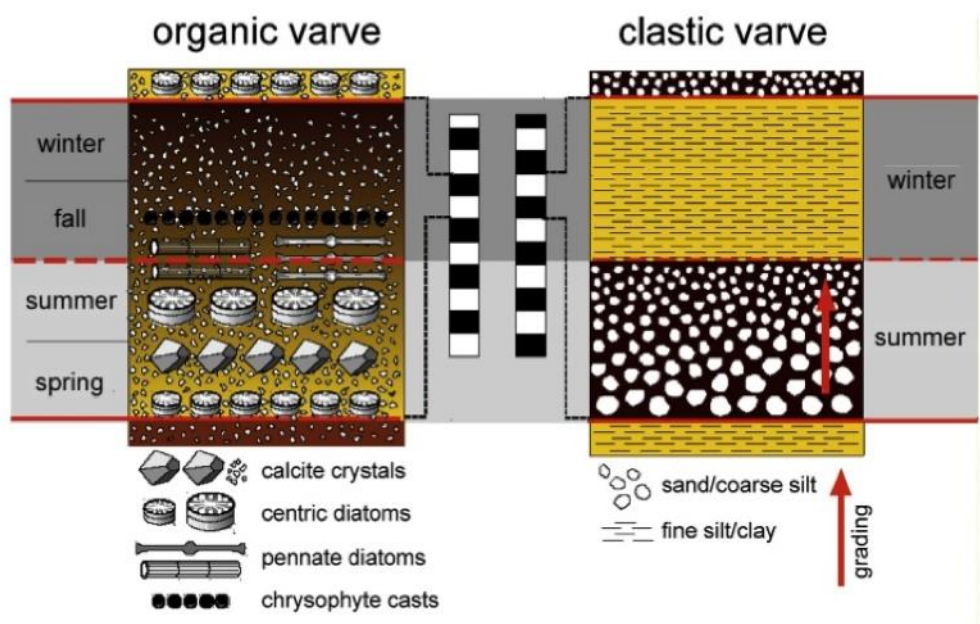


Figure 1.5 : Modèles simplifiés pour les dépôts d'une varve organique calcaire (mixte) et d'une varve clastique (adapté de Zolitschka et al. 2015).

1.5 Composition des sédiments (annuellement) laminés

Les sédiments lacustres peuvent être classés de deux manières : composition génétique ou provenance (Zolitschka et al. 2015). Sur la base de la composition génétique, ils sont décrits comme clastiques, biogènes et endogènes. Les sédiments clastiques sont constitués de particules minérogéniques, souvent silico-clastiques, déposées par des processus détritiques tels que le transport fluvial ou éolien. Les varves clastiques sont généralement caractérisées par une couche de décharge printanière généralement claire et de granulométrie grossière et une couche d'hiver de couleur foncée (Figure 1.5). Les varvés biogéniques sont principalement composées de particules riches en matière organique et / ou biominéralisées, telles que la silice biogénique ou les carbonates, qui se forment dans la colonne d'eau du lac (Figure 1.6-1, 1.6-2, 1.6-3). Les sédiments endogènes (varvés) sont composés de particules résultant de la cristallisation et / ou de la précipitation dans la colonne d'eau du lac, généralement associées à l'évaporation (Figure 1.6-4) (Zolitschka et al. 2015). Le terme «endogène» décrit dans la synthèse par Zolitschka et al. (2015) regroupe des catégories telles que les sédiments ferrogéniques et / ou calcaires (O'Sullivan 1983), les sédiments chimiques (Schnurrenberger et al. 2003) et les sédiments évaporitiques (Zolitschka 2007).

Selon leur origine, les sédiments sont classés comme autochtones ou allochtones. Des sédiments autochtones se forment *in situ* dans le lac, tandis que les sédiments dits allochtones sont transportés du bassin versant et déposés dans le fond du lac (O'Sullivan 1983; Zolitschka et al. 2015).

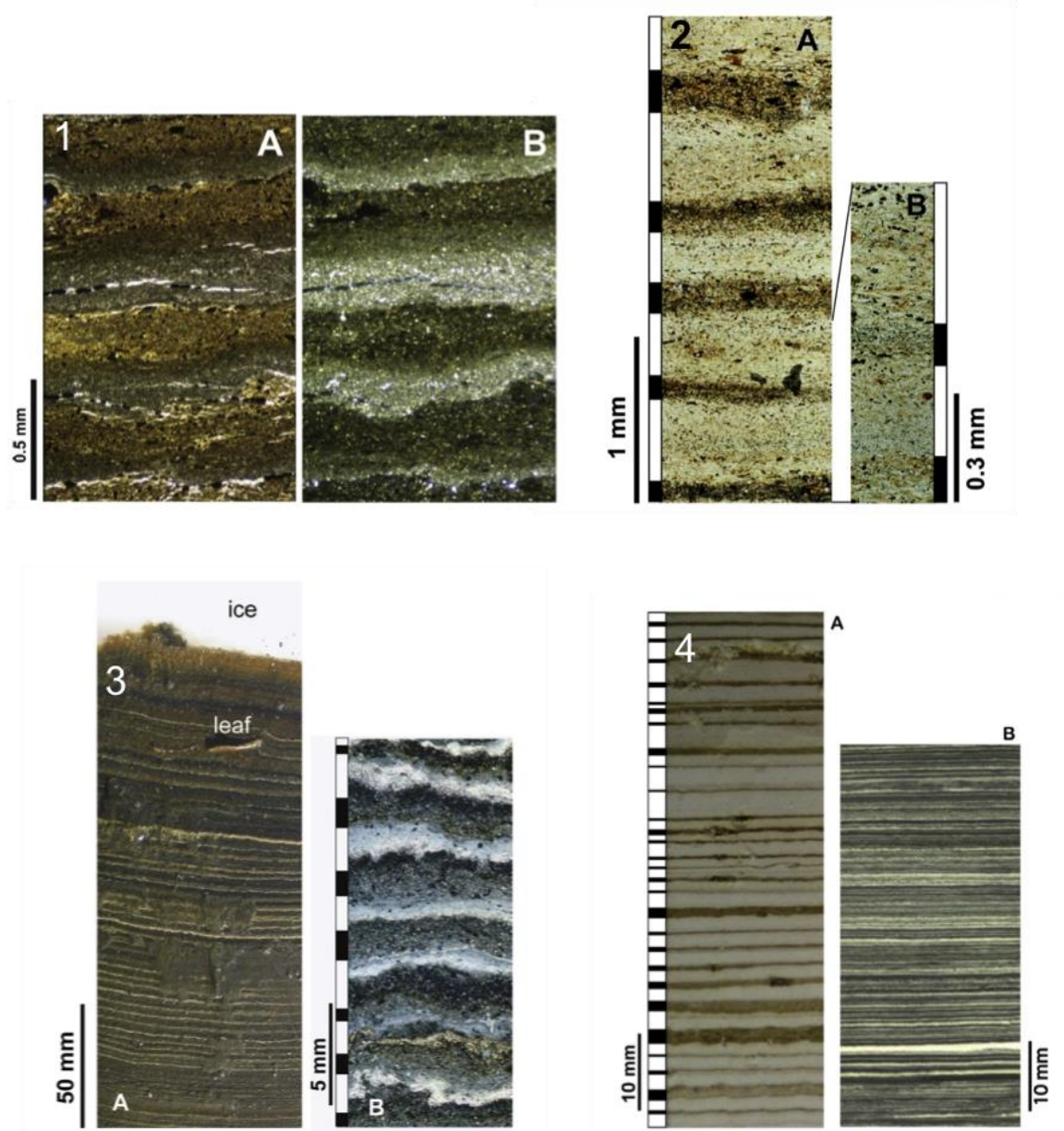


Figure 1.6 : Exemples de types de varves. (1.6-1) Varves clastiques-biogènes (mixtes) d'Alimmainen Savijarvi en Finlande (Ojala et al. 2000); (1.6-2) Varves biogéniques d'holocène moyen du lac Holzmaar, Allemagne (Zolitschka et al. 2000); (1.6-3) Varves calciques-biogènes de Sacrower See, Allemagne (Bluszcz et al. 2009; Lüder et al. 2006); (1.6-4) Varves endogènes (évaporitiques) (A) de la paleo Mer Morte du Pléistocène tardif (formation de Lisa) et (B) à 105,8 m au-dessous du fond du lac (projet de forage profond ICDP Dead Sea, Israël) (adapté de Zolitschka et al. 2015).

1.6 Une brève revue de l'origine des études des sédiments varvés

Le terme suédois «varve» (signifiant «cycle») a été introduit pour la première fois par De Geer (1912) pour décrire un cycle annuel lequel est caractérisé par une couche de grains grossiers déposée en été et une couche sombre à grains fins déposée en hiver dans un environnement proglaciaire. Plus tard, Sturm (1979) a défini les varves en termes de structure double caractérisée par une couche de texture grossière (silts ou sable) et une couche mince (argile) séparée de la suivante par une surface d'érosion. Renberg (1981) a déclaré que les varves désignent les sédiments déposés au cours d'une année, quel que soit le processus de dépôt, qu'il soit physique, chimique ou organogène. Cependant, la définition de De Geer (1912) a été largement acceptée par les chercheurs comme se référant aux «varves classiques».

Depuis les trois dernières décennies, la définition des varves s'est élargie pour inclure les sédiments de l'Holocène pour plusieurs raisons. Celles-ci comprennent : 1) des techniques de carottage améliorées (carottier à piston et carottier à percussion); 2) l'effet croissant des activités anthropiques sur les bassins versants des lacs, par exemple l'augmentation de l'eutrophisation (et de la pollution) (Jenny et al. 2013; Kinder et al. 2019a), et 3) la recherche d'enregistrements à haute résolution de sédiments lacustres annuellement laminés non glaciaires (Kinder et al. 2013; Kinder et al. 2019b; O'Sullivan 1983; Renberg 1981; Ridge and Larsen 1990; Saarnisto 1986; Tylmann et al. 2013). Zolitschka et al. (2015) fournissent une synthèse détaillée des sédiments lacustres varvés. Ceux-ci montrent que les sédiments annuellement laminés sont caractérisés par au moins deux couches saisonnières de couleur, de texture, de structure et de composition différentes qui s'insèrent dans le cycle annuel de dépôt. Le cycle annuel des sédiments varvés peut différer de l'année civile (de janvier à décembre), et être largement dépendante de la localisation géographique du site d'étude et inhérente au profil hydrologique de chaque région. Par exemple, dans les régions boréales telles que la Côte-Nord du Québec, la présence de sédiments laminés est modulée par l'alternance des périodes de fonte nivale (avril-mai) et des précipitations estivales et automnales (juin-octobre).

1.7 Une brève revue des études sur les varves au Québec

L'étude des varves glaciaires au Québec a débuté dans les années 1920 avec les rapports d'Ernst Antevs (Antevs 1922, 1925, 1928, 1931) qui établissait une corrélation entre les enregistrements de varves de plusieurs lacs proglaciaires influencés par le retrait de l'*Inlandis laurentidien* (LIS) (Breckenridge et al. 2012). La figure 1.7 montre l'emplacement des sites de la frontière Québec–Ontario étudiés par Antevs (1925, 1928), puis par Hughes (1959), Paulen (2001) et Breckenridge et al. (2012). À la frontière entre le Québec et l'Ontario, divers enregistrements couvrent une période de plus de 2000 ans et s'étendent du bassin du lac Témiscamingue, au sud, au bassin de la baie d'Hudson au nord (Breckenridge et al. 2012). Le lac glaciaire du bassin du lac Témiscamingue était désigné sous le nom du lac Barlow (Wilson 1918), tandis que le lac glaciaire du bassin de la baie d'Hudson

était désigné sous le nom de lac Ojibway (Coleman 1909). Anteys (1925) a proposé le nom de bassin Barlow-Ojibway pour désigner le lac glaciaire qui recouvrait les deux bassins. Cependant, les varves de tous les segments du lac «Barlow, Barlow-Ojibway et Ojibway» ont été simplement désignées sous le nom du lac Ojibway (Breckenridge et al. 2012). Dans le bassin du lac Ojibway, un enregistrement de la ré-avancée de l’Inlandis laurentidien (LIS), appelée Cochrane, a commencé avant le drainage du lac. La cause principale de la ré-avancée était cependant inconnue (Occhietti et al. 2004).

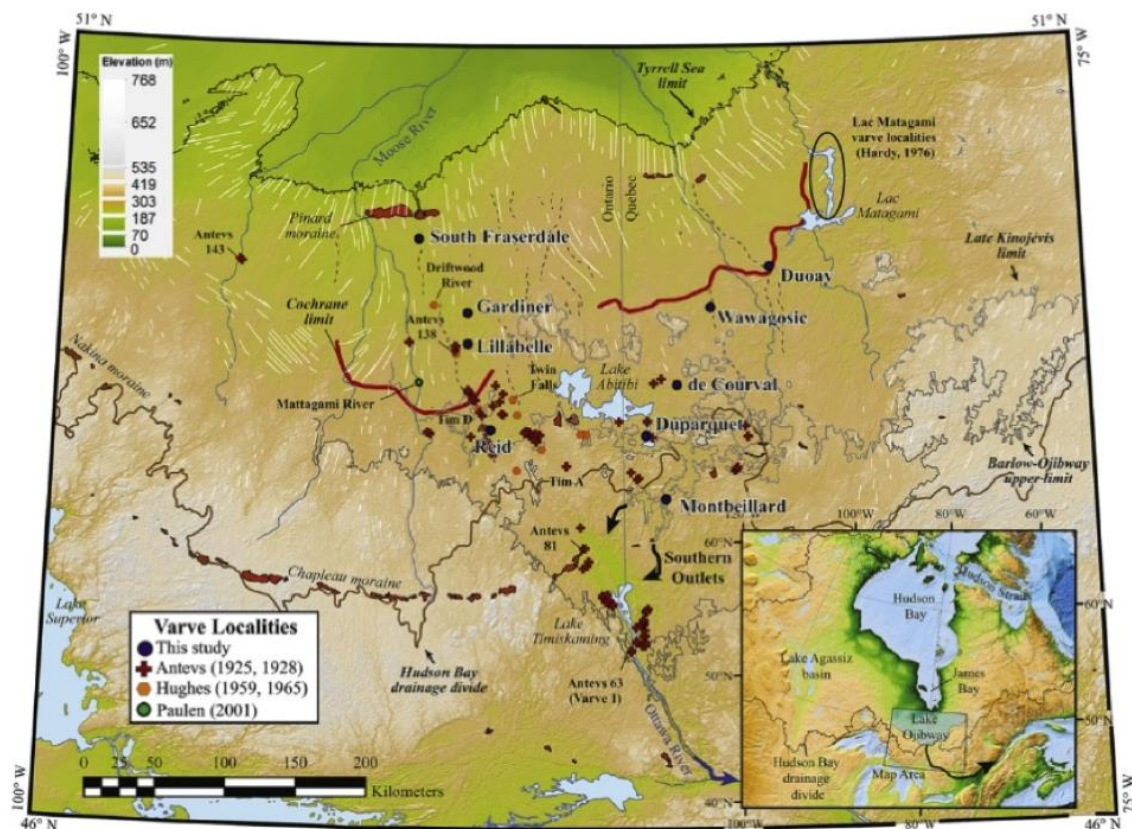


Figure 1.7 : Carte générale montrant les sites de sédiments varves du lac glaciaire Ojibway d'après les études d'Anteys (1925, 1928), Hughes (1959, 1965), Paulen (2001) et Breckenridge et al. 2012 (indiqués comme "cette étude" sur la carte). Les caractéristiques de la carte sont affichées (détailées dans Breckenridge et al. 2012).

Anteys (1925, 1928) a construit un enregistrement varvé de ~2027 ans en mesurant les épaisseurs des varves à l'aide d'un ruban adhésif maintenu directement sur l'affleurement. Il a créé une série de varve appelée «Timiskaming» en comparant l'épaisseur des varves sur différents sites, étiquetés avec une lettre et un chiffre (Breckenridge et al. 2012). Les varves au bas de la série étaient caractérisées par des sédiments à grain grossier liés à la glace proximale et étaient appelées «varves de fond». Les varves du bas ont servi de proxy pour interpréter la position de la marge de glace de LIS (Breckenridge et al. 2012).

Hughes (1959, 1965) a confirmé la détection de la séquence varvée d'Anteys et a également

découvert une nouvelle série de 60 varves d'une épaisseur anormale, appelée séquence de Connaught, plus jeunes que la séquence varvée identifiée par Antevs. Hardy (1977) a découvert 600 varves le long des rives du lac Matagami (Figure 1.7), y compris deux périodes d'épaisseur des varves relativement élevées liées aux avancées de la marge de glace, nommées «Cochrane I» et «Cochrane II» (Breckenridge et al. 2012). Antevs (1928) et Hughes (1959) ont cartographié des varves discontinues dans le till de Cochrane et ont suggéré que le lac Ojibway était partiellement asséché à cette époque. Paulen (2001) a décrit des couches d'argile dans le till de Cochrane dans la séquence des varves glaciaires dans le Nord de l'Ontario. Certains chercheurs ont cartographié les varves glaciaires des basses terres du bassin de la baie d'Hudson (McDonald 1969; Smith 1962), sans toutefois publier d'informations sur leur épaisseur. Breckenridge et al. (2012) ont corrélé le nombre de varves du lac Ojibway (Figure 1.8) et ont pu contraindre l'âge des varves entre 10570 à 8470 (\pm 200) cal BP en fonction des dates du bassin du Lac Supérieur.

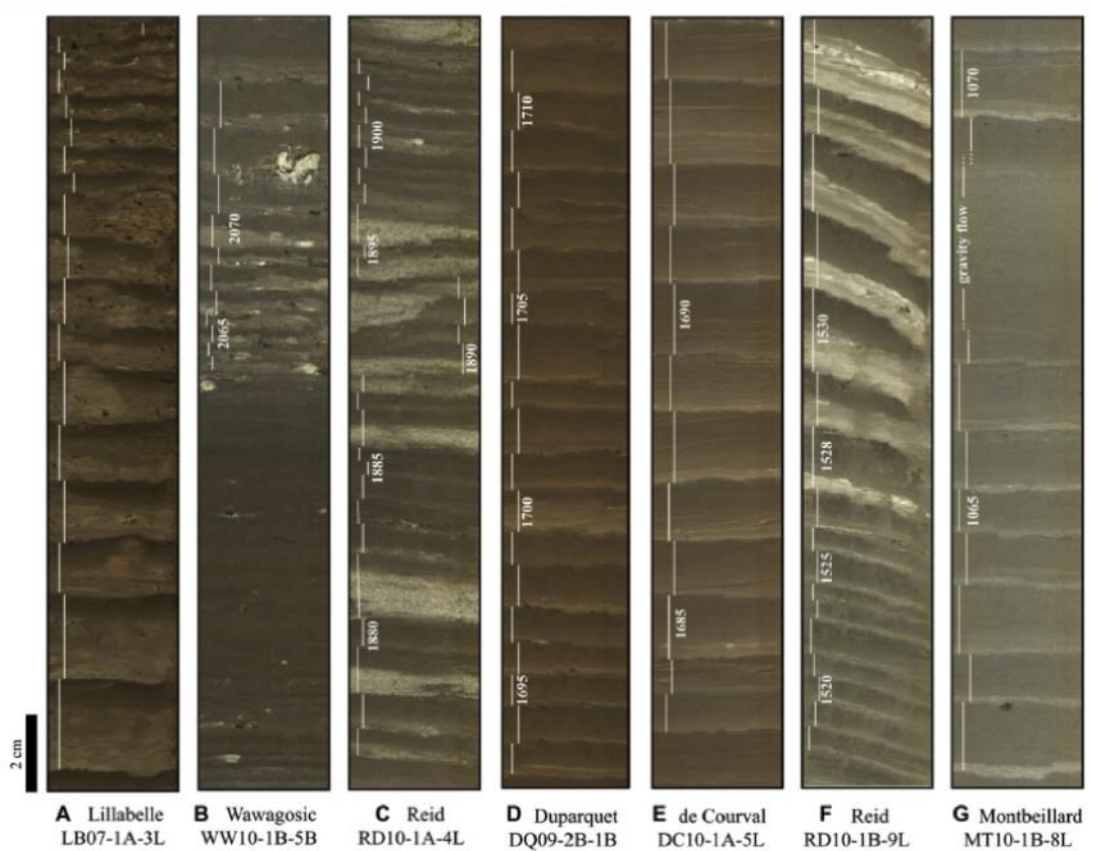


Figure 1.8 : Images sélectionnées de varves du lac Ojibway, Québec-Ontario, basées sur des études de Breckenridge et al. 2012. Les lignes verticales indiquent les couplets de laminae (varves) (tiré de Breckenridge et al. 2012).

Dans la vallée du Saint-Laurent, Besré and Occhietti (1990) ont étudié la stratigraphie et les structures sédimentaires de sédiments glaciolacustres provenant de différents endroits et ont délimité six unités rythmiques et / ou varvées. Ceux-ci comprennent : 1) les rythmites pré-Deschaillons ; 2) les varves de

Deschaillons ; 3) les rythmites de Leclerville (Besré and Occhietti 1988; Occhietti 1989) ; 4) les varves de déglaciation, possiblement l'équivalent des rythmites de Pré-Deschaillons ; 5) les rythmiques plus anciennes que les sédiments de Saint-Pierre ; et 6) les varves de Danville (Parent 1987) et autres argiles laminées (Figure 1.9). L'interprétation de ces unités a été basée sur l'épaisseur des varves et les variations des lames saisonnières.

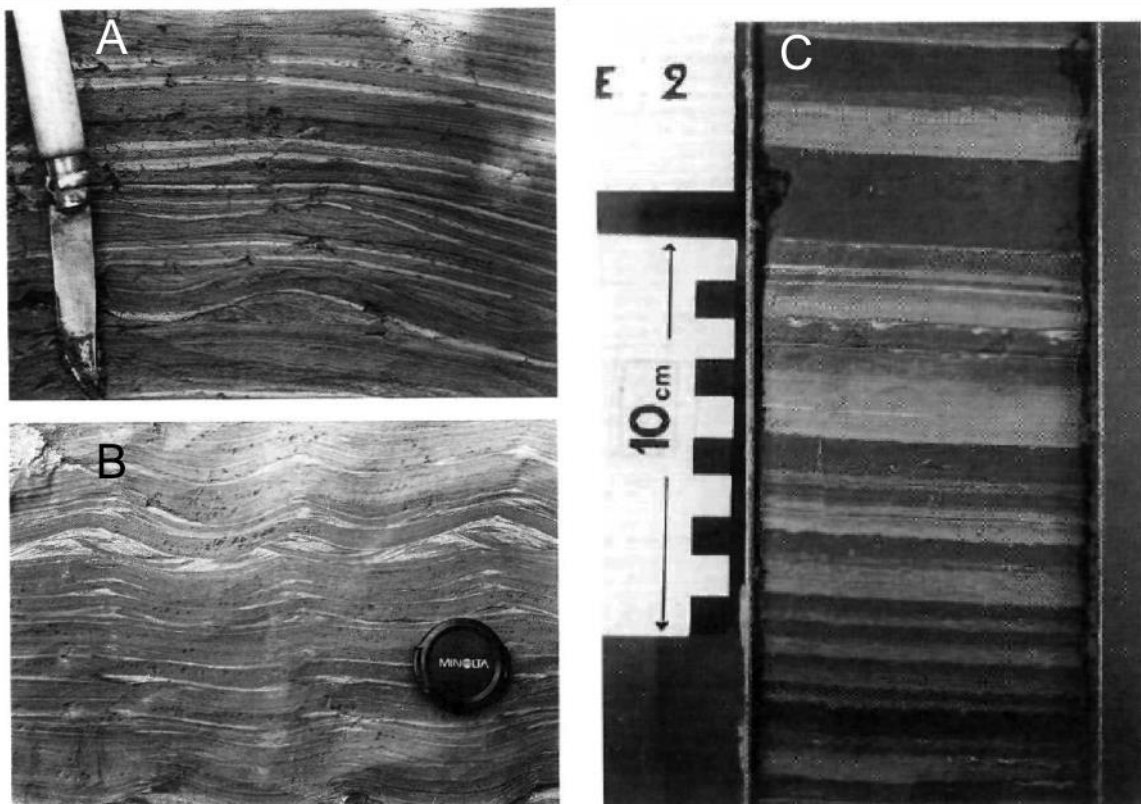


Figure 1.9 : Rides de courant dans les rythmites du Saint-Maurice : A) aux Vieilles-Forges et B) à Sainte-Anne-de-la-Pérade, et C) Les rythmites des Leclercville (tiré de Besré et Occhietti 1990).

Philibert (2012) a décrit les rythmites du lac Jacques-Cartier, dans la Réserve faunique des Laurentides, qui ont été interprétées comme des varves et attribuées à deux origines : 1) des varves clastiques déposées par un apport sédimentaire fluvial; 2) des varves glaciolacustres avec des lames épaisses (cm) et les couches sombres riches en sulfites (Figure 1.10). Ces interprétations étaient basées sur l'analyse de faciès et la stratigraphie acoustique.

Les études sur les varves dans les sédiments non-glaciaires au Québec sont plutôt rares. Les études de reconnaissance de Fortin et al. (2012) ont suscité un intérêt de recherche dans la région de la Côte-Nord (lacs Pentecôte, Walker et Pasteur) dans la région de Québec-Labrador (Grand lac) ainsi que dans certaines parties de l'est du Québec (Lac Yasinki) et dans la région frontalière Québec-Ontario

(Lac d'irrigation) (Figure 1.4). Des modèles d'âge holocène basés sur le comptage des varves existent au Lac Noir, sud du Québec (Neil and Gajewski 2018; Paquette and Gajewski 2013). Des études récentes fournissent des preuves de la présence de varves dans le lac Walker (Nzekwe et al. 2018) et potentiellement à Grand Lake, Labrador qui est actuellement analysé par Gagnon-Poiré et al. (2018).

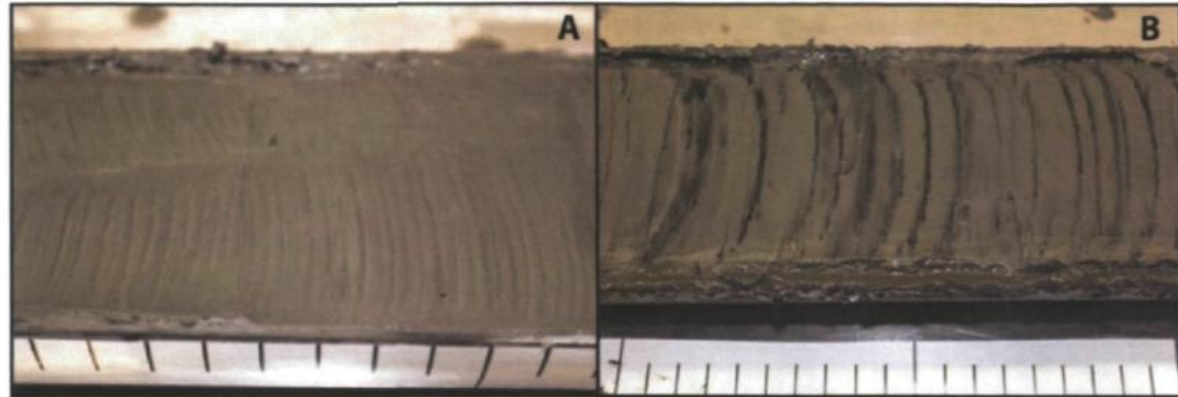


Figure 1.10 : Rythmites décrites dans les réserves fauniques du Lac Jacques-Cartier et des Laurentides, au Québec:
A) sous un régime nival ; B) en tant que varves glaciolacustres (adapté de Philibert 2012).

1.8 Objectifs de la thèse

L'objectif principal de cette thèse de doctorat est de reconstituer les conditions paléoenvironnementales à l'aide de sédiments (annuellement) laminés de trois lacs profonds (lacs Walker, Pentecôte et Pasteur) dans la région de la Côte-Nord du Québec. Les objectifs spécifiques sont les suivants :

- i) Évaluer la présence de sédiments laminés dans ces lacs et indiquer s'ils sont effectivement varvés. Cela implique la description et les preuves du dépôt de lamines au niveau spatial dans les lacs. Évaluer l'état de préservation des sédiments laminés et de leurs caractéristiques saisonnières et / ou annuelles continues ou discontinues, en fonction de leurs propriétés physiques, texturales, géochimiques et microscopiques.
- ii) Établir un modèle de profondeur-âge pour l'Holocène supérieur fondé en premier lieu sur le comptage des laminations à l'aide d'images haute-résolution au microscope électronique à balayage (MEB). Comparer ensuite ces comptages avec les mesures radiométriques (^{210}Pb , ^{137}Cs , ^{14}C) et paléomagnétiques pour fournir un modèle d'âge robuste.
- (iii) Intégrer les propriétés physiques, texturales, géochimiques et microscopiques des sédiments (annuellement) laminés dans l'identification des cycles milléniaux à saisonniers dans les séquences

sédimentaires. Cela implique l'acquisition de données générées par des instruments de haute-résolution. Parmi ceux-ci, l'atténuation des rayons gamma au GEOTEK (MSCL), l'absorption des rayons-X mesurée par tomographie axiale (CT-scan), les analyses géochimiques issues de la microfluorescence par rayons-X (μ -XRF), une analyse détaillée des facies grâce aux lames minces ainsi qu'aux images obtenues par microscopie électronique à balayage (MEB).

iv) Documenter les environnements sédimentaires successifs depuis le dernier maximum glaciaire jusqu'au début de l'Holocène. Cela implique des analyses multi-paramètres incluant la granulométrie, la palynologie, et le paléomagnétisme, ainsi que la modélisation hydraulique (Gagnon-Poiré 2016).

1.9 Hypothèses de recherche

Sur la base des objectifs énumérés ci-dessus, quatre hypothèses principales ont été évaluées dans cette recherche doctorale.

1.9.1 Hypothèse 1

Les trois lacs étudiés (lacs Walker, Pentecôte et Pasteur) sur la Côte-Nord du Québec contiennent des sédiments annuellement laminés.

Cette hypothèse a été formulée à partir d'études de reconnaissance (Fortin et al. 2012) suggérant que les lacs étudiés étaient favorables à la présence de sédiments annuellement laminés, comme indiqué ci-dessus (Figure 1.3). Les conditions préalables jugées favorables étaient les suivantes : 1) les lacs sont relativement profonds ; 2) le climat boréal est marqué par un fort contraste saisonnier et ; 3) les lacs reçoivent un apport de sédiments saisonnier constant provenant des bassins versants de rivières à fort débit (D. Fortin, communication personnelle, 2015). La principale question de recherche pour la présente étude était donc la suivante : ces conditions préalables sont-elles suffisantes pour garantir la formation et la préservation des varves dans ces lacs?

Afin de vérifier cette hypothèse, les carottes extraites lors de mission reconnaissance au lac Walker en 2011 (par David Fortin, Alexandre Normandeau et son équipe) ont été analysées afin de détecter la présence de laminations régulières (Figure 1.11). Dans le cadre d'une étude pilote, des lames minces ont été préparées à partir de l'une des anciennes carottes (WA11-W5-R). Des analyses radiométriques (^{210}Pb et ^{137}Cs) ont été faites sur cette carotte afin d'établir un modèle d'âge pour les sédiments récents. La comparaison du comptage de laminations (à l'aide des lames minces de cette carotte) avec ce modèle âge-profondeur a montré que les sédiments étaient fort probablement annuellement laminés. Ce fait a motivé la poursuite des études sur ce site et donc la planification d'un travail de terrain au printemps 2014, au cours duquel 42 carottes de sédiments courtes ont été collectées le long de transects dans les lacs Pentecôte, Walker et Pasteur. Une carotte de référence a été collectée et analysée dans chaque lac selon le même protocole que la carotte de reconnaissance : analyse de faciès,

analyse par lames minces, datation radiométrique (^{210}Pb et ^{137}Cs) et comparaison avec le modèle âge-profondeur.

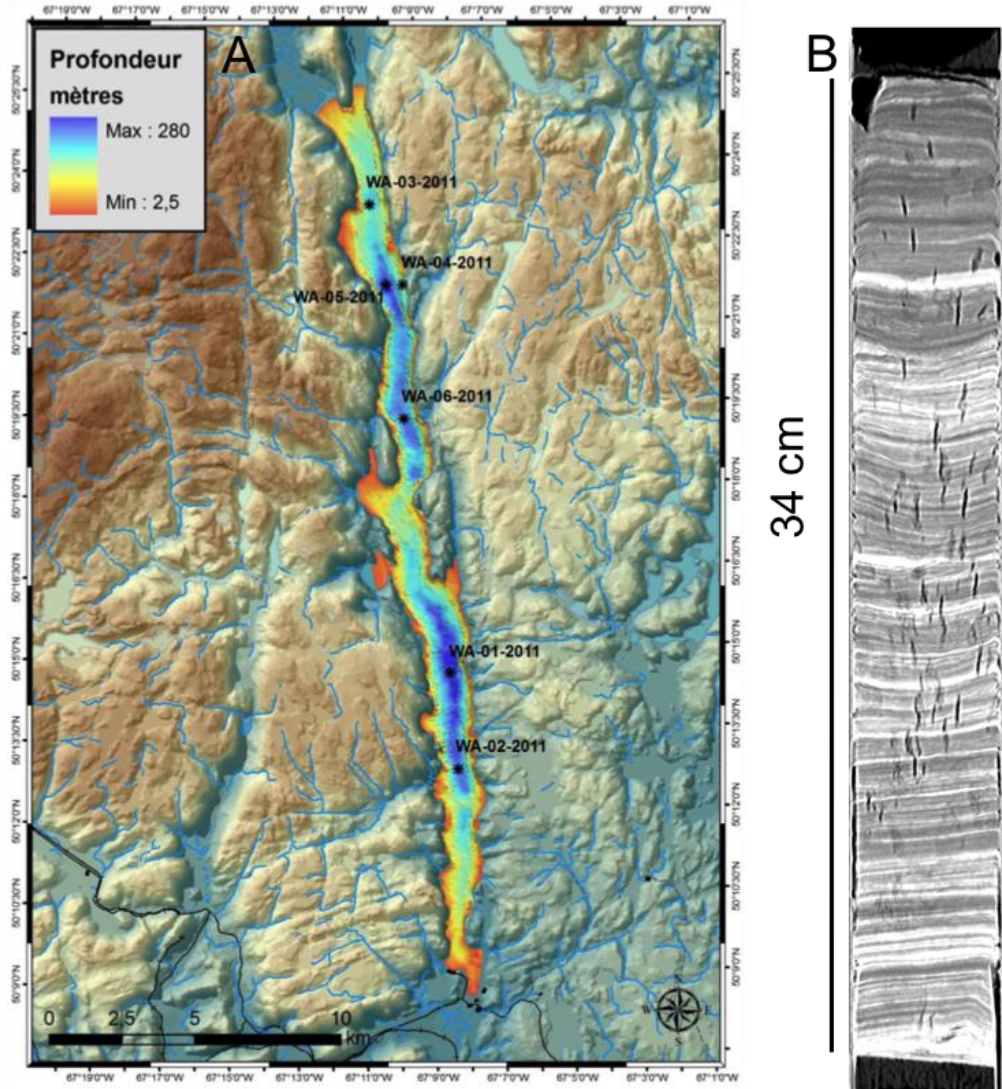


Figure 1.11 : (A) Carte bathymétrique montrant la localisation des carottes sédimentaires extraites du lac Walker lors d'étude de reconnaissance par Fortin et al. (2012). B) Image tomodensitométrique d'un carotte montrant les lamination régulières du sédiments (tiré de Fortin et al. 2012).

Tableau 1.1 : Liste des carottes sédimentaires récupérées du lac Walker lors d'étude de reconnaissance in 2011.

| S/N | Carotte |
|-----|------------|
| 1 | WA-1B-2011 |
| 2 | WA-02-2011 |
| 3 | WA-03-2011 |
| 4 | WA-04-2011 |
| 5 | WA-05-2011 |
| 6 | WA-06-2011 |

De plus, plusieurs formules empiriques rapportant un lien potentiel entre la préservation des lamination sédimentaires et la morphométrie de petits lacs ($<3 \text{ km}^2$) ont été testées afin de déterminer si elles sont applicables aux grands lacs tels que les lacs Pentecôte, Walker et Pasteur. Les paramètres morphométriques qui sont pris en compte sont les suivants : profondeur relative (Hutchinson 1957); limite critique (Larsen et MacDonald 1993) ; limite critique maximale (Larsen et al. 1998) ; fetch moyen, fetch maximum et exposition topographique (Tylmann et al. 2013). En outre, les variations de température dans le bassin du lac Walker ont été surveillées sur une période de deux ans afin d'évaluer le modèle de stratification thermique dans le lac (voir le chapitre 2).

Des plus, le modèle de distribution des sédiments laminés a été comparé à la bathymétrie dans les lacs étudiés. Par exemple, la figure 1.12 montre une évaluation simplifiée de cette hypothèse basée sur des études comparatives de la distribution des sédiments laminés dans le lac Suminko (Tylmann et al. 2012). Tel qu'illustré, les couches de stratification thermique dans le bassin du lac Suminko correspondent à la distribution suivante des sédiments : les sédiments laminés caractérisent le monimolimnion ; des sédiments homogènes et / ou laminés caractérisent la chimiocline et des sédiments homogènes marquent le mixolimnion (Zolitschka et al. 2015). De même, un test a été effectué pour confirmer si une telle tendance existait dans les lacs Pentecôte, Walker et Pasteur. Une description détaillée de la méthodologie et des résultats des lacs étudiés (lacs Walker, Pentecôte et Pasteur) est décrite au chapitre 2. Dans cette recherche, la définition de varves de Zolitschka et al. (2015) a été utilisée.

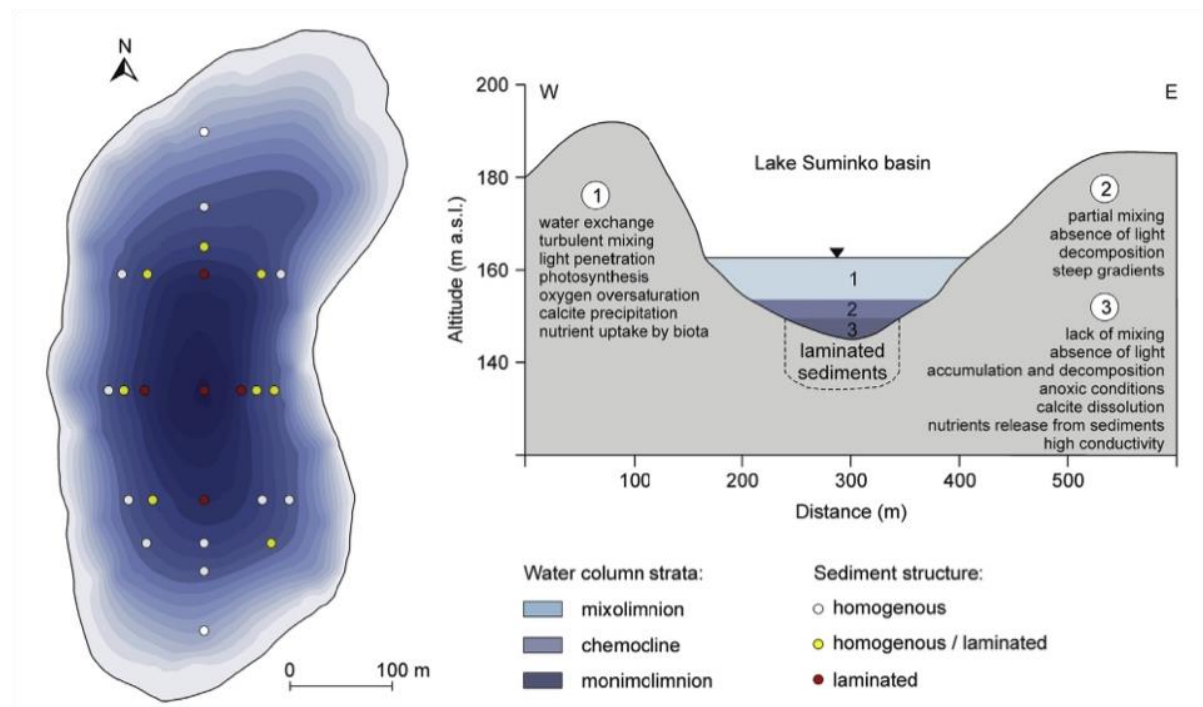


Figure 1.12 : Illustration de l'étendue latérale et des conditions générales de la distribution des sédiments varvés dans le lac Suminko (Tylmann et al. 2012). La stratification du lac est décrite comme suit : (1) mixolimnion, 2) chimiocline, 3) monimolimnion (adapté de Zolitschka et al. 2015).

1.9.2 Hypothèse 2

Les laminations annuelles trouvées dans ces lacs contiennent un enregistrement climatique dépassant le dernier millénaire.

Cette hypothèse a été formulée en partant de l'hypothèse que si l'un des trois lacs étudiés est réellement varvé, il est susceptible de contenir un enregistrement paléoenvironnemental des derniers millénaires (c'est-à-dire +1000 dernières années). Les résultats de la première hypothèse (chapitre 2) indiquent que seul le lac Walker contient des sédiments varvés récents (déposés au cours des 150 dernières années), en raison de caractéristiques morphologiques plus favorables (profondeur relative plus élevée, profondeur moyenne, profondeur maximale et exposition topographique). Par conséquent, la deuxième hypothèse a fait l'objet d'analyses plus poussées sur les sédiments du lac Walker.

Les principales questions de recherche étaient les suivantes : 1) les sédiments de l'Holocène supérieur sont-ils varvés? 2) Quelles méthodes seraient efficaces pour établir une chronologie de varves, et 3) comment l'épaisseur de varves varie-t-elle avec la profondeur? Pour répondre à ces questions, une séquence composite d'environ 4 m de long a été analysée à l'aide des images tomodensitométriques et de photographies haute résolution, ce qui a permis de localiser et sélectionner un intervalle avec des laminations continues. Afin de construire une chronologie varvée, deux méthodes indépendantes ont été comparées : le comptage manuel multiparamétrique à l'aide du logiciel PeakCounter et le comptage manuel sur des images en lames minces.

La première méthode (Figure 1.13) s'est révélée efficace sur les sédiments laminés du lac Suigetsu au Japon (Marshall et al. 2012). Cette méthodologie impliquait de comparer les variations élémentaires obtenues par μ -XRF (par exemple, Si, Fe, Mn) aux côtés des radiographies aux rayons-X (avec les valeurs d'échelle de gris) ainsi qu'aux images numériques. Dans le lac Suigetsu, les données μ -XRF et de radiographies ont été acquises à une résolution de 60 μm , avec un temps d'exposition de 4 s pour les mesures XRF. Ces paramètres ont été utilisés pour compter les sédiments laminés avec une épaisseur de varve moyenne entre 0,8–1 mm (Marshall et al. 2012) (Figure 1.13). Nous allons donc tester cette méthodologie sur un intervalle de 4 m de long du lac Walker en utilisant différents paramètres instrumentaux. Plus de détails sont fournis au chapitre 3 (voir les méthodes, résultats et discussion).

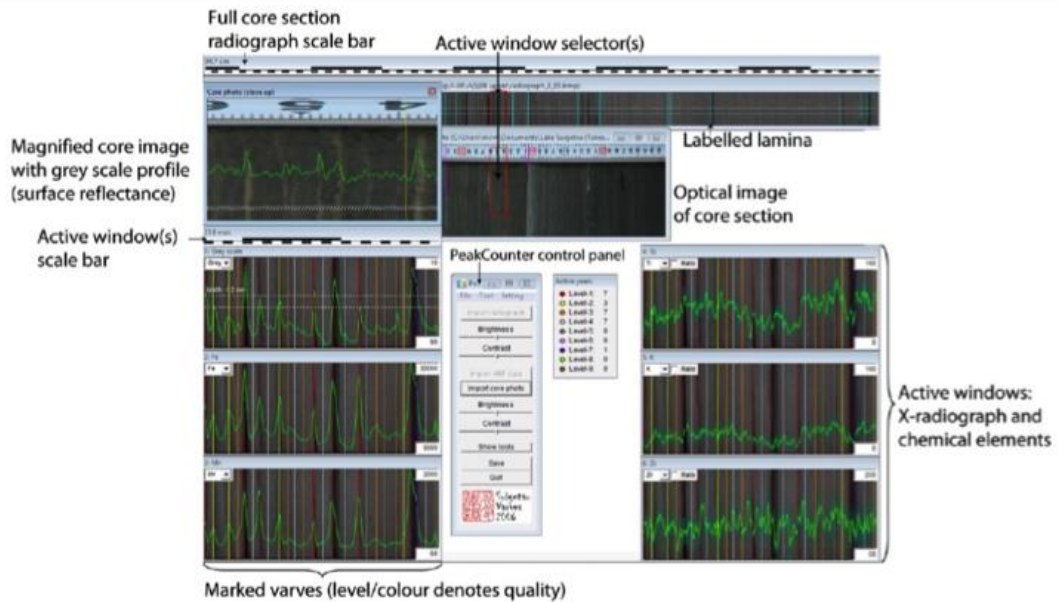


Figure 1.13 : Capture d'écran illustrant une approche multi-paramètres avec le logiciel PeakCounter pour le comptage des lamines / varves sur les sédiments du lac Suigetsu au Japon. Épaisseur moyenne de couche: 0,8 - 1 mm, résolution minimale: 60 µm (adapté de Marshall et al. 2012).

En ce qui concerne la deuxième méthode, cela a été utilisé avec succès sur deux lacs de la région arctique canadienne, à savoir, East Lake Cape Bounty et South Sawtooth Lake (Lapointe et al. 2012; Lapointe et al. 2019). Ces études ont montré que seule l'analyse des lames minces réalisée au MEB était appropriée pour établir une chronologie robuste. La méthodologie implique la fabrication des lames minces fabriquées à partir de sédiments imprégnés dans la résine époxy, leur numérisation à haute-résolution (2400 dpi) pour pouvoir réaliser un comptage. Des images au microscope électronique à balayage (MEB) ont ensuite été acquises à l'aide d'un logiciel développé à l'INRS-ETE (Francus et Norbert 2007). Une estimation d'erreur a été calculée sur la base de la différence du nombre de varves comptées par deux chercheurs ou plus.

Il a été noté que dans la plupart des lacs varvés l'épaisseur des varves diminue avec l'augmentation de la profondeur (Zolitschka et al. 2015), par exemple dans le lac Szurpily (Kinder et al. 2013) (Figure 1.14). Dans ce lac, les varves sont organo-clastiques (Kinder et al. 2013) et la diminution notable de l'épaisseur des varves avec l'augmentation en profondeur dans le lac Szurpily est attribuée aux changements dans les taux d'accumulation de sédiments pendant l'Holocène et, dans une moindre mesure, à la compaction due à la pression lithostatique (Zolitschka et al. 2015). Ces hypothèses seront testées pour vérifier leur validité pour le lac Walker (les détails sont fournis au chapitre 3).

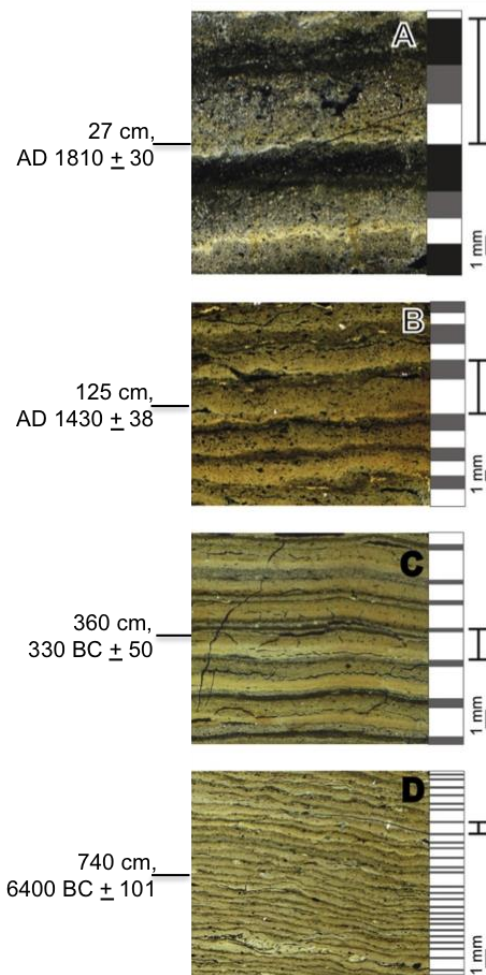


Figure 1.14 : Structure des sédiments varvés dans le lac Szurpily, en Pologne (modifié de Kinder et al. 2013). La composition de varve est similaire à toutes les profondeurs dans le lac, respectivement. Des barres grises et blanches délimitent les couples de varve. Les profondeurs centrales et l'âge des images sont marqués. La diminution notable de la variabilité avec l'augmentation de la profondeur des taux d'accumulation de sédiments au cours de l'Holocène et, dans une moindre mesure, en raison du compactage (adapté Zolitschka et al. 2015).

1.9.3 Hypothèse 3

Les lacs étudiés contiennent un enregistrement sédimentaire de la déglaciation qui peut aider à améliorer la compréhension des processus géologiques et géomorphologiques et préciser la chronologie de cette transition climatique majeure.

Cette hypothèse a été formulée à partir de relevés de terrain montrant que les lacs étudiés possèdent des bassins profonds ressemblants à des fjords en bordure de la limite sud de la Côte-Nord du Québec. Ils pourraient donc contenir des sédiments préservés lors de la dernière déglaciation (Lajeunesse 2014). Les données sismiques recueillies par le Laboratoire de géomorphologie marine (Université Laval, Québec) à l'aide d'un profileur fonctionnant à une fréquence de 3,5 kHz appuient cette hypothèse (Lajeunesse 2014). La figure 1.15 présente un profil sismique illustrant une topographie de

vallée à l'intérieur d'une vallée, avec des bancs rocheux supérieurs et un profil inférieur en V dans le lac Walker. Lajeunesse (2014) a suggéré que cette dernière était plus ancienne que la dernière déglaciation. Celle-ci aurait probablement été créée par un système de drainage fluvial préglaciaire incisé à un niveau de base inférieur. De telles vallées en forme de V existaient sous l'Inlandis laurentidien, celles-ci pouvant ainsi contenir des sédiments interglaciaires préservés pendant plusieurs glaciations.

Les résultats de la recherche de Lajeunesse (2014) sont corroborés par des données bathymétriques recueillies en 2014 qui révélaient des vallées en forme de V similaires dans les bassins des lacs Pentecôte, Walker et Pasteur (Gagnon-Poiré 2016; Gagnon-Poiré et al. 2019) (Figure 1.16). Sur la base de cette dernière étude, quatre unités sismostratigraphiques ont été identifiées dans les bassins lacustres : sous-acoustique, transport de sédiments par la glace; limons et argiles laminées, et sédiments paraglaciaires et postglaciaires. Les datations radiocarbonées montrent une transition de la sédimentation glaciaire à une sédimentation paraglaciaire / postglaciaire entre 8000-8160 cal BP et 7845 à 7950 cal BP dans les bassins versants des lacs Pentecôte et Walker (Gagnon-Poiré et al. 2019). Cependant, aucune étude n'a fait l'objet d'une interprétation sédimentologique détaillée de la transition glaciaire à postglaciaire. Par conséquent, il y a un intérêt particulier pour les questions suivantes : (1) comment peut-on fournir une preuve sédimentologique claire de la transition glaciaire à paraglaciaire / postglaciaire dans les lacs étudiés? (2) la transition a-t-elle été abrupte ou progressive?

Afin de répondre à la question ci-dessus, une analyse multi-paramètres de carottes longues extraites des lacs Pentecôte et Walker a été réalisée afin de décrire la lithostratigraphie et les faciès sédimentaires. La méthodologie utilisée comprend la granulométrie, la palynologie et le paléomagnétisme (de Vernal et al. 2010; St-Onge et al. 2007; Stoner et St-Onge 2007). Plus de détails sont fournis au chapitre 4.

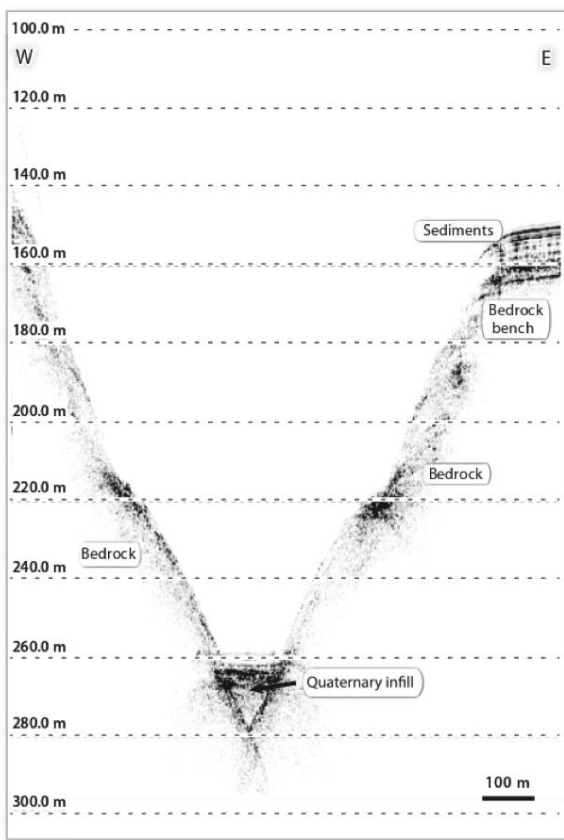


Figure 1.15 : Données de sismo-stratigraphie montrant une topographie de vallée à l'intérieur d'une vallée avec des bancs rocheux supérieurs et un profil en forme de V inférieur au lac Walker. Cela prouve que la vallée transversale en forme de V est plus ancienne que la dernière déglaciation (adapté de Lajeunesse 2014).

1.9.4 Hypothèse 4

Ces bassins profonds en forme de fjords étaient propices à l'apparition de lacs sous-glaciaires.

Cette hypothèse a été formulée sur la base de l'hypothèse de Lajeunesse (2014), selon laquelle les vallées en forme de V du lac Walker (et de certains lacs glaciaires proches de l'estuaire du Saint-Laurent, par exemple le lac Témiscouata) pourraient être le résultat de l'érosion sous-glaciaire des eaux de fonte. Cependant, l'idée a été rejetée sur la base 1) de l'uniformité des morphologies (davantage imputable à l'érosion préglaciaire), et 2) du modèle inhabituel d'érosion sous-glaciaire (Lajeunesse 2014). L'hypothèse a été réexaminée dans l'étude de Gagnon-Poiré (2016) et Gagnon-Poiré et al. (2019), ceux-ci n'ont pas confirmé cette hypothèse en raison de l'absence de preuves sédimentologiques à l'appui et faute de datation robuste. Cependant, l'hypothèse a été réévaluée dans ce projet doctoral à partir des résultats d'analyses multi-paramètres obtenus et des datations au radiocarbone (20 à 4 ka cal BP) des carottes longues recueillies dans les lacs Pentecôte et Walker (Chapitre 4). La méthodologie dans le chapitre 4 inclus : 1) une révision des étapes d'avancée et de recul du LIS sur la Côte-Nord du Québec (Syvitski 1991) (Figure 1.17) ; 2) la modélisation glaciologique selon la méthode de (Tarasov et al. 2012) (Figure 1.18) ; 3) des modèles conceptuels

pour la formation de lacs sous-glaciaires (Gagnon-Poiré 2016; Syvitski and Praeg 1989; Willis et al. 2015) (par exemple Figure 1.19) et modèles régionaux paléoenvironnementaux dans la zone d'étude (Casse et al. 2017; Dietrich et al. 2016; Gagnon-Poiré et al. 2019; Occhietti et al. 2011). La méthodologie détaillée et les résultats sont fournis dans le troisième article (Chapitre 4).

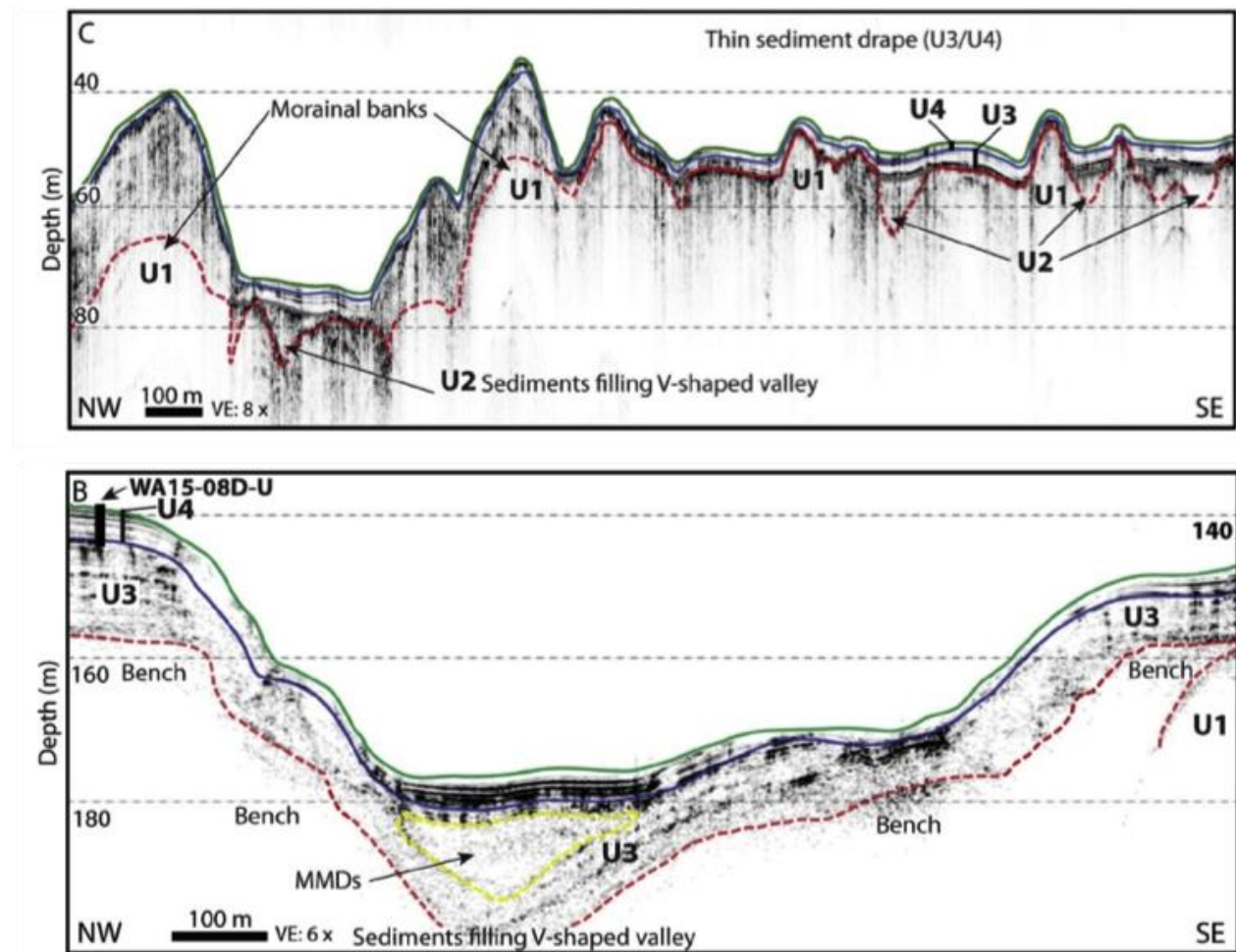


Figure 1.16 : Profils acoustiques de sous-surface dans (A) Lake Pentecôte et (B) Lake Walker montrant un mince drap sédimentaire (U3 : sédiments laminés rythmiquement et U4 : sédiments paraglaciaires et postglaciaires) sur la morphologie ondulante reposant sur le socle acoustique U1 (Gagnon-Poiré et al. 2019). La vallée en forme de V est remplie de sédiments supposés s'être déposés avant les dernières glaciations (tirés de Gagnon-Poiré et al. 2019).

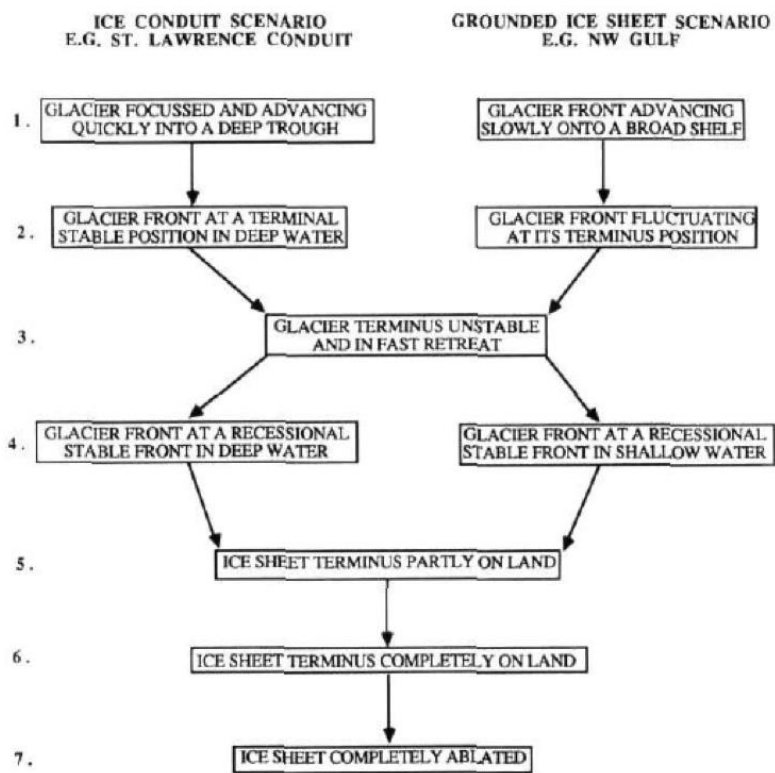


Figure 1.17 : Les sept étapes d'une avance sur glace et d'une retraite qui affectera ou contribueront à la sédimentation sur un plateau continental (Syvitski et Praeg 1989).

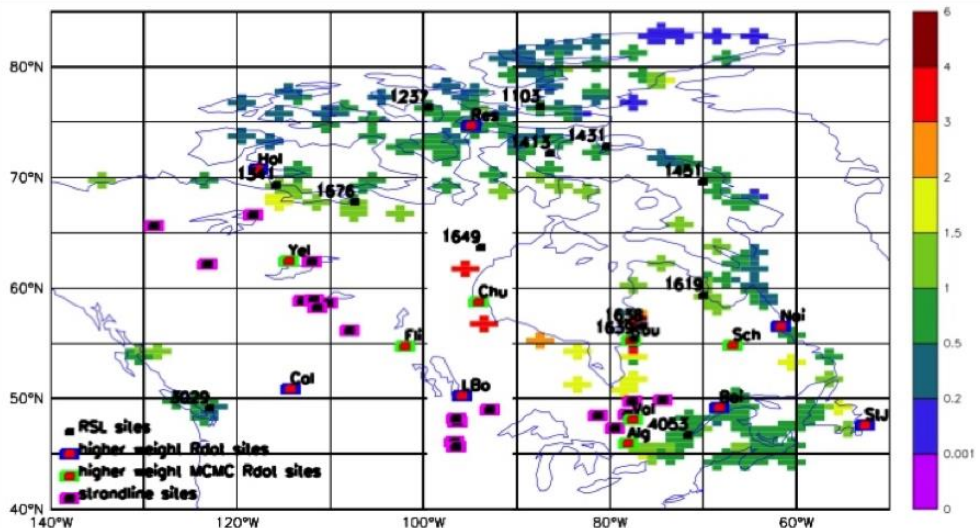


Figure 1.18 : Sélection des données d'étalonnage pour la modélisation glaciologique (tiré de Tarasov et al. 2012). Les données de cette étude ont été utilisées pour la modélisation hydraulique des lacs étudiés sur la Côte-Nord du Québec par Gagnon-Poiré et al. (2016).

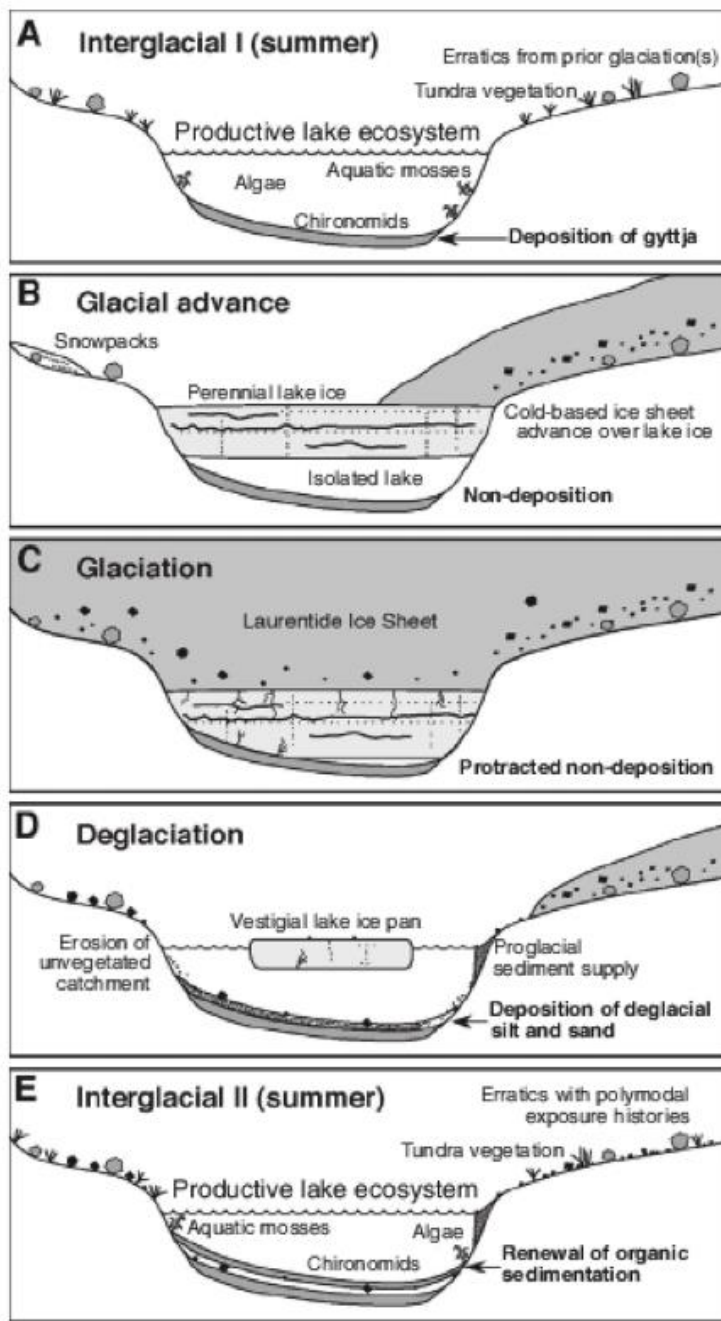


Figure 1.19 : Modèle conceptuel de sédimentation dans le lac CF8 (l'île de Baffin, Canada) au cours du cycle glaciaire complet, montrant la formation et la préservation des unités interglaciaires, le hiatus de sédimentation pendant les intervalles glaciaires et les sédiments minéraux sédimentaires glaciaires (tiré de Briner et al. 2007).

1.10 Cadre régional

1.10.1 Zone d'étude

Les lacs étudiés (les lacs Pentecôte, Walker et Pasteur) sont situés dans la région de la Côte-Nord au Québec, dans l'est du Canada. Ces lacs pittoresques sont situés dans la réserve faunique de Port-Cartier – Sept-Îles (Figure 1.20). Les activités humaines telles que le dragage et l'extraction de sable ne les ont guère perturbés, à l'exception de la pêche et de la navigation de plaisance (Nzekwe et al. 2018).

La région de la Côte Nord compte environ 95 000 habitants ; la majorité vit dans des habitations linéaires situées le long des principaux axes de transport ou près du littoral (Tourisme Québec 2016). L'accès à la région est possible via la route 138 du Québec, qui longe les rives du fleuve Saint-Laurent. Par exemple, à partir de Ville de Québec, on passerait vers le nord-est, traversant les villes de Forestville, Baie-Comeau et Port-Cartier, en direction de Sept-Îles (Figure 1.21). Pour arriver à l'un des lacs étudiés, il faut passer de la route 138 sur des routes non goudronnées.

Les travaux sur le terrain ont été effectués cinq fois pour ce projet doctoral : en été 2014 (pour obtenir des carottes de sédiments courtes), en automne 2014 (pour des mesures hydrogéochimiques), en hiver 2015 (pour obtenir des carottes longues de sédiments), en été 2016 et en automne 2016 (pour récupérer les pièges à sédiments) (voir un aperçu en Annexe I, Figure S1). Des informations additionnelles sur les travaux de terrain, la liste des carottes sédimentaires et les autres données se trouvent à la section 1.13 et aux chapitres 2 à 4).

Les données climatiques pour la zone d'étude sont disponibles auprès de stations météorologiques isolées, la plus proche étant l'aéroport de Sept-Îles, situé à environ 60 km à l'est du lac Walker. La région de la Côte-Nord a un climat subarctique caractérisé par deux saisons principales, soit l'hiver et l'été, tandis que le printemps et l'automne se caractérisent par de courtes périodes ne durant généralement que quelques semaines. L'hiver, froid et neigeux, débute à la fin octobre et se termine à la fin avril. À Sept-Îles, la température moyenne variait de -9,8 à -20,9 °C en janvier et de 19,5 à 10,8 °C en juillet (1981-2010; Environnement Canada).

1.10.2 Géomorphologie et géologie

Les profondeurs maximales des lacs Pentecôte, Walker et Pasteur sont de 130, 271 et 70 m (Nzekwe et al. 2018) avec une altitude maximale de 84, 115 et 86 m, respectivement (Gagnon-Poiré et al. 2019). Ces lacs se situent sous la limite marine (130 m dans la région de la Côte-Nord du Québec) de la dernière déglaciation, ils ont donc été submergés lors de la transgression de la mer de Goldthwait associée à la dépression glacio-isostatique (Gagnon-Poiré et al. 2019). De par leur superficie, les lacs Pentecôte ($18,9 \text{ km}^2$), Walker (41 km^2) et Pasteur ($19,3 \text{ km}^2$) (Gagnon-Poiré et al. 2019) sont plus

grands que la plupart des petits lacs ($> 3 \text{ km}^2$) qui ont servi à des études limnologiques (Larsen and MacDonald 1993; Nzekwe et al. 2018). Une étude détaillée de la relation entre la morphométrie et les caractéristiques limnologiques de ces lacs est présentée au chapitre 2 (Nzekwe et al. 2018).

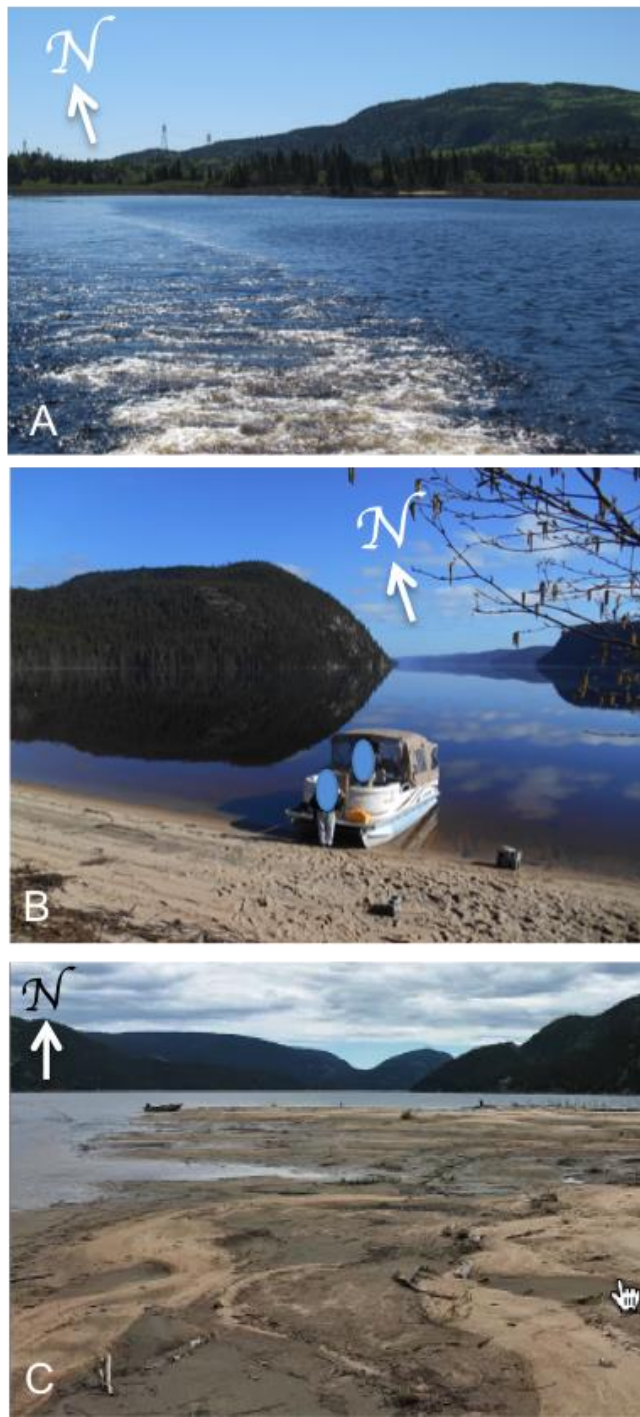


Figure 1.20 : Vues panoramiques des lacs étudiés: (A) Lac Pentecôte, (B) Lac Walker et (C) Lac Pasteur, qui illustrent une série de longues vallées glaciaires orientées nord-sud ($> 60 \text{ km}$).

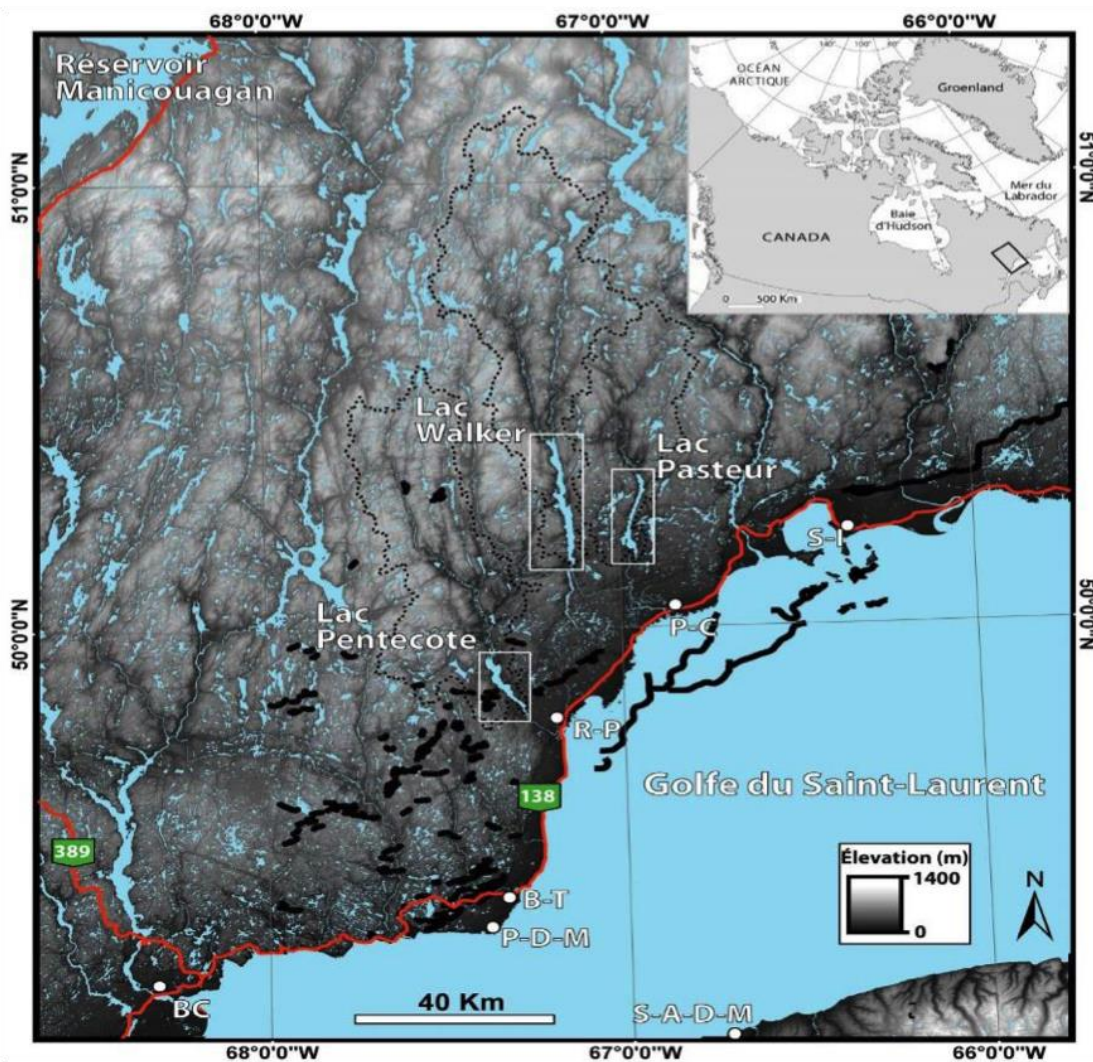


Figure 1.21 : Localisation des lacs Pentecôte, Walker et Pasteur et leur bassin versant (ligne noir pointillée) sur la Côte-Nord, Québec (Est du Québec). B-C: Baie-Comeau; P-D-M: Pointe-Des-Monts; B-T: Baie-Trinité; R-P: Rivière-Pentecôte; P-C: Port-Cartier; S-I : Sept-Îles (tiré de Gagnon-Poiré 2016).

Morphologiquement, le lac Pentecôte comprend trois bassins situés au nord, au centre et au sud (Gagnon-Poiré et al. 2019). Le lac Walker a deux bassins principaux dans les parties nord et sud, tandis que le lac Pasteur possède un bassin relativement profond dans la partie nord (Gagnon-Poiré et al. 2019; Nzekwe et al. 2018). Les caractéristiques géomorphologiques détaillées des lacs ont été décrites par Normandea et al. (2016) et Gagnon-Poiré et al. (2019).

La région de la Côte-Nord du Québec est située dans la province de Grenville, au nord de l'estuaire du Saint-Laurent (Figure 1.22). La géologie du substratum rocheux est constituée de roches précambriennes d'âge archéen ou protérozoïque. Les roches archéennes comprennent principalement de la migmatite et du gneiss, tandis que les roches protérozoïques comprennent des roches mafiques à ultramafiques ainsi que des roches sédimentaires (paragneiss, quartzite) (Ministère des ressources naturelles du Québec 2002).



Figure 1.22 : Carte géologique du Québec (tire de Ministère des Ressources naturelles et de la Faune du Québec 1997).

1.11 Déglaciation du Québec

1.11.1 La déglaciation au Québec du Wisconsinien supérieur à l'Holocène

La glaciation Wisconsinienne peut être divisée en trois épisodes : le début, l'interglaciaire et le fin du Wisconsinien (Occhietti et al. 2011). Ces épisodes ont été corrélés aux stades isotopiques marins (MIS) 2, 3, 4 et 5 (a à d) par Fulton (1984). Johnsen et al. (2001) ont associé les phases MIS aux changements de température pendant la glaciation du Wisconsinien à l'aide des carottes de glace GRIP $\delta^{18}\text{O}$ de Summit, au Groenland (Figure 1.23A). Des carottes de glace issues du projet Groenland Ice Sheet Project (GISP) ont aussi été utilisées pour reconstituer les changements climatiques intervenus depuis la dernière glaciation sur la base de rapports $^{18}\text{O}/^{16}\text{O}$ mesurés dans la glace (Johnsen et al. 2001; Stuiver et al. 1995) (Figure 1.23B-C).

L'histoire glaciaire de la glaciation wisconsinienne au Québec comprend trois zones principales : 1) le couloir Saint-Laurent (y compris la vallée, l'estuaire et le golfe du Saint-Laurent), 2) la région des Appalaches et 3) le Bouclier canadien (y compris la Côte-Nord de Québec) (Occhietti et al. 2011). Pendant la glaciation du Wisconsinien, la masse continentale du Québec était en grande partie recouverte par l'Inlandsis laurentidien (LIS) (Occhietti et al. 2011). Le LIS existait principalement comme dôme de glace central à l'Est du Bouclier canadien. Après le dernier maximum glaciaire (LGM), le LIS a commencé à se fragmenter le long de ses marges glaciaires par des processus tels que l'ablation et le retrait mécanique (Occhietti et al. 2011).

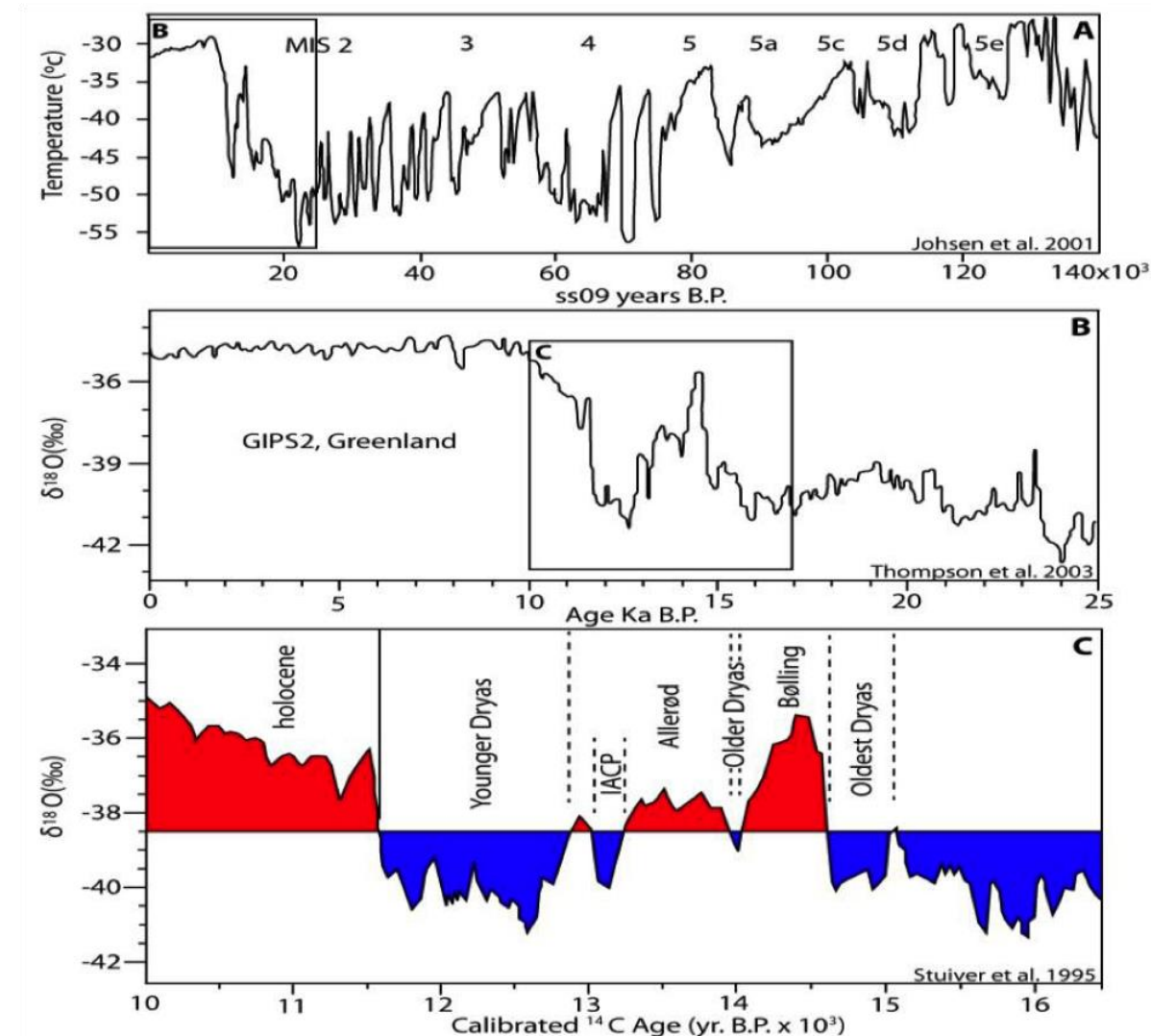


Figure 1.23 : (A) Le modèle de changements des températures pendant la glaciation Wisconsinne extraite de la carotte GRIP $\delta^{18}\text{O}$ du Groenland (Johnsen et al. 2001), (B) la courbe $\delta^{18}\text{O}$ des derniers 25,000 ans (Thompson et al. 2003); et (C) les changements climatiques majeurs extraite de la carotte GISP2 du Groenland par $\delta^{18}\text{O}$ (Stuiver et al. 1995) (Graphique tiré de Gagnon-Poiré 2016).

1.11.2 Déglaciation de la Côte-Nord du Québec

Plusieurs chercheurs ont étudié la déglaciation du golfe du Saint-Laurent, y compris la Côte-Nord du Québec et les régions adjacentes à l'océan Atlantique (Hughes 1998; Josenhans and Lehman 1999; Josenhans 2001; Lajeunesse et al. 2019; Occhietti et al. 2011; Shaw et al. 2002; Shaw et al. 2006; St-Onge et al. 2011; Syvitski and Praeg 1989). La déglaciation du golfe du Saint-Laurent peut être divisée en deux phases principales : 1) la phase précoce, antérieure à environ 14,8 ka BP, au cours de laquelle le retrait des glaces est principalement influencé par le vêlage; et 2) la phase tardive, soit le retrait de la glace au niveau terrestre (Shaw et al. 2006). La figure 1.24 présente une illustration graphique du retrait du LIS dans la région par Shaw et al. (2006).

Au dernier maximum glaciaire (LGM; ~ 21 ka BP), l’Inlandsis laurentidien a atteint son étendue maximale près du plateau continental (Figure 1.24A) et avait la forme d'un grand dôme divisé en deux sous-dômes. À 20 ka BP (~ 23,5 ka cal BP) (Figure 1.24B), toujours au niveau de la Côte-Nord du Québec, la glace, soudée au substrat du fleuve, s'est transformée en une plate-forme de glace. À 18 ka BP (~ 23,5 ka cal BP) (Figure 1.24C), les marges de glace se sont retirées lentement sur le plateau continental. L'élévation de la glace dans les régions intérieures a diminué en raison de l'apport progressif de glace de vêlage vers l'estuaire du Saint-Laurent et dans l'océan. À 16 ka BP (~ 19 ka cal BP), le retrait de la glace restante était encore relativement lent (Figure 1.24D). À 14 ka BP (~ 16,8 ka cal BP), la banquise s'est retirée à un rythme relativement rapide alors que la marge de glace était en grande partie sur la terre ferme (Figure 1.24E). Le plateau continental est devenu une zone d'eau de marée proche des côtes modernes, mais le niveau marin relatif était plus élevé que l'époque moderne. Les glaces se retirant sur la terre ferme se sont enracinées dans des zones d'eaux peu profondes, accompagnées du dépôt de moraines. (Piper and Macdonald 2001) ont noté que de la glace était présente à l'entrée du chenal Laurentien. L'eau libre a commencé à occuper le chenal entre la Gaspésie et l'île d'Anticosti (Rodrigues 1992). L'étendue marine dans le golfe du Saint-Laurent, appelée la mer de Goldthwait par Elson (1969), a commencé à s'infiltrer dans la vallée du Saint-Laurent, immergeant notamment une partie de la ville de Québec (Hetu 1998). À peu près 12 ka BP (~ 14 ka cal BP), l’Inlandis laurentidien étant essentiellement terrestre, le recul de l’Inlandis laurentidien était davantage influencé par les facteurs climatiques et moins affecté par le vêlage de glace (Figure 1.24F). Plus d'informations sont fournies par Shaw et al. (2006).

Selon Occhietti et al. (2011), l'histoire de la déglaciation au Québec après 16 ka cal BP est composée de trois étapes : (1) le courant glaciaire et ses effets (16,0 à 13,0 ka cal BP), (2) le Dryas Récent (YD) (12,9 à 11,7 ka cal BP). Le YD représente une phase froide qui se retrouve dans tout l'Hémisphère Nord (Occhietti 1980; Occhietti et al. 2011). Au Québec, la moraine de Saint-Narcisse (datée du 12,8 au 12,2 ka cal BP), qui correspond au premier épisode froid du YD, est une caractéristique distincte corrélée au YD. Elle constitue également une phase d'ancre de LIS (Occhietti et al. 2011). (3) La

déglaciation de l'Holocène inférieur (Occhietti et al. 2011; Stuiver et al. 1995). La masse de glace recouvrant l'est du Québec, au nord du corridor Saint-Laurent, s'est lentement dispersée entre 13 et 6 ka cal BP. Les traces résiduelles de glace ont finalement disparu vers 6,0 ka cal BP (Occhietti et al. 2011) (Figure 1.25).

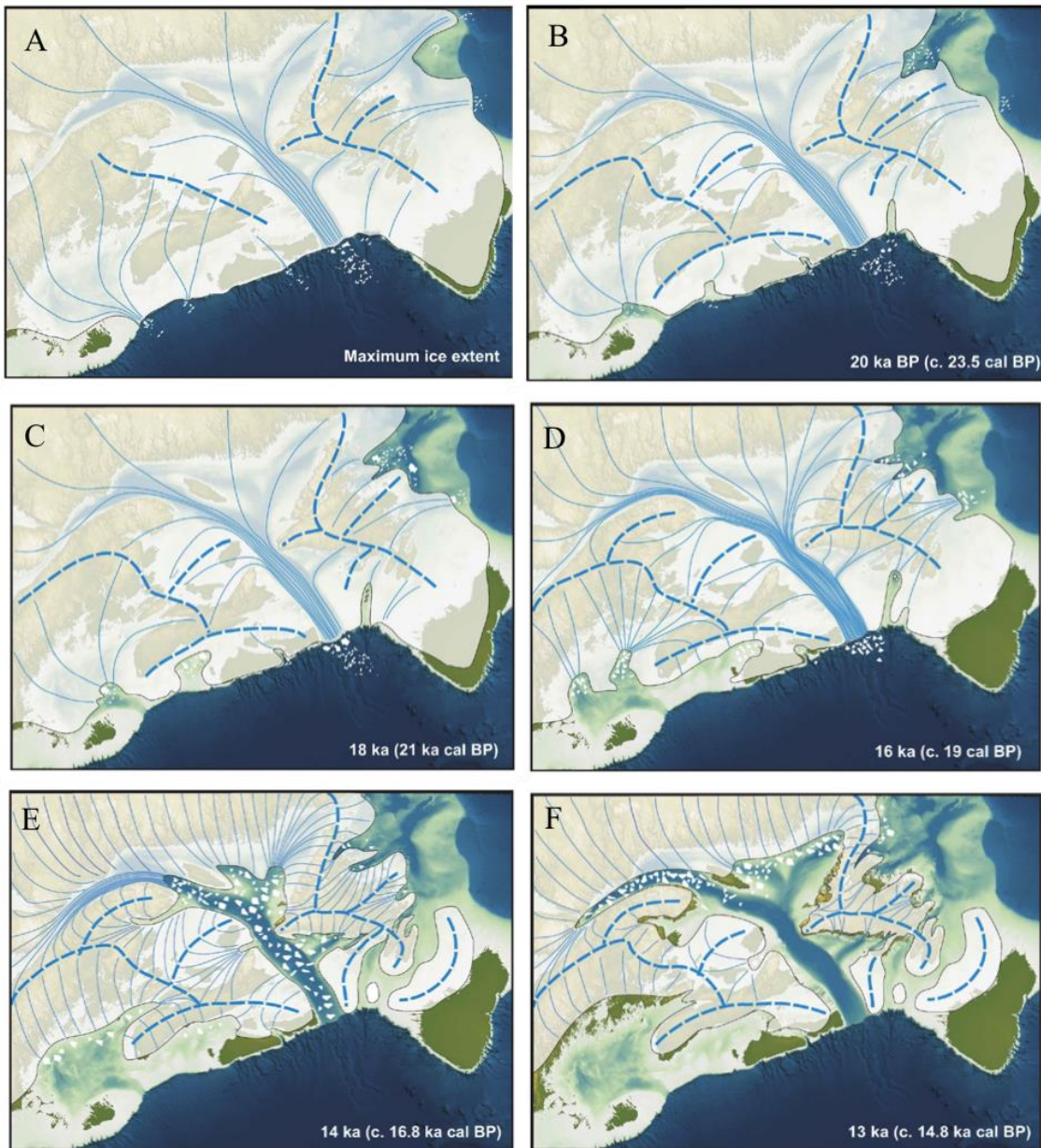


Figure 1.24 : Marge glacée et configuration de retrait de l’Inlandis laurentidien à : (A) étendue maximale de glace, (B) 20 ka, (C) 18 ka, (D) 16 ka, (E) 14 ka, (F), 13 ka (tiré de Shaw et al. 2006).

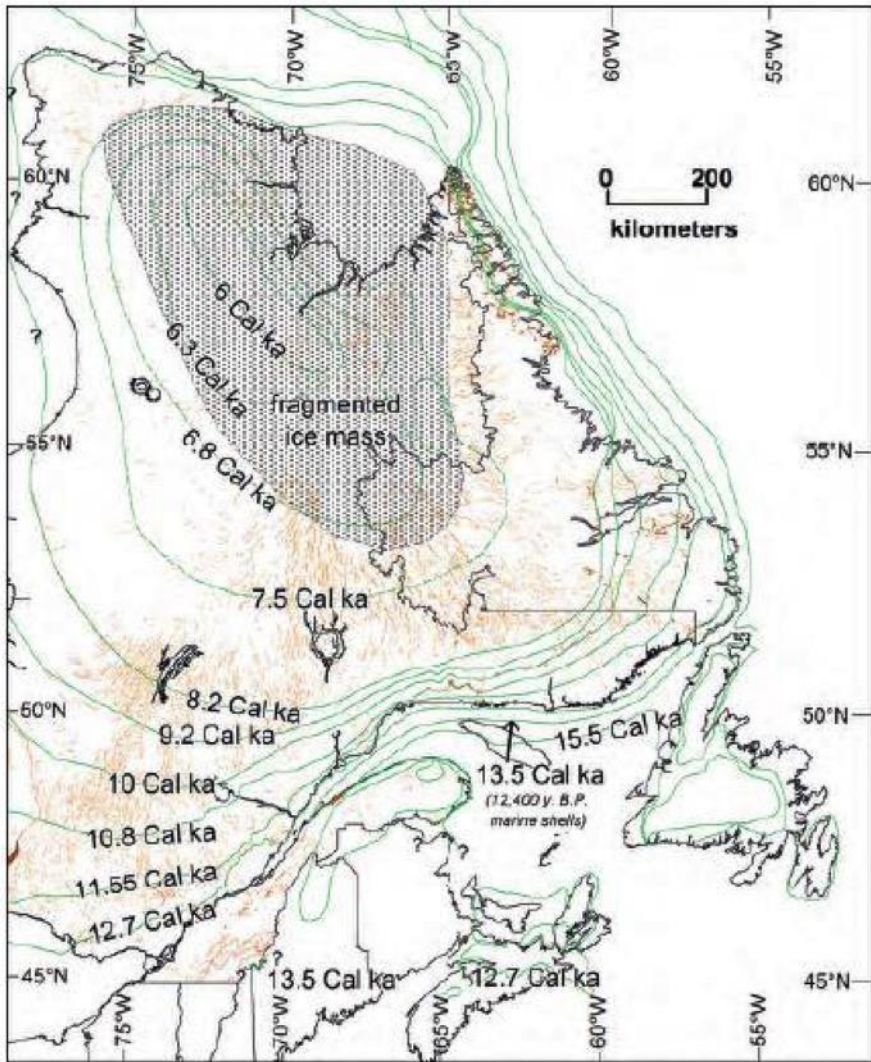


Figure 1.25 : Modèle du retrait de l’Inlandsis laurentidien au Québec entre 13,5 et 6 cal. ka BP, proposé par Occhietti et al. (2011).

Selon Occhietti et al. (2011), les deux types de défis limitant un modèle complet de déglaciation sur la Côte-Nord québécoise sont : 1) les défis chronologiques liés à la datation et 2) la nécessité de disposer de preuves géologiques sur le terrain. Dès lors, cette thèse de doctorat explore des réponses à ces questions dans les chapitres 2 à 4.

1.12 Les travaux de terrain réalisés durant cette étude

Des données bathymétriques à haute résolution ont été acquises à l'aide d'un sonar multifaisceaux et d'un interféromètre (sous la supervision de Patrick Lajeunesse) afin de combler le manque de connaissances paléolimnologiques et géomorphologiques des lacs étudiés. Cela a fourni des informations sur la morphologie du bassin lacustre et la nature des dépôts de sédiments. Des informations détaillées sur les données acoustiques à haute résolution des trois lacs étudiés ont été présentées par Gagnon-Poiré (2016) et Gagnon-Poiré et al. (2019).

Quarante-deux carottes courtes de sédiments mesurant de 30 à 100 cm ont été prélevées dans les lacs Pentecôte, Walker et Pasteur à l'aide d'un carottier gravitaire (également appelé carottier roquette) (Tableau 1.2). Au Lac Walker, 16 carottes de sédiments ont été récupérées à bord du bateau ponton du 3 au 10 juin 2014, tandis qu'au lac Pentecôte 10 carottes de sédiments ont été récupérées à bord du bateau RV Louis-Hamelin du 10 au 14 juin 2014 (par l'équipe de Obinna Nzekwe, Jean-Philippe Jenny, Gabriel Loyal, Antoine-Gagnon-Poiré, François Xavier L'Heureux-Houde, Étienne Brouard et Patrick Lajeunesse). Au Lac Pasteur, 16 carottes de sédiments ont été obtenues à bord d'un bateau pneumatique du 18 au 24 juin 2014 (par l'équipe de Alexandre Normandeau, Jean-Philippe Jenny et Annie-Pier Trottier).

Des carottes longues de sédiments (> 1 m) ont été prélevées du lac Pentecôte à l'aide d'un carottier à percussion du 17 au 18 février 2015 (Tableau 1.3). Dans le lac Walker, un ensemble de carottes longues de sédiments (provenant de trois forages : 08B, 08C et 08D) a été récupéré à l'aide d'un carottier à piston UWITEC du 25 au 28 mars 2015 (Tableau 1.4). Ces carottes ont permis d'établir une séquence composite d'environ 8 m, dénommée WA15-08-U. La figure 1.26 illustre la corrélation des longues carottes collectées dans le lac Walker en 2015 pendant le travail sur le terrain. Une carotte gravitaire (WA15-08B-G) a été récupérée en premier, puis des carottes de deux trous de forage, 08C et 08D qui étaient espacés de 50 cm pour faciliter la corrélation des sections et combler les lacunes entre les sections. Des sections de carotte d'environ 200 cm ont été recueillies à des intervalles en total d'environ 8 m de profondeur (figure 1.26). Cependant, au moins 200 cm de sédiments ont été perdus pendant la récupération (indiquée par une interruption, figure 1.26).

Une révision de la section composite (figure 1.26) a été effectuée après une analyse minutieuse des images acquises par la tomographie axiale (CT-scan) et la microfluorescence X (Figure 1.27). Plus précisément, les images des carottes ont été redimensionnées pour représenter la longueur réelle de chaque carotte, puis corrélées en utilisant des lits marqueurs tels qu'une succession particulière de laminations et les couches déposées rapidement (St-Onge and Long 2009). Par exemple, la figure 1.28 montre un marqueur (couche déposée rapidement) sur des images CT-scan qui a été utilisé pour corrérer des carottes parallèles à environ 352 cm cd). Les lithofaciès des séquences sédimentaires sont également décrits (figure 1.27).

Un avantage de la séquence composite révisée (figure 1.27) par rapport à la précédente (figure 1.26) est qu'elle ne montre qu'un seul hiatus (370 - 400 cm cd) dans toute la séquence composite au lieu de plusieurs hiatus dans chaque intervalle de 200 cm. Sur la base des objectifs / hypothèses de l'étude (section 1.9), la section composite a été divisée en deux sections : la partie supérieure (0 - 400 cm cd) représente l'Holocène supérieur et a été utilisée pour évaluer l'hypothèse 2 (chapitre 3), tandis que la partie inférieure de la section composite (400 - 740 cm cd) représente la sédimentation depuis la fin des glaciers au début de l'Holocène et a été utilisée pour analyser les hypothèses 3 et 4.

Tableau 1.2 : Liste des carottes courtes de sédiments échantillonnées dans les trois lacs étudiés.

| S/N | Carotte | Lac | Date obtenu | Latitude (°) | Longitud e (°) | Water depth (m) | Length (m) |
|-----|-----------|-----------|-------------|-----------------|-------------------|--------------------|---------------|
| 1 | PC14-01-R | Pentecôte | 09/06/2014 | 49.880944 | 67.356639 | 43 | 37 |
| 2 | PC14-02-R | Pentecôte | 09/06/2014 | 49.882444 | 67.354611 | 38 | 37 |
| 3 | PC14-03-R | Pentecôte | 09/06/2014 | 49.883556 | 67.353667 | 50 | 35 |
| 4 | PC14-04-R | Pentecôte | 09/06/2014 | 49.884944 | 67.353167 | 40 | 39 |
| 5 | PC14-05-R | Pentecôte | 09/06/2014 | 49.886306 | 67.351250 | 45 | 39 |
| 6 | PC14-06-R | Pentecôte | 09/06/2014 | 49.869208 | 67.331844 | 80 | 38 |
| 7 | PC14-07-R | Pentecôte | 09/06/2014 | 49.858361 | 67.331056 | 130 | 42 |
| 8 | PC14-08-R | Pentecôte | 09/06/2014 | 49.858361 | 67.318028 | 90 | 41 |
| 9 | PC14-09-R | Pentecôte | 09/06/2014 | 49.837972 | 67.296222 | 39 | 39 |
| 10 | PC14-10-R | Pentecôte | 09/06/2014 | 49.829611 | 67.286444 | 40 | 40 |
| 0 | WA14-00-R | Walker | 04/06/2014 | 50.394111 | 67.172389 | 161 | 43 |
| 1 | WA14-01-R | Walker | 05/06/2014 | 50.369750 | 67.167861 | 216 | 54 |
| 2 | WA14-02-R | Walker | 05/06/2014 | 50.369083 | 67.170806 | 178 | 55 |
| 3 | WA14-03-R | Walker | 05/06/2014 | 50.368250 | 67.174694 | 140 | 48 |
| 4 | WA14-04-R | Walker | 05/06/2014 | 50.367722 | 67.177083 | 121 | 46 |
| 5 | WA14-05-R | Walker | 05/06/2014 | 50.367361 | 67.178556 | 69 | 44 |
| 6 | WA14-06-R | Walker | 05/06/2014 | 50.380306 | 67.174028 | 151 | 49 |
| 7 | WA14-07-R | Walker | 06/06/2014 | 50.379083 | 67.176306 | 140 | 48 |
| 8 | WA14-08-R | Walker | 06/06/2014 | 50.377361 | 67.177083 | 140 | 45 |
| 9 | WA14-09-R | Walker | 06/06/2014 | 50.377083 | 67.181806 | 57 | 40 |
| 10 | WA14-10-R | Walker | 06/06/2014 | 50.376639 | 67.184139 | 31 | 35 |
| 11 | WA14-11-R | Walker | 06/06/2014 | 50.375917 | 67.185750 | 11 | 30 |
| 12 | WA14-12-R | Walker | 06/06/2014 | 50.381417 | 67.170028 | 156.5 | 44 |
| 13 | WA14-13-R | Walker | 06/06/2014 | 50.382889 | 67.165361 | 130 | 46 |
| 14 | WA14-14-R | Walker | 06/06/2014 | 50.368111 | 67.172028 | 165 | 48 |
| 15 | WA14-15-R | Walker | 06/06/2014 | 50.367917 | 67.175694 | 139 | 43 |
| 2 | PA14-02-R | Pasteur | 22/06/2014 | 50.318667 | 66.927083 | 30 | 38 |
| 3 | PA14-03-R | Pasteur | 22/06/2014 | 50.318583 | 66.927361 | 39 | 39 |
| 4 | PA14-04-R | Pasteur | 22/06/2014 | 50.318722 | 66.927639 | 45.6 | 35 |
| 5 | PA14-05-R | Pasteur | 22/06/2014 | 50.318778 | 66.927889 | 49.6 | 41 |
| 6 | PA14-06-R | Pasteur | 22/06/2014 | 50.318833 | 66.928222 | 54.5 | 36 |
| 7 | PA14-07-R | Pasteur | 22/06/2014 | 50.318806 | 66.928417 | 59 | 39 |
| 8 | PA14-08-R | Pasteur | 22/06/2014 | 50.318806 | 66.928722 | 64.8 | 42 |
| 9 | PA14-09-R | Pasteur | 22/06/2014 | 50.318917 | 66.929083 | 68.6 | 39 |
| 10 | PA14-10-R | Pasteur | 22/06/2014 | 50.319583 | 66.934972 | 38 | 28 |
| 11 | PA14-11-R | Pasteur | 22/06/2014 | 50.319175 | 66.932806 | 62 | 38 |
| 12 | PA14-12-R | Pasteur | 22/06/2014 | 50.319167 | 66.932528 | 66.5 | 36 |
| 13 | PA14-13-R | Pasteur | 22/06/2014 | 50.324806 | 66.933778 | 45 | 34 |
| 14 | PA14-14-R | Pasteur | 22/06/2014 | 50.332333 | 66.935083 | 60 | 40 |
| 15 | PA14-15-R | Pasteur | 23/06/2014 | 50.334167 | 66.937056 | 57 | 48 |
| 16 | PA14-16-R | Pasteur | 24/06/2014 | 50.318972 | 66.929944 | 71 | 73 |
| 17 | PA14-17-R | Pasteur | 25/06/2014 | 50.318861 | 66.928694 | 64.8 | 77 |

Tableau 1.3 : Liste des carottes longues récupérées du lac Pentecôte en 2015.

| S/N | Carotte | Date obtenu | Latitude (N) | Longitude (W) | Profondeur (m) | Longeur de carotte (cm) |
|-----|------------|-------------|-----------------|------------------|-------------------|-------------------------------|
| 1 | PC15-04B-P | 17/02/2015 | 67.357211 | 49.881904 | 193 | 12 |
| 2 | PC15-04A-P | 17/02/2015 | 67.35182833 | 49.87595167 | 95 | 9 |
| 3 | PC15-04C-P | 17/02/2015 | 67.35182833 | 49.87595167 | 79 | 9 |
| 4 | PC15-03-P | 17/02/2015 | 67.326788 | 49.872330 | 185 | 10 |
| 5 | PC15-07B-P | 18/02/2015 | 67.365911 | 49.922101 | 121 | 32 |
| 6 | PC15-05-P | 18/02/2015 | 67.376462 | 49.915184 | 113 | 23 |
| 7 | PC15-08-P | 18/02/2015 | 67.365042 | 49.908167 | 131.5 | 21 |
| 8 | PC15-02A-P | 18/02/2015 | 67.32347 | 49.864778 | 153 | 35 |
| 9 | PC15-02B-P | 18/02/2015 | 67.321879 | 49.865501 | 23 | 19 |
| 10 | PC15-02C-P | 18/02/2015 | 67.321879 | 49.865501 | 43 | 19 |
| 11 | PC15-01-P | 18/02/2015 | 67.291448 | 49.834852 | 116 | 47.5 |

Tableau 1.4 : Liste des carottes longues récupérées du lac Walker en 2015.

| S/N | Carotte | Date obtenu | Latitude (N) | Longitude (W) | *Profondeur de l'eau (cm) | Longeur de carotte (cm) |
|-----|------------------|-------------|-----------------|------------------|---------------------------------|-------------------------------|
| 1 | WA15-08B-G | 25/03/2015 | 50.37738 | 67.17712 | ~140 | 149.5 |
| 2 | WA15-08C-I-U-1 | 26/03/2015 | 50.37722 | 67.17694 | 138.5 | 137.2 |
| 4 | WA15-08C-II-U-1 | 26/03/2015 | 50.37722 | 67.17694 | 138.5+ | 97 |
| 5 | WA15-08C-II-U-2 | 26/03/2015 | 50.37722 | 67.17694 | 138.5+ | 97.5 |
| 6 | WA15-08C-III-U-1 | 27/03/2015 | 50.37722 | 67.17694 | 138.5+ | 152 |
| 7 | WA15-08C-IV-U-1 | 27/03/2015 | 50.37722 | 67.17694 | 138.5+ | 154.2 |
| 8 | WA15-08D-I-U-1 | 27/03/2015 | 50.37722 | 67.17694 | ~140 | 90.8 |
| 9 | WA15-08D-I-U-2 | 27/03/2015 | 50.37722 | 67.17694 | ~140+ | 91.4 |
| 10 | WA15-08D-II-U-1 | 27/03/2015 | 50.37722 | 67.17694 | ~140+ | 91.9 |
| 11 | WA15-08D-II-U-2 | 27/03/2015 | 50.37722 | 67.17694 | ~140+ | 91.2 |
| 12 | WA15-08D-III-U-1 | 27/03/2015 | 50.37722 | 67.17694 | ~140+ | 85.8 |
| 13 | WA15-08D-III-U-2 | 28/03/2015 | 50.37722 | 67.17694 | ~140+ | 86.9 |
| 14 | WA15-08D-IV-U-1 | 28/03/2015 | 50.37722 | 67.17694 | ~140+ | 83.2 |
| 15 | WA15-08D-IV-U-2 | 28/03/2015 | 50.37722 | 67.17694 | ~140+ | 82 |

*La figure 1.26 montre la stratigraphie de carottes qui a été construite pendant le travail sur le terrain, tandis que la figure 1.27 montre la stratigraphie après révision en utilisant la corrélation des laminations.

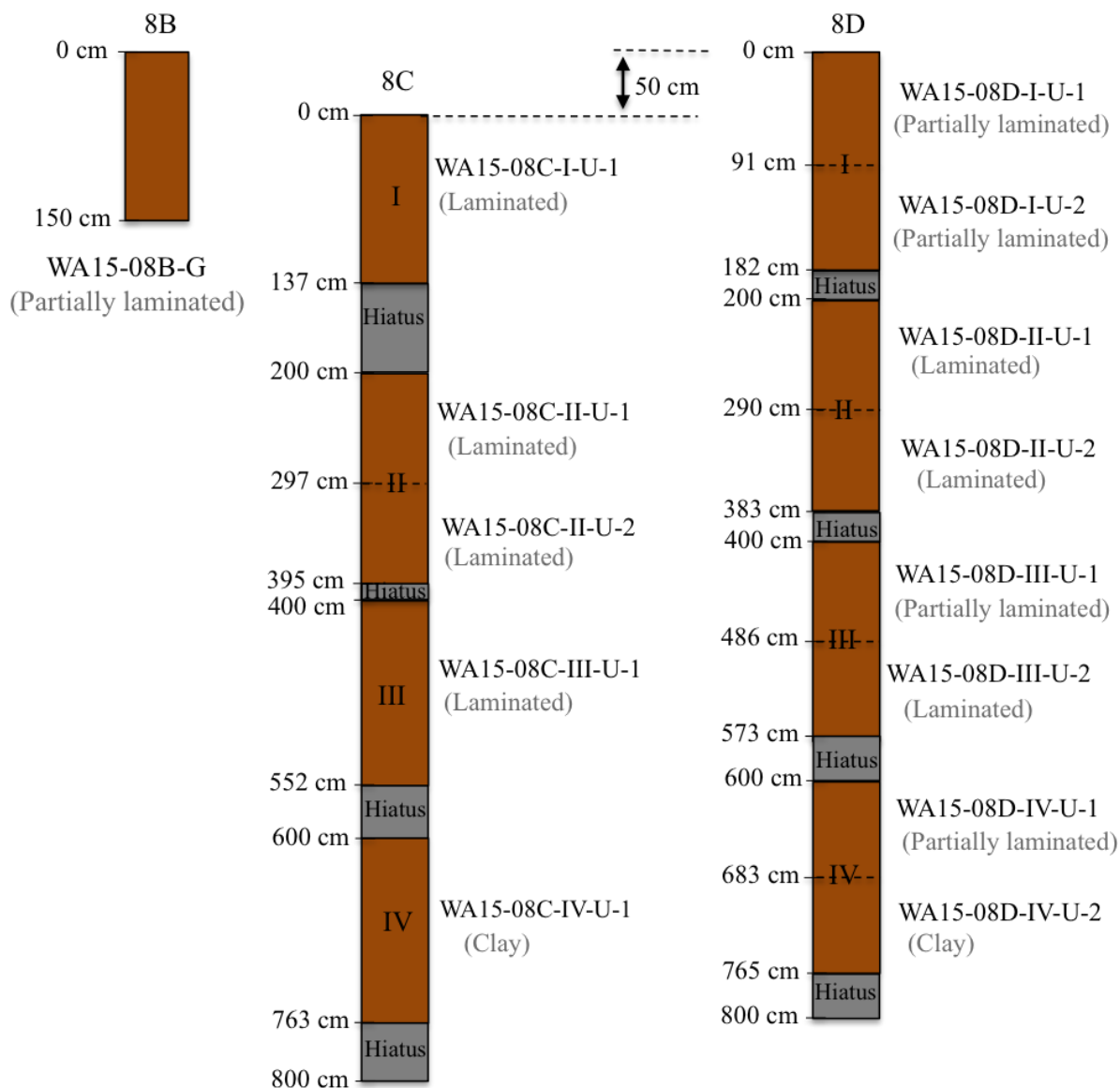
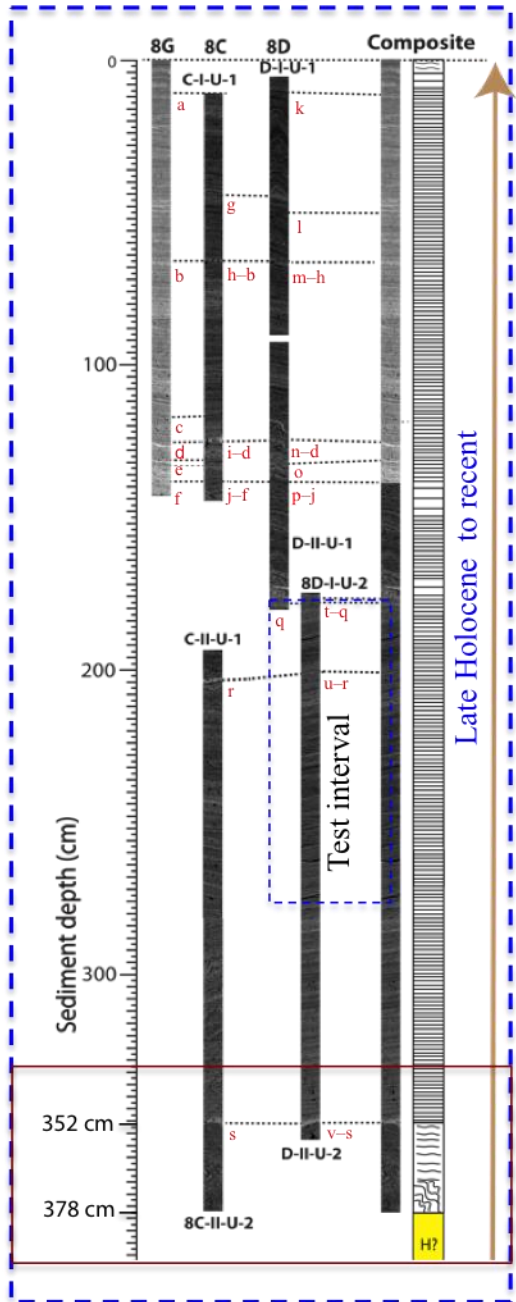


Figure 1.26 : Illustration schématique sur le terrain des carottes longues (tableau 1.4) recueillies dans le lac Walker en 2015, qui ont été utilisées pour reconstruire la carotte composite (WA15-08-U) (pas à l'échelle).

Cette étude (Hypothèse 2)



Cette étude (Hypothèses 3 et 4)

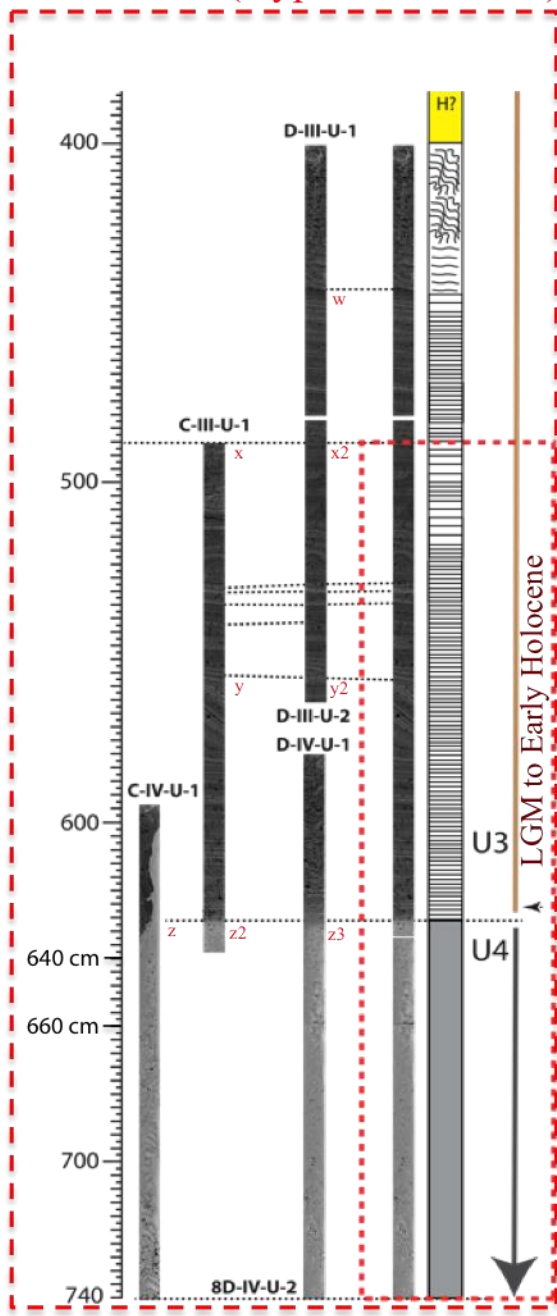
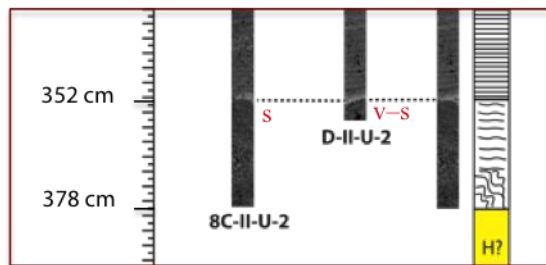


Figure 1.27 : Illustration de la séquence composite WA15-08-U (0 – 740 cm cd) basée sur la corrélation des carottes en utilisant des marqueurs (par exemple des lamination) et le redimensionnement des photos pour représenter les longueurs réelles de chacun carottes. La légende est montrée dans la figure 1.28. Liste des lamination / marqueurs utilisées pour la corrélation est fourni en tableau 1.5. L'insert (boîte rouge, gauche) montre un exemple de lamination / marqueur à haute fiabilité pour la corrélation entre des carottes.



Legend

- Crudely laminated sediments
- Slump/disturbed sediment
- H? Hiatus?
- Partially laminated sediments
- Laminated sediments (post glacial)
- Laminated sediments (Proglacial)

Figure 1.28 : Illustration de la révision de la séquence composite basée sur la corrélation des carottes en utilisant des marqueurs (par exemple des lamination) et le redimensionnement des photos pour représenter les longueurs réelles de chacun carottes. Des lithofaciès sont également décrits.

Tableau 1.5 : Liste des laminations utilisées pour corréler des carottes pour construire la séquence composite WA15-08-U (Lac Walker).

| Carotte | Label de lamination | Profondeur (cm) | Profondeur composite (cm cd) | Niveau de confiance de lamination |
|------------------|---------------------|-----------------|------------------------------|-----------------------------------|
| WA15-08B-G | a | 9 | 9 | L |
| WA15-08B-G | b | 65 | 65 | L |
| WA15-08B-G | c | 118 | 118 | L |
| WA15-08B-G | d | 126 | 126 | L |
| WA15-08B-G | e | 130 | 130 | L |
| WA15-08B-G | f | 138 | 138 | L |
| WA15-08C-I-U-1 | g | 37 | 46 | M |
| WA15-08C-I-U-1 | h-b | 56 | 65 | M |
| WA15-08C-I-U-1 | i | 117 | 126 | M |
| WA15-08C-I-U-1 | j | 129 | 138 | M |
| WA15-08D-I-U-1 | k | 6 | 10 | L |
| WA15-08D-I-U-1 | l | 44 | 50 | M |
| WA15-08D-I-U-1 | m-h | 59 | 65 | H |
| WA15-08D-I-U-2 | n-d | 32 | 124 | L |
| WA15-08D-I-U-2 | o | 40 | 132 | L |
| WA15-08D-I-U-2 | p-j | 46 | 138 | L |
| WA15-08D-I-U-2 | q | 2 | 178 | L |
| WA15-08C-II-U-1 | r | 10 | 204 | L |
| WA15-08C-II-U-1 | s | 154 | 348 | H |
| WA15-08D-II-U-1 | t-q | 0 | 178 | L |
| WA15-08D-II-U-1 | u | 172 | 348 | H |
| WA15-08D-II-U-1 | v-s | 42 | 352 | H |
| WA15-08D-III-U-1 | w | 0 | 442 | M |
| WA15-08C-III-U-1 | x | 0 | 4 | M |
| WA15-08C-III-U-1 | y | 79 | 567 | M |
| WA15-08C-IV-U-1 | z | 32 | 628 | H |
| WA15-08D-III-U-2 | x2 | 6 | 488 | L |
| WA15-08D-III-U-2 | y2 | 74 | 556 | M |
| WA15-08C-IV-U-1 | z2 | 48 | 628 | H |

Niveau de confiance des laminations : L- bas, M - moyen, H - haut

CHAPITRE 2

ARTICLE 1

2 RECENT SEDIMENTATION IN THREE ADJACENT FJORD-LAKES ON THE QUÉBEC NORTH SHORE (EASTERN CANADA): FACIES ANALYSIS, LAMINAe PRESERVATION AND POTENTIAL FOR VARVE FORMATION

Obinna P. Nzekwe¹, Pierre Francus¹, Guillaume St-Onge², Patrick Lajeunesse³, David Fortin⁴,
Antoine G. Poiré³, Édouard G. H. Philippe^{2, 5}, Alexandre Normandeau^{3, 6}

¹Institut National de la Recherche Scientifique, Centre - Eau Terre Environnement, Québec, QC G1K
9A9, Canada, Canada Research Chair in Environmental Sedimentology & GEOTOP

²Institut des sciences de la mer de Rimouski (ISMER), Université du Québec à Rimouski, QC G5L
2Z9, Canada, Canada Research Chair in Marine Geology & GEOTOP

³Centre d'études nordiques, Département de géographie, Université Laval, Québec, G1V 0A6, Canada

⁴School of Earth Sciences and Environmental Sustainability, Northern Arizona University, Flagstaff,
AZ 86011, USA

⁵Institut des sciences de la mer de Rimouski (ISMER), Université du Québec à Rimouski, Canada and
Institut de Physique de Globe de Paris, Paris, France & GEOTOP

⁶Geological Survey of Canada (Atlantic), Bedford Institute of Oceanography, Dartmouth, Nova Scotia
B2Y 4A2, Canada

¹Corresponding author. Obinna Nzekwe (obinna_peter.nzekwe@ete.inrs.ca)

Keywords: Limnogeology, sedimentary structures, laminations, varves, CT-scan, Québec North Shore

Article publié dans la revue Canadian Journal of Earth Sciences (2018) 55: 138-153

Date de soumission : 3 avril 2017

Date d'acceptation : 11 octobre 2017

Date de publication en ligne : 30 octobre 2017

DOI: <https://doi.org/10.1139/cjes-2017-0070>

Sédimentation récente dans trois lacs de fjord sur la Côte-Nord, Québec (est du Canada) : l'analyse des faciès, la préservation de la stratification et le potentiel de formation de varve

Résumé

Cet article analyse de courtes carottes gravitaires échantillonnées le long de transects dans trois lacs de profonds adjacents (les lacs Pentecôte, Walker et Pasteur) sur la Côte-Nord de Québec (est du Canada), afin d'évaluer la répartition de sédiments laminés et le potentiel de formation de varves. L'analyse de faciès basée la description lithologique, des photos numériques, des images par tomodensitométrie et des données bathymétriques, a permis l'identification de quatre principaux facies sédimentaires : des sédiments laminés, des sédiments partiellement laminés, des sédiments bioturbés, et des sédiments massifs. Des preuves directes sur la stratification thermique du Lac Walker ont été acquises de 2014 à 2016. Les taux de sédimentation moyens et les flux de sédimentation postglaciaires dans les bassins distaux des trois lacs étudiés sont $\leq 0,12 \text{ cm a}^{-1}$ et 0,03 à $0,16 \text{ g cm}^{-2} \text{ a}^{-1}$, respectivement, à la lumière de la datation aux ^{210}Pb (concentration initiale constante), ^{137}Cs et radiocarbone (par la spectrométrie de masse atomique). Sur la base de l'analyse d'images de lames minces et d'un modèle de chronologie du ^{210}Pb (concentration initiale constante), le Lac Pentecôte contient des sédiments principalement massifs à partiellement laminés, alors que le Lac Pasteur contient des sédiments partiellement laminés et des sédiments laminés non annuels ressemblants à des varves. Le Lac Walker contient toutefois des sédiments laminés qui sont vraisemblablement des varves. Le plus grand potentiel de préservation de laminations observé pour le lac Walker par rapport aux lacs Pentecôte et Pasteur est associé à des caractéristiques morphologiques plus favorables, dont sa profondeur relative, sa profondeur moyenne, sa profondeur maximum et son exposition topographique plus favorable.

Mots-clés : limnogéologie, structures sédimentaires, laminations, varves, tomodensitométrie, Côte-nord, Québec

Contribution des auteurs

La planification de la campagne de carottage «carottes courtes» dans les trois lacs a été réalisée par Obinna Nzekwe, Jean-Philippe Jenny, Antoine Gagnon-Poiré, Pierre Francus, Guillaume St-Onge et Patrick Lajeunesse. Obinna Nzekwe, Édouard Philippe, Jean-Philippe Jenny ont participé à la campagne de carottage aux Lac Walker et Lac Pentecôte, tandis que Jean-Philippe Jenny et Alexandre Normandeau ont participé à la campagne de carottage au Lac Pasteur. Les données bathymétriques à haute résolution et les profils acoustiques de sous-surface (Chirp) ont été acquis par Alexandre Normandeau et Antoine Gagnon-Poiré sous la supervision de Patrick Lajeunesse. Toutes les lames minces ont été fabriquées par Obinna Nzekwe ainsi que l'échantillonnage pour la datation radiocarbone et les modèles d'âge. Les analyses XRF ont été effectués par Obinna Nzekwe. Le comptage des laminations et / ou des varves à l'aide des lames minces ont été réalisés par Obinna Nzekwe sous la direction de Pierre Francus et avec l'aide de Patrick Lajeunesse et Guillaume St-Onge. L'interprétation des résultats et l'écriture de l'article ont été réalisés par Obinna Nzekwe. Tous les auteurs ont contribué à la relecture du manuscrit.

2.1 Abstract

This paper analyzes short gravity cores sampled along transects in three adjacent deep fjord-lakes (lakes Pentecôte, Walker and Pasteur) on the Québec North Shore, Eastern Canada, in order to evaluate the distribution of laminated sediments and potential for varve formation. Facies analysis based on lithological description, digital photos, CT-scan images and bathymetric data allowed for the identification of four main sediment facies, namely: laminated sediments, partially laminated sediments, bioturbated sediments, and massive sediments. Direct evidence that Lake Walker undergoes thermal stratification was monitored from 2014–2016. Mean sedimentation rates and sedimentation fluxes of postglacial sediments in the distal basin of the three studied lakes are ≤ 0.12 cm a⁻¹ and 0.03–0.16 g cm⁻² a⁻¹, respectively based on ²¹⁰Pb, ¹³⁷Cs and AMS radiocarbon dating. On the basis of thin section image analysis and ²¹⁰Pb (CIC) chronology model, Lake Pentecôte contains mainly massive–partially laminated sediments, while Lake Pasteur contains partially laminated sediments and non-annual varve-like sediments. However, Lake Walker contains laminated sediments that are likely varves. The increased potential for laminae preservation observed in Lake Walker compared to lakes Pentecôte and Pasteur is associated with more favourable morphological characteristics including higher relative depth, mean depth, maximum depth and topographic exposure.

2.2 Introduction

Lacustrine environments are subject to physical, chemical and biological processes that influence the nature of sediment deposition (Schnurrenberger et al. 2003; Tylmann et al. 2012; Zolitschka et al. 2015). Lake sediments are characterized by sedimentary facies that reflect the processes driving their deposition such as settling, wind-, or density-driven currents (Tylmann et al. 2012). Sedimentary structures such as laminations can be particularly useful for paleoenvironmental reconstructions when they are annually laminated, i.e., formed by seasonal deposition of autochthonous (formed within the lake basin) and/or allochthonous (transported from the watershed to the lake basin) materials under favourable conditions (Larsen and MacDonald 1993; O'Sullivan 1983; Saarnisto 1986; Zolitschka et al. 2015). However, the combination of several environmental and morphological conditions facilitate the preservation of laminations: (1) the absence of sediment-water mixing due to wave or wind-driven circulations, (2) presence of gentle to flat lake bottom that reduces the frequency of mass movements, (3) a deep basin that favours seasonal or permanent anoxia, (4) reduced biological activity of benthic organisms, (5) a seasonally contrasted sedimentary supply, and (6) sufficient sedimentation rates (Jenny et al. 2013; Larsen and MacDonald 1993; Larsen et al. 1998; O'Sullivan 1983; Schnurrenberger et al. 2003; Tylmann et al. 2012; Wetzel and Likens 1991; Zolitschka et al. 2015). It has been argued that there is a relationship between the distribution of laminated sediments and the lake morphometry (Zolitschka et al. 2015). Several authors have reported empirical assumptions using morphometric variables in order to improve the chances of recovering laminated sediments during reconnaissance field surveys or in areas where prior studies are relatively limited (Gorham and Boyce 1989; Larsen and MacDonald 1993; Larsen et al. 1998; O'Sullivan 1983; Ojala et al. 2000; Zolitschka et al. 2015).

On the Québec North Shore, in the southeastern Canadian Shield (Eastern Canada), three lakes (lakes Pentecôte, Walker and Pasteur) were studied for the possible occurrence of annually laminated sediments. High-resolution swath bathymetry, subbottom acoustic profiles and sediment cores were collected to reconstruct the Late Quaternary geomorphological evolution of these fjord-like lakes in response to deglaciation and postglacial sedimentary processes (Gagnon-Poiré 2016; Normandieu et al. 2016). In this paper, short gravity cores retrieved from these three adjacent lakes are analysed in order to evaluate laminae preservation and the potential for varve formation. The specific objectives are to: (1) identify the sedimentary facies present in the short gravity cores and assess their distribution and depositional environments, and (2) evaluate laminae visibility, sedimentation rates and the potential for establishing a varve chronology in the uppermost sediments from the lakes, using radiometric dating (^{210}Pb and ^{137}Cs) and image analysis of thin sections.

2.3 Regional setting

Lakes Pentecôte, Walker, and Pasteur are located on the Québec North Shore, in the northwestern Gulf of St. Lawrence in Eastern Canada (Figure 2.1). In the local context, the studied lakes are located within the *Reserve faunique de Port-Cartier–Sept-Îles*. They have been fairly undisturbed by anthropogenic activities such as dredging or hydropower generation, except for controlled fishing, boating and wood harvesting. The maximum depths of lakes Pentecôte, Walker and Pasteur are 130, 271 and 70 m, respectively (Gagnon-Poiré 2016); their elevation above sea level (asl) is 84, 115 and 86 m, respectively. The studied lakes have steep sidewalls and relatively deep bottoms, forming a fjord-type morphology. The lakes lie below the limit of the deglacial transgression associated with glacio-isostatic depression, which is at 130 m asl in the region (Dredge 1983).

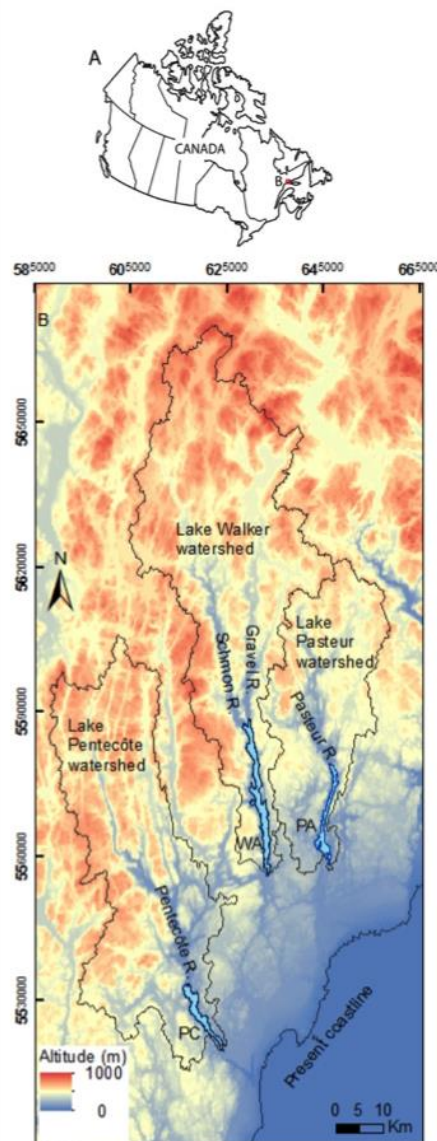


Figure 2.1: (A) Geographic location of the Québec North Shore region in Eastern Canada. The insert (B) shows the location of lakes Pentecôte (PC), Walker (WA) and Pasteur (PA) (shown in blue background) and the extent of their respective watersheds (marked by dark lines). Major river inflows in the northern area of each lake are also shown.

The Québec North Shore region has a subarctic climate where spring snowmelt, which constitutes the peak of the annual runoff period, occurs usually between April and May. The studied lakes are typically covered by ice from December until April. The lake basins receive seasonal inflows from major rivers and small streams that drain areas covered with glacial fine and marine sediments (Figure 2.1). In Lake Walker, the Schmon and Gravel rivers flow into the northwestern and northeastern parts, respectively (Figure 2.1). Lakes Pentecôte and Pasteur are principally fed by Pentecôte and Pasteur rivers that both flow into their northern parts (Figure 2.1). Land cover is largely a boreal forest comprising fir, black spruce, poplar, aspen and shrubs. Morphological and other characteristics of the lakes are shown in Table 2.1.

The Québec North Shore region lies within the geologic province of Grenville. Bedrock geology consists of Precambrian rocks that are Archean or Proterozoic in age (Ministère des ressources naturelles du Québec 2002). Archean rocks comprise migmatite and gneiss, which contain plagioclase, biotite and/or hornblende and/or amphibolite. Proterozoic rocks comprise mafic to ultramafic rocks, as well as sedimentary rocks, which contain paragneiss and quartzite (Ministère des ressources naturelles du Québec 2002). Gneissic rocks underlie most parts of lakes Walker and Pentecôte watersheds, while paragneissic rocks underlie most parts of Lake Pasteur. The history of the sedimentation in the watersheds of studied lakes during the transition from late Quaternary glacial to postglacial has been discussed by Gagnon-Poiré (2016), Normandeau et al. (2016) and Gagnon-Poiré et al. (2019). The fjord-type lakes in the southeast Canadian Shield region have been formed by preglacial fluvial erosion during a lower base level, which carved out V-shaped valleys subsequently occupied by Quaternary sediments preserved below the Laurentide Ice Sheet (LIS) (Lajeunesse 2014).

2.4 Methods and materials

2.4.1 Fieldwork and sediment coring

Short sediment cores ranging from 30 to 100 cm were collected from lakes Pentecôte, Walker and Pasteur in June 2014. Efforts were made to carefully retrieve undisturbed sediment/water interface from suitable locations based on multibeam bathymetry and subbottom profiler data, which provided insight on the lake basin morphology and nature of sediment deposition. Detailed information on high-resolution subbottom acoustic data from the three studied lakes have been presented by Gagnon-Poiré (2016) and Gagnon-Poiré et al. (2019). Sediment cores were obtained in the central and southern parts of Lake Pentecôte and along two transects in the northern part of Lake Walker (Figures 2.2A and 2.2B). Coring was restricted to the northern part of Lake Pasteur due to limited accessibility (Figure 2.2C). A free fall gravity corer (modified after Hvorsley and Stetson (1946)) equipped with metal bars as load was used to improve sediment penetration at depths. In total, 42 short gravity cores were collected: 10 cores at Lake Pentecôte, 16 at Lake Walker and 16 at Lake Pasteur (Table 2.2).

The sediment cores were collected on board a pontoon boat on lakes Pentecôte and Walker and from an inflatable boat on Lake Pasteur. All boats were positioned with DGPS systems (*ca* 60 cm precision; Hemisphere GPS, Calgary, Canada).

Table 2.1: Characteristics of the studied lakes and empirical parameters relating laminated sediments to lake morphometry.

| Lake | Pentecôte | Walker | Pasteur |
|--|---------------|---------------|----------------|
| Latitude (°) | 49.867 | 50.267 | 50.217 |
| Longitude (°) | -67.333 | -67.15 | -66.067 |
| Altitude (m) | 84 | 115 | 86 |
| Maximum depth, Zm (m) | 130 | 271 | 70 |
| Maximum lenght, L _{max} (km) | 15 | 30 | 18 |
| Maximum width, b _{max} (km) | 2.8 | 2.3 | 1.9 |
| Lake area (km ²) | 18.9 | 41 | 19.3 |
| Area of watershed (km ²) | 1710 | 2173 | 1020 |
| Salinity (PSU) | 1.2 - 1.4 | 1.2 - 1.5 | |
| Conductivity (mS) | 1.75 - 1.9 | 1.75 - 1.9 | |
| Thermal lake type | D | D | D |
| Catchment Geology | G, T, S, C, P | G, T, S, C, P | Pg, T, S, C, P |
| Dominant sediment facies | MS, PLS | LS | PLS |
| Empirical parameters | | | |
| Relative depth, Z _r (m) | 2.7 | 3.9 | 1.4 |
| Critical boundary, Zm ₁ (m) | 71.5 | 89.8 | 72.5 |
| Mean depth (m) | 59.5 | 125 | 54.7 |
| Exposure index (km) | 31.8 | 32 | 35.3 |
| Maximum wind fetch (km) | 5.3 | 6.1 | 2.3 |
| Mean wind fetch (km) | 1.6 | 1.9 | 0.9 |
| Topographic exposure (km) | 28.4 | 125.6 | 52.2 |
| Shoreline development (%) | 5 | 3 | 1 |
| Shoreline afforestation (%) | 80 | 85 | 70 |

Basic morphometric characteristics according to (Gagnon-Poiré 2016; Gagnon-Poiré et al. 2019; Normandeau et al. 2016). Thermal lake type: D - dimictic. Catchment geology: G gneiss, Pg paragneiss, T morainic till, S sand and gravel, C clay and silt, P peat. Empirical assumptions (Hutchinson 1957; Larsen and MacDonald 1993; Larsen et al. 1998; Tylmann et al. 2013). Facies legend is given in Figure 2.5.

Temperature sensors (Onset Hobo Water Temp Pro v2 and Tidbit v2 models) were deployed in Lake Walker on June 5th 2014, in order to determine whether the lake undergoes thermal stratification. The deployment location (50°23'17.2" N, 67°10'23.4" W) was chosen for its relative proximity to the area of coring and to the inflow of the two rivers in the northern part of the lake (Figure 2.2B). The temperature sensors were placed along a polypropylene rope and set to take readings every hour for a two-year period, after which they were retrieved. To ensure upright suspension of the sensors, a load

(concrete block) was tied to the base of the mooring while two buoys located 20 m apart were attached at the upper end of the rope.

Table 2.2: List of short sediment cores sampled from the three studied lakes.

| S/N | Core name | Lake | Latitude (N) | Longitude (W) | Water depth (m) | Length (m) | Main sediment facies (Remark) |
|-----|-----------|-----------|--------------|---------------|-----------------|------------|-------------------------------|
| 1 | PC14-01-R | Pentecôte | 49.880944 | 67.356639 | 43 | 37 | PLS |
| 2 | PC14-02-R | Pentecôte | 49.882444 | 67.354611 | 38 | 37 | PLS |
| 3 | PC14-03-R | Pentecôte | 49.883556 | 67.353667 | 50 | 35 | PLS |
| 4 | PC14-04-R | Pentecôte | 49.884944 | 67.353167 | 40 | 39 | PLS (Reference) |
| 5 | PC14-05-R | Pentecôte | 49.886306 | 67.351250 | 45 | 39 | PLS |
| 6 | PC14-06-R | Pentecôte | 49.869208 | 67.331844 | 80 | 38 | PLS |
| 7 | PC14-07-R | Pentecôte | 49.858361 | 67.331056 | 130 | 42 | MS |
| 8 | PC14-08-R | Pentecôte | 49.858361 | 67.318028 | 90 | 41 | PLS |
| 9 | PC14-09-R | Pentecôte | 49.837972 | 67.296222 | 39 | 39 | PLS |
| 10 | PC14-10-R | Pentecôte | 49.829611 | 67.286444 | 40 | 40 | MS |
| 0 | WA14-00-R | Walker | 50.394111 | 67.172389 | 161 | 43 | LS |
| 1 | WA14-01-R | Walker | 50.369750 | 67.167861 | 216 | 54 | LS |
| 2 | WA14-02-R | Walker | 50.369083 | 67.170806 | 178 | 55 | LS |
| 3 | WA14-03-R | Walker | 50.368250 | 67.174694 | 140 | 48 | LS |
| 4 | WA14-04-R | Walker | 50.367722 | 67.177083 | 121 | 46 | LS |
| 5 | WA14-05-R | Walker | 50.367361 | 67.178556 | 69 | 44 | LS |
| 6 | WA14-06-R | Walker | 50.380306 | 67.174028 | 151 | 49 | LS |
| 7 | WA14-07-R | Walker | 50.379083 | 67.176306 | 140 | 48 | LS (Reference) |
| 8 | WA14-08-R | Walker | 50.377361 | 67.177083 | 140 | 45 | LS |
| 9 | WA14-09-R | Walker | 50.377083 | 67.181806 | 57 | 40 | LS |
| 10 | WA14-10-R | Walker | 50.376639 | 67.184139 | 31 | 35 | BS |
| 11 | WA14-11-R | Walker | 50.375917 | 67.185750 | 11 | 30 | BS |
| 12 | WA14-12-R | Walker | 50.381417 | 67.170028 | 157 | 44 | LS |
| 13 | WA14-13-R | Walker | 50.382889 | 67.165361 | 130 | 46 | LS |
| 14 | WA14-14-R | Walker | 50.368111 | 67.172028 | 165 | 48 | LS |
| 15 | WA14-15-R | Walker | 50.367917 | 67.175694 | 139 | 43 | LS |
| W5 | WA11-W5-R | Walker | 50.362310 | 67.165650 | 270 | 43 | LS (Reconnaissance) |
| 2 | PA14-02-R | Pasteur | 50.318667 | 66.927083 | 30 | 38 | PLS |
| 3 | PA14-03-R | Pasteur | 50.318583 | 66.927361 | 39 | 39 | PLS |
| 4 | PA14-04-R | Pasteur | 50.318722 | 66.927639 | 46 | 35 | PLS |
| 5 | PA14-05-R | Pasteur | 50.318778 | 66.927889 | 50 | 41 | PLS |
| 6 | PA14-06-R | Pasteur | 50.318833 | 66.928222 | 55 | 36 | PLS |
| 7 | PA14-07-R | Pasteur | 50.318806 | 66.928417 | 59 | 39 | PLS |
| 8 | PA14-08-R | Pasteur | 50.318806 | 66.928722 | 65 | 42 | PLS |
| 9 | PA14-09-R | Pasteur | 50.318917 | 66.929083 | 69 | 39 | PLS |
| 10 | PA14-10-R | Pasteur | 50.319583 | 66.934972 | 38 | 28 | PLS |
| 11 | PA14-11-R | Pasteur | 50.319175 | 66.932806 | 62 | 38 | PLS |
| 12 | PA14-12-R | Pasteur | 50.319167 | 66.932528 | 67 | 36 | PLS |
| 13 | PA14-13-R | Pasteur | 50.324806 | 66.933778 | 45 | 34 | PLS |
| 14 | PA14-14-R | Pasteur | 50.332333 | 66.935083 | 60 | 40 | PLS |
| 15 | PA14-15-R | Pasteur | 50.334167 | 66.937056 | 57 | 48 | PLS |
| 16 | PA14-16-R | Pasteur | 50.318972 | 66.929944 | 71 | 66 | LS (Reference) |
| 17 | PA14-17-R | Pasteur | 50.318861 | 66.928694 | 65 | 77 | PLS |

Note: Sediment facies: LS, Laminated sediments; PLS, partially laminated sediments; BS, bioturbated sediments; MS, massive sediments.

On September 25th 2014, during another fieldwork, an S4 current meter (InterOceans Systems Inc. USA) was used to measure temperature and salinity. Two measurements were collected at Lake Pentecôte and three at Lake Walker, at points where the water depths ranged from 40 to 100 m (Table 2.3). None were collected at Lake Pasteur due to logistical constraints.

2.4.2 Computed tomography and digital photography

Whole core sections were analyzed using a SIEMENS SOMATOM Definition Volume Access sliding gantry medical CT-scanner at the *Institut National de la Recherche Scientifique, Centre Eau Terre Environment* (INRS-ETE). The CT-Scan allowed for the non-destructive acquisition of longitudinal and transverse images showing the internal structures of the cores. The acquisition was performed at a voltage of 140 keV, current of 410 mA and a rotation time of 1000 ms/rot. The resulting images were displayed in gray scale, with lighter and darker areas indicating higher and lower X-ray attenuations, respectively. Gray scale values are expressed as CT numbers or Hounsfield units (HU). X-ray attenuation is related to sediment bulk density, porosity and mineralogy (Boespflug et al. 1995; Cremer et al. 2002; Fortin et al. 2013). Analysis of CT-scan images was done using the Siemens software or the Image J software® (Schneider et al. 2012).

Shortly after splitting and prior to oxidation of the sediment core surface, the split sediment cores were photographed with a GEOTEK™ Geoscan IV line-scan camera (50-µm pixel size) mounted on a GEOTEK™ Multi-Sensor Core Logger (MSCL; Geotek Ltd., UK.) at the *Institut des sciences de la mer de Rimouski* (ISMER), Canada. Subsequently, another high-resolution line camera mounted on an ITRAX core scanner (Cox Analytical Systems, Sweden) at INRS-ETE was used to acquire RGB colour images (50-µm pixel size) of the split cores. The advantage of the latter over the former is that the images are relatively free from the effects of glare from water on the sediment surface, due to polarizers of the ITRAX.

2.4.3 Facies- and image analysis

Sediment cores were described and grouped into facies based on qualitative identification of textural properties such as colour, grain size and sedimentary structures through a combination of visual inspections and analysis of digital photos, CT-scan images and ITRAX line scan images. Colour of sediments was expressed based on the Munsell Soil Colour Chart (Munsell Color Xrite). A qualitative index, the “Lamination visibility index (LVI)” was introduced to describe the visibility of laminations, as observed from the digital images, with values as follows: 0 - none, 1 - faint, 2 - visible, 3 - clear, and 4 - distinct. One reference core was selected for each lake based on the presence of laminations and evidence of minimal sediment disturbance, namely PC14-04-R (Pentecôte), WA14-06-R (Walker) and PA14-16-R (Pasteur), respectively.

Undisturbed sections were subsampled from the selected reference cores using overlapping metal slabs made of thin aluminium (measuring 18 x 1.5 x 0.5 cm), and thin sections were made based on freeze-drying and epoxy-resin embedding techniques (Francus and Asikainen 2001). Image observation of scanned thin-section slabs was performed using software developed at INRS-ETE (Francus and Nobert 2007). This allowed for further description of the laminae visibility (using the LVI index), and for microscopic counting of laminations on the digital scans (Francus 2006). Laminae were counted by two independent researchers and counting error (%) was estimated based on the difference in the number of counted laminae couplets along the thin sections (Zolitschka et al. 2015).

2.4.4 Sediment dating

For ^{210}Pb analysis, the upper 10 cm section of the three reference cores was sampled at intervals of 0.4 cm. In addition, another core, WA11-W5-R that was retrieved ~2 km southeast of core WA14-06-R during a reconnaissance survey in Lake Walker in 2011, was included in the analysis for comparison (hereafter referred to as reconnaissance core, Figure 2.2B). Core WA11-W5-R was previously sampled at intervals of 0.5 cm. Freeze-dried samples (ca. 2g) were analysed for ^{210}Pb activity using a high-resolution germanium diode gamma detector and multichannel analyzer gamma counter at the Centre d'études Nordiques (CEN), Université Laval (Canada) for core WA11-W5-R, and subsequently with a similar instrument at INRS-ETE for the reference cores. ^{210}Pb activities were analysed as function of depth expressed in form of cumulative dry mass in order to account for the effect of compaction (Appleby and Oldfield 1978). The profiles of ^{210}Pb unsupported were used as input for three possible dating models: (1) the constant rate of sedimentation (CRS) model that takes into account variable sedimentation rates, but constant fluxes of ^{210}Pb , (2) the constant initial concentration (CIC) model that simultaneously takes into account varying sedimentation rates and fluxes of ^{210}Pb , and (3) the constant flux - constant sedimentation model (CF-CS) that simultaneously takes into account constant rate of sedimentation and input of ^{210}Pb (Appleby et al. 1979; Robbins and Edgington 1975). Confidence intervals were calculated by first-order error analysis of counting uncertainty (Appleby and Oldfield 1978; Appleby et al. 1979). This was done in order to determine the age (a), sedimentation rate (cm a^{-1}), and sediment (mass) accumulation rates ($\text{g cm}^{-2} \text{ a}^{-1}$) for the past ~150 years (Zolitschka et al. 2015). ^{137}Cs was used to identify sediments deposited during the peak of atmospheric nuclear testing between the periods from 1963 to 1964 (Appleby and Oldfield 1978).

Terrestrial plant macrofossils (wood fragments) were collected from core WA14-06-R at a depth of 36.5 cm. Bulk sediment from another core, PC15-04B-P-CD that was sampled from Lake Pentecôte in 2015 was included for comparison (Gagnon-Poiré et al. 2019). The samples were prepared at CEN and analysed using accelerator mass spectrometry (AMS) at the Earth System Science Department Keck Carbon Cycle AMS Facility at the University of California at Irvine. The dates were calibrated

using the Calib 7.1 software using the INTCAL2013 calibration curve (Stuiver and Reimer 1993) and are presented with 2 sigma standard deviation (Table 2.4).

2.4.5 Loss on ignition

Within the intervals sampled for ^{210}Pb dating, sediments were extracted to perform loss-on-ignition (LOI) measurements. Organic matter content was calculated as the difference in weight between sediment dried at 60 °C and the ash produced after ignition at 550 °C for 4 hours. Furthermore, the percentage of calcium carbonate was calculated as the difference in weight between ash produced after ignition at 550 and 1000 °C within a high temperature furnace (Heiri et al. 2001).

2.5 Results

2.5.1 Physical limnology

Figure 2.3A shows a clear evidence of temperature variations measured at 35 and 170 m depths (below water level) over a 2-year period (June 5th 2014 – August 4th 2016) in Lake Walker. In the upper part of the lake (~35 m), temperature varied between 3.4 and ~7.0 °C and fluctuated intermittently to 10.0 °C between June and November. It decreased from 3.4 to 2.0 °C during winter. In the lower part of the lake (~170 m), temperature was ~4 °C between June and November, decreasing to ~3.5 °C during winter. Lake mixing, evidenced by temperature reversals across the two depth intervals, occurred twice each year, in May and November, which correspond to the time of ice breakup and ice formation, respectively.

Figures 2.3B and 2.3C show point measurements of temperature and salinity in lakes Pentecôte and Walker measured in September 2014 (Table 2.3). In Lake Pentecôte, profiles from the northern (S4_PC_01) and southern (S4_PC_03) parts of the lake show a temperature decrease from ~15–12 °C at the surface and ~12–8 °C at 20 meters, and slight increase in salinity from 1.1–1.3 and 1.8–1.9 PSU. Between 20 and 40 m, the northern profile indicates a temperature trend from ~12–9 °C, and slight increase in salinity from 1.2–1.3 PSU, while the southern one shows that towards ~60 m depth, temperature and salinity steadied at ~8 °C and ~1.4 PSU, respectively.

In Lake Walker, profiles from the southern (S4_WA_01) and northern (S4_WA_03) parts (locations in Table 2.3) show comparable trends between 0–60 m: temperature decreases from ~14–8°C and salinity increases slightly from 1.2–1.4 PSU. Further down, the three parameters stabilize. However, a profile from the central (S4_WA_02) part of the lake indicates that within 0–30 m, temperature decreases from 11–6 °C, while salinity increases slightly from 1.3–1.5 PSU (Figures 2.3C-1 and 2.3C-2). These data show that thermal stratification occurs in Lake Walker.

Table 2.3: List of sampling points for measurement of physico-chemical parameters in lakes Pentecôte and Walker.

| Code | Lake | Latitude (N) | Longitude (W) | Parameter measured | Depth (m) | Relative location |
|-------------|-----------|--------------|---------------|--------------------|-----------|-------------------|
| S4_PC_01 | Pentecôte | 49.918368 | 67.362836 | T, S | 40 | North |
| S4_PC_03 | Pentecôte | 49.842510 | 67.305110 | T, S | 60 | South |
| S4_WA_01 | Walker | 50.222500 | 67.150833 | T, S | 100 | South |
| S4_WA_02 | Walker | 50.299067 | 67.182238 | T, S | 60 | Central |
| S4_WA_03 | Walker | 50.377083 | 67.181806 | T, S | 80 | North |
| T1 (Onset) | Walker | 50.338111 | 67.173167 | T | 35 | North-central |
| T12 (Onset) | Walker | 50.338111 | 67.173167 | T | 170 | North-central |

Parameter: T - temperature, S – salinity. Measurement points and profiles are shown on Figures 2.2 and 2.3, respectively.

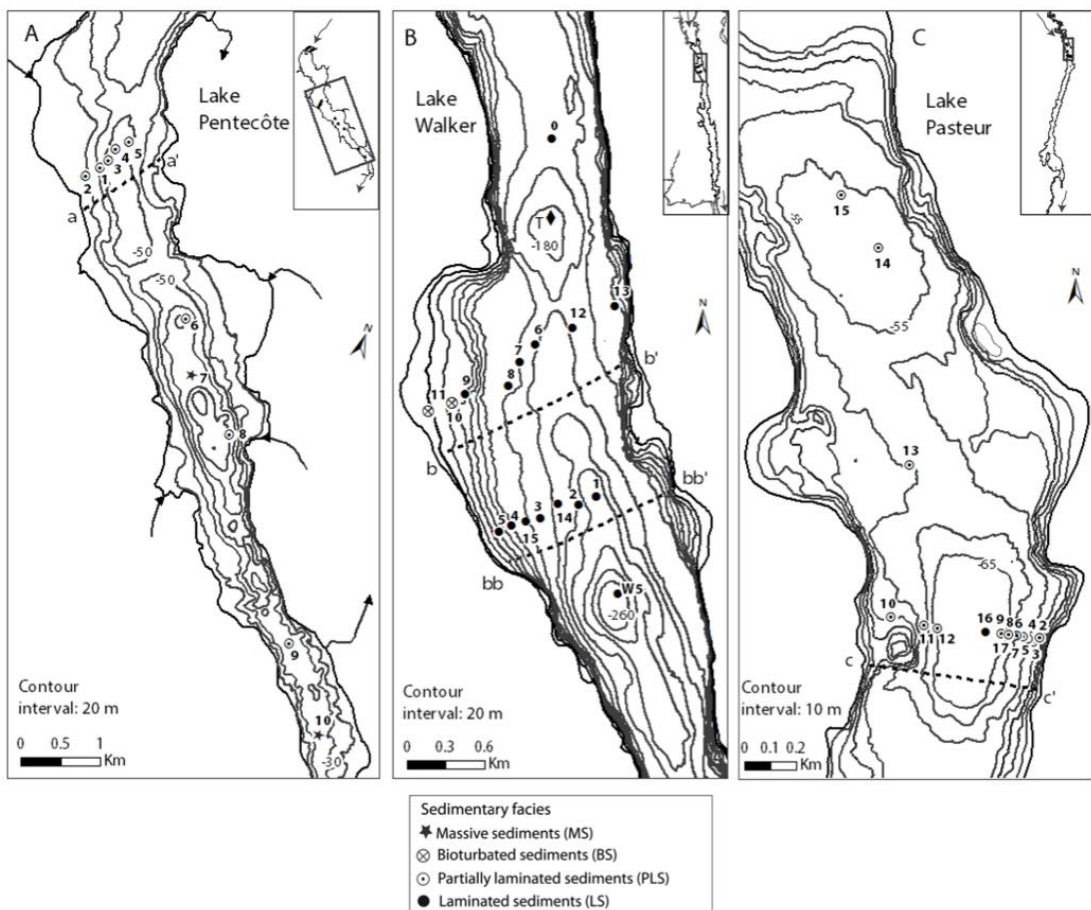


Figure 2.2: Maps showing bathymetry, location of sediment cores and the sediment facies described in (A) Lake Pentecôte, (B) Lake Walker and (C) Lake Pasteur. Core names are abbreviated as serial numbers e.g. WA14-06-R written as 6 (Table 1). W5 refers to the reconnaissance core, WA11-W5-R from Lake Walker (see text). Also shown is the deployment location of Onset temperature sensors in Lake Walker, labelled as T. Schematic subbottom profiles along marked transects are shown in Fig. 3. Core names along transect c-c', Lake Pasteur, are clearer in Figure 2.4D.

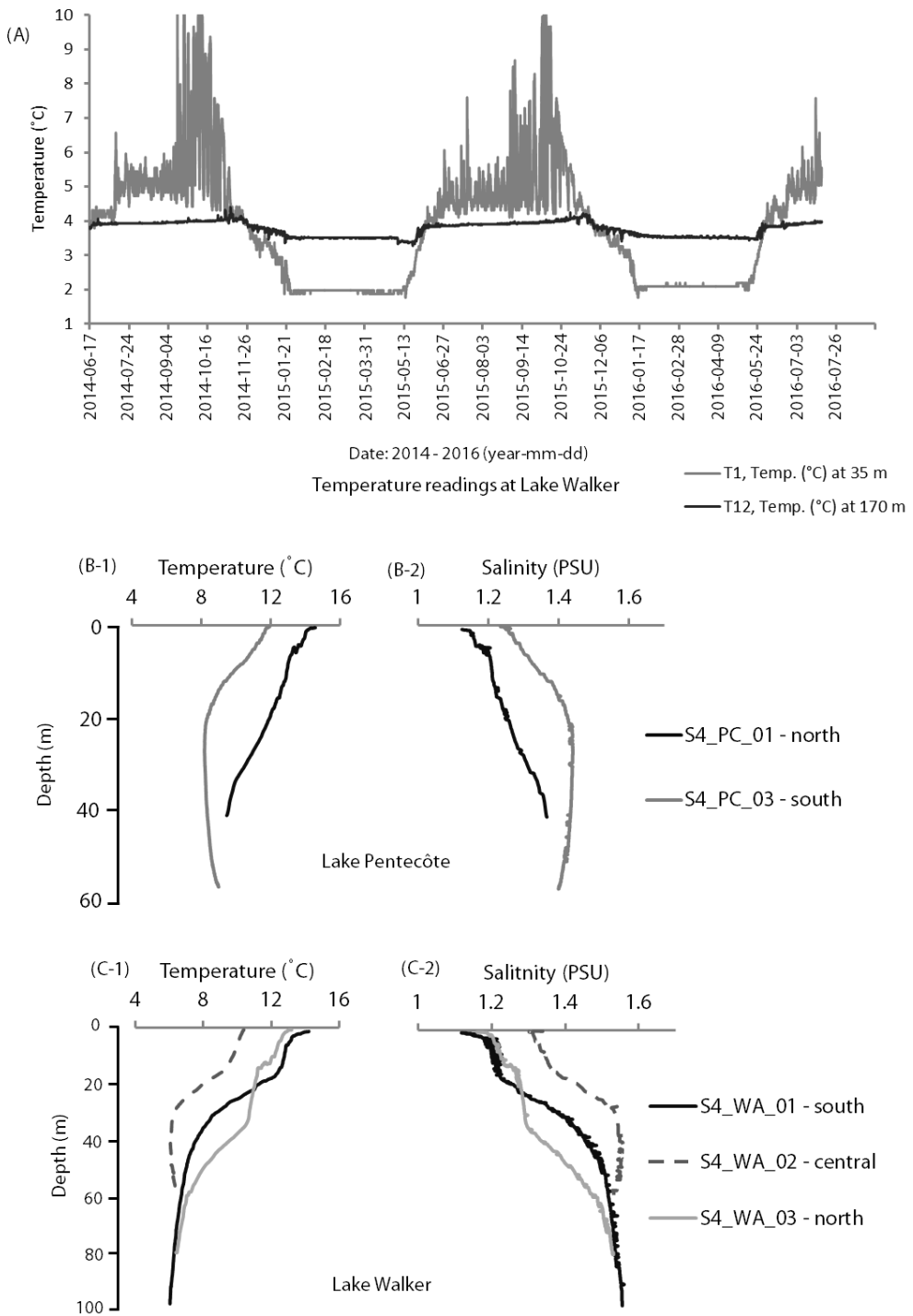


Figure 2.3: Measurement of physical parameters: (A) Temperature variations in the water column of Lake Walker at 35 and 170 m depths below water level measured using Onset Hobo temperature sensors over a 2-year period (June 2014 - August 2016). Deployment location of sensors is marked as T in the Figure 2.2 (B and C) Profiles of temperature and salinity measured in lakes Pentecôte and Walker, respectively using an S4 current meter on September 24 2014 (sampling points are described in Table 2.3).

2.5.2 Sedimentary facies

The following distinct sedimentary facies were identified based on qualitative analysis: laminated, partially laminated, bioturbated and massive sediments. Rapidly deposited layers and turbidite deposits were also identified (Figures 2.2, 2.4 and 2.5).

2.5.2.1 Laminated sediments (LS)

The two basic units that compose the laminated sediment facies are a silty minerogenic material (silty lamina) and a clay and organic rich material (clayey lamina). The silty lamina is grayish brown to dark gray (Munsell colour: 2.5Y 5/2 to 4/2), whereas the clayey lamina is dark gray to very dark gray (Munsell colour: 2.5Y 5/2 to 3/2). LS facies have visible to distinct laminations (LVI index 2–4). The thickness of lamina couplets ranges from 0.2 to 1 cm. Laminations are usually horizontal, although sometimes inclined due to disturbance during deposition or coring and transportation. CT number varies from 1100 to 1500 HU (Figure 2.5).

The distribution of the LS facies in the three lakes is shown on Figures 2.2 and 2.4. Of the ten short sediment cores collected from Lake Pentecôte, none was laminated along its entire length. In Lake Walker, 81% (13 out of 16) of cores were characterised entirely by the LS facies. These cores were retrieved at water depths ranging from 60 to 270 m, which correspond to the deep central part of the lake basin (Figures 2B, 4B and 4BB). In Lake Pasteur, 6% (1 out of 16) of cores contained LS facies along the entire core. It was retrieved at a depth of 70 m, which corresponds to the deepest part of the lake's basin (Figures 2.2C and 2.4C).

2.5.2.2 Partially laminated sediments (PLS)

Partially laminated sediments (PLS) comprise olive gray silty lamina and dark to very dark olive gray clayey lamina (Munsell colour: 5Y 3/15 and Y 4/2 to 3/2, respectively). They are characterized by similar grain size as the LS facies, but with parallel or inclined laminations that range from faint to clear (LVI index 1–3) at intervals within the same core (Figure 2.5). In this study, PLS facies is used to distinguish sediments that are neither laminated or massive (e.g. Larsen et al. 1998). Laminations in the PLS facies are at irregular intervals and are clear to obscure in appearance. Laminae thickness ranges from 0.4 to 1 cm. Wood fragments are more common in the PLS than in the LS facies. CT number varies from 1200 to 1600 HU.

In Lake Pentecôte, partially laminated sediments characterized 80% (8 out of 10) of collected cores. The cores were retrieved from water depths ranging from 39–130 m, representing the shallow to deep parts of the lake (Figures 2.2A and 2.4A). In Lake Walker, none were partially laminated, while in Lake Pasteur, 94% (15 out of 16) of sediment cores were partially laminated. They were collected at

water depths ranging from 28–48 m, representing the shallow to moderately deep parts of the lake (Figures 2.2C and 2.4C).

2.5.2.3 *Bioturbated sediment (BS)*

Bioturbated sediments (BS facies) are marked by colour mottling, with variation from light yellowish brown to light olive brown and gray to dark grayish brown silty clay and clay materials (Munsell colour: 10YR 6/4 to 4/1, 2.5Y 6/1 to 5/2). The laminations appear faint to visible (LVI index 1– 2) and are parallel to inclined, sometimes disturbed. CT number ranges from 1400 to 1500 HU (Figure 2.5B). BS facies contain more traces of organic matter than massive sediments (described below). The term “bioturbated” is actually “inferred” rather than “indicative” based on their characteristics (mottling, and organic matter content (St-Onge et al. 2012).

The BS facies was encountered in the upper part of two cores from Lake Walker, which were retrieved at depths of 10–30 m that correspond to the proximal and shallow parts of the lake (Figures 2.2B and 2.4B).

2.5.2.4 *Massive sediments (MS)*

Massive sediments consist of olive gray and dark gray silty and clayey materials (Munsell colour: 5Y 4/2 to 4/1, respectively). Unlike the bioturbated sediments, massive sediments are marked by relatively uniform colour (and/or absence of mottling). There is no clear evidence of visible laminae pattern though faint laminations (LVI index 0-1) are occasionally present (Figure 2.5E). This facies contains organic materials such as wood fragments and deformations due to gas expansion that were more evident after core splitting. The transition between the PLS and MS facies are rather subtle.

Of the three studied lakes, sediment cores that present the MS facies were retrieved only in Lake Pentecôte. In that lake, MS facies characterized two cores (Figure 2.2A) and also the lower part of another core, PC14-04-R (Figure 2.5A). The cores were sampled at water depths of 39–42 m, which corresponds to the shallow parts of the lake (Figure 2.2A).

2.5.2.5 *Rapidly deposited layers (RDLs)*

Within the LS and PLS facies, there is evidence of a distinct sub-facies that is characterized by light gray to dark yellowish brown silty and clayey materials (Munsell colour: 2.5Y 7/1 to 4/2, 5.Y 3/1), with clearly visible boundaries (LVI index 2–3) that is marked by an abrupt change in CT number from 1300–1500 HU, compared to the LS/PLS facies (Figure 2.5). They are interpreted as rapidly deposited layers (RDLs) (St-Onge et al. 2012). They range from few mm to >1 cm in thickness and are noticeable on CT-scan images and the ITRAX line scan images, but may be obscure under the

naked eye (Figures 2.5A and 2.5C). RDLs show a sequence of reverse to normal grading (Figure 2.5F) St-Onge et al. 2012) and were encountered in several cores from the three studied lakes, irrespective of coring depth.

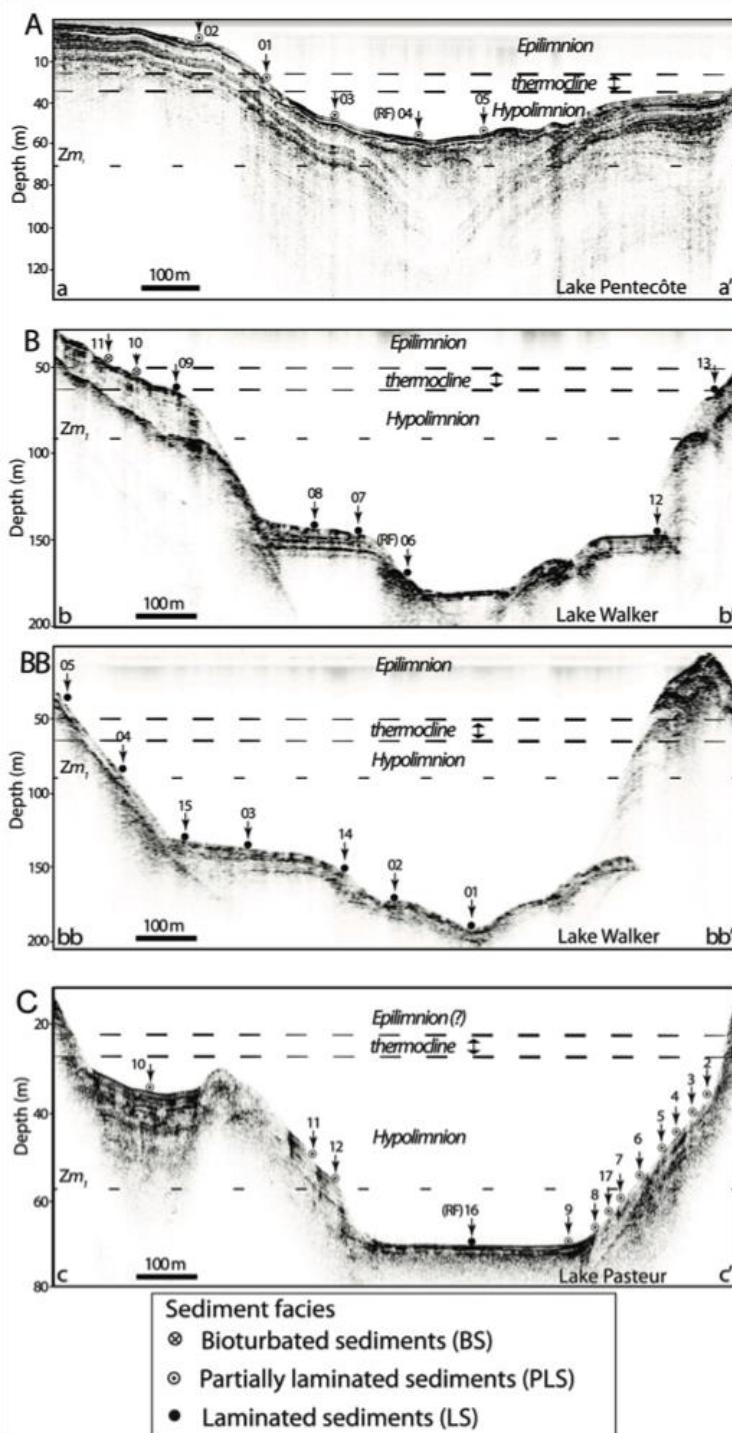


Figure 2.4: Schematic subbottom profiles along the transects shown in Fig. 2. (A) a – a', Lake Penticôte; (B) (b – b', bb – bb'), Lake Walker) and (C) c – c', Lake Pasteur. The location of cores retrieved and the sediment facies encountered are shown (see full legend in Figure 2.2). Core names are abbreviated as serial numbers (see Table 1). RF indicates the reference core for each lake. Thermal stratification zones are inferred from temperature measurements (see text). Also shown are the empirical depths of the critical boundary (Zm₁) described for each lake (See text and Table 2.1).

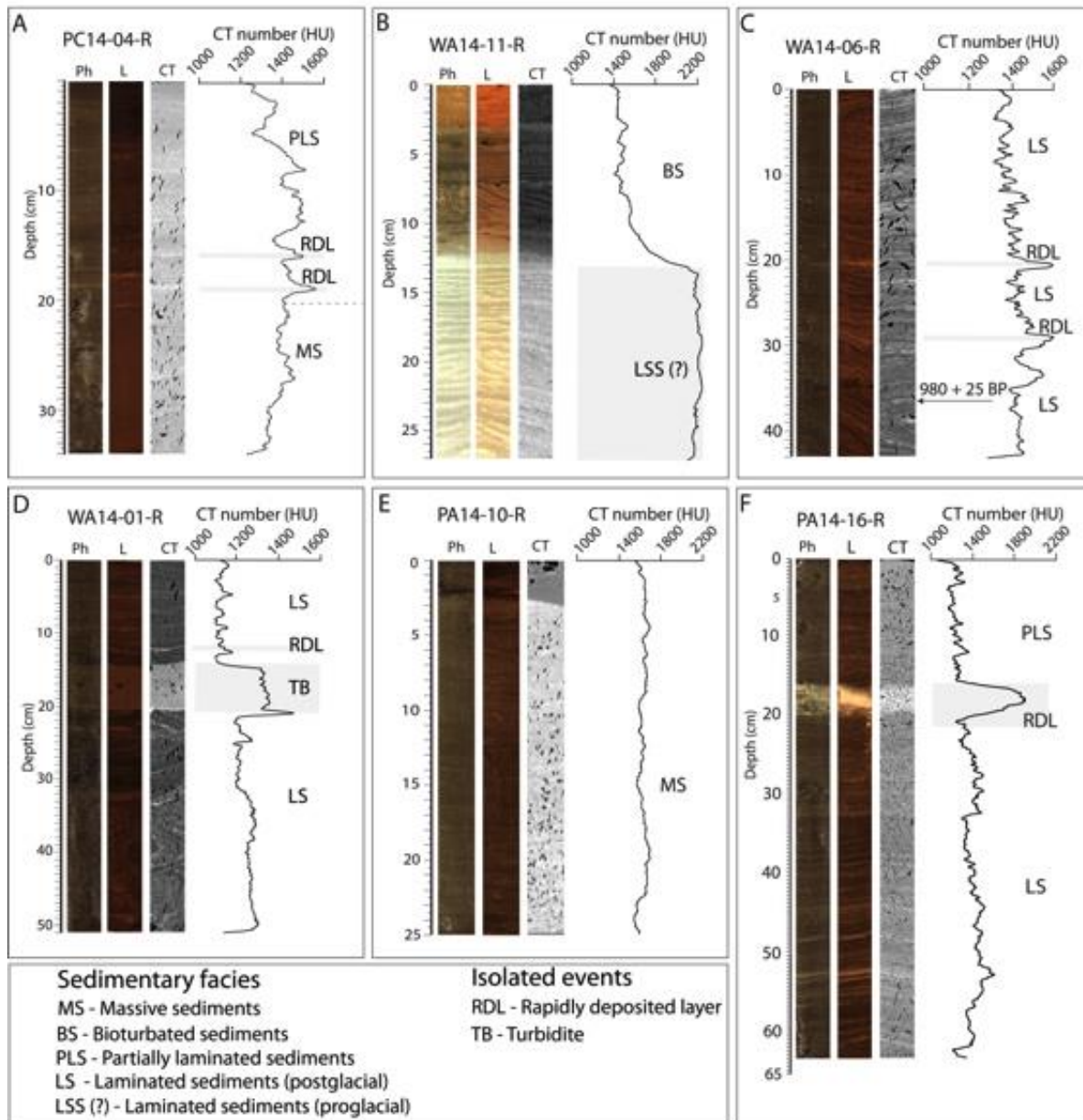


Figure 2.5: Digital photo (Ph), ITRAX line scan images (L) and CT-scan frontal view (CT) showing example images of the sedimentary facies described in lakes Pentecôte, Walker and Pasteur. Rapidly deposited layers (RDLs) and turbidites (TB) represent isolated events. The LLS (?) represents Late Quaternary glacial facies that was encountered (below the BS facies, 2.5B) but not discussed in detail in this study (see core PC15-04-P-CD; Gagnon-Poiré et al. 2019). Note that corresponding images may appear slightly different because they were taken along different slices/views of the respective sediment cores.

RDLs observed to be normally graded were characterized by light-coloured silt-rich base (associated with high density; CT-number) that fines upwards into silty and clayey materials (e.g., St-Onge et al. 2012). However, a 5 cm thick RDL is clearly noticeable on one core, PA14-16-R from Lake Pasteur (Figure 2.5F), which exhibits reversed grading. In this case, the base of the RDL is characterized with clayey materials that coarse upwards into silty materials and afterwards fines upwards into clayey materials (Figure 2.5F).

2.5.2.6 Turbidites

Another sub-facies, characterized by fine grained (silty clay) materials and coarse grained (sandy) materials and which is non-laminated and normally graded, was observed. Its lower and upper boundaries are marked by sharp contacts with the underlying and overlying LS facies, and are evidenced by abrupt change in CT number from 1300 to 1500 HU (Figure 2.5D). It is interpreted as a turbidite deposit (St-Onge et al. 2004). It was encountered only in Lake Walker, on one core, WA14-01-R that was collected at a depth of ~200 m (Figures. 2.4BB and 2.5D).

2.5.3 Thin section image analysis

Laminae visibility index was used to describe thin sections from the three reference cores, PC14-04-R, WA14-06-R and PA14-16-R, and are plotted on Figure 2.6. Counting of laminae in cross-polarized light was preferred due to higher birefringence of silty particles relative to the fine clay matrix. Image observation of thin sections from core PC14-04-R, collected from Lake Pentecôte at a depth of ~40 m, indicates that it is characterized by MS facies in the lower section that pass into PLS facies in the upper section. The uppermost part appears disturbed near the sediment/water interface. The laminae are faint (LVI index ≤ 2) and occurrence is discontinuous (Figure 2.6A). Consequently, replicate counting of laminae was not performed and thus no counting errors were estimated for this lake.

On thin sections of core WA14-06-R, collected from Lake Walker at 151 m depth, the laminae visibility index shows that laminations appear visible to distinct (index 3–4) in lower to upper intervals, which facilitated replicate counting, but passes into faint laminations (index 0–1) in the uppermost part of the core near the sediment/water interface (Figure 6B). Approximately 400 lamina couplets were counted along the 43 cm long core, with varying error estimation within successive thin sections. A plot of error estimation versus depth shows that error limit decreases with increasing depth, ranging from 4% for the lowermost part of the core, where distinct laminae were most evident, to 10% for the topmost (5 cm) sediment interval (Figures 2.6B and 2.7B).

On thin sections of core PA14-16-R, collected from Lake Pasteur at 70 m depth, laminations are visible to clear (LVI index 2–3) in the lower part of the core, which facilitated replicate counting (Figures 2.6C and 2.7C), passing into discontinuous and faint (LVI index 0–1) in the uppermost section near the sediment/water interface. Approximately 560 lamina couplets were counted along the 63 cm core. Error estimation versus depth illustrates that the error limit varies irregularly between 3–54% down core (Figure 2.6C). Laminae boundaries are noticeably obscured within RDLs, consequently higher error limits were observed where RDLs occur (e.g. between 15–20 cm on core PA14-16-R, Figure 2.6C).

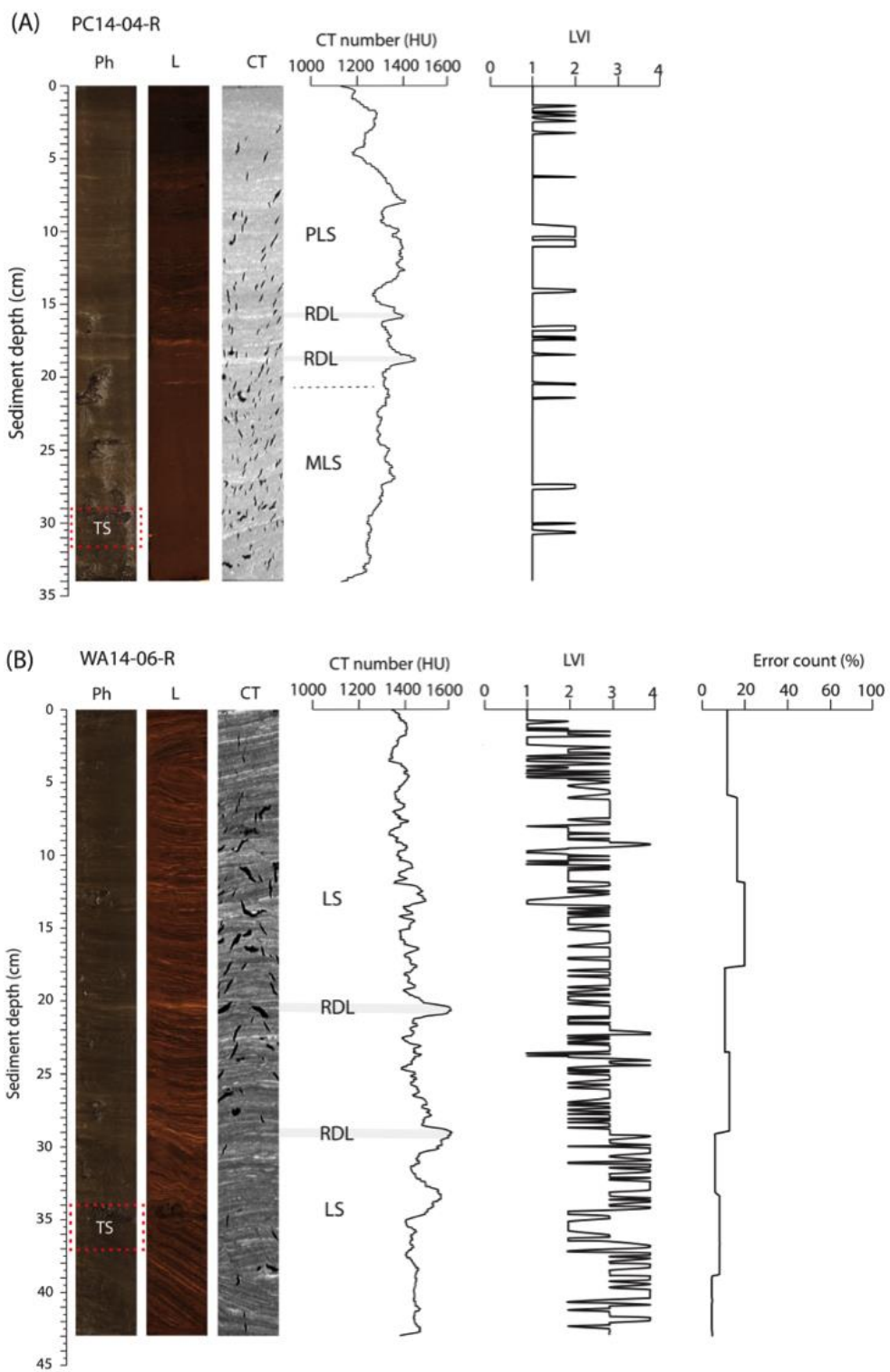


Figure 2.6: Profiles with the digital photo (Ph), ITRAX line scan image (L) and CT-scan frontal view (CT), and results of sedimentological analysis: laminae visibility index (LVI) and laminae counting error estimate for the reference cores (A) PC14-04-R, (B) WA14-06-R and (C) PA14-16-R from lakes Pentecôte, Walker and Pasteur, respectively. LVI index: 0 - none, 1- faint, 2 - visible, 3 - clear, 4 - distinct. Thin-sections from the lower part (marked "TS" on the digital photos) are shown in Figure 2.7.

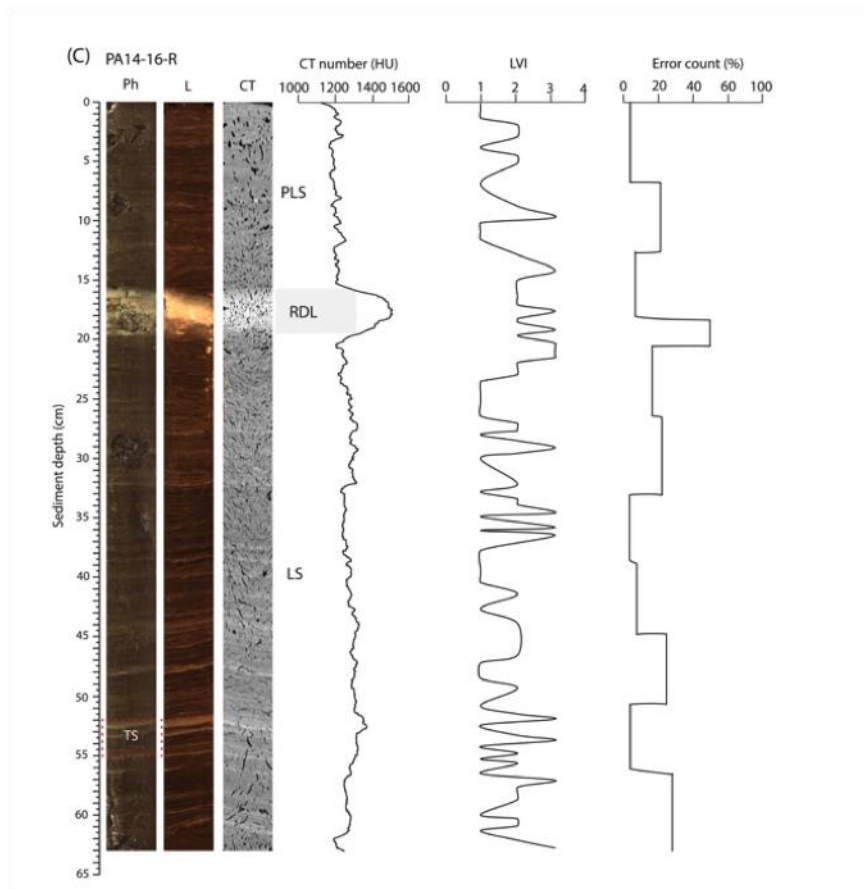


Figure 2.6: (continued, 6C) Profiles with the digital photo, CT-scan frontal view, line scan image (ITRAX) and results of sedimentological analysis: laminae visibility index (LVI) and laminae counting error estimate for the core PA14-16-R from Lake Pasteur. LVI index: 0 - none, 1- faint, 2 - visible, 3 - clear, 4 - distinct. Thin-sections from the lower parts (marked “TS” on the digital photos) are shown in Figure 2.7.

Table 2.4: AMS ^{14}C age of the dated materials from lakes Pentecôte and Walker.

| Core name | Depth (cm) | Material | Laboratory no. | ^{14}C a (BP) | ^{14}C a cal BP |
|----------------|------------|---------------|----------------|------------------------|--------------------------|
| WA14-06-R | 36.5 | Wood fragment | UCIAMS-161059 | 930 ± 25 | 790-920 |
| PC15-04B-P-CD* | 101 | Bulk sediment | UCIAMS-162978 | 7240 ± 25 | 7996-8159 |

*Gagnon-Poiré et al. (2019)

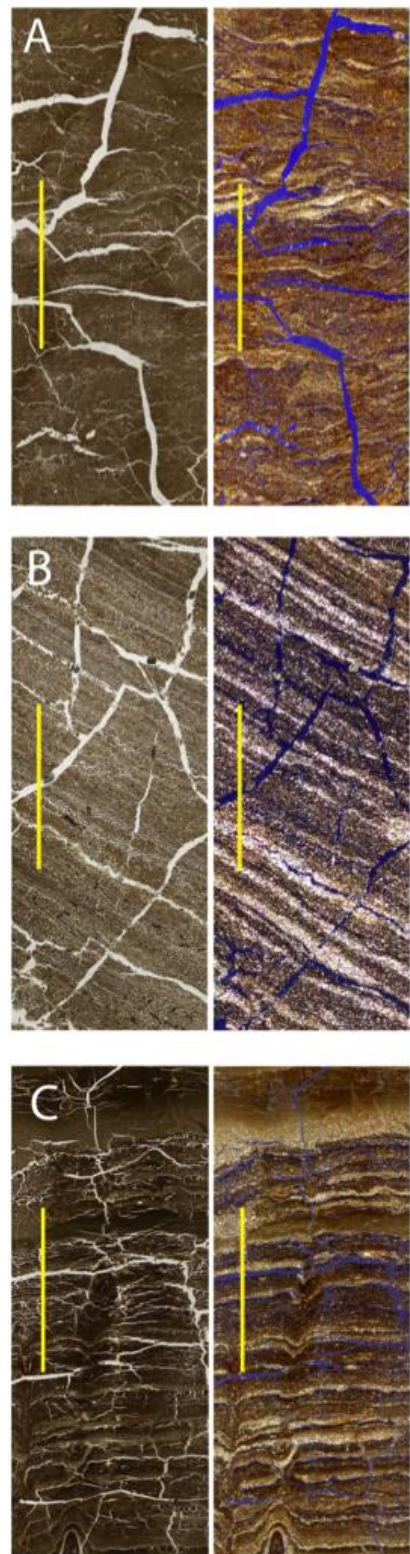


Figure 2.7: Image observation of laminae structure in lower intervals of the reference cores: (A) PC14-04-R, (B) WA14-06-R and (C) PA14-16-R using thin-sections viewed in plane (left) and cross polarized light (right). Scale is 1 cm. Blue backgrounds in the cross-polarized light are due to the embedding resin. In the WA14-06-R and PA14-16-R, visible-distinct laminae couplets comprising a silty lamina and a clayey lamina with sharp contact with the overlying laminae can be seen.

2.5.4 Age-depth models and sedimentation rates

2.5.4.1 ^{210}Pb and ^{137}Cs age models

Figure 2.8 (A-1, B-1 and C-1) depicts ^{210}Pb activity versus depth profiles for the three reference cores. The mean sedimentation- rates and fluxes derived from the three ^{210}Pb models (CRS, CIC and CF-CS) are comparable (Table 2.5). The ^{210}Pb CIC model was selected as the most suitable model because (1) it is least susceptible to the low activity levels of ^{210}Pb measured on the reference cores (where $^{210}\text{Pb}_{\text{total}} < 0.1 \text{ Bq g}^{-1}$ except for the top 2 cm), (2) it takes into account the varying sedimentation rates and fluxes of ^{210}Pb that were observed (Annexe II, Figure S1), and (3) it shows a near-constant slope profile for the three reference cores (Figures 2.8A-1, B-1, and C-1). Moreover, the ^{210}Pb CIC model is in close correspondence with the CRS model in the upper sections of cores PC14-04-R and WA14-06-R; and the mean sedimentation rates averaged from both models are similar (Table 2.5). On the other hand, the ^{210}Pb CF-CS model was the least suitable, as it was most susceptible to decrease in ^{210}Pb unsupported activity levels towards equilibrium, which is evidenced by the wavy outline and age reversals observed (Figures 2.8A-2, B-2 and C-2).

On core PC14-04-R (Lake Pentecôte), mean sedimentation rate of $\sim 0.07 \text{ cm a}^{-1}$ and mean sedimentation flux of $0.03 \text{ g cm}^{-2} \text{ a}^{-1}$ were calculated based on the ^{210}Pb CIC model, respectively (Table 2.5). ^{137}Cs activity starts at 1.8 cm and reaches a peak at 0.6 cm sediment depth (Figures 2.8A-1 and A-2).

On core WA14-06-R (Lake Walker), mean sedimentation rate of 0.07 cm a^{-1} and mean sedimentation flux of $0.03 \text{ g cm}^{-2} \text{ a}^{-1}$ were calculated based on the ^{210}Pb CIC chronology model, respectively. ^{137}Cs activity starts at 1.4 cm and reaches a peak at 0.6 cm (Figures 8B-1 and B-2). These values were compared to results from the reconnaissance core, WA11-W5-R (Annexe II, Figure S2). On that core, mean sedimentation rate of 0.002 cm a^{-1} and mean sedimentation flux of $0.01 \text{ g cm}^{-2} \text{ a}^{-1}$ were calculated based on the ^{210}Pb CIC model, respectively (Table 2.5). ^{137}Cs activity starts at 2.3 cm and reaches a peak at $\sim 1.3 \text{ cm}$ (Annexe II, Figure S2). The equilibrium depth of ^{210}Pb unsupported (where values tend to zero) corresponds to $\sim 3.75 \text{ cm}$.

On core PA14-16-R (Lake Pasteur), mean sedimentation rate of $\sim 0.12 \text{ cm a}^{-1}$ and mean sedimentation flux of $0.09 \text{ g cm}^{-2} \text{ a}^{-1}$ were calculated based on the ^{210}Pb CIC model, respectively (Table 2.5). ^{137}Cs activity starts at 2.2 cm and reaches a peak at 1.8 cm (Figure 2.8C-1 and C-2).

2.5.4.2 Radiocarbon age

A wood fragment collected from core WA14-06-R at 36.5 cm dated $980 \pm 25 \text{ years } ^{14}\text{C BP}$ (790-920 cal BP, UCIAMS-161059), which allowed for estimation of a mean sedimentation rate of $\sim 0.04 \text{ cm a}^{-1}$

for the entire core (Figure 2.5C). Bulk sediment sampled at 101 cm from another core, PC15-04B-PCD from Lake Pentecôte dated 7240 ± 25 years ^{14}C BP (7996-8156 cal BP, UCIAMS-162978) (Gagnon-Poiré et al. 2019) and allowed for estimation of a mean sedimentation rate of $\sim 0.09 \text{ cm a}^{-1}$ for the entire core (Table 2.5).

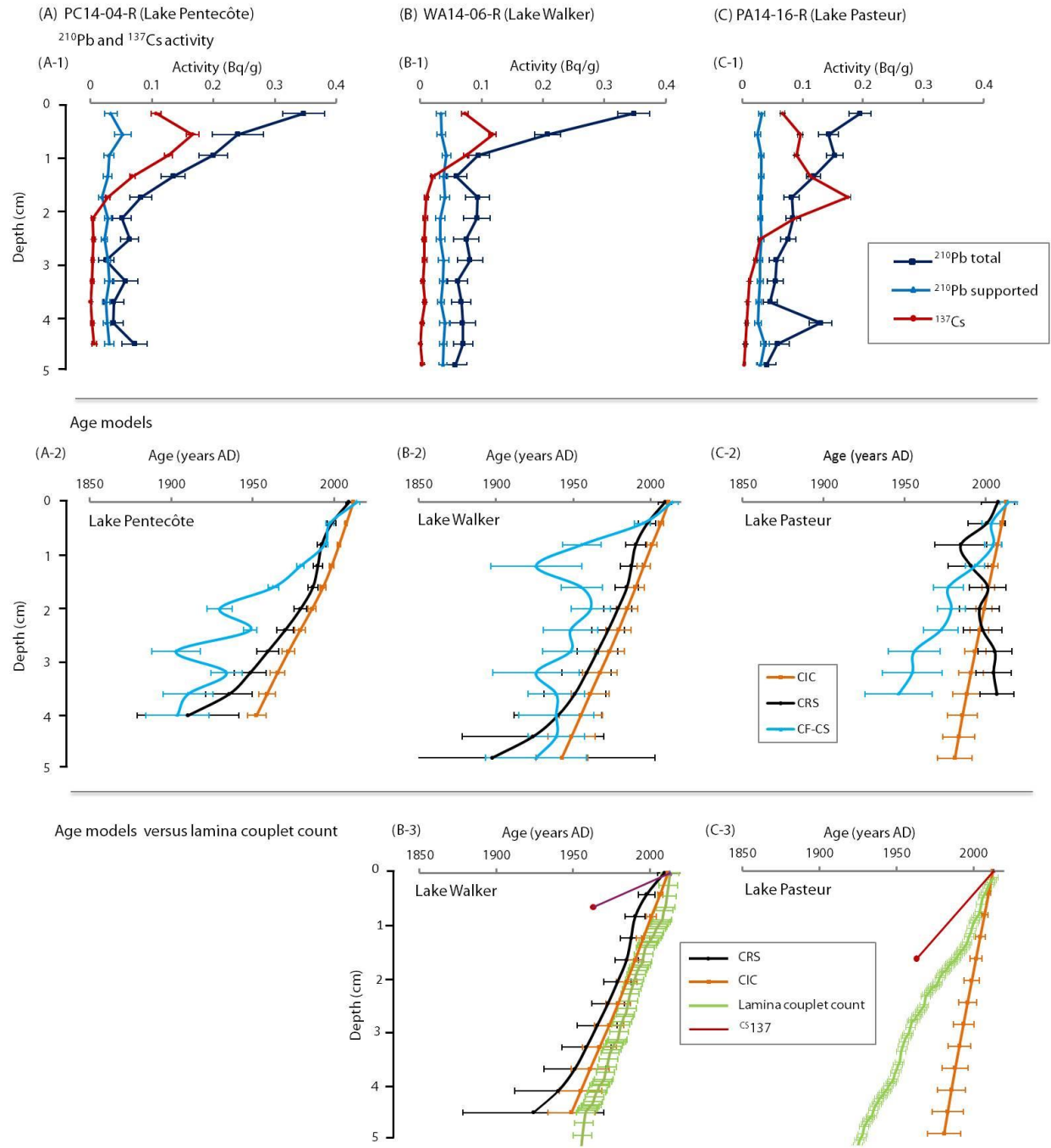


Figure 2.8: Recent chronology (^{210}Pb and ^{137}Cs) for the reference cores from (A) Lake Pentecôte, (B) Lake Walker and (C) Lake Pasteur, respectively: (A-1, B-1, and C-1) Total (measured) and supported (from ^{226}Ra decay) ^{210}Pb activity and ^{137}Cs activity; (A-2, B-2, and C-2) Chronology models based on the constant rate of supply (CRS), the constant initial concentration (CIC) and constant flux–constant sedimentation (CF-CS); (B-3, and C-3) Comparison of applicable age models (CIC/CRS) to lamina couplet counts in the upper sediments of lakes Walker and Pasteur.

Table 2.5: Comparison of sedimentation- rates and fluxes derived from sediment dating from surface cores from lakes Pentecôte, Walker and Pasteur.

| Core | Sedimentation rate (mm a^{-1})* | | | | Sedimentation flux ($\text{g cm}^{-2} \text{a}^{-1}$) | | |
|----------------|--|--------------------------|----------------------------|------------------------|---|--------------------------|----------------------------|
| | ^{210}Pb CRS | ^{210}Pb CIC | ^{210}Pb CF-CS | AMS ^{14}C | ^{210}Pb CRS | ^{210}Pb CIC | ^{210}Pb CF-CS |
| PC14-04-R | 0.64 | 0.68 | 0.48 | | 0.03 | 0.03 | 0.02 |
| WA14-06-R | 0.65 | 0.70 | 0.95 | 0.40 | 0.03 | 0.03 | 0.05 |
| PA14-16-R | 0.04 | 1.15 | 0.87 | | 0.03 | 0.09 | 0.06 |
| WA11-W5-R | 0.11 | 0.02 | 0.02 | | 0.03 | 0.01 | 0.16 |
| PC15-04B-P-CD* | | | 0.90 | | | | |

2.5.5 Comparison of laminae counts to radiometric dating

In order to test the hypothesis that the studied lakes could be annually laminated, laminae counts were compared to the ^{210}Pb model and ^{137}Cs chronology for cores WA14-06-R and PA14-16-R from lakes Walker and Pasteur, respectively. Lake Pentecôte was excluded due to low laminae visibility index (index ≤ 2) irrespective of depth.

In Lake Walker, Figure 2.8B-3 illustrates that the profile of the ^{210}Pb CIC model is consistent with that of laminae couplet counts. Both profiles plots within the error limit (± 6 years) of the other for the uppermost 3 cm sediments interval, and relatively close at lower depths. If the CRS model is considered, there is still close correspondence between the ^{210}Pb CIC versus CRS model and laminae count. The error margin is, however, larger for the CRS model in the lower (3–5 cm) part of the core (Figure 2.8B-3). The CF-CS model was excluded in the comparison due its high margin of error.

In Lake Pasteur, there is divergence between the ^{210}Pb CIC model and laminae counts. The ^{210}Pb CRS and CF-CS models were less comparable due to age reversals and divergence that are associated with that core (Figure 2.8C-3). Figures 2.8B-3 and 2.8C-3 show that there is divergence between the profiles of the ^{137}Cs versus ^{210}Pb chronology (CIC) models and also laminae count.

2.6 Discussion

2.6.1 Catchment and local controls over sediment deposition

The recent sedimentation in lakes Pentecôte, Walker and Pasteur is influenced by interacting factors including limnological, climatic, morphological and possibly dynamic processes. These lakes undergo thermal stratification typical of the boreal climate in that region, and this was confirmed by instrumentation in Lake Walker (Figure 2.3). The transitions between the lower part of the lakes

(containing cooler water) and the upper part (containing warmer water), inferred from measured data (30–40 m in Lake Pentecôte and 50–60 m in Lake Walker; Figures 2.3B and 2.3C) corresponds to the summer thermocline in those lakes (Håkanson and Jansson 2002). Temperature reversals observed in Lake Walker indicate that mixing of the water column occurs twice each year, in May and November (Figure 2.3A), which implies that it is dimictic. Circulation in its water column occurs to ≤ 170 m.

Sediment coring in Lake Pentecôte was fairly extensive compared to lakes Walker and Pasteur due to its accessibility. However, the frequency of partially laminated and massive sediments in Lake Pentecôte could be attributed in part to shallow coring depths (generally < 45 m, Table 2.2) or the influence of processes that inhibit laminae preservation such as sediment mixing due to wind or current driven circulations across the lake's basin (Larsen and MacDonald 1993; O'Sullivan 1983). In Lake Walker, the uniform distribution of laminated sediments (75%) in the distal part of the river deltas (Figures 2.2B, 2.5B and 2.5BB) suggests that sediment deposition is dominated by low-energy suspension settling (Smith 1978; Smith and Ashley 1985). The occurrence of bioturbated facies in two cores that were retrieved in the proximal part of the lake (< 55 m; Figures 3.2B and 3.4B) indicates that sediment disturbance and/or mixing are restricted to the shallow parts of the lake, near the sediment/water interface. It also implies that current and oxic conditions exists in proximal areas near the lake shore, possibly allowing bioturbation (O'Sullivan 1983). Similarly, in Lake Pasteur, the only core that contained LS facies (6 %) was in a deep part, while other cores with PLS facies (94 %) were retrieved from shallower depths (Figures 2.2C and 2.4C).

Lakes Pentecôte, Walker and Pasteur are principally fed by the Pentecôte River, the Gravel and Schmon rivers, and the Pasteur River, respectively from the northern part into the lakes' basin. Although Lake Walker receives fluvial input from two major rivers on its northern part, compared to lakes Pentecôte and Pasteur that receive from one, respectively, the sedimentation rates and fluxes in the central part of the three lakes are of the same order of magnitude, considering the ^{210}Pb models (Figures 2.2, Table 2.5). Also, overall composition of the sediment is similar based on bulk density, calcium carbonate and organic matter contents (Annexe II, Figure S3). Nevertheless, the low mean sedimentation rates in lakes Pentecôte, Walker and Pasteur ($\leq 0.12 \text{ cm a}^{-1}$) are similar to those described in other lakes in southern Québec [e.g. Lake aux Sables: 0.08 cm a^{-1} ; Lake St-Joseph: 0.07 cm a^{-1} ; and Lake Mékinac: 0.18 cm a^{-1} (Trottier et al. 2018)] and other Canadian provinces [e.g. Birchbark Lake: 0.08 cm a^{-1} ; Miller Lake 0.11 cm a^{-1} and Whitemouth Lake (0.15 cm a^{-1}) (Turner and Delorme 1996)].

2.6.2 Relating the presence of laminations to lake morphometry using empirical assumptions

Some researchers have applied empirical relationships to predict laminae formation and preservation in small lakes using morphometric parameters (e.g. Gorham and Boyce 1989; Larsen and MacDonald

1993; Larsen et al. 1998; O'Sullivan 1983; Ojala et al. 2000; Zolitschka et al. 2015). However, there are insights from applying some of those empirical parameters in fjord lakes such as Pentecôte, Walker and Pasteur that are of larger areal size and different geographical context (Table 2.1). For example, a relevant parameter is the relative depth, Z_r (Hutchinson 1957), which was used by O'Sullivan (1983) to illustrate that lakes with stratified water columns might contain laminated sediments, by relating maximum depth (Z_{max}) and lake surface area (A) [where $Z_r = 50Z\sqrt{\pi}/\sqrt{A}$]. In this regard, the relative depth of lakes Pentecôte, Walker and Pasteur is « $Z_r = 2.7, 3.9$ and 1.4 » respectively (Table 2.1). These values fall within the range of those of some large lakes in Europe and North America with significant maximum depth ($Z_m > 70$), in which laminated sediments have been found [e.g. Lac D'Annecy, $Z_m = 82$ (Dearing 1979); Pääjärvi, $Z_m = 87$ (Ojala et al. 2000); Lillooet lake, $Z_m = 137$ (Desloges and Gilbert 1994; Gilbert 1975) and Zugsersee, $Z_m = 197$ (Thompson and Kelts 1974)].

Larsen and MacDonald (1993) demonstrated that small lakes ($<3 \text{ km}^2$) with maximum depths deeper than their critical boundary Z_{m_l} , might preserve laminated sediments, while those with maximum depth Z_m less than the depth of Z_{m_l} , are likely to contain non-laminated sediments. That assumption is valid in a general sense when applied to lakes Pentecôte, Walker and Pasteur (with surface area of 18.9, 41 and 19.3 km^2 respectively), based on obtained Z_{m_l} values and facies distribution (Figure 2.4; Tables 2.1 and 2.2). However, a modified form of Z_{m_l} , the maximum critical boundary (Z_{m_m}) by Larsen et al. (1998) is inapplicable to lakes Pentecôte, Walker and Pasteur because Z_{m_m} is shallower than the depths from which all cores (except two from Pentecôte) were retrieved.

Alternative variables that describe lake basin morphology, for example by considering both size and depth using mean depth of sampled cores, mean- and maximum wind fetch and exposure index (e.g. (Tylmann et al. 2013; Wetzel and Likens 1991) were considered to evaluate facies distribution in lakes Pentecôte, Walker and Pasteur. Table 2.1 shows that Lake Walker has a mean depth ($m = 125$) that is significantly deeper than lakes Pentecôte and Pasteur ($m = 59.5$ and 54.7 respectively), though the three lakes have more or less the same exposure index (ratio of surface area to mean depth). Compared to the other two lakes, Lake Walker also has a longer maximum wind- and mean wind fetch (that describe the distance between coring location and lake shore) due to its greater maximum length ($\sim 30 \text{ km}$) and surface area (41 km^2), which suggests that it is exposed to stronger winds that would likely have its water column mixed at relatively greater depths (Wetzel and Likens 1991). However, the fact that LS facies were preserved on 75% of cores collected from Lake Walker compared to lakes Pentecôte and Pasteur (0 and 6% respectively) indicates that the effects of the longer maximum wind and mean wind fetch are likely compensated by the higher mean depth and maximum depth in the former, as opposed to the latter (Wetzel and Likens 1991). Topographic exposure index calculated for Lake Walker (which is twice as much as the next lake, Pasteur, Table

2.1) is also a factor favouring laminae preservation (Wetzel and Likens 1991). Thus, morphologically, Lake Walker can be distinguished from lakes Pentecôte and Pasteur based on its unique characteristics: higher relative depth, mean depth, maximum depth and topographic exposure (Table 2.1).

2.6.3 Laminated vs possibly varved sediments in the three deep fjord-lakes

The potential of establishing a varve chronology differs in the three studied lakes based on the laminae counts and ^{210}Pb dating. In Lake Pentecôte, the prevalence of massive to partially laminated sediment facies and absence of distinct laminations on core PC14-04-R suggest low potential for annual rhythmicity. In Lake Pasteur, the occurrence of partially laminated sediments and the divergence between the ^{210}Pb CIC model versus laminae counts of core PA14-16-R indicate that it contains laminated sediments that are non-annual.

In Lake Walker, close agreement between laminae counts and the ^{210}Pb CIC and CRS chronology models of core WA14-06-R support the hypothesis that the sediments are likely varves. The validity of the depth of ^{137}Cs peak (supposedly 1963) from two cores from Lake Walker is, however, questionable. On core WA14-06-R, the mean sedimentation rate is 0.07 cm a^{-1} (from the CIC model) and the time span between 1963 (^{137}Cs peak) and 2013 (anchor year for the laminae count) is ~ 50 years. Thus, the supposed depth for the ^{137}Cs peak should be $\sim 3.5 \text{ cm} \ll 50 \text{ a} * 0.07 \text{ cm a}^{-1} = 3.5 \text{ cm} \gg$ rather than the actual depth, 0.6 cm (Figure 2.8B-1). On the reconnaissance core, WA11-05-R, retrieved 3 years earlier, the ^{137}Cs peak is at 1.25 cm (Annexe II, Figure S2), while the supposed depth should be $\sim 0.094 \text{ cm} \ll 47 \text{ a} * \sim 0.002 \text{ cm a}^{-1} = 0.094 \text{ cm} \gg$. In these two cores, the disparity between the supposed and actual depths of ^{137}Cs peak, yet sharp aspect of the ^{137}Cs peak in the profile suggests possible migration of ^{137}Cs in the sediments, which should be interpreted with caution (Davis et al. 1984; Turner and Delorme 1996). Another hypothesis is that coring operations using a free-fall gravity corer (also called rocket corer) at great depth (>100 m) do somehow wash away the very unconsolidated water/sediment interface, even if a clear water/sediment interface is apparent in the core tubes. Systematic errors in laminae counting and the chronologies presented could have resulted from technical sources such as sediment sampling that are associated with thin-section preparation, subjective counting of very fine laminae and/or artefacts of the dating models applied (Appleby and Oldfield 1978; Turner and Delorme 1996; Zolitschka et al. 2015). The hypothesis that the laminations in Lake Walker are varves needs to be verified by recovering sediments with other coring techniques, or extensive radiocarbon dating down core where laminae are better preserved, or sediment trap studies (initial deployment of two sediment traps in Lake Walker was unsuccessful). Nevertheless, this study showed that by comparing several ^{210}Pb (CIC, CRS and CF-CS) and ^{137}Cs models, with laminae counts that varves are likely preserved in the upper part of the sedimentary sequence in Lake Walker.

2.7 Summary and conclusions

This paper analysed short sediment cores collected across transects alongside subbottom profiles in three deep fjord-lakes (lakes Pentecôte, Walker, Pasteur) on the Québec North Shore, Eastern Canada. The main results are as follows:

- Based on visual description of textural properties supported by CT-scan images and ITRAX line scan images, the following postglacial sedimentary facies were identified: Laminated sediments (LS), Partially laminated sediments (PLS), Bioturbated sediments (BS), and Massive sediments (MS). Rapidly deposited layers (RDLs) and a turbidite deposit were also identified. These facies were deposited under modern conditions, and reflect the influence of interacting factors including seasonality, sedimentation rate and depth.
- Morphological parameters, including relative depth, maximum depth and some variables (mean depth, mean wind fetch, maximum wind fetch and topographic exposure) favour laminae preservation in Lake Walker compared to lakes Pentecôte and Pasteur.
- Lake Pentecôte contains mainly massive to partially laminated sediments, while Lake Pasteur contains (partially) laminated facies that reflect non-annual deposition. On the other hand, Lake Walker contains laminated sediments that are better preserved with increasing depth. Despite inconsistencies in ^{137}Cs dating, there is evidence of close correspondence between laminae counts and the ^{210}Pb (CIC and CRS) chronology models, which support the hypothesis that Lake Walker is likely a varved lake. Therefore, Lake Walker is a promising archive for future varve-based paleoenvironmental reconstructions.

2.8 Acknowledgement

The authors thank the Editor, Ali Polat and two anonymous reviewers for constructive reviews in improving this paper. This research was funded by the Natural Sciences and Engineering Research Council of Canada (NSERC) Discovery grants and Ship Time grant, and by the Fonds de Recherche du Québec: Nature et Technologies (FRQNT) – recherche en équipe to P.F, G.S and P.L. Graduate scholarships from GEOTOP (2015) and NSERC CREATE EnviroNorth (2016) to O.N are acknowledged. Reinhard Pienitz at Université Laval is acknowledged for comments and literature that inspired some ideas in this paper. The authors thank members of their research teams: Jean-Philippe Jenny, Arnaud De Coninck, François Lapointe and Thibault Labarrre at INRS-ETE; Etienne Brouard, Annie-Pier Trottier, Francois-Xavier L'Heureux-Houde, Gabriel Joyal and Daniel Deschênes at Université Laval, and Quentin Beauvais, Elissa Barris and Melissa Étorre at UQAR-ISMER for their assistance during fieldwork and/or in the laboratory. Lastly, we thank the management and staff at *La Réserve faunique de Port-Cartier-Sept-Îles* for ease of access to the lakes.

CHAPITRE 3

ARTICLE 2

3 THIN-SECTION ANALYSIS AND DATING OF A NEW ~900-YEAR (LATE HOLOCENE) VARVED RECORD IN LAKE WALKER, QUÉBEC NORTH SHORE, EASTERN CANADA

Obinna P. Nzekwe¹, Pierre Francus¹, François Lapointe^{1, 2}, Guillaume St-Onge³, Patrick Lajeunesse⁴, David Fortin^{1, 5}, Jean-Philippe Jenny⁶, Arnaud De Coninck¹, Édouard G. H Philippe^{3, 7}, Thibault Labarre^{1, 4}

¹Institut National de la Recherche Scientifique, Centre - Eau Terre Environnement, Québec, QC G1K 9A9, Canada, & Canada Research Chair in Environmental Sedimentology & GEOTOP

²Climate Science Center, Department of Geosciences, University of Massachusetts, Amherst, MA 01003, USA

³Institut des sciences de la mer de Rimouski (ISMER), Université du Québec à Rimouski, Canada, & Canada Research Chair in Marine Geology & GEOTOP

⁴Centre d'études nordiques, Département de géographie, Université Laval, Québec, QC G1V 0A6, Canada

⁵Department of Geography and Planning, University of Saskatchewan, SK S7N5C8 Canada

⁶Université Savoie Mont Blanc, INRA, CARRTEL, 74200 Thonon-les-Bains, France

⁷Institut de Physique du Globe de Paris, Sorbonne Paris-Cité, UMR 7154 CNRS, Paris, France

¹Corresponding author: Obinna Nzekwe (obinna_peter.nzekwe@ete.inrs.ca)

Keywords: Laminations, varves, thin-section, Image analysis, scanning electron microscope, Québec North Shore

Article prêt à être soumis au Journal of Paleolimnology

L'analyse de lames minces et la datation d'un nouvel enregistrement de varves d'environ 900 ans (Holocène tardif) au Lake Walker, Côte-Nord, Québec, Est du Canada

Résumé

Cet article présente un nouvel enregistrement de sédiments annuellement laminés (varves) provenant du Lac Walker (région de la Côte-Nord, Québec) pour la période de 2340 à 3200 ± 20 cal BP. Une analyse multi-échelle des laminations d'une séquence composite de ~4.0 m de long a été réalisée à l'aide de la tomodensitométrie et de photographies en haute résolution afin de sélectionner un intervalle avec des laminations régulières et continues. La chronologie de la séquence varvée a été construite selon deux méthodes : le comptage manuel multiparamétrique à l'aide du logiciel PeakCounter et le comptage sur des photos de lames minces au microscope électronique à balayage (MEB). La comparaison des deux méthodes indique que la chronologie des varves construite à l'aide de lames minces présente une meilleure corrélation avec les âges obtenus par datation au radiocarbone. L'épaisseur moyenne des varves est de 0,86 mm. Sur la base de la taille des particules et de l'analyse par microfluorescence aux rayons X, les varves du lac Walker sont principalement «clastiques». Des corrélations de rang de Spearman « rs » entre l'épaisseur des varves et la taille des particules pour toutes les variables calculées, à savoir le diamètre médian apparent (mD_0), écart type (sD_0), percentile 75% (D_{75} µm), 95% (D_{95} µm), 98% (D_{98} µm), 99% (D_{99} µm) et le diamètre maximum apparent ($\max D_0$) sont faibles, positives et monotones ($n = 923$, $p < 0,01$). La plus forte corrélation obtenue est ($r_s = 0,2184$; $p\text{-value} = 0,0001$) entre l'épaisseur des varves et le percentile 75% (D_{75}). Ce nouvel enregistrement varvé offre ainsi une perspective unique pour développer une plus longue reconstitution paléoclimatique à haute résolution dans une région où des enregistrements similaires sont relativement rares.

Mots-clés : Laminations, varves, lames minces, analyse d'images, microscope électronique à balayage, Côte-Nord

Contribution des auteurs

La planification de la campagne de carottage a été réalisée par Obinna Nzekwe, Jean-Philippe Jenny, Pierre Francus et Patrick Lajeunesse. Obinna Nzekwe, Guillaume St-Onge, Édouard Philippe et Thibault Labarre ont participé à la campagne de carottage au Lac Walker en mars 2015. Obinna Nzekwe, Guillaume St-Onge, David Fortin, Édouard Philippe, Patrick Lajeunesse et Pierre Francus ont participé à l'établissement de la séquence composite «WA15-08-U». Toutes les lames minces ont été fabriquées par Obinna Nzekwe ainsi que l'échantillonnage pour la datation radiocarbone et les modèles d'âge. Les analyses XRF ont été effectuées par Obinna Nzekwe après des formations par Arnaud De Coninck. Le comptage des laminations et / ou des varves à l'aide du logiciel PeakCounter ainsi que les analyses statistiques ont été effectués par Obinna Nzekwe. Le comptage de varves à l'aide des lames minces, les ~1000 images prises au MEB et le traitement de celles-ci ont été réalisés par Obinna Nzekwe (O.P.N) en collaboration avec François Lapointe (F.L). Le comptage des varves en lames minces a été effectué indépendamment par O.P.N et F.L. L'interprétation des résultats et l'écriture de l'article ont été réalisées par Obinna Nzekwe en collaboration avec François Lapointe sous la supervision de Pierre Francus. Tous les auteurs ont contribué à la relecture du manuscrit.

3.1 Abstract

This paper presents a new annually laminated record (varves) from Lake Walker, Québec North Shore (eastern Canada) spanning the period from ~2340 to 3200 ± 20 cal BP. The methodology involved multi-scale analysis of laminations from a ~4.0 m long composite sequence using computed tomography and high-resolution photographs in order to select an interval with regular and continuous laminations. The varve chronology was built based on two methods: manual multi-parameter counting using the *PeakCounter* software, and manual counting on thin-section images obtained by scanning electron microscopy (SEM). Comparison of both methods indicates that the varve chronology established using thin-sections correlates more closely with the ages derived from AMS radiocarbon dating, and suggests that thin-section analysis is a more reliable counting technique. The varved sediments from Lake Walker are classified as principally clastic based on particle size and X-ray microfluorescence analyses. Mean varve thickness is 0.86 mm Statistical analysis using Spearman's rank correlation indicates that a low, positive, monotonic association ($n=923$, $p<0.01$) exists between varve thickness and most particle size proxies, including: medium disk apparent parameter (mD_0), standard deviation (sD_0), percentile 75% ($D_{75} \mu\text{m}$), 95% ($D_{95} \mu\text{m}$), 98% ($D_{98} \mu\text{m}$), 99% ($D_{99} \mu\text{m}$) and maximum ($\text{max}D_0$). The strongest correlation with varve thickness is obtained with the 75th percentile ($r_s = 0.2184$, $p\text{-value} = 0.0001$). Results from this study thus indicate that the new varve chronology from Lake Walker presents remarkable prospects of developing a longer and high-resolution paleoclimatological reconstruction in a region where similar records are relatively scarce.

3.2 Introduction

Annually laminated (varved) sediments can serve as reliable archives of past environmental conditions because of the quality of their chronology (Francus et al. 2013a; Ojala et al. 2012; Ojala et al. 2013). Indeed, counting sediment successions deposited over the course of 1 year or less allows establishing precise varved-based chronologies with annual and/or seasonal resolution (Francus et al. 2013b; O'Sullivan 1983; Ojala et al. 2012; Schnurrenberger et al. 2003; Zolitschka et al. 2015).

Knowledge about past climate conditions in the Québec North Shore (Eastern Canada) region during the late Holocene is very limited. To date, only instrumental data and paleoclimatic reconstructions from tree rings and stable isotopes from tree stems covering the past 200-years to the last millennium are available in northern Québec (Arseneault et al. 2013; Naulier et al. 2014; Nicault et al. 2014). However, annually laminated sediments from that period have been generally difficult to find. Hence, discovering a new varved sequence from this boreal region could provide an increased potential to reconstruct regional past modes of climate variability (Figure 3.1).

On the Québec North Shore, in the southeastern Canadian Shield (eastern Canada), three adjacent deep fjord-lakes (lakes Pentecôte, Walker and Pasteur) were studied in order to evaluate laminae preservation and potential for varve formation. Facies analysis of short sediment cores using digital images and thin-sections revealed that the lakes contain bioturbated, partially laminated and well-laminated sediments (Nzekwe et al. 2018). It has been demonstrated that of the three earlier-studied lakes, Lake Walker is characterized by morphological factors that better favour the preservation of sediment laminae, which include higher relative depth, mean depth, maximum depth, critical depth and topographic exposure (Nzekwe et al. 2018). Based on comparison of laminae couplet counts to the chronology derived from ^{210}Pb measurements from a short core (core WA14-06-R from Lake Walker), the uppermost (recent) sediments are believed to be annually laminated (Nzekwe et al. 2018). More so, it was suggested that laminated sediments in Lake Walker are better preserved in deeper parts of the lake based on laminae visibility index (LVI), a semi-quantitative index that was established using image observation of thin sections from core WA14-06-R (Nzekwe et al. 2018). However, the hypothesis that annual rhythmicity exists in sediments older than the last 150 years (Late Holocene) in this lake has not been confirmed yet. Hence, a parallel set of long cores that form a ~400-cm long composite section “WA15-08-U” was collected from Lake Walker in March 2015, which provides a longer sediment sequence compared to the previously analysed 43-cm long core. Therefore, the specific objectives of the present study are to: (1) establish a depth-age model for the Late Holocene from the composite core (WA15-08-U) based on radiocarbon dating, 2) evaluate laminated intervals in the composite core and verify the hypotheses that they are varved, and that laminae preserved improve with increasing depth (Nzekwe et al. 2018), 3) establish a new varve chronology using manual counting and/or conventional thin-section counts, and 4) characterize the

sediment composition.

3.3 Site description

Lake Walker ($50^{\circ} 16.02' N$, $67^{\circ} 9' W$) is a picturesque lake situated on the Québec North Shore, north west of the Gulf of St. Lawrence in eastern Canada (Figure 3.1A-B). The maximum depth of the lake is 271 m (Figure 3.2A) and the elevation above modern sea level is 115 m. It has a ~30-km long predominantly longitudinal north-south oriented basin (Gagnon-Poiré et al. 2019). Morphologically, it is typically U-shaped, with steep sidewalls and relatively deep V-shaped bottom (150–271 m), and thus described as a fjord-lake (Gagnon-Poiré et al. 2019; Lajeunesse 2014). It consists of two deep basins in the northern and southern parts, separated by a central sill. The area of the lake covers 41 km² while its watershed extends over 2187 km² (Gagnon-Poiré et al. 2019).

Lake Walker is dimictic and receives seasonal inputs of surficial material from two rivers, the Schmon and Gravel Rivers that flow into the northwestern and northeastern parts of the lake, respectively (Nzekwe et al. 2018). The headwaters of these rivers originate northwards from the boreal forests around Lake Manicouagan and the Caniapiscau River (Figure 3.1A). The Québec North Shore has a subarctic climate where spring runoff occurs between April and May. Instrumental climatic data for the region are available from isolated meteorological stations, the closest being the Sept-Îles airport ($50^{\circ} 13'00'' N$, $66^{\circ} 15'00'' W$, 52.60 m asl), which is ~70 km east of Lake Walker (Centre d'expertise hydrique 2016). Detailed morphological and limnogeological characteristics of Lake Walker have been presented by Gagnon-Poiré et al. (2019), Normandeau et al. (2016) and Nzekwe et al. (2018).

3.4 Methods and materials

3.4.1 Sediment coring and construction of the composite sequence

The coring location was selected based on previously obtained multibeam bathymetric and subbottom profiler data (Gagnon-Poiré et al. 2019) and short sediment coring (Nzekwe et al. 2018) (Figure 3.2A). A succession of core sections ranging from 100 to 200 cm in length were obtained from Lake Walker at a water depth of ~140 m using a UWITEC piston corer on the lake ice cover (~15 cm) in March 2015 (Figure 3.2A-B). The core sections were retrieved from two boreholes (08C and 08D), which were used to name individual core sections (Table 3.1). A gravity core was also retrieved at the site (08B-G). Collected sediment cores were stratigraphically realigned using marker beds (such as visible laminae, image artefacts and/or rapidly deposited layers) to construct a 352-cm long composite sequence, WA15-08-U (Table 3.1). Hereafter, stratigraphical positions are expressed in composite depths (cm cd).

Since this study mainly aims at establishing the annual nature of the late Holocene sediment

laminations from Lake Walker and the best protocol for their analysis, the entire composite sequence WA15-08-U (0~400 cm cd) was not analysed. Instead, a test interval was selected (~175–263 cm cd; Table 1) based on the quality of laminations preservation and continuity as observed on digital images as described below.

3.4.2 Computed tomography

Whole core sections were analysed using a SIEMENS SOMATOM Definition AS+ 128 Volume Access sliding gantry medical CT-scanner (SIEMENS AG, Munich, Germany) at the *Institut National de la Recherche Scientifique, Centre Eau Terre Environnement* (INRS-ETE). The resulting images (0.6 mm resolution) were shown in gray scale. Gray scale values are expressed as CT numbers or Hounsfield units (HU), a proxy for sediment bulk density, porosity and mineralogy (Boespflug et al. 1995; Cremer et al. 2002; Fortin et al. 2013). Lighter and darker areas indicate higher and lower X-ray attenuations, respectively (St-Onge et al. 2007).

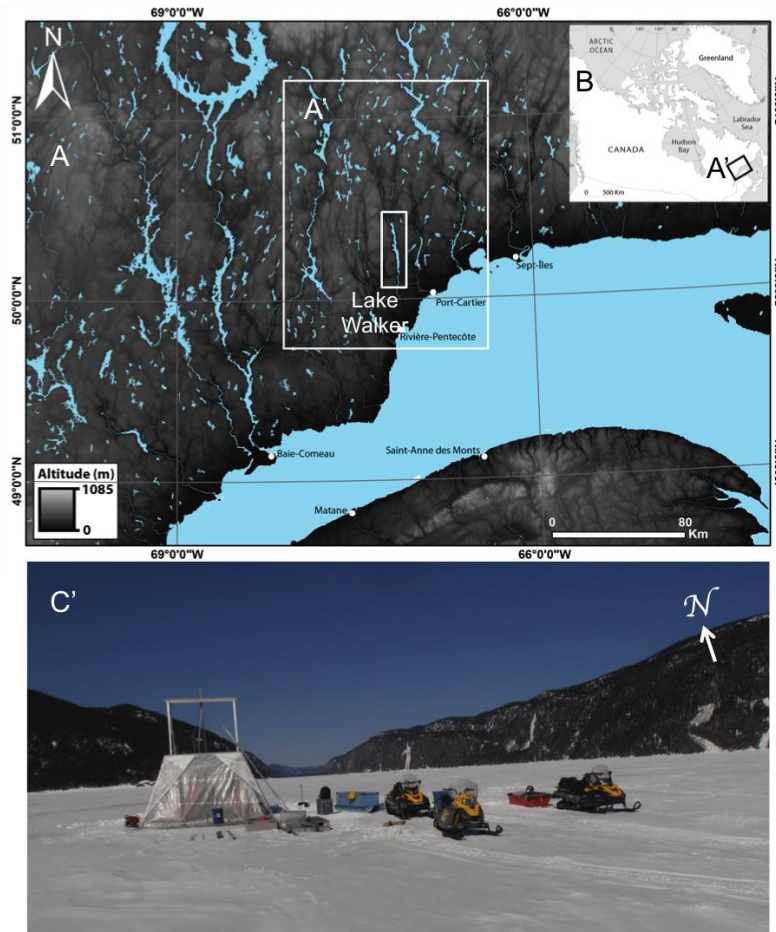


Figure 3.1: (A) Regional setting and geographic location of Lake Walker situated on the Québec North Shore (A') in southeastern Canada, as shown in the insert (B). (C) Panoramic view of Lake Walker (N-S direction). As illustrated, coring in Lake Walker posed technical challenges due to its remote location and geomorphology.

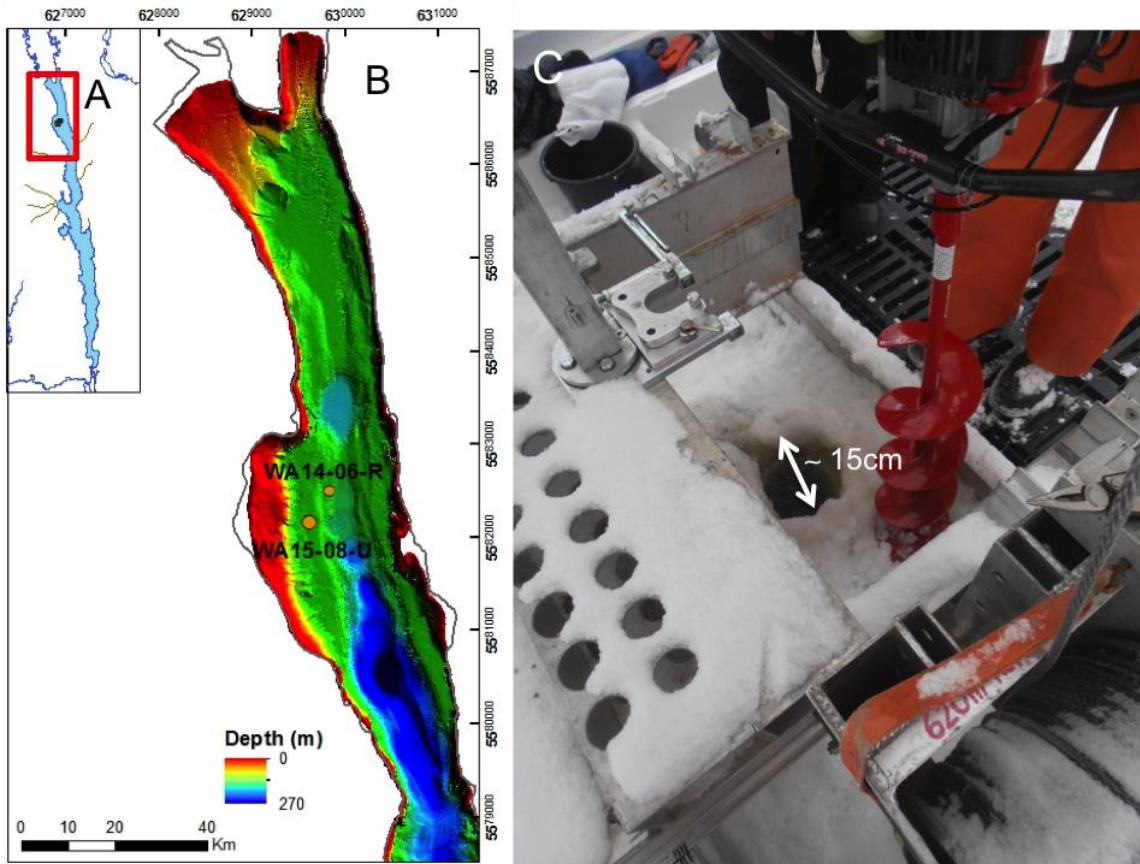


Figure 3.2: A) Showing the northern part of Lake Walker that was cored. B) Multi-beam bathymetry of the cored area (modified from Gagnon-Poiré et al. 2019). Also shown are the location of two cores: core WA14-06-R previously analysed (Nzekwe et al. 2018), and the composite core WA15-08-U (this study); C) shows a photo of the UWITEC piston corer that was used to retrieve cores WA15-08B-G, WA15-08C-U and WA15-08D-U (Table 1) over lake ice cover.

Table 3.1: List of sediment cores used to reconstruct the (~4 m upper part of) composite core WA15-08-U (Lake Walker).

| Core sections | Sections Length (cm) | Core sections depth interval (cm) | Core section depths used to construct composite (cm cd) |
|-----------------|----------------------|-----------------------------------|---|
| WA15-08B-G | 143 | 0–143 | 0–139 |
| WA15-08D-I-U-1 | 84 | 6–90 | |
| WA15-08C-I-U-1 | 134 | 10–144 | |
| WA15-08D-I-U-2 | 90 | 90–180 | *139–178 |
| WA15-08D-II-U-1 | 87.5 | 175–262.5 | *178–262.5 |
| WA15-08C-II-U-1 | 89 | 193–282 | |
| WA15-08D-II-U-2 | 89.5 | 262.5–352 | 262.5–352 |
| WA15-08C-II-U-2 | 96 | 282–378 | |

*Part of the composite core that was subsampled for thin-section analysis. Geographic location of core is shown in Figure 3.2. Correlation panel of cores and list (including depths) of laminations that were used to reconstruct the composite sequence are shown in Appendix III (Figure S1, Table S1).

3.4.3 X-ray microfluorescence and X-radiography

An ITRAX core scanner with a molybdenum tube (Cox Analytical Systems, Mölndal, Sweden) was used to acquire microgeochemical (μ -XRF) and microdensity (radiography) variations in the split long sediment cores at INRS-ETE. Prior to measurement, RGB colour images (50 μm resolution) of the cores were taken using the ITRAX line scan camera. The number of counts for each element in a spectrum acquired for a specific depth interval was normalized by the total number of counts of that spectrum (expressed in counts per second, cps). “Inc” is the incoherent scattering or Compton scattering and “coh” is the coherent or Rayleigh scattering (Croudace et al. 2006). The inc/coh ratio is inversely proportional to the average atomic weight (Croudace et al. 2006). μ -XRF data was acquired at a down-core resolution of 100 μm at an exposure time of 5 s, using a voltage of 30 kV and current of 45 mA. Data were analysed using Q-Spec 8.6.0 software (Croudace et al. 2006). Additional high-resolution radiographs of the split cores were also obtained using a voltage of 50 kV, current of 45 mA and an exposure time of 70 ms.

3.4.4 Stratigraphy, chronology and radiocarbon dating

Terrestrial plant macrofossils (wood fragments) and bulk sediments (in the absence of datable fossils) were collected at various depths from the composite core WA15-08-U (Table 3.2). The samples were prepared for ^{14}C dating at the *Centre d'études Nordiques* (CEN), *Université Laval* and analysed using accelerator mass spectrometry (AMS) at the Earth System Science Department Keck Carbon Cycle AMS Facility at the University of California at Irvine. The dates were calibrated using Calib 7.1 software using the Northern Hemispheric calibration curve INTCAL2013 (Reimer et al. 2013). The age-depth model was established using the Clam software version 2.2 (Blaauw 2010a) interface with the R software (Blaauw 2010b), which allowed for plotting the “best fit” with 95% confidence interval. For the reconstruction of the varve chronology, only the ^{14}C ages within the selected sediment depth interval were considered (Table 3.2).

3.4.5 Lamination and varve counting

A semi quantitative index, the “Lamination visibility index (LVI)” was used to describe the visibility of laminations: 0 - none, 1 - faint, 2 - visible, 3 - clear, and 4 - distinct (Nzekwe et al. 2018) on the composite sequence WA15-08-U. For the reconstruction of the varve chronology, two methods were considered: manual counting using the *PeakCounter* software, and manual counting on thin-sections.

3.4.5.1 Manual counting using PeakCounter

A multi-parameter approach of manual counting using the freeware *PeakCounter* 1.6.4 (Marshall et al. 2012) was used to count the laminations on core WA15-08-U (~175–263 cm cd). In order to

analyse the laminations, the X-ray radiograph (with gray scale values), optical image (from ITRAX line scan camera) and five traceable (XRF) elemental variations (Si, Ti, K, Fe and Ca) and also the inc/coh ratio were evaluated adjacently (e.g. Marshall et al. 2012; Nakagawa et al. 2012). The following pre-defined criteria were set in order to facilitate varve counting using *PeakCounter*: (1) the μ -XRF was run at a high resolution (100 μm) such that peaks in elemental compositions would represent sub-layers in the laminae couplet (varve) structure, and (2) the μ -XRF step size and the X-radiography resolution were the same (100 microns) in order to facilitate correlation of elemental composition and digital images. Considering the mean laminae couplet thickness of ~0.7 mm (minimum laminae couplet thickness is 0.18 mm, maximum laminae couplet thickness is 3.85 mm and the standard deviation is 0.57) in the uppermost (recent) sediments from Lake Walker (Nzekwe et al. 2018), seven μ -XRF measurements (0.1 mm) were obtained on average per laminae couplet.

Similar to the LVI, a varve quality Index (VQI), otherwise described as varve “levels” in the PeakCounter 1.6.4 software (Marshall et al. 2012) was used to describe varves on the core section (~175–263 cm cd) as follows: Level 1: distinct – where high peaks/lows in all selected XRF elements correlate and are distinguishable with laminae/varve boundaries in the digital images. Level 2: clear – where high to medium peaks/lows in at least four XRF elements correlate and are distinguishable with laminae/varve boundaries in the digital images; Level 3: visible – where medium to low peaks in at least three elements correlate but are indistinguishable with laminae/varve boundaries in the digital images; Level 4: faint – where medium to low peaks in two or less XRF elements correlate but are indistinguishable with laminae/varve boundaries in the digital images.

3.4.5.2 Thin-section and grain size analyses

Undisturbed sediments were subsampled using aluminium slabs (measuring 8 x 1.5 x 0.5 cm), freeze-dried and epoxy-resin embedded (Francus and Asikainen 2001). The thin-section slabs were scanned to obtain digital images that were analysed for microscopic counting of laminations using an in-house software developed at INRS-ETE (Francus and Nobert 2007). An error estimate was calculated based on the difference in the number of laminae couplets counted by two independent researchers (O.P.N and F.L.).

Image analysis of thin sections allowed for identification of regions of interest (ROIs) on the flatbed digital scans. Images of the identified ROIs were acquired using SmartSEM software and further analysed using a Zeiss Evo5.0[®] scanning electron microscope (SEM) in backscattered electron (BSE) mode at INRS-ETE. 8-bit gray-scale BSE 1024 x 768 pixels images, with a pixel size of 1 μm , were obtained at a tilt angle of 0°, working distance of 8.5 mm, and accelerating voltage of 20 kV, in order to optimize contrast between clastic grains and clay matrix (Francus et al. 2008; Lapointe et al. 2012). Approximately 1000 BSE images were analysed. For each laminae couplet, the following particle size

distribution (PSD) indices were calculated: medium disk apparent parameter (mD_0) (Francus 1998), standard deviation (sD_0), percentile 75% (D_{75} μm), 95% (D_{95} μm), 98% (D_{98} μm), 99% (D_{99} μm) and maximum ($\text{max}D_0$).

3.4.6 Statistical analysis of proxy data

The physical properties of the laminated sediments such as varve thickness (VT) and particle size indices (mD_0 , sD_0 , D_{75} μm , D_{95} μm , D_{98} μm , D_{99} and $\text{max}D_0$ μm) were analysed using the Paleontological Statistic (PAST) software (Hammer et al. 2001). Univariate analysis was used to calculate measures of location (mean and median), and measures of spread (variance and standard deviation). Normality test using Shapiro-Wilk test indicated that the sample data (VT and particle size indices) were not normally distributed (Annexe III, Table S2), thus statistical correlation of VT and particle size variables was done using a non-parametric test, the Spearman's rank order correlation coefficient (r_s) (Dodge 2003; Hammer et al. 2001). Principal component analysis (PCA) was used to transform the multivariate XRF elements into groups that highlight similarities and differences (Hammer et al. 2001).

3.5 Results

3.5.1 Stratigraphy, chronology and radiocarbon dating

Table 3.2 presents the results of thirteen radiocarbon ages obtained from the laminated intervals in the composite core WA15-08-U (~0–400 cm cd) from Lake Walker. This corresponds to the Late Holocene sedimentation. The age-depth model is constrained by ten AMS ^{14}C ages that span from 4169 ± 50 cal BP to 891 ± 40 cal BP. Three ages derived from bulk sediment sampled at 176, 207 and 350 cm cd, respectively were considered as outliers because they were plotted outside the line of best fit (marked in red colour; Figure 3.3A). Based on the age model, the mean sedimentation rate in Lake Walker during the last ~4 ka BP ranges from 0.52 to 1.75 mm a^{-1} .

The test interval that was selected for varve studies (~175–263 cm cd) spans from 3417 ± 20 cal BP to 2347 ± 20 cal BP (Figure 3.3B). Besides the outliers (as noted above), an age reversal was noticed on the upper part of the selected section, where bulk sediments sampled at 176 cm cd dated 2803 ± 20 cal BP, while wood fragment sampled at 179 cm cd dated 2361 ± 5 cal BP (Table 3.2) (discussed below).

Table 3.2: AMS ^{14}C age of dated materials from the composite core WA15-08-U (Lake Walker).

| Core name | Material | Core section depth (cm) | Composite Depth (cm cd) | UC Irvine Lab # | Université Laval # | ^{14}C a BP | ^{14}C cal BP |
|-----------------|---------------|-------------------------|-------------------------|-----------------|--------------------|----------------------|------------------------|
| WA15-08D-I-U-1 | Bulk sediment | 45 | 47 | UCIAMS-179151 | ULA-6395 | 980 ± 15 | 891 ± 40 |
| WA15-08D-I-U-2 | Bulk sediment | 10.5 | 104.5 | UCIAMS-179152 | ULA-6396 | 1265 ± 15 | 1223 ± 30 |
| WA15-08C-I-U-1 | Wood fragment | 119 | 128 | UCIAMS-179988 | ULA-6442 | 1565 ± 15 | $1466 + 40$ |
| WA15-08D-I-U-2 | Bulk sediment | 51 | 145 | UCIAMS-179153 | ULA-6397 | 1750 ± 15 | 1666 ± 30 |
| WA15-08D-II-U-1 | Bulk sediment | 6 | 176 | UCIAMS-179953 | ULA-6399 | 2735 ± 15 | $2803 \pm 20^*$ |
| WA15-08D-I-U-2 | Wood fragment | 32 | 179 | UCIAMS-179985 | ULA-6441 | 2370 ± 15 | $2361 + 5$ |
| WA15-08D-I-U-2 | Bulk sediment | 89 | 207 | UCIAMS-179154 | ULA-6400 | 2320 ± 15 | 2347 ± 20 |
| WA15-08D-II-U-1 | Bulk sediment | 41.5 | 217.5 | UCIAMS-217742 | ULA-8512 | 2765 ± 20 | 2853 ± 30 |
| WA15-08D-II-U-1 | Bulk sediment | 65 | 241 | UCIAMS-217743 | ULA-8513 | 3035 ± 20 | 3272 ± 40 |
| WA15-08D-II-U-1 | Bulk sediment | 85 | 260 | UCIAMS-179954 | ULA-6400 | 3190 ± 15 | $3417 \pm 20^*$ |
| WA15-08D-II-U-2 | Bulk sediment | 11 | 273 | UCIAMS-179955 | ULA-6401 | 3360 ± 15 | 3608 ± 20 |
| WA15-08D-II-U-2 | Bulk sediment | 50 | 312 | UCIAMS-179956 | ULA-6402 | 3785 ± 15 | 4169 ± 50 |
| WA15-08D-II-U-2 | Bulk sediment | 88 | 350 | UCIAMS-179979 | ULA-6435 | 6180 ± 15 | 7081 ± 15 |

*Dates from the test interval of the composite core (cm cd) from which thin-section were subsampled. Correlation panel of core sections is shown in Appendix III (Figure S1; Table S1).

3.5.2 Laminae visibility and counting

The composite core WA15-08-U (~0–400 cm cd) comprises mainly laminated and partially laminated sediments (Nzekwe et al. 2018) (Figure 3.4). The laminations observed are generally horizontal and continuous (Figures 3.4a, 3.4b). Their “Lamination visibility index” (LVI) (Nzekwe et al. 2018) is between 2 and 4 (visible to distinct) over the entire interval. Within the test interval (~175–263 cm cd; Figure 3.4b–d), the laminations appear clear to distinct (LVI: 3–4).

Figure 3.5 illustrates the downcore XRF data for selected elements (Ti, K, Zr) on core WA15-08-U (~0–400 cm cd), which were transformed into depths based on alignment with sediment laminae. The lower part of the core is characterized by relatively steady and regular elemental variations compared

to the upper part of the core that is characterized by a generally decreasing upward profile. The relatively steady XRF variation within the sediment interval selected for varve analysis (~175–263 cm cd) formed the basis of manual counting of lamination/varves.

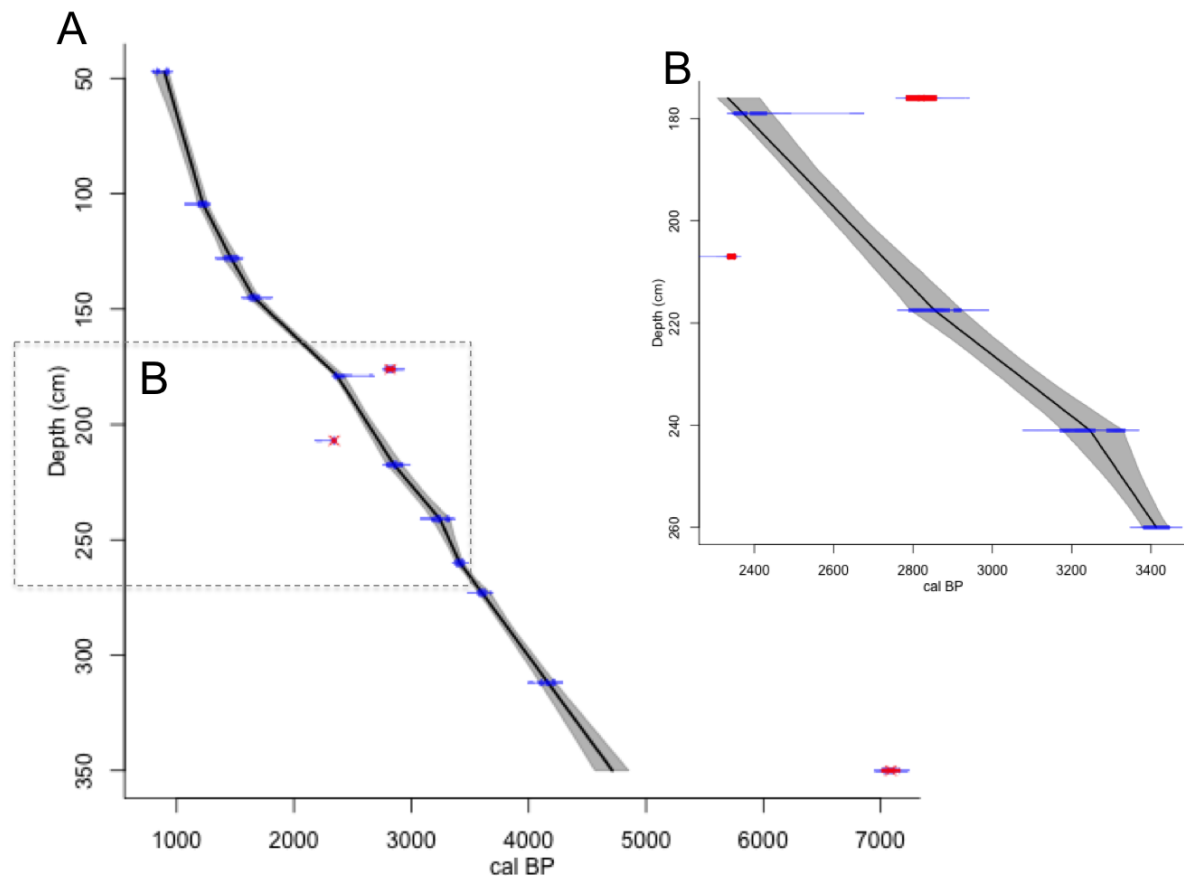


Figure 3.3: (A) Age-depth model of the composite core WA15-08-U (~ 50–350 cm cd) from Lake Walker based on radiocarbon dating. The model is constrained by ten dates, with three other dates as outliers (sampled at 176, 207 and 350 cm cd and derived from bulk sediment; Table 3.2). The insert (B) shows the age-depth model of the section of core WA15-08-U (~175–263 cm cd) that was analyzed for varve occurrence.

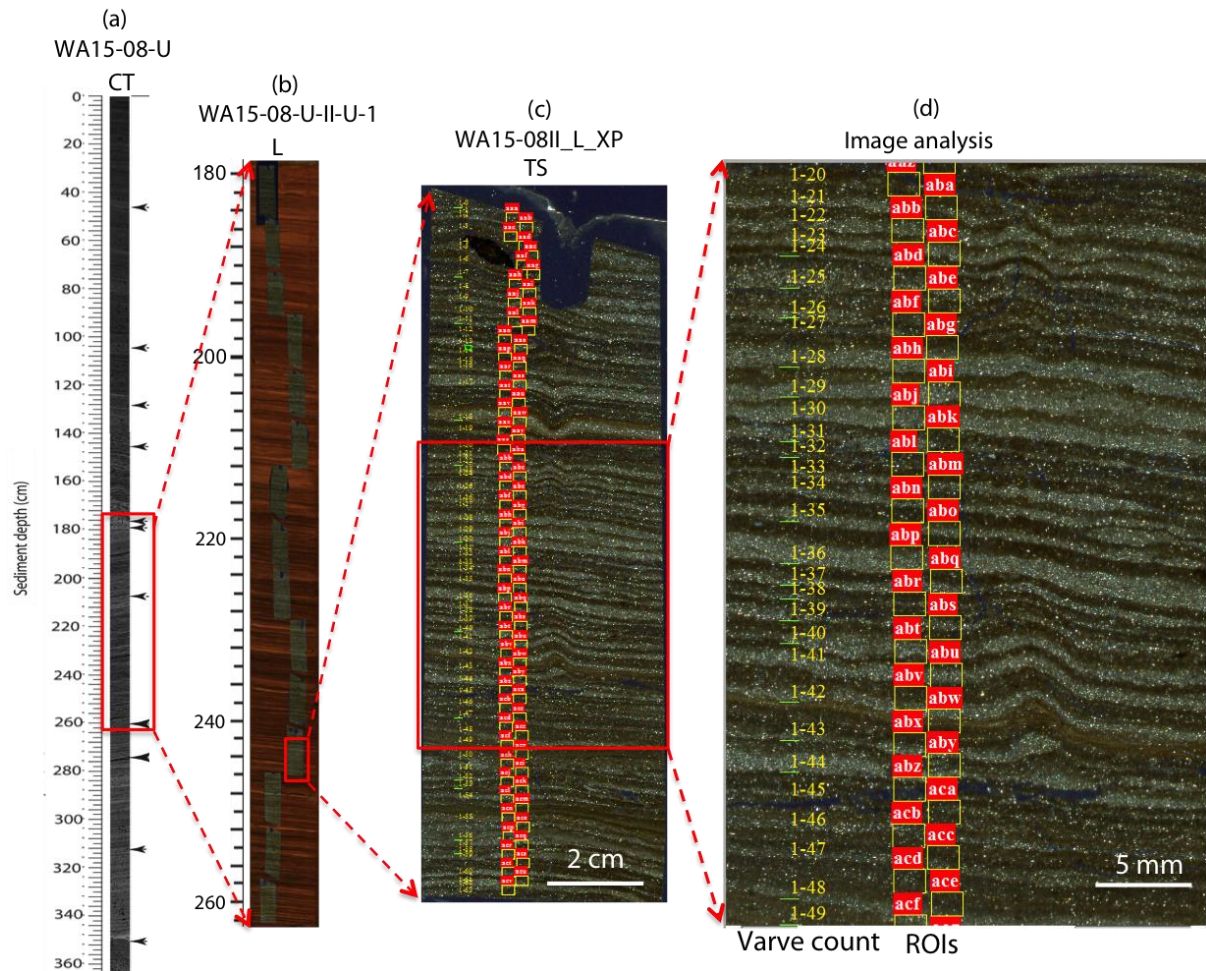


Figure 3.4: Illustration of multi-scale image analyses of the composite core WA15-08-U (Lake Walker) to select a laminated interval and establish a varve record: a) CT-scan of the upper ~4 m part of the core to delineate laminated intervals (black arrows indicate depths sampled for ^{14}C dating); b) Line-scan image of a selected interval with regular laminations; c) Thin-section from the selected interval showing laminae with clear-distinct boundaries; d) Image analysis of varve counts and selection of regions of interests for particle size analysis using SEM.

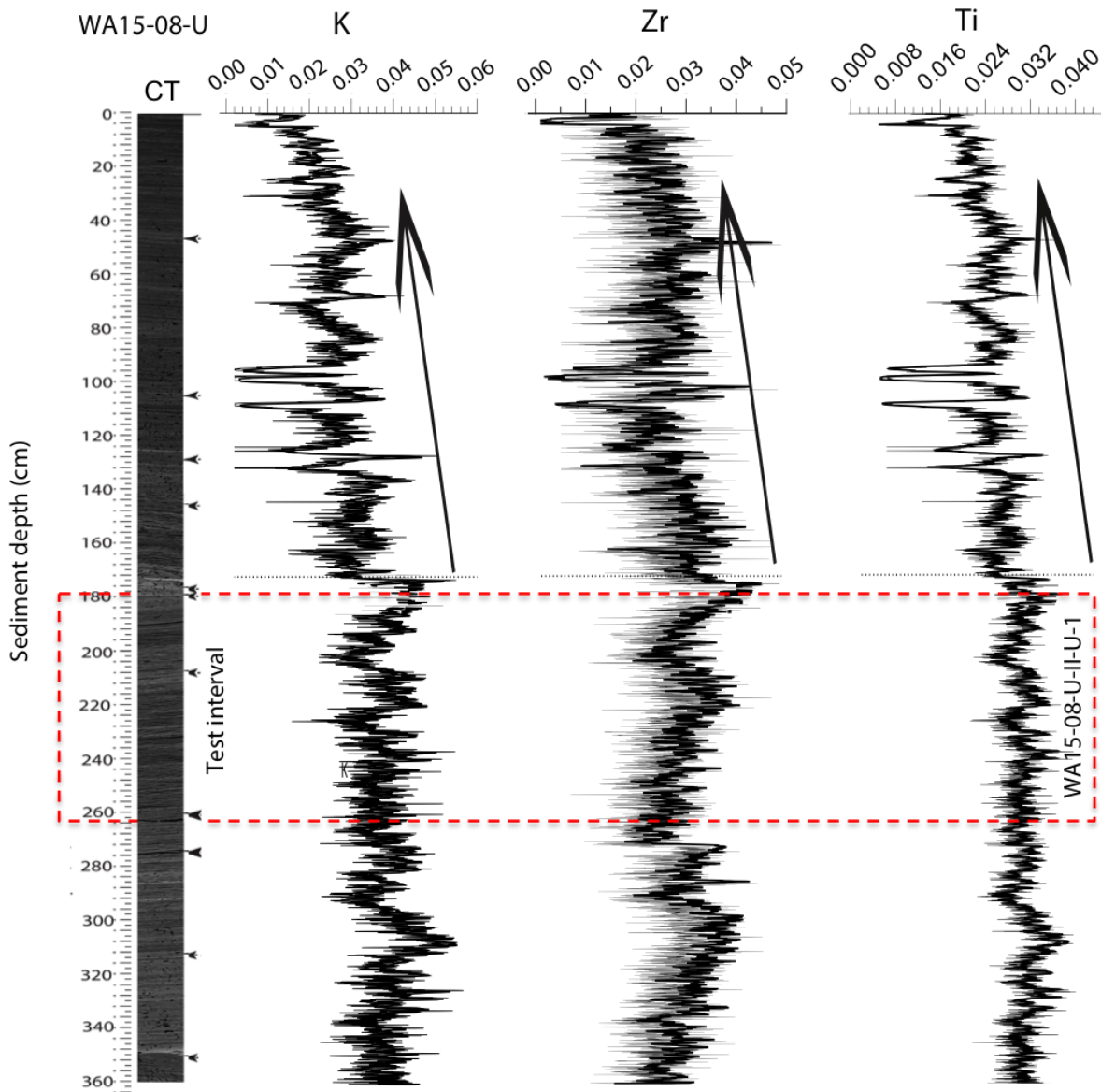


Figure 3.5: XRF data for the composite core WA15-08-U showing CT-scan frontal view (CT) and vertical profiles of selected elements along the core. The number of counts for each element in a spectrum acquired for a specific depth interval was normalized by the total number of counts of that spectrum (expressed in counts per second, cps). Elemental variations are relatively more regular in the lower part of the core compared to the upper part, where they show general upward reduction. For preliminary attempts to establish a varve chronology, the middle part of the core (~175–263 cm cd) was selected for analysis using PeakCounter software (compare with Marshall et al. 2012; see Figure 1.13).

3.5.2.1 Manual counting of laminae couples using PeakCounter

Figure 3.6 presents results of laminae counting from the test interval of core WA15-08-U (~175–263 cm cd) using *PeakCounter*. Specifically, gray scale value from the ITRAX radiograph and five selected XRF elements (Fe, K, Si, Ti and the inc/coh ratio) with traceable concentrations were overlapped and compared within an active window (selected interval) within the core. As shown in Table 3.3, a total of 561 laminae couples were counted within the selected core section (~175–263 cm cd), which includes: 356 “level 1”, 183 “level 2”, 22 “level 3”, and 0 “level 4” laminae couples.

An estimate of 6 to 8 μ -XRF measurements was observed between successively marked laminae couplet boundaries (Annexe III, Figure S3). Three depositional events with thicknesses of ≥ 1 cm characterized by relatively high gray scale value, high Fe, medium Mn and high Si and Ti (not shown) were found at ~ 240 , 241 and 246 cm cd respectively (Appendix III, Figure S4). They are interpreted as rapidly deposited layers (St-Onge et al. 2012; St-Onge et al. 2007).

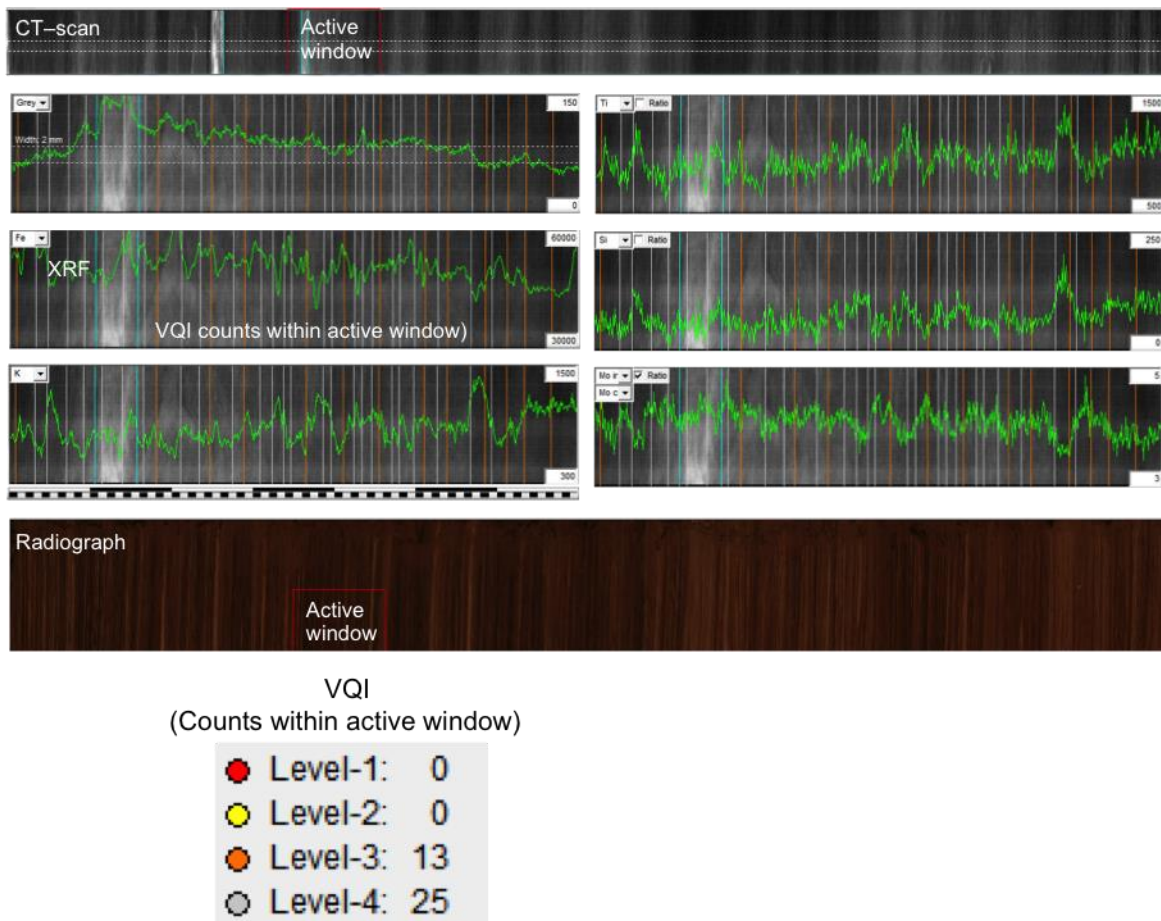


Figure 3.6: Illustration of the multi-parameter approach using the PeakCounter Software (Marshall et al. 2012) for lamina/varve counts on core WA15-08-U (Lake Walker). Parameters include: Radiograph (top) and optical image (below) of the core section (~ 175 – 263 cm cd, Table 3.1). (Middle) for an active window (see radiograph), grey scale and XRF elements (Fe, K, Ti, Si, inc/coh ratio) are overlapped, where vertical marked lines represent laminations labelled based on varve quality index (see levels 1 to 4 colours/marks, as shown in table 3.3).

Table 3.3: Summary data of varve counts on a section of the composite core WA15-08-U (~175–263 cm cd) using the PeakCounter software (Marshall et al. 2012). Level 1, 2, 3, 4 represent the varve quality indices used.

| *Composite depth (~cm cd) | Boundaries | Level-1 | Level-2 | Level-3 | Level-4 |
|------------------------------|----------------------|---------|---------|---------|---------|
| 175 | Core section top' | --- | 0 | 22 | 148 |
| 240 | 'RDL' | --- | 0 | 0 | 0 |
| 241 | 'RDL' | --- | 0 | 0 | 15 |
| 246 | 'RDL' | --- | 0 | 0 | 20 |
| 263 | Core section bottom' | --- | 0 | 0 | 71 |

*Composite depth on core section (WA15-08D-II-U-1; ~175–263 cm cd) that was analysed using PeakCounter software.

3.5.2.2 *Laminae couplet counts using thin-section and image analysis*

Figure 3.7 depicts that the laminae couplets from core WA15-08-U (~175–263 cm cd) comprise two main layers based on thin-section analysis and image analysis of particle size from SEM: a fine silt layer deposited between sprint melt and autumn, and a clay-rich layer deposited during winter. The clay-rich layer, otherwise referred to as clay cap (Francus et al. 2008; Zolitschka et al. 2015) was the main feature used to delineate the laminae couplet boundaries due to their relatively fine and more distinct borders compared to the silt-rich layer (Figure 3.7B). Laminae couplet counts by two independent researchers summed to 901 “varves” (O.P.N) and 923 varves (F.L). The difference between the two individual counts (O.P.N and F.L) ranged from ± 1 to ± 12 varve years per thin-section, with a total difference of approximately ± 22 years for the test interval (~175–263 cm cd). The error in counting ranges from ~0.1 to ~1.5% (Annexe III, Figure S5).

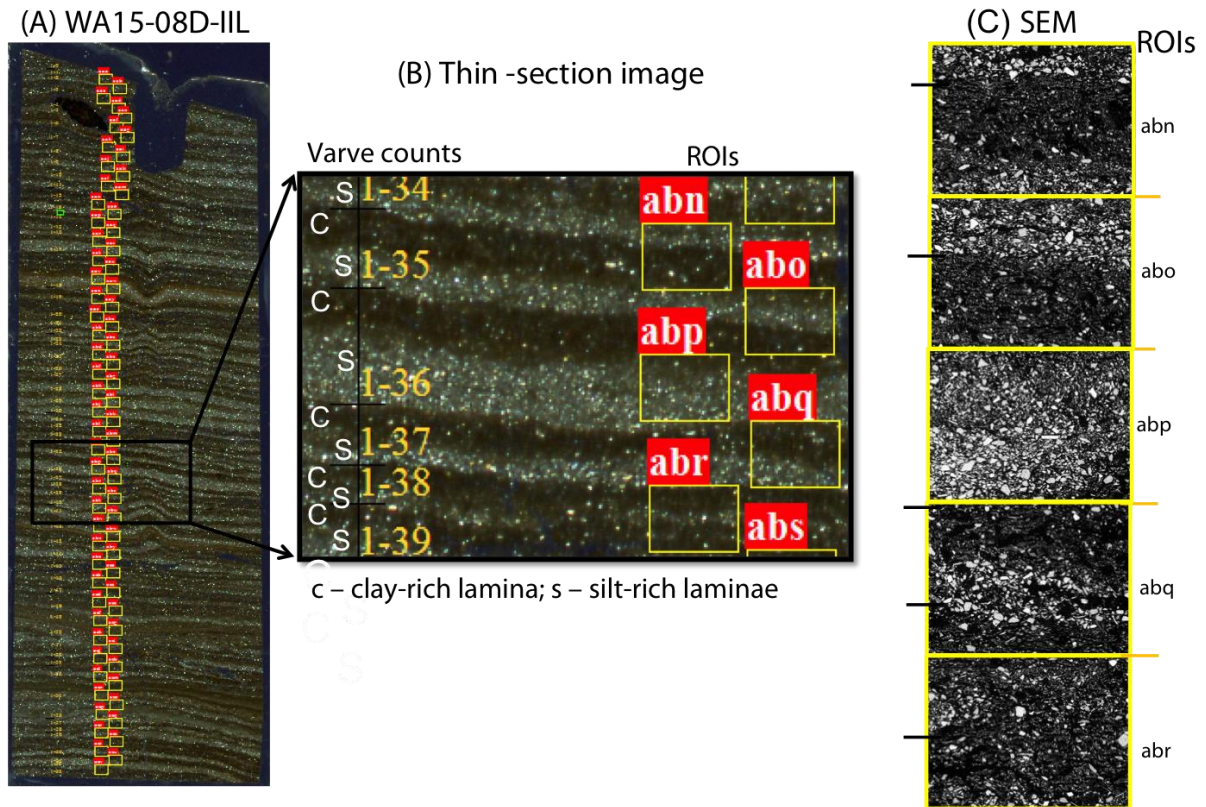


Figure 3.7: Illustration of typical varve structure from Lake Walker, interpreted as clastic varves: A) Flat-bed thin-section image showing (B) two main layers: clay-rich laminae (denoted as “c”) deposited during winter and silt-rich laminae (denoted as “s”) deposited between spring melt and autumn. Black horizontal bars indicate varve boundaries while numbers indicate varve counts (not in years). Regions of interest (ROIs) are shown at the right side lettered squares. (C) SEM images related to ROIs (as shown in B). SEM images show relatively clear contrast between clayey and silty laminae (letters and yellow squares indicate ROI boundaries, while black horizontal lines indicate varve boundaries.

Table 3.4: Univariate statistics of the physical parameters analysed using PAST software from the composite core WA15-08-U (~175–263 cm cd) Lake Walker.

| | VT | mDo | sDo | minDo | maxDo | P75_Do | P90_Do | P95_Do | P98_Do | P99_Do |
|------------|-------|-------|-------|----------|---------|--------|--------|--------|--------|--------|
| N | 923 | 923 | 923 | 923 | 923 | 923 | 923 | 923 | 923 | 923 |
| Min | 0.169 | 5.171 | 2.736 | 3.568 | 16.622 | 7.047 | 9.305 | 11.17 | 13.729 | 14.936 |
| Max | 7.620 | 9.271 | 6.945 | 3.568 | 109.645 | 13.446 | 19.278 | 24.067 | 32.047 | 37.701 |
| Mean | 0.861 | 6.378 | 4.265 | 3.568 | 31.758 | 9.483 | 13.211 | 16.094 | 19.889 | 22.566 |
| Std. error | 0.018 | 0.020 | 0.021 | 2.35E-15 | 0.264 | 0.030 | 0.047 | 0.063 | 0.087 | 0.107 |
| VAR. | 0.289 | 0.380 | 0.414 | 5.12E-27 | 64.232 | 0.848 | 2.053 | 3.648 | 7.053 | 10.594 |
| SD. | 0.537 | 0.616 | 0.643 | 7.15E-14 | 8.015 | 0.921 | 1.433 | 1.910 | 2.656 | 3.255 |

Note: VT – varve thickness (mm), VAR – Variance, SD – Standard deviation

3.5.3 Statistical analysis of particle size proxies

Table 3.4 presents univariate analysis of varve thickness (VT) and particle size data (mD_0 , sD_0 , D75 μm , D95 μm , D98 μm , D99 μm and $\text{max}D_0 \mu\text{m}$) extracted from the test interval of core WA15-08-U (~175–263 cm cd). The mean VT is 0.86 mm (minimum VT is 0.17 mm, maximum VT is 7.62 mm) with variance of 0.29 mm and standard deviation of 0.54 mm (Table 3.4). Spearman's rank correlation indicates that there is a low, positive, monotonic association ($n=923$, $p<0.01$) between VT and particle size parameters (mD_0 , sD_0 , D75 μm , D95 μm , D98 μm , D99 μm and $\text{max}D_0 \mu\text{m}$). Although the correlation coefficient (Spearman's rank order coefficient, r_s) is generally low ($r_s < 0.2$) for all variables, the strongest correlation with varve thickness is obtained with the 75th percentile ($r_s = 0.2184$, $p\text{-value} = 0.0001$; Table 3.5). Results of principal component analysis (PCA) of XRF elements from Core WA15-08-U reveal XRF elemental associations and possible sources of sediments (Appendix III, Figures S6, S7 and S8).

Table 3.5: Spearman's rank correlation of varve thickness and grain size parameters from the composite core WA15-08-U (175 – 262.5 cm cd), Lake Walker.

| VT | mDo | sDo | maxDo | P75_Do | P90_Do | P95_Do | P98_Do | P99_Do |
|---------|------------|------------|--------------|---------------|---------------|---------------|---------------|---------------|
| r_s | 0.1944 | 0.1929 | 0.1586 | 0.2184 | 0.2035 | 0.2042 | 0.166 | 0.1713 |
| p-value | 0.0001 | 0.0001 | 0.0001 | 0.0001 | 0.0001 | 0.0001 | 0.0001 | 0.0001 |

VT - Varve thickness, r_s - Spearman's rank correlation coefficient

3.6 Discussion

3.6.1 Classification of laminae couplets “varves” from Lake Walker

Varved lake sediments are broadly classified into three categories based on their composition, namely: clastic, biogenic and endogenic (Zolitschka et al. 2015). Based on the fine silt layer deposited between spring melt and autumn, and the clay-rich layer deposited during winter, which typically lasts for 5 months, from December to April (Nzekwe et al. 2018), the laminae couplets from core WA15-08-U (Lake Walker) are classified as clastic varves (Figures 3.8A-B). Furthermore, comparison of laminae couplets with XRF data (alignment of XRF with thin-section images) suggests that the fine silt-rich layer is richer in silicate minerals (Si, Ti and Rb), while the clay-rich element is richer in redox-sensitive elements (Fe, Mn).

3.6.2 Comparison of varve counting methods and error estimates

For the test interval of the composite core WA15-08-U (~175–263 cm cd) that was analysed for varve sediments, Figure 3.8 presents a comparison between the varve chronologies constructed using manual counts from the *PeakCounter* software and from individual counts from thin-sections, and the

AMS ^{14}C ages from within the counted interval. The varve chronology model constructed using *PeakCounter* has a steeper slope compared to the chronology constructed from individual thin-section counts, and plots progressively away from the radiocarbon age-depth model. However, the varve chronology model from thin-section counts has a gentler gradient and correlates closely with the radiocarbon age-depth model (Figure 3.8). The mean varve count from the thin-section (black line; Figure 3.8) depicts the average of the individual counts by two independent analysts (O.P.N and F.L). The difference between the two counts (O.P.N and F.L) and the mean varve count defines the standard deviation of the varve chronology (Figure 3.8; Table 3.4).

The difference in varve counts between the varve chronologies established using the *PeakCounter* software and thin-section ranges from ± 5 to ~ 350 varve years (Figure 3.8), which corresponds to an error of $\pm 40\%$. As noted already, error in individual laminae counts (O.P.N and F.L) using thin-section ranges from ~ 0.1 to $\sim 1.5\%$ (Appendix III, Figure S5). For *PeakCounter*, the VQI was used to estimate the error (counts by O.P.N only) based on maximum standard deviation of counts per VQI index. The VQI level 1 (with 356 counts out of 561 total counts) accounted for the maximum deviation, which indicates that the majority of counted varves were “faint”. In summary, the varve chronology established from the thin-sections is interpreted to be more reliable than that from the *PeakCounter* because it more closely follows the AMS ^{14}C (Figure 3.8). The varve chronology from the test interval of the composite core WA15-08-U (~ 175 – 263 cm cd) is anchored on four radiocarbon dates that range from $\sim 2340 \pm 20$ to 3200 ± 20 cal BP (Figure 3.8).

3.6.3 Chronology and radiometric dating

The age-depth model of core WA15-08-U (~ 0 – 350 cm cd) is constrained by ten radiocarbon ages, while 3 ages are considered as outliers. Two of the outliers (at 176 and 207 cm cd) are located near the depth interval where there is an age reversal (between 176 and 179 cm cd). These samples were sampled near the (~ 5 cm) edge of the individual core sections that make up the composite sequence (Tables 3.1 and 3.2), where some disturbance, and possible contamination can occur. As shown in Figure 3.3 (and Table 3.2), the fact that the ages of the two (2) wood fragments, at 128 and 179 cm cd (which are more reliable than bulk sediments) fit in a linear relationship with the ages of eight (8) bulk sediment-derived ages indicates that the radiocarbon age-depth model (Figure 3.8) is robust despite the exclusion of 3 dates. The occurrence of these three outliers and also the age reversal are common issues when dating bulk sediments in the absence of datable macrofossils (Grimm et al. 2009). The two older outlying dates (at 176 and 350 cm cd, respectively) could be attributed to the dating of reworked bulk sediment material, while the occurrence of the younger date (at 207 cm cd) suggest possible contamination during sediment deposition and/or laboratory analysis (Butler et al. 2004; Hajdas et al. 1995). In the case of the lowermost date (at 350 cm cd), it is likely caused by the dating of material from a relatively thick lamina, described as a rapidly deposited layer (St-Onge et al.

2012; St-Onge et al. 2007), which might have preserved older remobilised sediments (Gagnon-Poiré et al. 2019).

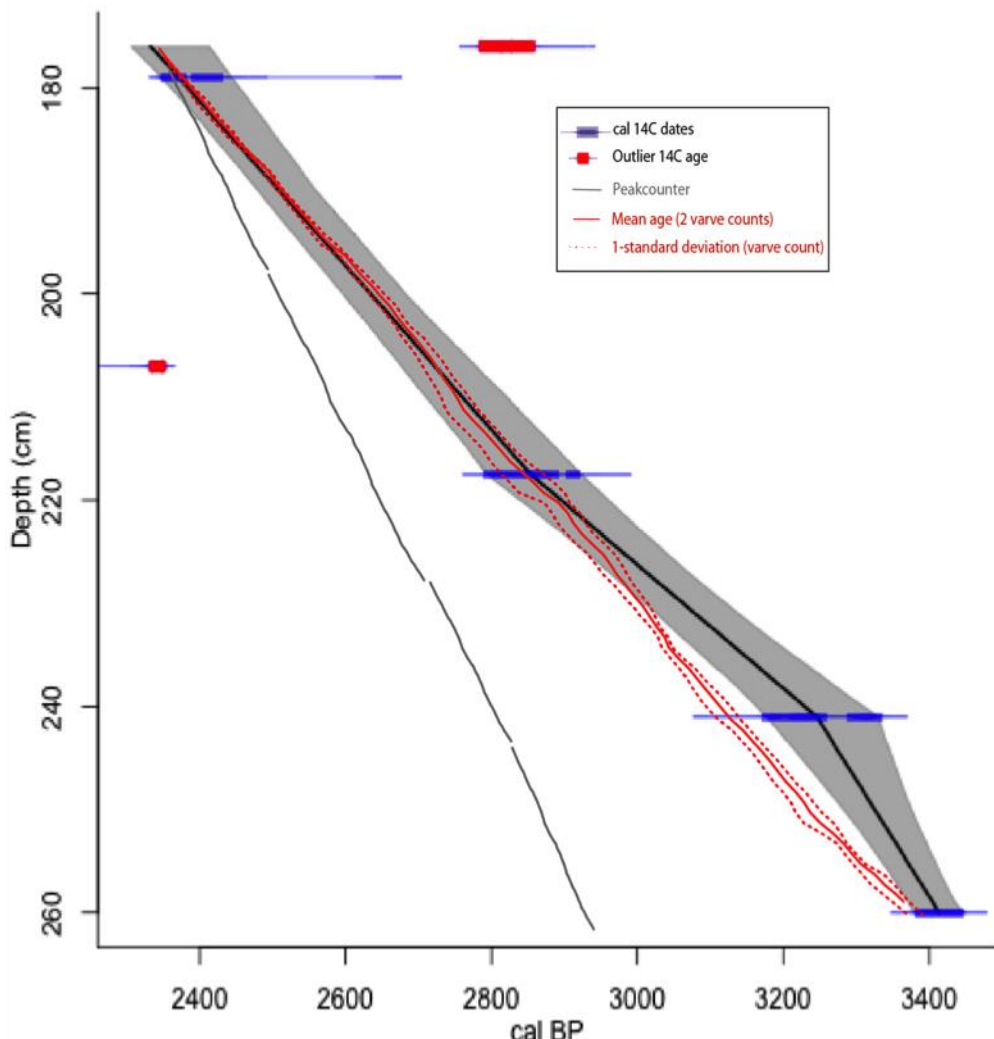


Figure 3.8: Comparison of age-depth models for the laminated interval of core WA15-08-U (~175–263 cm cd) based on AMS ^{14}C dating, semi-automatic counting using PeakCounter software (Marshall et al 2012); two individual varve counts based on thin-sections in this study (O.P.N and F.L); and the mean varve count by the two researchers.

The chronology of recent sedimentation (i.e., deposited during the last ~150 years) in Lake Walker was established by ^{210}Pb and ^{137}Cs dating (Nzekwe et al. 2018). Comparison of the recent sedimentation with the radiocarbon chronology from the present study indicates that the sedimentation rate in Lake Walker during the last ~3.5 ka cal BP ranged from $0.4\text{--}1.75 \text{ mm a}^{-1}$. Such sedimentation rates are comparable to those in lakes within the central and southern regions of the province of Québec, for example, in Lake Pentecôte: $0.48\text{--}0.90 \text{ mm a}^{-1}$ (Nzekwe et al. 2018); Lake Jacques-Cartier: 0.40 mm a^{-1} (Philibert 2012); Lake St-Joseph: 0.7 mm a^{-1} ; Lake Aux Sables: 0.8 mm a^{-1} ; and Lake Maskinongé: 1.8 mm a^{-1} (Trottier et al. 2018), though no varve records have been

reported from these lakes. In general, the sediment accumulation rate of Lake Walker and other nearby lakes suggests that the regional sedimentation rate ranges from 0.4 to \sim 2 mm a $^{-1}$.

This (~900-year) late-Holocene varve chronology from Lake Walker is novel because only limited varved sequences from lakes of similar size and morphology were previously identified in Northeastern America (Ojala et al., 2012). However, records from varved lakes with clastic sedimentation and similar glacial history exist elsewhere, for instance, in Steel Lake, WA, USA: 1.22 mm a $^{-1}$ (Tlan et al. 2005). In the Québec-Labrador region, there is only a similar site reported in recent studies suggesting that Grand Lake contains varve sediments (Fortin et al. 2012; Gagnon-Poiré et al. 2017), which is \sim 1000 km northeast of Lake Walker. Sedimentation rates in that lake range from \leq 1 to \leq 5 mm a $^{-1}$ (Gagnon-Poiré et al. 2018).

Late Holocene varves from Lake Walker are different both in age and laminae structure from glacial varves formed during the last deglaciation in the Northern Hemisphere. Indeed, glacial varves from Lake Hitchcock (Connecticut, USA) (Ridge et al. 2012); Lake Barlow-Ojibway (Ontario-Québec border) (Breckenridge et al. 2012); Lake Jacques-Cartier (Québec, Canada) (Philibert 2012); the Deschaillons varves in the St. Lawrence Valley, Québec (Besré and Occhietti 1990), and varves records from paleoearthquake studies in western Québec-northeastern Ontario (Brooks 2020) are marked by relatively thicker ($>$ 1 cm) varves comprising predominantly clay, and deposited in proglacial environments.

3.6.4 Hypotheses on laminae formation and varve preservation

Favourable conditions for the deposition of varved sediments in clastic environments include: a seasonally contrasted sedimentary supply, adequate sedimentation rates, seasonal or permanent anoxia, and a relatively deep basin (Jenny et al. 2013; Larsen and MacDonald 1993; Larsen et al. 1998; Nzekwe et al. 2018; O'Sullivan 1983; Schnurrenberger et al. 2003; Tylmann et al. 2012; Zolitschka et al. 2015). This study demonstrated that Lake Walker contains laminated and varved intervals during the period 3200 ± 20 to 2340 ± 20 cal BP, and that the preservation of varved sediments generally improves with increasing depth in the composite core.

Indeed, two previously formulated hypotheses on laminae formation and varve preservation in Lake Walker (Nzekwe et al. 2018) were verified based on thin-section analysis. Firstly, the hypothesis that Lake Walker contains varve sediments in deeper intervals has been confirmed (Figures 3.4, 3.7). Furthermore, the hypothesis that laminae preservation generally improves with increasing depth in Lake Walker was also verified, as shown in Appendix III, Figure S9 (Kinder et al. 2013). The error limits in varve counting decreases with increasing depths (Appendix III, Figure S5), suggesting improved laminae preservation (Nzekwe et al. 2018; Tylmann et al. 2012; Zolitschka et al. 2015), which is possibly due to favourable morphological factors such as higher relative depth, anoxia and

less sediment mixing potential (Larsen and MacDonald 1993; Larsen et al. 1998). Also, the LVI and VQI improve with increasing depth, while varve composition remains principally clastic at all depths (Appendix III Figure S9). These interpretations are valid within the test interval covered with thin-sections (~175–263 cm cd). Based on laminae visibility, this study suggests that there are possibly other varved intervals in the Lake Walker composite core (WA15-08-U).

3.6.5 Lake Walker varve record: prospects and challenges

Although laminae couplets on core WA15-08-U were generally visible on CT-scan images, line-scan photos and radiographs, it was, however, difficult to clearly delineate varve boundaries on them (mean varve thickness of 0.86 mm), because their resolution were insufficient, i.e., 0.6 mm, 50 µm and 100 µm, respectively. Using the PeakCounter software for laminae counting proved to be unsuccessful here at adequately delineating laminae couplet boundaries (Figure 3.7, Appendix III Figure S4) because it relies on the Itrax resolution that is 100 µm. Possible sources of error associated with varve counting using *PeakCounter* include: 1) technical challenges such as image resolution with respect to very fine laminae thickness and/or detectable thresholds of XRF elements. Indeed, considering a modal and median varve thickness of 0.65 and 0.74 mm, respectively, it means that more than 50% of the laminations are represented by only 6 to 7 data points, which is an insufficient number for delineating a couplet; 2) subjectivity of delineation of laminations/varves by the analyst (Schlolaut et al. 2012); and 3) depositional events such the presence of rapidly deposited layers (Appendix III, Figure S2), partial or incomplete laminations and low depositional rates (Zolitschka et al. 2015), as observed in Lake Walker.

On the contrary, thin-section and SEM images were more suitable to count varves due to their improved phase contrast and higher resolution (Figures 3.4 and 3.8) (Francus 2006; Francus and Karabanov 2000; Lapointe et al. 2012). Therefore, these images could provide the principal basis for counting laminations/varves from core WA15-08-U. Counting and measuring varves on SEM images were facilitated by the use of an in-house software (Francus and Nobert 2007), allowing multiple counts by different researchers. However, possible sources of error associated with this counting technique include: (1) technical challenges such as cracks in sediments generated during resin embedding and freeze-drying, and cutting successive thin-sections with adequate (at least 1 cm) sediment overlap, and (2) depositional factors, as stated above.

In future studies, the Lake Walker varve chronology could be extended, but will require a set of new thin-sections, possibly from new cores, however it seems clear that micro-facies analysis from SEM images of thin-sections are needed. Annually resolved particle size analysis was performed on the test section of Lake Walker (Figures 3.4, 3.7), opening the prospect of paleoenvironmental reconstructions as performed in other varved records (Lapointe et al. 2012; Lapointe et al. 2019).

The chronology of this sequence remains anchored on radiocarbon dates for the time being. New cores or independent chronostratigraphic methods such as paleomagnetic secular variation and tephrochronology could be useful to calibrate this chronology or to anchor it to another absolute time marker (Bradley 1999; Zolitschka et al. 2015). In the future, there might be a possibility to validate (Late Holocene) varved records from Lake Walker using tree ring data, which at present, extend to the last 1000 years in northern Québec (Naulier et al. 2014; Nicault et al. 2014). Nevertheless, based on radiocarbon dating, the new varve chronology from Lake Walker is reliable, and could possibly show significant links to past climate variability.

3.7 Summary and Conclusion

This study analysed laminated sediments from the composite core WA15-08-U (~0–400 cm cd) collected from Lake Walker, Québec North Shore region, eastern Canada using multi-scale analyses of laminations/varves: CT-scan, μ -XRF, PeakCounter software and SEM image of thin-sections. The main findings are as follows:

- The hypothesis made by Nzekwe et al. (2018) that Lake Walker contains annually laminated sediments from deeper intervals has been confirmed. The application of image analysis of thin-sections and SEM images of the finely laminated sediments from Lake Walker allowed for delineation of varves. Furthermore, the hypothesis that laminae preservation and varve quality generally improves with increasing depth in Lake Walker (Nzekwe et al. 2018) was verified.
- Comparison of the newly developed varve chronology using the *PeakCounter* software and that from thin-section varve counts with AMS ^{14}C ages indicates that the varve chronology model from thin-section correlates strongly with the radiocarbon age/depth model, while the varve chronology constructed using the PeakCounter software correlates weakly. Indeed, due to the very fine lamination typical in Lake Walker (mean varve thickness is 0.86 mm) subsequent studies focussing on thin-section image analysis are recommended.
- This study presents data on the first ~900-year varved record from Lake Walker, Québec North Shore region spanning the interval ~3200 to 2340 cal BP. Based on AMS ^{14}C dating, the new varve chronology from Lake Walker is reliable, and there is a high potential to establish a longer record from other laminated intervals from this lake.

3.8 Acknowledgement

This research was funded by the Natural Sciences and Engineering Research Council of Canada (NSERC) Discovery grants and Ship Time grant, and by the *Fonds de Recherche du Québec: Nature et Technologies* (FRQNT) – recherche en équipe to P.F, G.S and P.L. Graduate scholarships from GEOTOP (2015) and NSERC CREATE EnviroNorth (2016) to O.P Nzekwe are acknowledged. The

authors particularly thank Richard Niedereiter of UWITEC (Mondsee, Austria), Sylvain Boulianne of the *Québec Ministères de Forêts, Faune et Parks* and Thibault Labarre (INRS-ETE) for their assistance during fieldwork in the winter of 2015. Also, thanks to David Fortin (Northern Arizona University), Louis-Frederic Daigle and Mathieu Des Roches (INRS-ETE), Quentin Beauvais (UQAR-ISMER), and Antoine-Gagnon-Poiré (INRS-ETE) for their assistance in the laboratory, respectively. Lastly, the management and staff at La Réserve faunique de Port-Cartier-Sept-Îles are appreciated for easing the access to the lakes.

CHAPITRE 4

ARTICLE 3

4. GLACIAL TO PARAGLACIAL/POSTGLACIAL DEPOSITIONAL TRANSITION IN FJORD-LAKES PENTECÔTE AND WALKER, QUÉBEC (EASTERN CANADA) SINCE THE LAST GLACIATION: A MULTI-PROXY APPROACH

Obinna P. Nzekwe^{1, 5}, Pierre Francus^{1, 5}, Antoine Gagnon-Poiré¹, Patrick Lajeunesse², Guillaume St-Onge^{3, 5}, Alexandre Normandeau⁴, Édouard G. H Philippe^{3, 7, 5}, Camille Brice⁵, Jean-Michel Lemieux⁶

¹Institut National de la Recherche Scientifique, Centre - Eau Terre Environnement, Québec, QC G1K 9A9, Canada, Canada Research Chair in Environmental Sedimentology

²Département de géographie, Université Laval, Québec, QC G1V 0A6, Canada

³Institut des sciences de la mer de Rimouski (ISMER), Université du Québec à Rimouski, QC, G5L 3A1 Canada, Canada Research Chair in Marine Geology

⁴Geological Survey of Canada (Atlantic), Bedford Institute of Oceanography, Dartmouth, NS, B2Y 4A2, Canada

⁵GEOTOP, Université du Québec à Montréal, P.O. Box 8888, succursale Centre-ville, Montréal, QC, H3C 3P8 Canada

⁶Département de géologie et de génie géologique & Centre d'études nordiques &, Université Laval, Québec, QC G1V 0A6, Canada

⁷Institut de Physique du Globe de Paris, 75005 Paris, France

¹Corresponding author. Email: obinna_peter.nzekwe@ete.inrs.ca

Keywords: Sediments, CT-scan, XRF, paleomagnetism, (De)glaciation subglacial, Québec North Shore

Article prêt à être soumis à The Depositional Record

**Transition de sédimentation glaciaire à paraglaciale / postglaciaire dans les fjords lacustres
Pentecôte et Walker, Côte-Nord du Québec (Canada) depuis la dernière glaciation : une
approche par multi-paramètres**

Résumé

Les propriétés sédimentologiques, géochimiques et palynologiques de carottes de sédiments collectées dans deux fjords lacustres sur la Côte-Nord du Québec ont été analysées afin d'accroître nos connaissances sur les changements paléoenvironnementaux qui se sont produits durant la transition du tardi-glaciaire au postglaciaire. À l'aide d'analyses par *Multi-Sensor Core Logger*, tomodensitométrie, microfluorescence aux rayons X, granulométrie, paléomagnétisme et palynologie, deux faciès sédimentaires ont été identifiés : des argiles rythmiquement laminées (RLC) déposées en milieu proglaciaire, et des silts et argiles laminées déposés en milieu paraglaciale à postglaciaire. Ce dernier faciès est divisé en deux groupes : des silts et argiles laminées riches en matière organique (LS-O) déposés en milieu paraglaciale et des sédiments laminés à partiellement laminés (LS) déposés en milieu postglaciaire. La transition de la sédimentation proglaciaire à la sédimentation paraglaciale et postglaciaire est caractérisée par un changement abrupt dans les propriétés texturales, des changements dans les signaux géochimiques (XRF), une augmentation de la diversité des palynomorphes ainsi qu'un changement abrupt des inclinaisons paléomagnétiques. Les datations au radiocarbone suggèrent un hiatus d'âge et/ou de sédimentation entre ~22 et 8 ka cal BP dans le Lac Pentecôte et entre ~18 et 8 ka cal BP au Lac Walker. L'analyse du potentiel hydraulique suggère qu'un lac sous-glaciaire existait probablement dans les bassins des lacs Pentecôte et Walker pendant le Dernier Maximum Glaciaire (20-21 ka cal BP), ce qui pourrait limiter en partie l'érosion et favoriser la préservation des sédiments déposés dans ces bassins sédimentaires avant la déglaciation.

Mots-clés : Sédiments, tomodensitométrie, XRF, paléomagnétisme, (dé) glaciation, sous-glaciaire, Côte-Nord, Québec

Contribution des auteurs

Obinna Nzekwe, Guillaume St-Onge, Édouard Philippe et Thibault Labarre ont participé à la campagne de carottage de la séquence sédimentaire composite «WA15-08-U» au Lac Walker en mars 2015, tandis qu'Antoine Gagnon-Poiré a participé à la campagne de carottage au Lac Pentecôte en février 2015. La planification pour le carottage a été faite en collaboration avec Pierre Francus et Patrick Lajeunesse. Les données bathymétriques à haute résolution et les profils acoustiques de sous-surface (Chirp) ont été acquis par Alexandre Normandeau et Antoine Gagnon-Poiré sous la supervision de Patrick Lajeunesse. Les U-channels pour l'analyse paléomagnétique ont été collectés par Obinna Nzekwe et Edouard Philippe; l'interprétation de ces données a été faite par Édouard Philippe et Guillaume St-Onge. Les analyses palynologiques ont été réalisées par Obinna Nzekwe en collaboration avec Camille Brice. Les analyses de XRF ont été réalisées par Obinna Nzekwe. Le potentiel hydraulique a été modélisé par Antoine Gagnon-Poiré avec l'aide de Jean-Michel Lemieux. Obinna Nzekwe a analysé et réinterpréter les résultats des modèles hydrauliques à la lumière des nouvelles datations au radiocarbone obtenues dans le cadre de cette étude. Tous les auteurs ont contribué à l'interprétation des résultats. Obinna Nzekwe est l'auteur principal du manuscrit qui a été rédigé avec l'aide de Pierre Francus, Patrick Lajeunesse, Guillaume St-Onge et Alexandre Normandeau. Tous les auteurs ont relu la version finale du manuscrit.

4.1 Abstract

Along the Québec North Shore, eastern Canada, the sedimentological, geochemical and palynological properties of sediments from fjord-lakes Pentecôte and Walker were investigated in order to reconstruct Late-Quaternary paleoenvironmental changes that occurred during the transition from glacial to postglacial environments. The methodology involved a set of analyses including: multi-sensor core logger, computed tomography, X-ray microfluorescence, granulometry, paleomagnetism and palynology. Two main sediment facies were identified: a rhythmically laminated clay (RLC) facies deposited in a proglacial environment, and a laminated sediment facies deposited in paraglacial/postglacial environment. The latter is divided into two subfacies: laminated (organic-rich) silty clay and clay (LS-O) facies deposited in a paraglacial setting, and laminated to partially laminated sediments (LS) facies deposited in a postglacial setting. The transition from proglacial to para/postglacial sedimentation is characterized by abrupt changes in textural properties, shifts in geochemical (XRF) signatures, increase in palynomorph diversity, as well as negative paleomagnetic inclinations. Based on radiocarbon dating, age and/or sedimentation hiatus is inferred in lakes Pentecôte and Walker between ~22 and 8 ka cal BP and between ~18 and 8 ka cal BP, respectively. Hydraulic potential modeling indicates that subglacial lakes likely existed in the lakes Pentecôte and Walker basins during the Last Glacial Maximum (20-21 ka cal BP) prior to deglaciation, favouring the preservation of previously deposited sediments in both basins.

4.2 Introduction

Fjord-lakes refer to deep lakes with steep sidewalls situated in glacial and/or preglacial overdeepened valleys (Eyles et al. 1990; Gagnon-Poiré et al. 2019; Lajeunesse et al. 2016; Nasmith 1962). Due to their geomorphological characteristics, fjords provided preferential corridors during Quaternary glaciations for the ice flow from the interior of the ice sheet to the marine environment (Gagnon-Poiré et al. 2019; Syvitski and Shaw 1995; Syvitski and Praeg 1987). Sediments preserved at their bottom can provide useful information for reconstructing paleoenvironmental succession from glacial to postglacial sedimentary regimes (Bertrand et al. 2012; Boyd et al. 2008; Lajeunesse 2014; St-Onge et al. 2012). Fjords occurring in glacio-isostatically uplifted coastal lacustrine environments are useful in reconstructing the paleogeography of former neritic zones and/or paleo-terrestrial–ocean interactions through multi-proxy analyses including textural, mineralogical, geochemical and preserved fossilized remains (Antoniades 2017; Campos et al. 2014; Casse et al. 2017; de Vernal 2009; Rothwell and Croudace 2015).

During glaciation, fjord-lake and other deep lake basins provided favourable sites for the formation of subglacial lakes due to their deep geological basins (Christoffersen et al. 2008; Lesemann and Brennand 2009). Favourable conditions for the formation of subglacial hydraulic systems include: 1) geological valleys or cavities, 2) flat or low-angled ice sheets with warm bedded conditions, and 3) basal hydraulic systems that include the ponding and drainage of subglacial meltwater (Flowers 2015; Gagnon-Poiré 2016; Herman et al. 2011). Some studies report that such conditions existed below the Laurentide Ice Sheet (LIS) that covered the Gulf of St. Lawrence and Atlantic Canada (Christoffersen et al. 2008; Livingstone et al. 2012). Thus, subglacial lakes may have existed in some of the fjords-like lakes in that region (Dietrich et al. 2017b; Evatt et al. 2006; Gagnon-Poiré et al. 2019; Lajeunesse 2014; Syvitski and Praeg 1989).

Along the St. Lawrence Estuary and adjoining areas, the northward retreat of the Laurentide Ice Sheet (LIS) has been reconstructed based on the dating of ice-contact deposits (Occhietti 2007; Occhietti et al. 2011), delta morphostratigraphy (Dietrich et al. 2017a) and high-resolution acoustic stratigraphy (Gagnon-Poiré et al. 2019; Normandeau et al. 2016; Syvitski and Praeg 1989). According to Syvitski and Praeg (1989) five main seismo-stratigraphic units within the Quaternary sequence in the region include: 1) ice-contact deposits; 2) ice-proximal sediments; 3) ice-distal sediments; 4) paraglacial deltaic sediments that reflect the melting of terrestrially-based ice caps accompanied with rapidly falling sea; and 5) post-glacial sediments that reflect sediments deposited after the disappearance of glacier from the lake watershed. Dietrich et al. (2017a) noted that depositional systems formed in deltaic complexes of the Québec North Shore, eastern Canada during the LIS retreat include: 1) ice-contact deposits; 2) ice-distal glaciofluvial delta; and 3) paraglacial suites.

On the Québec North Shore, high-resolution swath bathymetry imagery, subbottom profiles and

sediment cores were recently collected from three adjacent fjord lakes (lakes Pentecôte, Walker and Pasteur) in order to reconstruct the geomorphological history in the watersheds of these lakes since deglaciation (Gagnon-Poiré 2016; Gagnon-Poiré et al. 2019; Normandeau et al. 2016). Four conformable units have been delineated in the basin of the three lakes based on acoustic stratigraphy, namely: acoustic basement; ice-loaded sediments; rhythmically laminated silts and clays; and postglacial sediments (Gagnon-Poiré et al. 2019). The transition from glacial to paraglacial/postglacial sedimentation in the watersheds of lakes Pentecôte and Walker was dated 8000–8160 cal BP and 7845–7950 cal BP, respectively based on accelerator mass spectrometry (AMS) radiocarbon dating of plant macrofossils and bulk sediment (Gagnon-Poiré et al. 2019). Although the geomorphology and Quaternary history of the lakes were previously presented (Gagnon-Poiré 2016; Gagnon-Poiré et al. 2019; Normandeau et al. 2016), a detailed understanding of the direct land-sea correlations and/or succession from glacial to postglacial conditions in the studied lake basins is still lacking.

This study explores multi-proxy analyses of long sediment cores retrieved from two of the three earlier-studied lakes (lakes Pentecôte and Walker) in order to constrain previous conceptual paleogeographical models of the lake basins (Gagnon-Poiré et al. 2019; Occhietti et al. 2011; Syvitski and Praeg 1989) with specific focus on the glacial to postglacial transition. The specific objectives are to: 1) describe the lithostratigraphy and sedimentary facies based on core scanning and logging, granulometry, palynology and paleomagnetism in order to reconstruct successive depositional transition from the glacial to postglacial sedimentary environments; 2) establish age-depth models for this transition using radiocarbon dating; and 3) test the hypothesis that a subglacial lake may have existed at the location of lakes Pentecôte and Walker (Gagnon-Poiré 2016), and its implication on the glacial history of the studied lakes.

4.3 Studied lakes

Lakes Pentecôte and Walker) have maximum depths of 130 and 271 m, respectively, and are located on the Québec North Shore, in the northwestern Gulf of St. Lawrence, eastern Canadian Shield (Figure 4.1A). The elevation of lakes Pentecôte and Walker is 84 and 115 m above sea level (asl) respectively. They lie below the marine limit reached by the deglacial sea transgression associated with glacio-isostatic depression, which is 130 m asl in the Québec North Shore region (Nzekwe et al. 2018). The lakes are located downstream of north-south trending glacial valleys, more specifically, in the transition zone between the Laurentian Highlands (>300 m asl) and the coastal lowlands (Gagnon-Poiré et al. 2019). Bedrock geology of the region falls within the Precambrian Grenville complex of the Canadian Shield. Granitic and paragneissic rocks underlie most parts of Lake Pentecôte (Mouksil et al. 2011), while Lake Walker is underlain by homogenous granitic gneiss complexes (Ministère des ressources naturelles du Québec 2002).

Morphologically, the Lake Pentecôte basin has an area of 18.9 km² and consists of three bathymetric zones: a northern sector that reaches 50 to 60 m-deep, a central basin that reaches 130 m-deep, and a southern sector characterized by a central narrow trough (Gagnon-Poiré et al. 2019) (Figure 4.1B). The Lake Walker basin spans 41 km² and consists of a northern basin that reaches 260 m-deep and a steep-sided southern basin that reaches 271 m-deep, separated by a central sill (Gagnon-Poiré et al. 2019) (Figure 4.1C). Detailed morphological and limnogeological characteristics of the lakes have been described by Normandeau et al. (2016), Gagnon-Poiré et al. (2019) and Nzekwe et al. (2018).

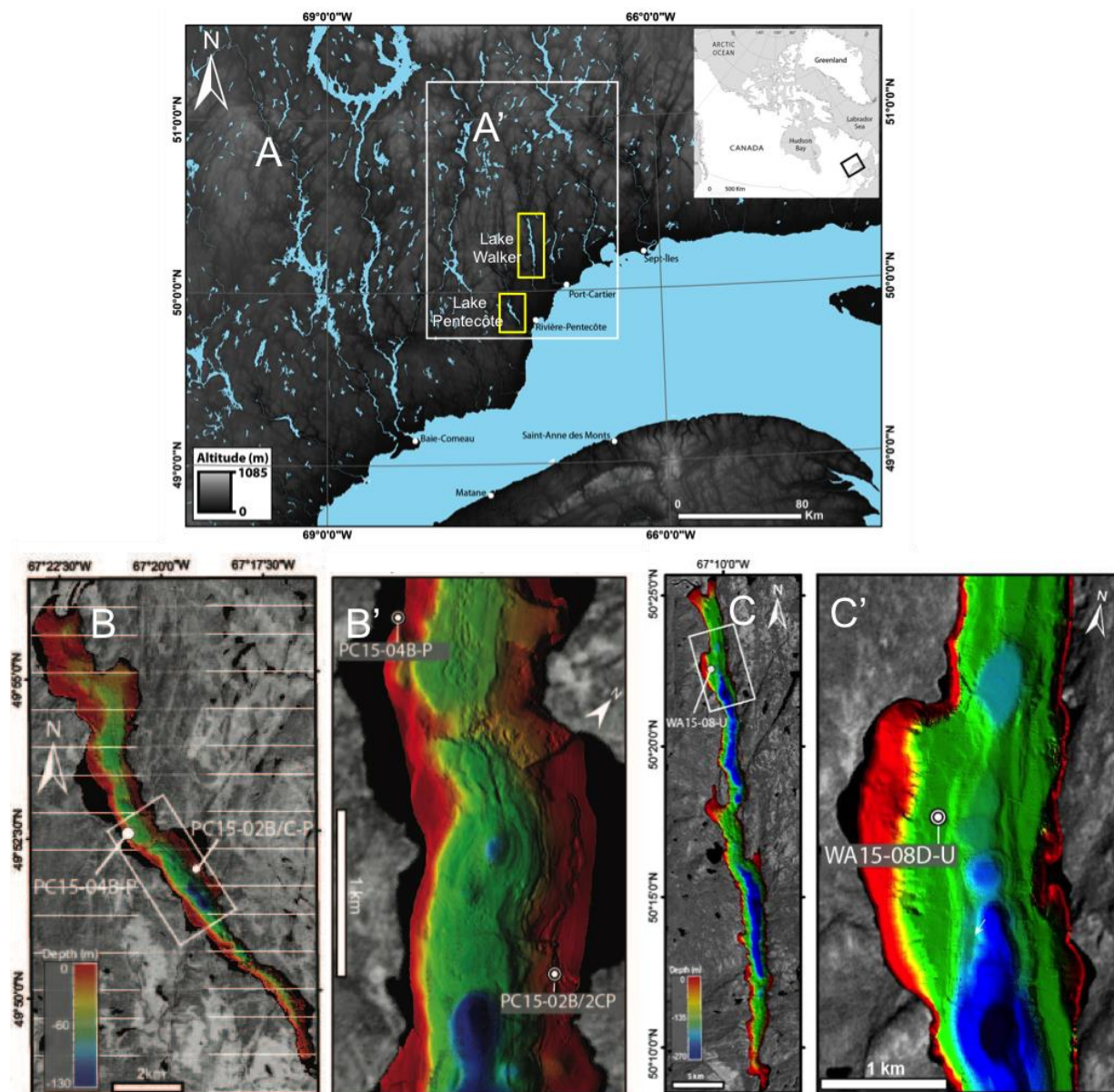


Figure 4.1: (A) Geographic location of the Québec North Shore region, eastern Canada. (A') indicates the location of lakes Pentecôte (PC) and Walker (WA) (shown within yellow rectangles). Also shown are images of multibeam bathymetry of (B) Lake Pentecôte (1-m resolution) and (C) Lake Walker (3-m resolution). The inserts (B', C') indicate the cored area in the both lakes and the location of analysed cores (Table 4.1) (adapted from Gagnon-Poiré et al. 2019).

4.4 Methods and materials

4.4.1 Fieldwork and sediment coring

Long sediment cores (>1 m) were collected from Lake Pentecôte using a universal percussion corer (Aquatic Research Systems, Idaho, USA) in February 2015. In Lake Walker, a parallel set of cores forming a composite section, WA15-08-U was recovered using a UWITEC piston corer (UWITEC, Mondsee, Austria) in March 2015. The individual cores forming the composite were realigned stratigraphically (using high-resolution images and marker beds); hence composite depths differ slightly from those that have been previously reported (Gagnon-Poiré et al. 2019). In order to focus on the transition from glacial to paraglacial/postglacial sedimentation in the two lakes, two cores (PC15-02C-P and PC15-04B-P) were selected from Lake Pentecôte (Figure 4.1B; Table 4.1), while the lower part of the composite core WA15-08-U, ~480–729 cm cd (established by Nzekwe et al.; Chapter 3) from Lake Walker was studied in detail (Figure 4.1C; Table 4.2).

Table 4.1: List of sediment cores analysed from the Lake Pentecôte.

| S/N | Core name | Lake | Latitude (°) | Longitude (°) | Depth (m) | Length (cm) | Remark |
|-----|------------|-----------|--------------|---------------|-----------|-------------|-----------------|
| 1 | PC15-04B-P | Pentecôte | 67.351828 | 49.875952 | 9 | 184 | Percussion core |
| 2 | PC15-02C-P | Pentecôte | 67.321879 | 49.865501 | 19 | 43 | Percussion core |

Table 4.2: List of sediment cores that were used to reconstruct composite core, WA15-08-U (~488-740 cm cd) from Lake Walker.

| Core | Lake | Latitude (°) | Longitude (°) | Length (cm) | Depth interval (cm) | Composite depth selected (cm cd) |
|------------------|--------|--------------|---------------|-------------|---------------------|----------------------------------|
| WA15-08C-III-U-1 | Walker | 67.176944 | 50.377221 | 79 | 488-638 | 488-634 |
| WA15-08D-IV-U-1 | Walker | 67.176944 | 50.377221 | 80 | 580-660 | 634-660 |
| WA15-08D-IV-U-2 | Walker | 67.176944 | 50.377221 | 83 | 660-740 | 660-740 |

Correlation panel of cores and list (including depths) of markers/laminations that were used to reconstruct the composite sequence of are shown in Appendix III (Figure S1).

4.4.2 Core scanning and logging

Whole core sections were analysed using a SIEMENS SOMATOM Definition AS+ 128 computer-axial tomography system (CT-scanner) (SIEMENS AG, Munich, Germany) at the Institut National de la Recherche Scientifique, Centre Eau Terre Environnement (INRS-ETE). The images derived are shown in gray scale, with values expressed as CT numbers or Hounsfield units (HU). Images were processed using ImageJ software (Schneider et al. 2012). Lighter and darker areas indicate higher and lower X-ray attenuations, respectively (St-Onge and Long 2009). Shortly after splitting and prior to

oxidation of the sediment core surface, digital photographs were taken using a GEOTEK Geoscan IV line-scan camera ($50\text{ }\mu\text{m}$ pixel size) attached on a GEOTEK Multi-Sensor Core Logger (MSCL; Geotek Ltd., Northamptonshire, UK) at the Institut des sciences de la mer de Rimouski (ISMER), Canada. Continuous physical properties including magnetic susceptibility were measured at 1 cm intervals from split sediment cores using the MSCL. Diffuse spectral reflectance was measured using a CM26000d spectrophotometer mounted on the MSCL and afterwards converted into the L*, a*, b* colour space of the International Commission on Illumination (CIE). L* value ranges from 0 (black) to 100 (white), while a* and b* vary from +60 (red) to -60 (green) and +60 (yellow) to -60 (blue), respectively (St-Onge et al. 2007).

An ITRAX core scanner with a molybdenum tube (Cox Analytical Systems, Mölndal, Sweden) was used to acquire microgeochemical (μ -XRF) variations on the split sediment cores at INRS-ETE. Before measurement, RGB colour images ($50\text{ }\mu\text{m}$ pixel size) of the cores were taken using the ITRAX line scan camera. The scanner emits a non-destructive beam that radiates the sample and uses the electron dispersive spectrum (EDS) to detect the energy of fluorescent radiation, which produces high-resolution relative concentration of elements, from aluminium to uranium (Croudace et al. 2006). The number of counts for each element in a spectrum acquired for a specific depth interval was normalized by the total number of counts of that spectrum (expressed in counts per second, cps). “Inc” is the incoherent scattering or Compton scattering and “coh” is the coherent or Rayleigh scattering. The inc/coh ratio is inversely proportional to the average atomic weight (Croudace et al. 2006) and has been used as a proxy for organic matter content (Guyard et al. 2013), sediment density (Thomson et al. 2006) and porosity (Jenkins 1999). μ -XRF data was acquired at a downcore resolution of $500\text{ }\mu\text{m}$ at an exposure time of 10s, using a voltage of 30 kV and current of 45 mA. Data were analysed using Q-Spec 8.6.0 software (Croudace et al. 2006) and graphs were plotted using PanPlot software (Sieger and Grobe 2013).

For paleomagnetic analysis, u-channels (plastic liners of $2\times 2\text{ cm}$ cross-section) were sampled from the composite core WA15-08-U from Lake Walker. The natural remanent magnetization (NRM) was measured using a 2-G Enterprise model 755.-1.65 DC cryogenic magnetometer at the Institut de Physique du Globe de Paris and 2-G Enterprise model 755 SRM cryogenic magnetometer at ISMER. Measurements from the upper and lower 5 cm of the u-channels were ignored in order to remove edge effects due to the response function of the magnetometer’s pick-up coils (Philippe et al. 2018; Weeks et al. 1993). The NRM was measured and subsequently demagnetized by an alternating field (AF) at 5 mT increments from 0 to 60 mT in order to determine the characteristic remanent magnetization (ChRM). The anhysteretic remnants magnetisation (ARM) was induced in a peak AF of 100 mT in the presence of a weak direct current (DC) biasing field of 0.05 mT, followed by demagnetization steps at peak AF fields of 0 to 80 mT (5 mT increments). Using the PaleoMacan Excel macro

developed by Cogné (2003), the median destructive field (MDF) was computed along with the ChRM inclinations and declinations. Maximum angular deviation (MAD) values were computed by principal component analysis (Kirschvink 1980). The MAD values can be used as a quantitative measure of the quality of the palaeomagnetic data, where values less than 5° suggest high-quality directional data (Stoner and St-Onge 2007).

4.4.3 Chronology and radiocarbon dating

Bulk sediment samples, and when present, terrestrial plant macrofossils (wood fragments) were cautiously collected at various depths from cores PC15-02C-P and PC15-04B-P (Lake Pentecôte) and WA15-08-U (Lake Walker) (Table 4.2). The samples were pre-treated (with HCl-NaOH-HCl) and combusted at the Radiocarbon dating laboratory, Centre d'études nordiques (CEN), Université Laval. Afterwards, samples were analysed using accelerator mass spectrometry (AMS) at the Earth System Science Department, Keck Carbon Cycle AMS Facility at the University of California at Irvine (UCI). The dates were calibrated with the Calib 7.1 software (Stuiver et al. 2018) using the INTCAL2013 (Reimer et al. 2013) and are presented with 2 sigma standard deviations (Table 4.2). Two previously dated intervals from core PC15-04B-P and the composite core WA15-08-U (Gagnon-Poiré et al. 2019) were included for comparison (Tables 4.3 and 4.4). Age-depth models were constructed using Clam software, version 2.2 (Blaauw 2010a) interface with R software (Blaauw 2010b).

Laminations from the lower unit (Unit 1) of cores PC15-02-P and PC15-04B-P (Lake Pentecôte) were counted on CT-images by two researchers (O.P.N and A.G-P). The laminae counts were then compared to radiocarbon dates from given depth (Table 4.2) in order to test the hypothesis that they could be annually laminated (Gagnon-Poiré et al. 2019). Core WA15-08-U (Lake Walker) was excluded because laminae were not clearly visible.

4.4.4 Grain size analysis

About 0.2 to 0.6 g of sediments were sampled from cores PC15-02C-P and PC15-04B-P (Lake Pentecôte) and WA15-08-U (Lake Walker) at intervals of 5 to 10 cm. The sediments were treated with ~5 mL of 30% hydrogen peroxide (H_2O_2) to remove organic matter, and with 30 mL of 10% sodium carbonate (Na_2CO_3) to remove biogenic silica, after which ~10 mL of sodium hexametaphosphate ($NaPO_3)_6$ was added as dispersant. Sediment grain size distributions were determined using a Beckman Coulter LS 13 320 laser diffraction particle size analyser (Beckman Coulter Inc., Brea, CA, USA) at INRS-ETE. A minimum of three measurements was done per sample to obtain average results. Grain size parameters were derived using the GRADISTAT software (Blott and Pye 2001) and classified based on the Wentworth scale (Wentworth 1922), while grain size statistics were calculated using the Folk and Ward (1957) method.

4.4.5 Sediment description

Sediment colours were described using the Munsell Soil Colour Chart (Munsell Color Xrite, USA). Unconsolidated sediments were taken from the selected cores (PC15-02C-P, PC15-04B-P and WA15-08-U) at various depths and embedded on glass to form smear slides, using a thin layer of hydro-matrix water-solved mounting medium (Micro Tech Lab, Graz, Austria), following the protocol developed by Myrbo et al. (2011). The smear slides were observed under a petrographic microscope at ~100 to 400x magnification (with minerals identified at 40x objective) for semi-quantitative compositional analysis of areas of interest (e.g., sediment facies and laminations). The main components were categorized as clastic (e.g., clay mineral, quartz, feldspar), authigenic (e.g., carbonates) or biogenic (e.g., organic matter, pollen) (Myrbo et al. 2011). However, in this study, “carbonates” is simply used instead of “authigenic”.

4.4.6 Palynological analysis

Sediments were subsampled from the selected cores (PC15-02C-P, PC15-04B-P and WA15-08-U) at intervals of 5 to 10 cm and prepared for palynological analysis using mechanical and chemical procedures to concentrate microfossils (e.g., pollen and spores), following the protocol developed by de Vernal et al. (2010). Mechanical separation involved wet sieving to remove silt size and sand fractions and/or dense liquid separation, while chemical procedures involved treating the sample with hydrochloric acid (HCl) and hydrofluoric acid (HF) macerations to dissolve silica particles. In order to facilitate the calculation of pollen concentration, lycopodium tablets (Stockmarr 1971) were added to the samples. Following treatment, the residue containing the palynomorphs was mounted on microscopic slides for analysis at the GEOTOP Research Centre (Montreal, Canada). The observation of terrestrial and/or marine palynomorphs (with dimensions generally at 5–150 µm) was done at high magnification (>250x) using an optical microscope in transmitted light. The concentration of palynomorphs was classified on a semi-quantitative scale: 0 - Absent; 1 - Rare (1–100 grains/cm³); 2 - Present (100–1,000 grains/cm³); 3 - Common (1000–10,000 grains/cm³), and 4 - Abundant (>10,000 grains/cm³). Palynomorph diagrams were compiled using the C2 software (Juggins 2007).

4.4.7 Evaluation of hydraulic potential model

Gagnon-Poiré (2016) tested the hypothesis that a subglacial lake existed at the location of lakes Pentecôte and Walker during the last glacial maximum (LGM). For clarity, a brief description of the model by Gagnon-Poiré (2016) is provided below. The model was done using the methodology described by Clarke (2005) and Guyard et al. (2011). The hydraulic potential below the ice sheet was derived using the following equation:

$$h_w = \frac{\rho_i}{\rho_w} (z_i - z_b) + z_b \quad (1)$$

where h_w is the subglacial hydraulic head (m), ρ_i (1000 kg/m^3) and ρ_w (910 kg/m^3) are the density of ice and water respectively, z_i is the elevation of the ice sheet surface and z_b is the elevation of the bedrock surface. The extent of the lake was defined based on the following assumptions: 1) the hydraulic potential is constant in the lake; 2) the ice is floating on the lake; and 3) the lake is filled to capacity (Gagnon-Poiré 2016). The elevation of the lake z_l , was obtained using the filled hydraulic head h_w^{fill} :

$$z_l = \frac{h_w^{\text{fill}} - (\rho_i / \rho_w) z_i}{1 - \rho_i / \rho_w} \quad (2)$$

ArcGIS software (ESRI 2014) raster calculator was used to run the model and calculate the potential based on given empirical equations. Input raster parameters included: 1) topography raster; 2) model for the ice sheet parameter (Tarasov et al. 2012); and 3) glacial surface topographic slope (see Gagnon-Poiré et al. 2016 for details).

In this study, an evaluation of the hypothesis by Gagnon-Poiré (2016) was done for two main reasons: 1) to test whether there are possible links between the proposed subglacial lake model and the new radiocarbon dates that were analysed (Table 4.2), and 2) to decipher any insights that could constrain the glacial model of the studied lakes (Gagnon-Poiré et al. 2019). For these reasons, several hydraulic potential runs were modelled for lakes Pentecôte and Walker (e.g., at the LGM ~20, 15 and 10 ka cal BP), considering the new age constraints (Table 4.2).

4.5 Results

4.5.1 ^{14}C age-depth models and sedimentation rates

Tables 4.3 and 4.4 present the radiocarbon ages from the selected cores (PC15-02C-P, PC15-04B-P and WA15-08-U).

4.5.1.1 Core PC15-02C-P, Lake Pentecôte (Figure 4.3)

Figure 4.2A illustrates the age-depth model of core PC15-02C-P (Figure 3), which is constrained by three AMS ^{14}C ages. Bulk sediments sampled near the base and top of the core, at 40 and 5 cm, yielded ages of 32435 ± 325 cal BP and 13820 ± 140 cal BP, respectively. The mean sedimentation rate is $\sim 0.002 \text{ cm a}^{-1}$. The age from the base of this core represents the oldest sediments collected from the lakes (Table 4.2).

Table 4.3: AMS ^{14}C age of the dated materials from Lake Pentecôte.

| Core name | Depth (cm) | Material | UCI Lab # | Université Laval # | $^{14}\text{C a}$ (BP) | $^{14}\text{C a}$ cal BP |
|-------------|------------|---------------|---------------|--------------------|------------------------|--------------------------|
| PC15-04B-P | 35 | Wood fragment | UCIAMS-191360 | ULA-7100 | 2900 ± 15 | 3034 ± 30 |
| PC15-04B-P | 54.5 | Wood fragment | UCIAMS-191359 | ULA-7099 | 3630 ± 15 | 3945 ± 25 |
| PC15-04B-P | 74 | Wood fragment | UCIAMS-205560 | ULA-7849 | 6060 ± 20 | 6924 ± 25 |
| PC15-04B-P* | 101 | Bulk sediment | UCIAMS-162978 | ULA-5436 | 7240 ± 25 | 8075 ± 55 |
| PC15-04B-P | 115 | Bulk sediment | UCIAMS-207669 | ULA-8007 | 18175 ± 45 | 21904 ± 336 |
| PC15-04B-P | 130 | Bulk sediment | UCIAMS-204634 | ULA-7850 | 18130 ± 60 | 21870 ± 345 |
| PC15-04B-P | 180 | Bulk sediment | UCIAMS-207671 | ULA-8009 | 19375 ± 45 | 23134 ± 261 |
| PC15-02C-P | 5 | Bulk sediment | UCIAMS-204635 | ULA-7851 | 11920 ± 35 | 13817 ± 142 |
| PC15-02C-P | 20 | Bulk sediment | UCIAMS-207674 | ULA-8012 | 17955 ± 45 | 21625 ± 335 |
| PC15-02C-P | 40 | Bulk sediment | UCIAMS-191357 | ULA-7097 | 27910 ± 240 | 32435 ± 325 |

*Gagnon-Poiré et al. (2018)

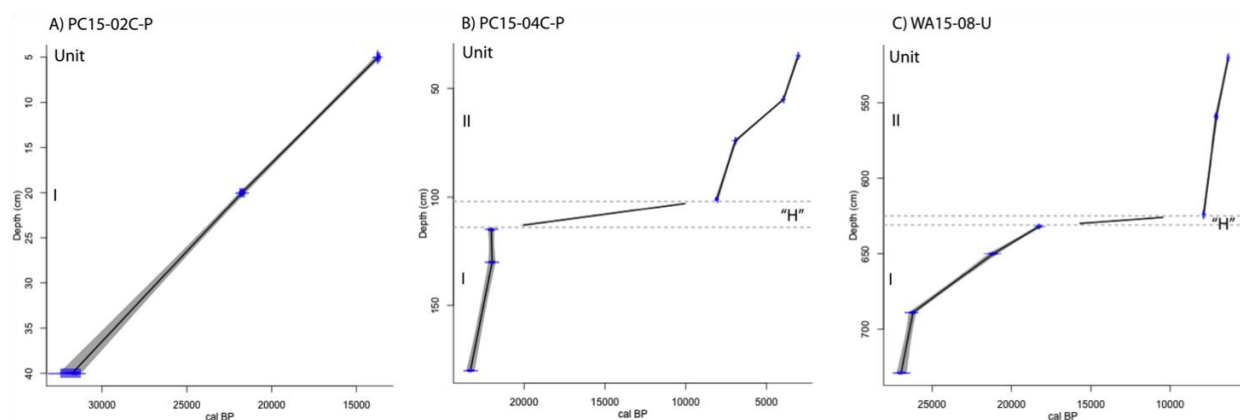


Figure 4.2: Age-depth models based on radiocarbon dating from: A) core PC15-02C-P and B) core PC15-04B-P (Lake Pentecôte) and composite core WA15-08-U (Lake Walker). In B and C, the model shows an age gap between the lower unit (Unit I) and the upper unit (II) of the cores, which suggests an age/sedimentation hiatus, indicated as "H".

Table 4.4: AMS ^{14}C age of the dated materials from the composite core, WA15-08-U (~488–740 cm cd) Lake Walker.

| Core name | Material | Core depth (cm) | Composite depth (cm cd) | UCI Lab # | Université Laval # | ^{14}C a BP | ^{14}C cal BP |
|------------------|---------------|-----------------|-------------------------|---------------|--------------------|----------------------|------------------------|
| WA15-08C-III-U-1 | Bulk sediment | 20 | 488 | UCIAMS-191358 | ULA-7098 | 5530 ± 20 | 6341 ± 40 |
| WA15-08D-III-U-2 | Bulk sediment | 41 | 520 | UCIAMS-179982 | ULA-6438 | 5525 ± 15 | 6309 ± 5 |
| WA15-08D-III-U-2 | Bulk sediment | 80 | 559 | UCIAMS-179983 | ULA-6439 | 6180 ± 15 | 7081 ± 40 |
| WA15-08D-IV-U-1* | Wood fragment | 50 | 624 | UCIAMS-161066 | ULA-5406 | 7060 ± 25 | 7904 ± 30 |
| WA15-08D-IV-U-1 | Bulk sediment | 52 | 632 | UCIAMS-207670 | ULA-8008 | 15030 ± 30 | 18264 ± 235 |
| WA15-08D-IV-U-1 | Bulk sediment | 70 | 650 | UCIAMS-204636 | ULA-7852 | 17510 ± 70 | 20931 ± 310 |
| WA15-08D-IV-U-2 | Bulk sediment | 30 | 689 | UCIAMS-207672 | ULA-8010 | 22010 ± 60 | 26420 ± 326 |
| WA15-08D-IV-U-2 | Bulk sediment | 70 | 729 | UCIAMS-207673 | ULA-8011 | 22610 ± 70 | 27340 ± 376 |

*Gagnon-Poiré et al. (2018)

4.5.1.2 Core PC15-04B-P, Lake Pentecôte (Figure 4.4)

Figure 4.2B shows the age-depth model of core PC15-04B-P (Figure 4.4), which is constrained by seven AMS ^{14}C ages (Table 4.2). Bulk sediments sampled at 180 cm, near the bottom of the core were dated at 23130 ± 260 cal BP, while a wood fragment collected at 35 cm, near the top, revealed an age of 3030 ± 30 cal BP (Table 4.2). The model indicates an abrupt change in age range at the transition between the lower unit (Unit I) and the upper unit (Unit II) of the core, which implies a probable age and/or sedimentation gap (hiatus). The lower and upper limits of the age hiatus, at 115 and 101 cm depth of the core, were dated at 21904 ± 336 cal BP and 8075 ± 55 cal BP, respectively. The mean sedimentation rate below the transition (Unit I) is ~ 0.04 cm a^{-1} , while rates above the transition (Unit II) range from 0.01 to 0.03 cm a^{-1} .

4.5.1.3 Composite core WA15-08-U, Lake Walker (Figure 4.7)

Figure 4.2C displays the age-depth model of the composite core, WA15-08-U (488–740 cm cd; Figure 4.7) from Lake Walker, which is constrained by seven AMS ^{14}C ages (Table 4.2). Bulk sediments collected near the bottom and top of the composite, at 729 and 488 cm cd, yielded ages of 27340 ± 376 cal BP and 6341 ± 40 cal BP, respectively. The model also depicts an abrupt change in age range between the lower unit (Unit I) and the upper unit (Unit II) of the core, implying a hiatus. Its lower and upper limits, at 624 and 559 cm cd, were dated at 18264 ± 235 cal BP and 7904 ± 30 cal

BP, respectively (Table 4.2). Mean sedimentation rates in the lower interval (Unit I) range from 0.001 to 0.07 cm a⁻¹, while rates in the upper interval (Unit II) range from 0.001 to 0.05 cm a⁻¹.

Table 4.5: Summary of multi-proxy analyses and their environmental interpretation

| Sediment Facies [Age] | Litho- stratigraphic unit [core] | Sedimentology | Geochemistry (XRF) | Palyno- stratigraphy | Depositional environment |
|--|---|--|--|---|-----------------------------|
| LS facies ~8 (?) ka cal BP to recent (Lake Pentecôte) ~7.9 ka cal BP to recent (Lake Walker) | Unit IIb: PC15-04B-P, WA15-08-U | Laminated to partially laminated Dark grayish clay and grayish brown silty clay laminae Thinly laminated (0.4–1 cm) Mean grain size: Medium silt Clay content: 0–15% | Low detritic inputs (Si, K, Ti, Rb, K/Ti) Low carbonate inputs (Ca, Sr) Low redox-sensitive (Fe, Mn, Fe/Ca) Moderate-high organic input (inc/coh) | High diversity: (Pollen, Pteridophytes spores, Sphagnum, Mushroom spores, Thecamoebians, Radiosperma, Stomata) | Postglacial |
| LS-O facies ~8 to ~? ka cal BP (Lake Pentecôte) | Unit IIa: PC15-04B-P | Laminated dark grayish clay and grayish brown laminae silty clay Organic-rich (peat) laminae Thinly laminated (0.4–1 cm) Mean grain size: Medium silt Clay content: 10–15% | Low detritic inputs (Si, K, Ti, Rb, K/Ti) Low carbonate inputs (Ca, Sr) High redox-sensitive (Fe, Mn, Fe/Ca) High organic input (inc/coh) | High diversity: (Pollen, Pteridophytes spores, Sphagnum, Mushroom spores, Thecamoebians, Radiosperma, Stomata) | Paraglacial |
| RLC facies ~32 to ~13 ka cal BP | Unit I: PC15-02C-P PC15-04B-P, WA15-08-U | Rhythmic greenish gray clay and dark gray silty clay Thickly laminated (1–2 cm) Mean grain size: Fine to very fine silt Clay content: 20–60% | High detritic inputs (Si, K, Ti, K/Ti) High carbonate input (Ca, Sr) Low redox-sensitive (Fe, Mn, Fe/Ca) Low organic input (inc/coh) | Low diversity: Almost no palynomorphs except sporadic pollens and Pteridophytes spores | Proglacial |

4.5.2 Lithostratigraphy and sedimentary facies

Two main sedimentary facies were identified from the analysed cores, namely: rhythmically laminated clay (RLC) and laminated silty clay and clay. The latter is divided into two subfacies: laminated (organic-rich) silty clay and clay (LS-O) and laminated to partially laminated sediments (LS-PLS, hereafter designated as “LS”) (Nzekwe et al. 2018). Table 4.5 summarizes the features and stratigraphic position of the identified facies (and subfacies). Distinctive characteristics of the three analysed cores are described below. The following XRF elements were selected to characterize the sediments: Si, Ti, Rb, Zr, Fe, Ca, Sr, and the inc/coh ratio and also, specific element ratios such as K/Ti (proxy for sediment provenance) and Fe/Ca (proxy for detrital:carbonate ratio) (Croudace et al. 2006; Rothwell and Croudace 2015).

4.5.2.1 Core PC15-02C-P, Lake Pentecôte

Figure 4.3 depicts that core PC15-02C-P, 43 cm long (Unit I: 43–0 cm) is characterized by rhythmic alternation of cm-thick argillaceous laminae comprising dark gray very fine silt and greenish gray fine to medium silt (Munsell colour: 5Y 6/4 to 5/3). The clay content ranges from 10–35%, while the mean grain size is fine to very fine silt (2–10 μm). The banded laminae couplets have a thickness of 1 to 2 cm. The CT number varies from 1700–2300 HU (Figure 4.3). L* varies from 25–50, a* from 0–1.3, and b* from 4–9. The sediment is generally poorly to very poorly sorted (2.5–5 μm), fine to coarsely skewed and mesokurtic (Folk and Ward 1957). The low field volumetric magnetic susceptibility (MS) varies from 50–350 * 10^5 SI (Figure S4.1). Smear slide analysis reveal that the dark gray and light laminae comprise 80–90% clastic, 20–5% carbonates (mainly calcite) and 0–5% biogenic components. The main identifiable mineral in both laminae is quartz (with angular grains) suspended in fine-grained (clay) matrix. μ -XRF profiles indicate positive co-variation of Si/cps, K/cps, Ti/cps and K/Ti ratio and also Ca/cps and Sr/cps, as well as background values of Fe/cps and Mn/cps. The dark gray silty laminae correspond to higher values of Si/cps, K/cps, Ca/cps and Sr/cps, while the light gray clayey laminae correspond to higher values of Fe/cps, Mn/cps, Fe/Ca and the inc/coh ratio. However, as observed in Figure 4.3, visual correlation of laminations with μ -XRF data is somewhat difficult because the laminations are inclined and/or rippled, possibly due to disturbance or pressure during percussion coring.

In order to test the hypothesis that the rhythmic laminations observed on core PC15-02-P (Unit I) could be annually laminated (Gagnon-Poiré et al. 2019), laminae counts on the CT-scan image were compared to the radiocarbon ages. Figure 4.3 illustrates that approximately 32 laminae couplets were counted between 32435 ± 325 cal BP and 13817 ± 142 cal BP. Each laminae couplet corresponds to ~550 years, thus they are non-annual.

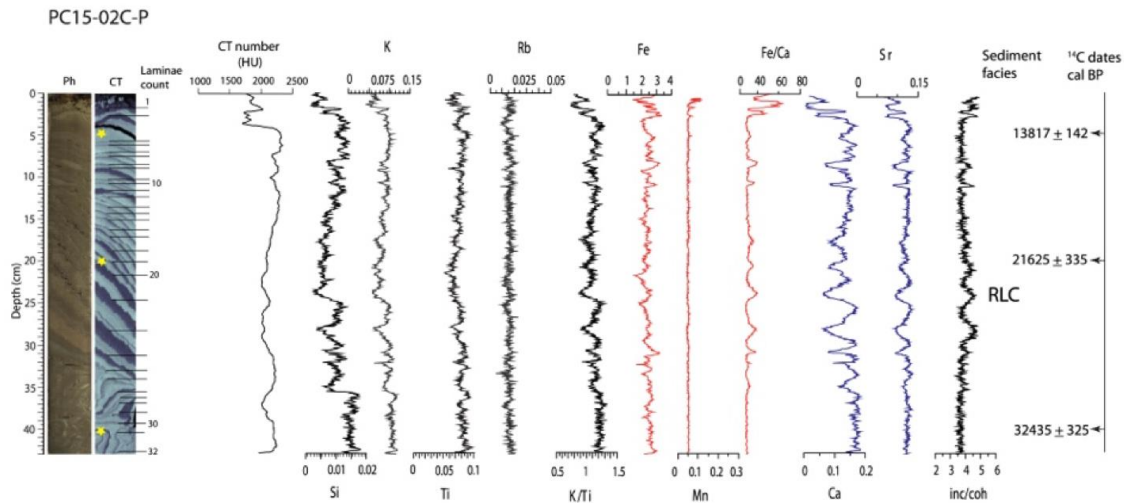


Figure 4.3: Multi-proxy analysis of core core PC15-2C-P (Lake Pentecôte). (From left to right, L-R): Digital photo (Ph), CT-scan image (CT), laminae counts on the CT-scan compared to age model based on radiocarbon dating (dated intervals are marked by yellow star). The laminations are non-annual. Also shown are XRF data for selected elements. Values are given in peak area integrals normalized by the total counts per second of each spectrum (cps = counts per second). Comparison of elemental variation is rather difficult due to laminae disturbance. However, elemental peaks show strong correlation with laminae structure: Si, K, Sr are higher within light gray laminae, while inc/coh ratio and Fe/Ca are higher within the dark gray laminae.

4.5.2.2 Core PC15-04B-P, Lake Pentecôte

Figure 4.4 illustrates that core PC15-04B-P, ~190 cm long, consists of two main units: a lower unit from 190–102 cm (Unit I) and an upper unit from 102–0 cm (Unit II). Unit I (190–102 cm) is characterized by a rhythmic alternation of light greenish gray and greenish gray (Munsell colour: GLEY 6/1 to 5/1) clayey material comprising fine silt and very fine silt. Clay content varies from 20–60%, while mean grain size is fine silt ($1.9\text{--}4 \mu\text{m}$). The unit is generally poorly sorted, fine to symmetrically skewed and mesokurtic (Figure 4.4). The thickness of laminae couplets is 0.2 to 1 cm. The CT number varies from >1500–2200 HU. L^* is ~43, a^* is ~-0.1, b^* is ~5, while MS is ~300 $k \cdot 10^5 \text{ SI}$ (Appendix IV, Figure S2). Smear slide analysis indicates 50–80% clastic, 30–10% carbonates (mainly calcite) and 20–10% biogenic components (Myrbo et al. 2011). The main identifiable mineral is quartz suspended in fine-grained (clay) matrix (Figure 4.5). Feldspar is also noticeable. In order to test the hypothesis that the rhythmic laminations observed in this unit could be annually laminated (Gagnon-Poiré et al. 2019), laminae counts on the CT-scan image were compared to the radiocarbon ages. Figure 4.4B depicts that on the CT-scan image, approximately 108 laminae couplets were counted between $21904 \pm 336 \text{ cal BP}$ and $23134 \pm 261 \text{ cal BP}$. Each laminae couplet corresponds to ~5–10 years (using the 2 sigma ages). The laminations are thus non-annual. μ -XRF elemental profiles for Unit I of core PC15-04B-P present co-variation of Si/cps, K/cps, Ti/cps and K/Ti ratio, and also Ca/cps and Sr/cps. Background (zero to low) values of Fe/cps, Mn/cps and Fe/Ca are noticeable. The inc/coh ratio ranges from 2.5–3.0 (Figure 4.6). There is a sharp transition between Unit I and the overlying unit (Unit II).

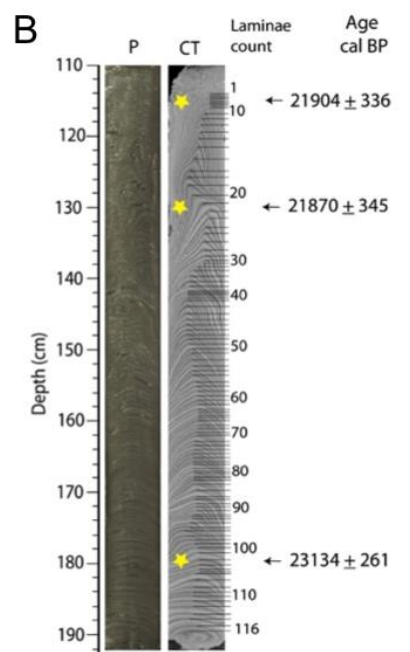
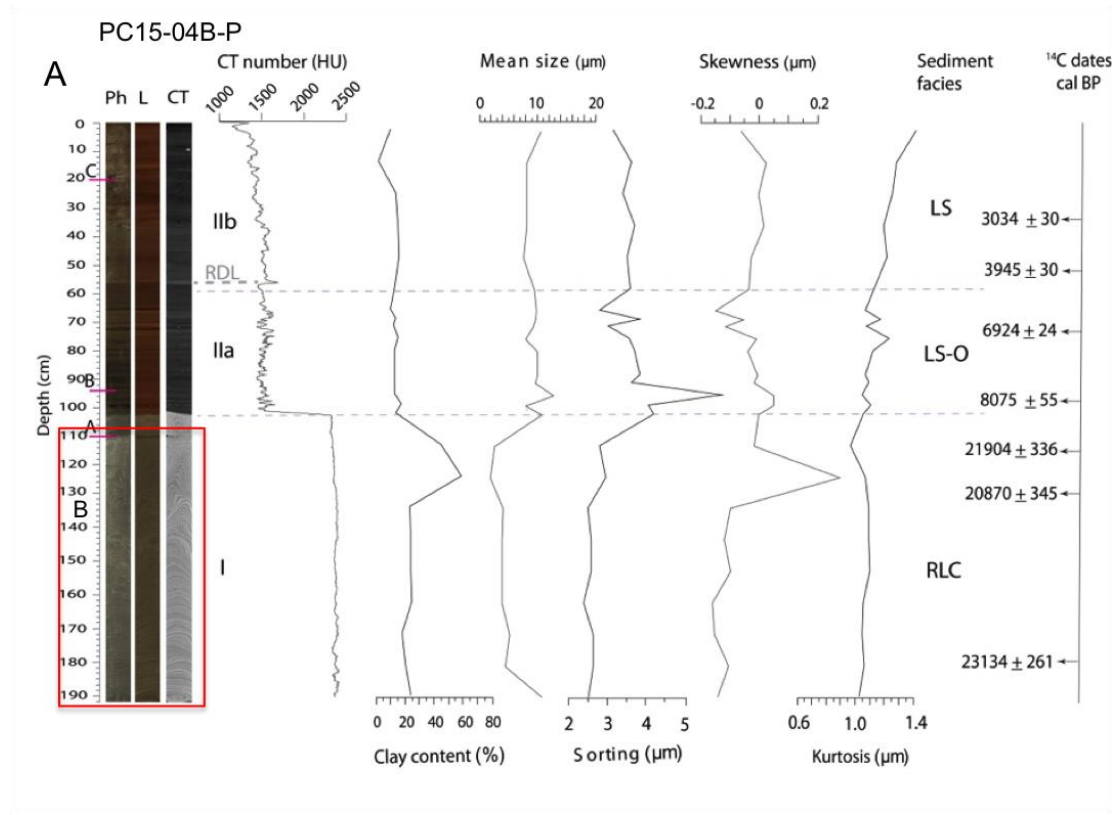


Figure 4.4: (A) Grain size analysis for core PC15-04B-P, Lake Pentecôte. (L-R): Digital photo (Ph), line scan image (L), CT-scan frontal view (CT) and CT number (HU), grain size statistical parameters (clay content, mean grain size, sorting, skewness and kurtosis) calculated by the GRADISTAT 4.0 software (Blott and Pye, 2001) using the Folks and Ward 1957 method. The lettering (A, B, C) on the digital photo indicates depths that were sampled for smear slide analysis, shown in Figure 4.5. Sediment facies are RLC rhythmically laminated clay sediments; LS-O laminated organic-rich silty clay and clay sediments; and LS - laminated sediments.

The upper unit of core PC15-04B-P, Unit II (from 102–0 cm) can be further divided into two subunits (Figure 4.4 and 4.6). Subunit IIa (PC15-04B-P), from 102–60 cm comprises regularly laminated dark grayish clay and grayish brown silty clay (Munsell colour: 5Y 4/1 to 4/2), and intermittent dark brown to black organic-rich laminae. A mm to cm-thick layer of silty clay that can relate to a rapidly deposited layer (RDL) (Gagnon-Poiré et al. 2019; St-Onge et al. 2012; St-Onge et al. 2007) is noticeable at ~55 cm (Figure 4.4 and 4.6). Clay content ranges from 10–15% and mean grain size is medium silt (8–13 μ m). The interval is poorly sorted, fine to symmetrically skewed and mesokurtic. The CT number varies from 1200–2200 HU (Figure 4.4). L* varies from 20 to 40, a* from 1–4, b* from 2–16 and MS from 0–250 * 10^5 SI (Appendix IV, Figure S2). The upper subunit of Unit II, Subunit IIb (from ~60–0 cm) consists of partially laminated dark grayish clay and grayish brown silt (Figure 4.4 and 4.6). Compared to Unit IIa, the RDL and organic-rich laminae are less noticeable, while clay content ranges from 0–15%. Mean grain size is also medium silt.

Smear slide analysis reveal that subunits IIa and IIb comprise clastic (70–50%; 75–60%), carbonates (10–25%; 10–20%) and biogenic (20–25%; 15–20%) components, respectively. Quartz and feldspar are common. However, in subunit IIa, organic matter (biogenic component) is noticeable as brown translucent amorphous algal material (Myrbo et al. 2011) (Figure 4.5B: B2-B3).

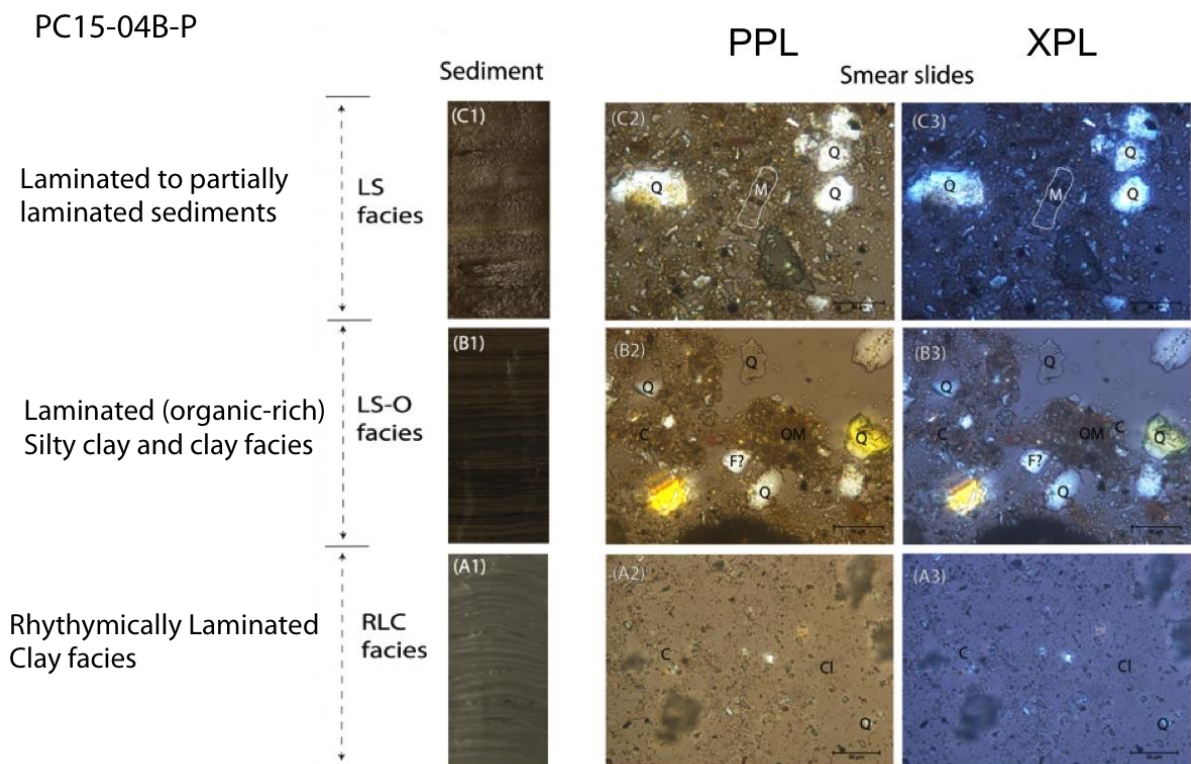


Figure 4.5: (A1 – C1) Sediment core image and smear slide images from core PC15-04B-P at selected depths, as seen in plane- and crossed-polarized light: (A) RLC facies, 110 cm; (B2-B3) LS-O facies, 94 cm; (C2-C3) LS facies. Identifiable minerals include: Q - quartz, F - feldspar, C - carbonates (calcite), M - muscovite, Ma - mafics, V - vivianite, Cl - clay minerals, OM - organic matter. Sediment facies are RLC rhythmically laminated clay sediments; LS-O laminated organic-rich silty clay and clay sediments; and LS - laminated sediments.

μ -XRF profiles for Unit II (subunits IIa and IIb) indicate abrupt decrease in Si/cps, K/cps, Ti/cps, Rb/cps, K/Ti, Ca/cps and Sr/cps, complemented by an increase in the inc/coh ratio, compared to Unit I below (Figure 4.6). The distinguishing signal appears to be peak variations of Fe/cps, Mn/cps and Fe/Ca within subunit IIa, which return to background values in subunit IIb.

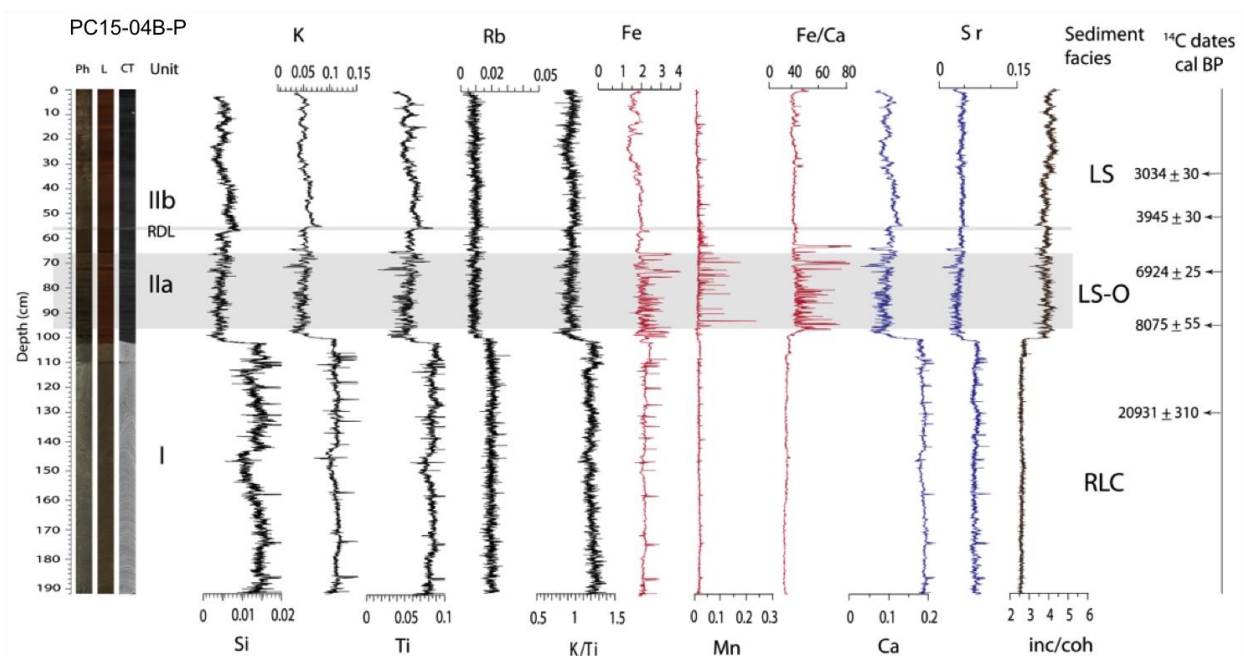


Figure 4.6: XRF data for core PC15-4B-P showing digital photo (Ph), line scan image (L) and CT-scan frontal view (CT), and vertical profiles of selected elements along the core. Values are given in peak area integrals normalized by the total counts per second of each spectrum (cps = counts per second). Sediment facies are RLC rhythmically laminated clay sediments; LS-O laminated organic-rich silty clay and clay sediments; and LS - laminated sediments.

4.5.2.3 Composite core WA15-08-U, Lake Walker

Figure 4.7 displays the part of the composite section WA15-08-U (Lake Walker) that was analysed. It comprises two main units: a lower unit (Unit I) from ~660–630 cm cd and an upper unit (Unit IIb), from 630–488 cm cd.

Unit I (~660–630 cm cd) comprises a rhythmic alternation of pale olive to dark olive gray (Munsell colour: 5Y 4/2 to 3/2) clayey fine-grained material comprising fine silt and very fine silt. Laminae thickness ranges from 0.4 to 1 cm. This unit is marked by CT numbers between 1500–2200 HU (Figure 7). L* varies from 35 to 50, a* from -1.31–0, b* from 5–10, and MS from 200–250 $\times 10^{-5}$ SI (Appendix IV, Figure S3). Clay content varies from 20–60% and mean grain size is fine silt ($\sim 1.9\text{--}4 \mu\text{m}$). It is poorly sorted, fine to symmetrically skewed ($<0.001 \mu\text{m}$) and mesokurtic ($\sim 1 \mu\text{m}$) (Figure 4.7). Smear slides analysis indicate 90–70% clastic, 10–30% carbonates (mainly calcite) and 0–20%

biogenic components (Myrbo et al. 2011). Identifiable minerals include quartz and feldspar (Appendix IV, Figure S4). μ -XRF profiles for Unit I indicate relatively steady values of Si/cps, K/cps, Ti/cps, Rb/cps and K/Ti ratio and Ca/cps and Sr/cps (Figure 4.8). Also, background values of Fe/cps, Mn/cps and Fe/Ca are noticeable. The inc/coh ratio is ~3.5.

Unit IIb (from 630–488 cm cd) of core WA15-08-U comprises regularly laminated olive gray clay and dark olive gray silty clay (Munsell colour: 5Y 4/2 to 3/2) with few RDLs. The CT number varies from 1200–2200 HU (Figure 4.7). L^* varies from 20–43, a^* from 0–3, b^* from 0–10 and MS from $40–215 * 10^5$ (SI) (Appendix IV, Figure S3). Clay content from 0–12%, while mean grain size is medium silt (8–13 μm). The interval is poorly sorted, fine to symmetrically skewed and mesokurtic ($\sim 1 \mu\text{m}$) (Figure 4.7). Smear slides indicate 75–90% clastic, 10–5% carbonates (calcite) and 15–5% biogenic components. Identifiable minerals include quartz, feldspars and muscovite. However, RDLs (e.g. at ~ 512 cm cd; Figure 4.7) contain 70–90% clastic, 15–10% carbonates and 5–0% biogenic components. The most identifiable mineral in RDLs is quartz, with angular to sub-angular grains (Appendix IV, Figure S4). At the transition into Unit IIb (~ 628 cm cd), there is a slight reduction in values of Si/cps, K/cps, Ti/cps, Rb/cps and K/Ti ratio, and also of Ca/cps and Sr/cps (Figure 4.8); their variations remain fairly stable up to the top of the core. On the other hand, Fe/cps, Mn/cps and Fe/Ca ratio show unsteady and sometimes peak variations between ~ 616 –584 and ~ 556 –514 cm cd (Figure 4.8).

Figure 4.9 illustrates the downcore variation of paleomagnetic inclination and declination and corresponding MAD values for the composite core WA15-08-U (Lake Walker). MAD values are very low ($< 5^\circ$) and indicate high quality data (Stoner and St-Onge 2007). However, at the transition between the two units (640–620 m cd), the inclination varies from -20 to 60° without a similar variation in declination. The normalized remanence ratio NRM/ARM is higher in unit I than in section IIb.

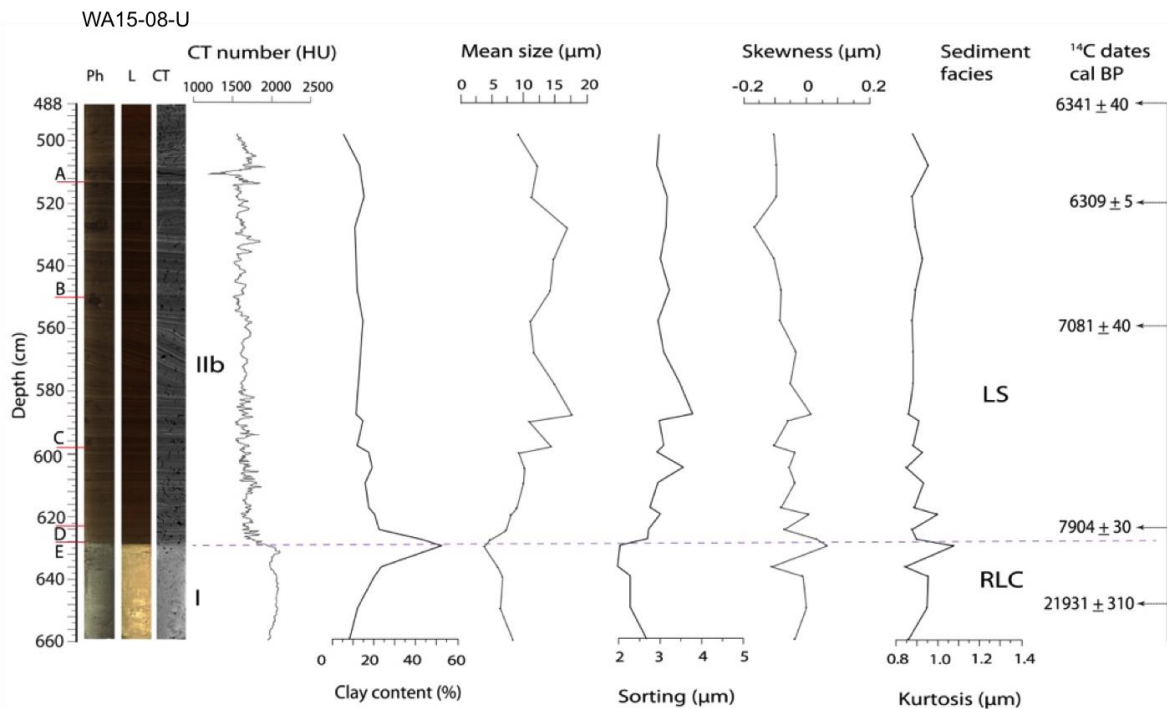


Figure 4.7: Grain size analysis for the composite core, WA15-08-U from Lake Walker, showing: digital photo (Ph), line scan image (L), CT-scan frontal view (CT) and CT number (HU), grain size statistical parameters (clay content, mean grain size, sorting, skewness and kurtosis) calculated by the GRADISTAT 4.0 software (Blott and Pye, 2001) using the Folks and Ward 1957 method. The letterings A, B, C, D, E on the digital photo indicate depths that were sampled for smear slide analysis, shown in Appendix IV, Figure S4. Sediment facies are RLC rhythmically laminated clay sediments, and LS - laminated sediments.

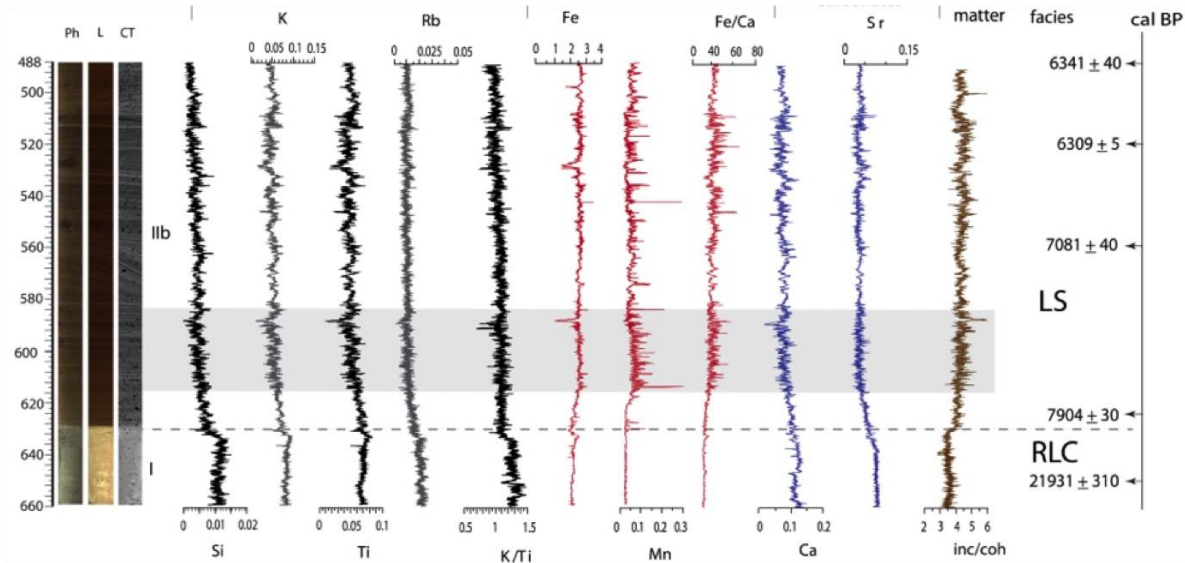


Figure 4.8: XRF data for core WA15-08-U from Lake Walker showing digital photo (Ph), line scan image (L), CT-scan frontal view, CT number (HU) and vertical profiles of selected elements along the core. Values are given in peak area integrals normalized by the total counts per second of each spectrum (cps = counts per second). Sediment facies are RLC rhythmically laminated clay sediments, and LS - laminated sediments.

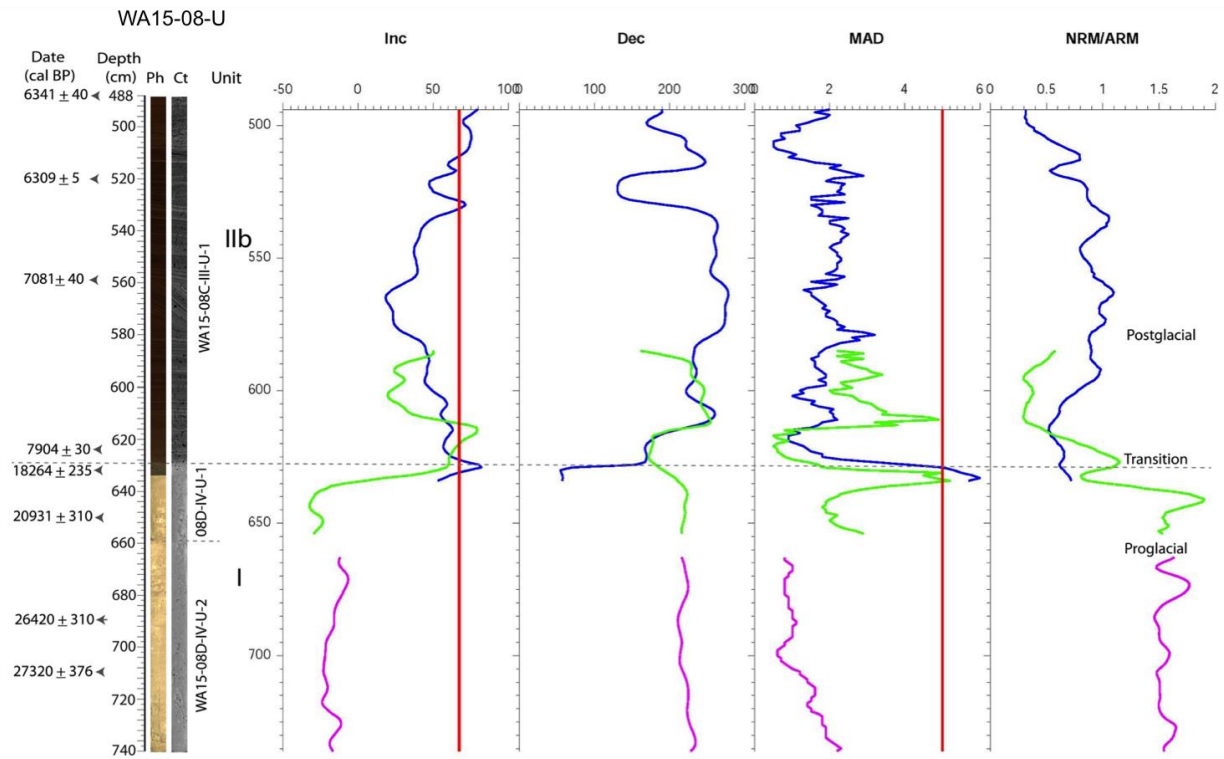


Figure 4.9: Paleomagnetic secular variation records (PSV) for the lower part of the composite section, WA15-08-U from Lake Walker, showing Inclination (inc), Declinations (dec), Maximum angular deviation (MAD), and Natural Remnant Magnetization (NRM) and Anhysteretic Remnant Magnetization (ARM) ratio. Each profile consists of segments that correspond to individual cores comprising the composite.

4.5.3 Palynological analysis

Optical images of selected palynomorphs observed in the analyzed cores are shown in Figure 4.10. For brevity, palynomorph diversity is described in terms of the identified sedimentary facies/subfacies, as shown in Table 4.3.

The RLC facies (Unit I of cores PC15-02C-P, PC15-04B-P and WA15-08-U) is characterized by a low diversity of palynomorphs. Pollen species (e.g., *Betula*, *Pinus*) and Pteridophytes spores are sporadically present (index 2: 100–1000 grains/cm³), while the other analysed species are absent (Figure 4.11A, B, C).

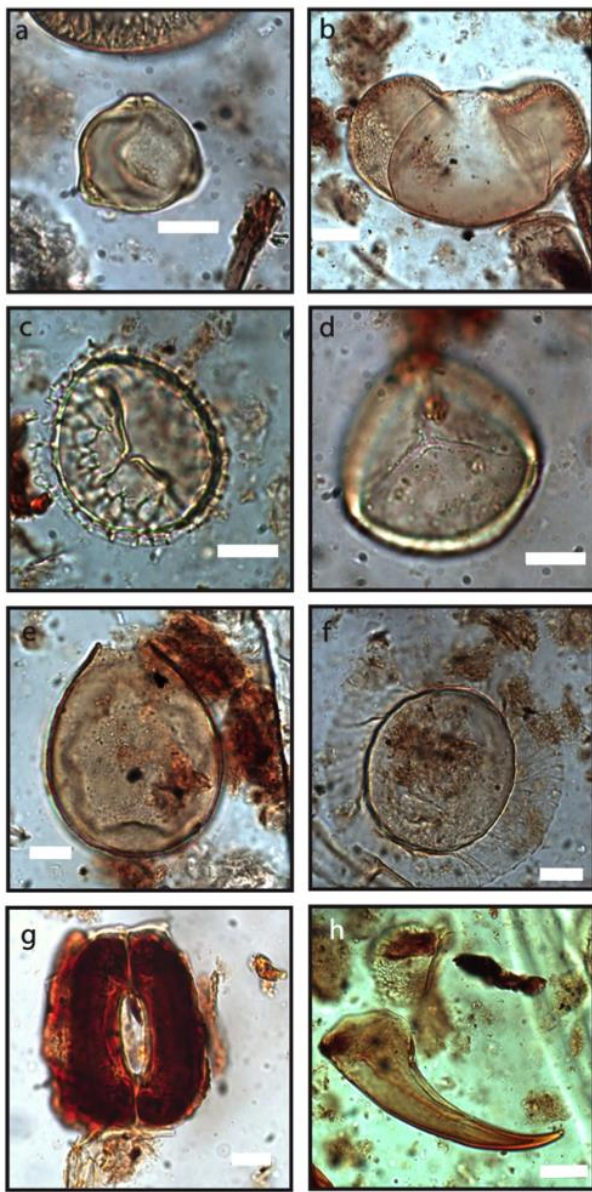


Figure 4.10: Optical images of selected palynomorphs observed in cores from lakes Pentecôte and Walker: (a) Betula Pollen, (b) Pinus Pollen, (c) Pteridophyte spores (d) Sphagnum, (e) Thecamoebian (Testate amoebae), (f) Radiosperma, (g) Stomata (h) Arthropoda segment. Scale bar (in white colour) in images a–h is 10 µm, except for image b where it is 20 µm.

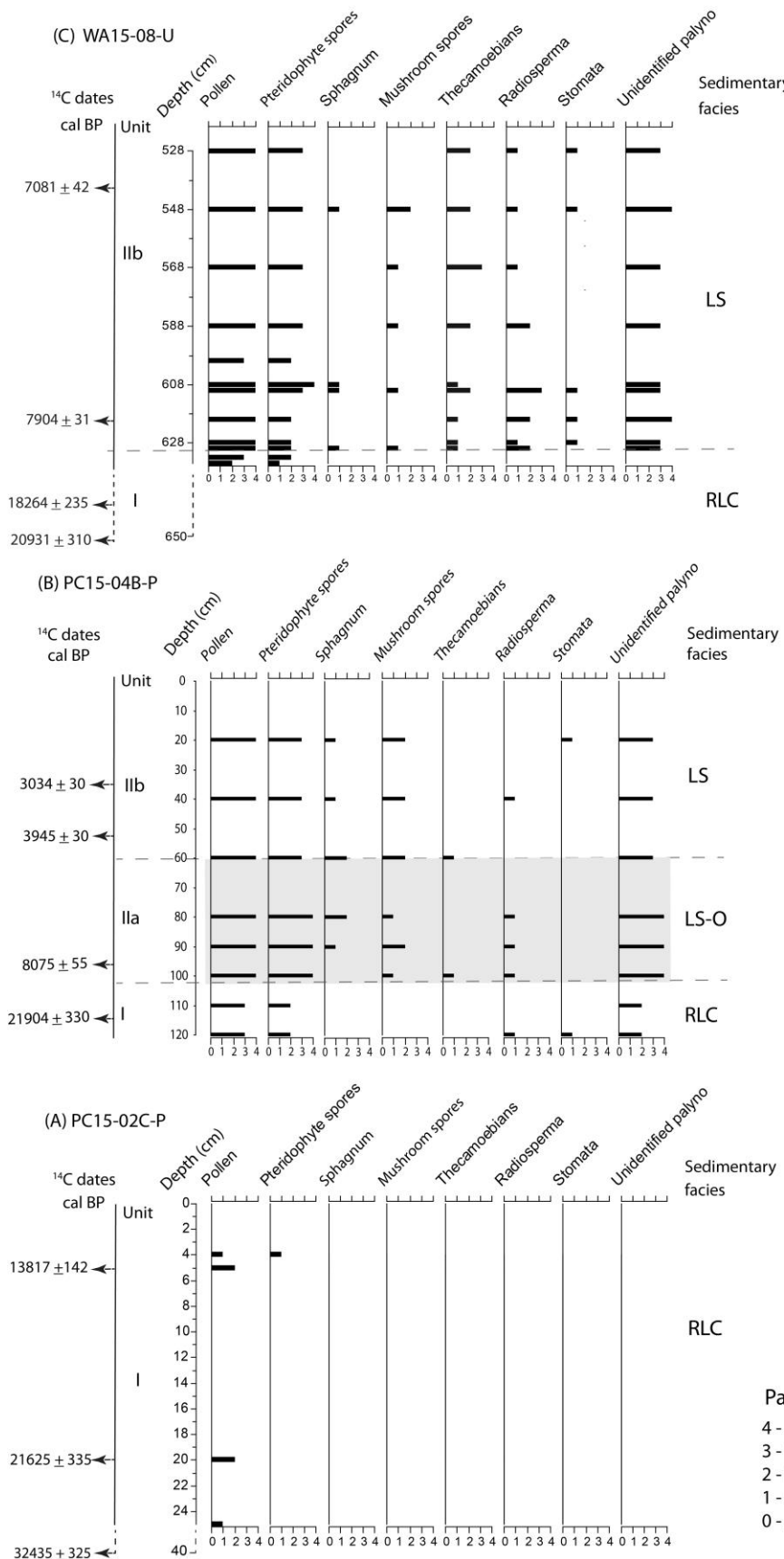


Figure 4.11: Simplified palynostratigraphy of selected cores showing palynomorph counts against depths and calibrated years BP. (A) PC15-02B-P and (B) PC15-04B-P from Lake Pentecôte, and (C) WA15-08-U from Lake Walker.

The LS-O subfacies (Unit IIa of core PC15-04B-P) and LS subfacies (Unit IIb of cores PC15-04B-P and WA15-08-U) are both characterized by relatively sharp increase in palynomorph diversity. Pollen species (*Pinus*, *Betula*) and Pteridophytes spores are abundant (index 4: >10,000 grains/cm³), while other palynomorphs including Sphagnum, mushroom spores, Thecamoebians, Radiosperma and Stomata are present to common (index 2–3: 100–10,000 grains/cm³) (Figure 4.11A, B, C).

4.5.4 Evaluation of Hydraulic potential model

Evaluation of the hydraulic potential model by Gagnon-Poiré (2016) supports the hypothesis that a subglacial lake may have existed in the lakes Pentecôte and Walker basins during the Last Glacial Maximum (LGM; ~20-21 ka). The model output parameters include: hydraulic potential of the lake, depth of the lake and topographic profiles at the LGM, as illustrated in Figures 4.12 and 4.13. Based on higher fluid pressures observed at the base of the LIS compared to those in the lake basin depression, there was most probably storage of subglacial water within lakes Pentecôte and Walker (Gagnon-Poiré 2016). In Lake Pentecôte, the model indicates the existence of narrow, shallow and discontinuous subglacial lakes with maximum depth of 39 m within the central northern and southern basins (Figure 4.12A-B). In Lake Walker, the model indicates the existence of a subglacial lake marked by a modern central sill that separates the large southern basin from the northern basin of the lake (Figure 13A-B). The subglacial lake has an area of ~13 km². Its maximum depth is 132 m, with an average depth of ~45 m (Figure 13A-B). As shown in Figures 12 and 13, the subglacial lake is inferred to have an inclined geometry that is partly caused by the direction of ice flow and the ice sheet surface slope (Livingstone et al. 2012; Occhietti et al. 2011).

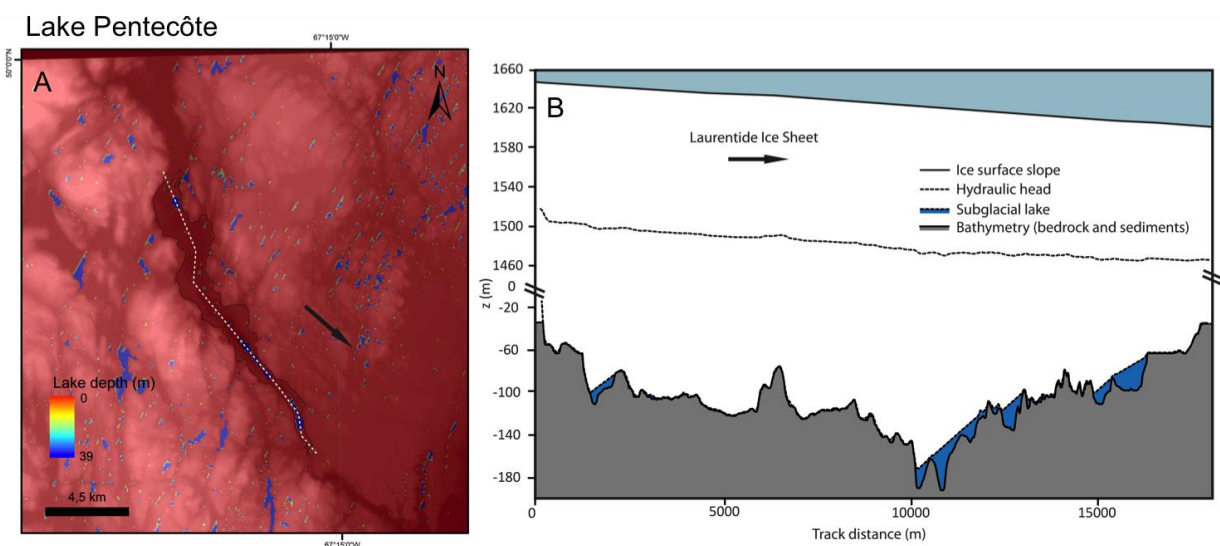


Figure 4.12: Hydraulic potential for the Lake Pentecôte basin at the Last Glacial Maximum (LGM: 20-21 ka) following a southeastern ice flow direction (shown by black arrows; Dredge, 1983), considering a 1650 m ice thickness (Tarasov et al. 2012) and an ice sheet surface slope of 0.17. (A) Lake Pentecôte subglacial lake depth (m); (B) Geometry along longitudinal profile of the subglacial lake basin. The current lake shoreline is represented by the black dashline (Modified from Gagnon-Poiré 2016).

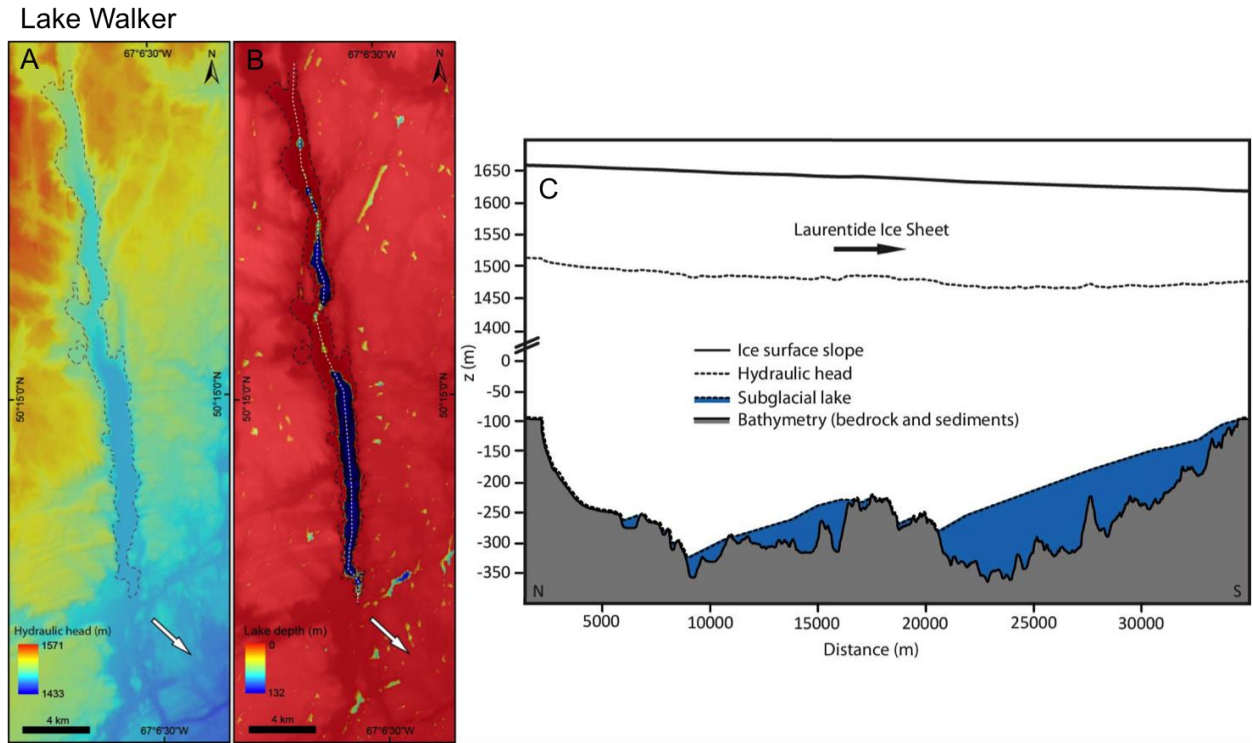


Figure 4.13: Hydraulic potential for the Lake Walker basin at the Last Glacial Maximum (LGM: 20 ka) following a south-eastern ice flow direction (shown by white arrows; Dredge, 1983), considering a 1650 m ice thickness (Tarasov et al. 2012) and an ice sheet surface slope of 0.17. (A) Hydraulic head (m) for Lake Walker; (B) Lake Walker subglacial lake depth (m); (C) Geometry along longitudinal profile of the subglacial lake basin (illustrated by white dashed line in B). The current lake shoreline is represented by the black dashline (Modified from Gagnon-Poiré 2016).

4.6 Discussion

4.6.1 Environmental interpretation of the sedimentary facies

In this discussion, the classification of successive depositional environments are based on the definitions by Syvitski and Praeg (1989), which are 1) ice-contact deposits; 2) ice-proximal sediments; 3) ice-distal sediment; 4) paraglacial sediment and 5) post-glacial sediment. Below the first three environments are grouped under “proglacial”, while the other two (paraglacial and postglacial) are discussed separately.

4.6.1.1 Proglacial environment

The RLC facies occurs at the lowermost stratigraphic position of the analysed cores (Unit I: cores PC15-02C-P, PC15-04B-P and WA15-08-U), and is interpreted to be deposited in a setting proximal to the ice (Appendix IV, Figure S5 and S6; Table 4.3). Nzekwe et al. (2018) recently interpreted this sedimentary facies as proglacial laminated sediments (LLS facies) based on qualitative grain size analysis and radiocarbon dating, while Gagnon-Poiré et al. (2019) interpreted it as glaciomarine

and/or glaciolacustrine sediments based on acoustic stratigraphy. However, a new lithological descriptive name, rhythmically laminated clay (RLC) facies is proposed in this study based on the following: 1) quantitative grain size analysis that indicates high clay content (20–60%) and mean grain size of fine to very fine silt; 2) CT values of >2000 HU that indicate higher density of the clay-rich materials relative to overlying sediments, and 3) visible rhythmic laminae.

Some characteristics of this facies points to a glaciomarine setting: L* values of 35–50 (Figures S1 and S2) and higher Ca and Sr contents (Figures 4.3, 4.6 and 4.8) points to a carbonate-rich input that are typical of marine sediments (St-Onge et al. 2007). Other features points to a glaciolacustrine setting: 1) it was not possible to detect more marine associated elements (e.g. Cl and Br) as they showed background values, and 2) Co-variation of detritic elements (Si/cps, K/cps, Ti/cps, K/Ti) suggest that terrigenous input was significant (Rothwell and Croudace 2015). However, palynostratigraphy employed (this study) focussed on pollen and spores. It did not include diatoms, or other index fossils that have been used to characterize transition from late-glacial to postglacial (Bouchard et al. 2017; Rolland et al. 2008) foraminiferas were not found during sample preparation, and the fine mean grain-size and CT numbers around 2000 HU are similar to lacustrine proglacial varves, such as the one of Lake Jacques-Cartier (Philibert 2012). Low organic productivity in the RLC facies is inferred from relatively low inc/coh ratios (Figures 4.7, 4.10, 4.12).

4.6.1.2 Glacial-deglacial transition phase

The glacial/deglacial transition (from proglacial sediments to overlying paraglacial/postglacial sediments) is marked by abrupt shifts in input of detritic (Si/cps, Ti/cps, K/cps, K/Ti) and pH-sensitive element (Ca/cps, Sr), which correlate well to glacial/deglacial transitions (Rothwell and Croudace 2015). The marked shift from sporadic appearance of pollen species and pteridophytes spores to abundance of these palynomorphs (including appearance of sphagnum, mushroom spores, thecamoebians, radiosperma and stomata) reflect changes to relatively warmer conditions (de Vernal 2009).

4.6.1.3 Paraglacial to postglacial transitional environment

The LS-O facies corresponds to Unit IIa of core PC15-04B-P (Lake Pentecôte) and is interpreted to be deposited in a paraglacial-postglacial environment. It is difficult to clearly delineate the transition from paraglacial-postglacial on the sediment core (PC15-04B-P) because the LS-O facies grades gradually into postglacial (LS) facies, with both having similar mean grain size (medium silt) and palynological characteristics (Figures 4 and 11). Possible markers of the paraglacial depositional system are the peak variations of redox-sensitive elements (Fe/cps, Mn/cps and Fe/Ca; Figure 4.6), which reflects oxic conditions (Rothwell and Croudace 2015). The oxic conditions could be attributed

to: 1) fluctuation of water levels associated with rapid retreat of glacier ice from watershed of Lake Pentecôte (Svytski 1991; Svytski and Praeg 1989), and/or 2) exposure of the lake water column to influence from external factors such as wind and/or currents, which would thus promote water mixing (Tylmann et al. 2012; Zolitschka et al. 2015). Perhaps the presence of lamination in the LS-O facies suggest that fluctuating water level and/or sediment/water mixing were relatively limited to the lake water surface, thus did not reach (critical) depths that would otherwise hinder laminae preservation (Larsen and MacDonald 1993; Larsen et al. 1998; Nzekwe et al. 2018). The beginning of the paraglacial (LS-O facies) in Lake Pentecôte is dated 8075 ± 55 cal BP, however its exact end could not be dated in this study.

4.6.1.4 Postglacial environment

The LS facies occurs at the upper stratigraphic position (Unit IIb) of cores PC15-04B-P (Lake Pentecôte) and WA15-08-U (Lake Walker) and is interpreted to be deposited during postglacial period. As observed, the postglacial period in the studied lakes is marked by steady input of silicate elements (Si/cps, K/cps, Ti/cps, K/Ti) (Rothwell and Croudace 2015) suggesting terrigenous input from the watershed into the lakes. Unlike the paraglacial, the shift from peak to background values of redox-sensitive elements (Fe/cps, Mn/cps and Fe/Ca) in the postglacial environment suggests that glacier ice has completely retreated from of the watershed of the lakes (Gagnon-Poiré et al. 2019). Thus, the lakes Pentecôte and Walker water basins became more exposed to limnological factors (e.g., seasonality) and morphological factors (e.g., topographic exposure) that favoured the deposition of laminated sediments, respectively (Larsen et al. 1998; Nzekwe et al. 2018; Zolitschka et al. 2015). Furthermore, the progressive increase of palynomorphs diversity during the postglacial reflects steady input from terrestrial vegetation into the lakes Pentecôte and Walker basin (Barnekow et al. 2007; de Vernal 2009). Based on radiocarbon dating, the postglacial period started in Lake Walker at ~7 ka cal BP (Table 4.2). However, in Lake Pentecôte, its exact onset is not clear due to the overlap with the paraglacial (as noted above).

4.6.2 Chronological challenges and/or local controls

The radiocarbon age-depth models from cores PC15-02B-P and PC15-04B-P (Lake Pentecôte) and WA15-08-P (Lake Walker) may have been influenced by technical and/or paleoenvironmental factors (Figure 4.2A–C). Despite careful sampling and pre-treatment, the chronological challenges observed include: 1) a general lack of datable macrofossils, especially in the proglacial sediments (RLC facies), hence the use of bulk sediments; 2) age reversals on cores PC15-04B-P (Lake Pentecôte) and WA15-08-U (Lake Walker); and 3) significant age difference between the proglacial and the paraglacial/postglacial sediments inferred a “hiatus” in the cores (Figures 4.3 and 4.4: Table 4.2).

The age reversals observed could be attributed to possible artefacts and/or sediment disturbance, for example, the rippled concave downward laminae shown on CT-scan images (Figure 4.3B). However, the age hiatus inferred between the proglacial and paraglacial/postglacial sediments (ca. ~22 to 8 ka cal BP; Table 2) may have resulted from any of the following: 1) the radiocarbon ages obtained represent the age of the proglacial sediments in both lakes, within given error limits (Table 4.2). For example, ¹⁴C ages of the proglacial sediments from lakes Pentecôte and Walker are comparable to those reported from some other coastal areas in Québec, e.g., Lake Jacques-Cartier (Philibert 2012) and the Charlevoix region (Brouard et al. 2016); 2) possible contamination by old carbon (Occhietti et al. 2011); and/or 3) the hiatus probably only exists because of the core location in relatively shallow water where there is some evidence of erosion on the sub-bottom profiles. The hiatus might not exist if the core was sampled from another part of the lake, not affected by erosion (Appendix IV, Figure S7). Nevertheless, radiocarbon dating especially from bulk sediments needs to be interpreted with caution (Grimm et al. 2009).

4.6.3 Inference from paleomagnetic reconstruction

On core WA15-08-U (Lake Walker), the variation of inclination from -20 to 60° without similar variation of declination (Figure 4.9) might be associated with any of the following: 1) a sampling artefact; 2) compaction or deformation of the sediment such as a slump, debris flow or other mass movement mechanisms (St-Onge et al. 2004); or (3) in case of no deformation, an excursion of Earth's magnetic field (Singer 2014; Singer et al. 2014; Stoner and St-Onge 2007). Considering the above-stated factors, the obtained results were of high quality as evidenced by MAD values below 5° (Stoner and St-Onge 2007). The dating and especially the duration of the negative event (close to 10 ka cal BP), which is present only in the clay layer (RLC facies) exclude any possible excursions, which have a much shorter duration of 1 to 2 ka (Lund et al. 2006) and are seen in both inclination and declination (Channell et al. 2012). Similarly, the NRM/ARM ratio often used as a relative paleointensity proxy (Stoner and St-Onge 2007) indicates higher normalized remanence values, which is contrary to what is observed during excursions. These observations suggest that the negative inclinations and higher normalized remanence values represent lithological variations that could be associated with movement/deformation and/or coring disturbance in the clay layer rather than genuine geomagnetic changes. Indeed, some significant deformations can clearly be observed on the CT-scan images (Appendix IV, Figure S5).

4.6.4 Last glacial maximum (LGM), deglaciation and transitional phases

Figure 4.14 illustrates a conceptual hydraulic potential model for the evolution of the Lake Walker basin from the LGM to the Late Holocene (i.e., 20-21 to 10 ka cal BP) following a southeastern ice flow direction. At ~20-21 ka cal BP, there is a high possibility that a subglacial lake existed below the

LIS in the Lake Walker basin (Figure 4.14A) based on a combination of the following: 1) the relatively flat, thick ice sheet surface; 2) the deep geological basin of Lake Walker, and its sediment storage potential (Christoffersen et al. 2008; Evatt et al. 2006; Munro-Stasiuk 2003); 3) low structural connectivity of the Lake Walker deep basin with the open coast lowlands (Gagnon-Poiré et al. 2019); and 4) associated warm-based subglacial water systems that helped to lubricate the ice flow (Margold et al. 2015). At ~15 ka cal BP (Figure 4.14B), thinning and/or steepening of the ice sheet possibly triggered less favorable conditions for the subglacial lake existence, leading to reduction in size of the subglacial lake system.

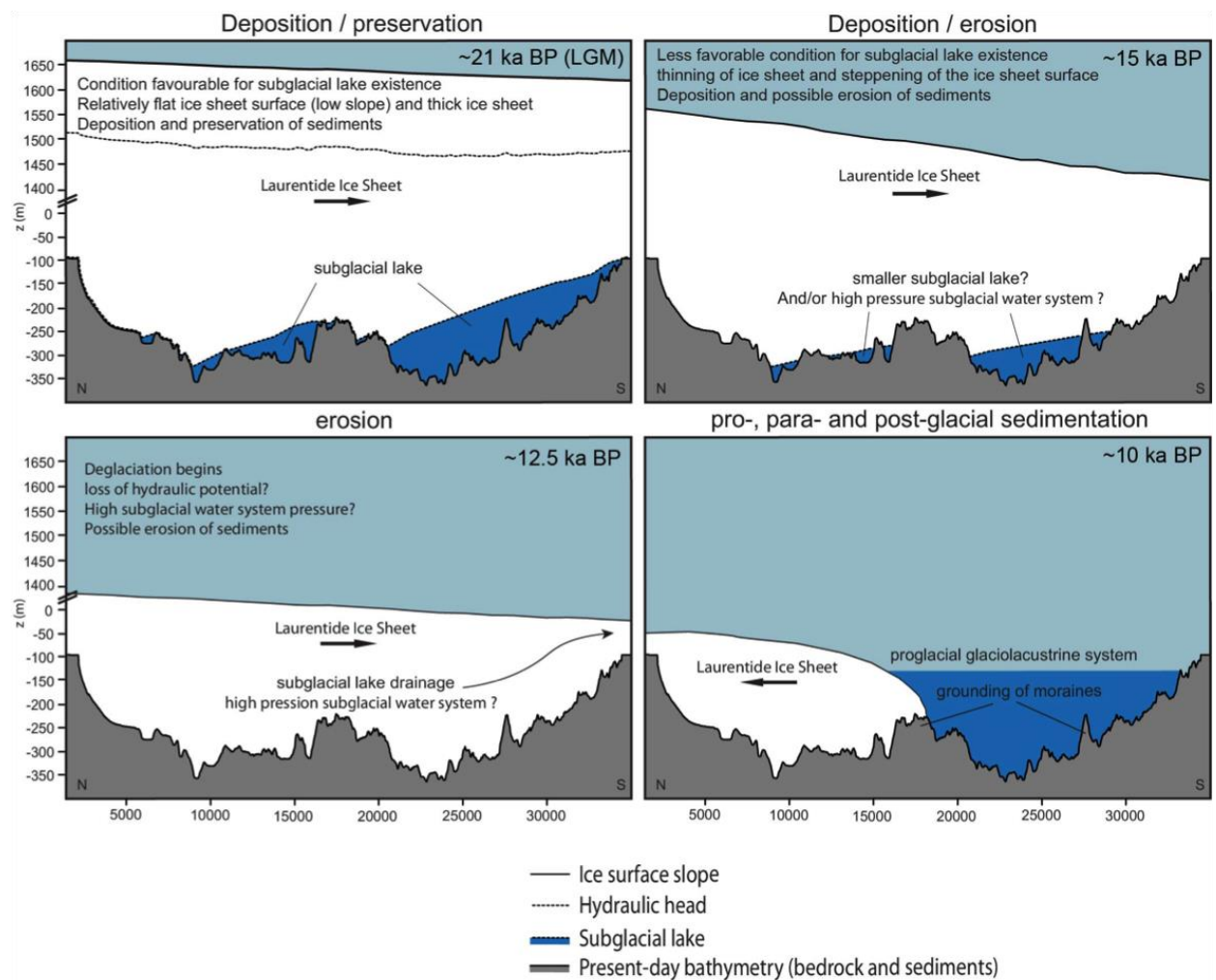


Figure 4.14: Conceptual hydraulic potential model for the evolution of the Lake Walker basin from the Last Glacial Maximum (LGM: 20 Ka) to the Late Holocene following a south-eastern ice flow direction considering a 1650 m ice thickness (Tarasov et al. 2012) and an ice sheet surface slope of 0.17. (A) at 20-21 ka BP, (B) 15 ka BP, (C) 12.5 ka BP, and (D) 10 ka BP.

At the onset of deglaciation (~12.5 ka cal BP), warm-based conditions (over 75%) at the LIS (Marshall and Clark 2002) possibly triggered high-pressure subglacial water system (Gagnon-Poiré 2016), and subsequently drainage of subglacial water from the fjord-like Lake Walker basin (Figure 4.14C) (Bamber et al. 2013). However, the V-shaped valleys observed at the base within the glacial valleys were likely not eroded by the LIS during Quaternary glaciations (Gagnon-Poiré et al. 2019; Lajeunesse 2014) and are likely able to preserve older sediments (Figure 4.14D) (Briner et al. 2007). With a similar morphometry, Lake Pentecôte could also have had the potential for the ponding of subglacial meltwater, although to a lesser extent as Lake Walker, as illustrated in Figures 4.12 and 4.13.

Sources of errors associated with glaciological modelling of the LIS have been detailed by Tarasov et al. (2012). However, in this study, the error limits of the hydraulic models are relatively minimal due to the following: 1) availability of previously computed relative sea level chronologies over the North American ice complex (Tarasov et al. 2012); 2) smaller extent of the study area (i.e., the lake Pentecôte and Walker basins) relative to larger dataset, and 3) integration of data constraints including high-resolution bathymetric data (Gagnon-Poiré et al. 2019), sediment core data, and radiocarbon ages that span the LGM to early Holocene (Tables 4.1 and 4.2).

However, this study presents relatively important gaps, mainly with regard to (1) depositional hiatuses (Figure 4.2) and (2) the interpretation of sediments in which radiocarbon dating has provided ages older than 15 ka cal BP. In the present model (Table 4.5; Figure 4.14), the older sediments (> 15 ka cal BP) are included in the proglacial environment (RLC facies), though they could be subglacial (based on hydraulic modelling results), and/or interstadial or interglacial sediments (Briner et al. 2007). If the hypothesis is true, it is arguable that RLC facies from core PC15-02C-P (Lake Pentecôte) that were dated 13–32 cal BP possibly represent subglacial and/or interglacial sediments; which might explain the occurrence of non-annual (rather centennial) laminae couplets (Figure 4.3). On the other hand, the RLC facies delineated in cores PC15-04B-P (Lake Pentecôte) and WA15-08-U (Lake Walker) represent the proglacial sediments, as already indicated (Table 4.5).

Deglacial models according to Occhietti et al. (2011), Dietrich et al. (2017a), Gagnon-Poiré et al. (2019) suggest that the retreat of the LIS in the watershed of lakes Pentecôte and Walker did not occur synchronously, partly due to differences in their relative elevation above sea level and from marine limit. Deglaciation of the Québec North Shore began at ~12.5 ka cal BP (Occhietti et al. 2011). Of the two lakes, Lake Pentecôte was the first that began to be deglaciated (Gagnon-Poiré et al. 2019) and the first to be invaded by the Goldthwait Sea at ~11.5 ka cal BP (Occhietti et al. 2011). Its elevation at 84 m asl suggests that the lake was rapidly invaded by the Goldthwait Sea that reached a maximum limit of 130 m asl at ~10.8 ka cal BP (Occhietti et al. 2011).

Lake Walker, located at 115 m asl some 30 km north of the coastline was deglaciated after Lake Pentecôte (Gagnon-Poiré et al. 2019). As the Goldthwait Sea reached its maximum limit (130 m asl) in the watershed of Lake Walker at ~10.8 ka cal BP (Occhietti et al., 2011), the LIS margin steadied ~10 km south of the lake (Lajeunesse 2016). After deglaciation in Lake Walker, there was possibly less drastic transition into glaciolacustrine setting and subsequently postglacial conditions, partly due to narrow structural connectivity with the Goldthwait Sea (Gagnon-Poiré et al. 2019), which is evidenced by relatively gentle shifts in textural and geochemical parameters compared to Lake Pentecôte (Figure 4.8). Thus, the relatively gentle shifts in these (textural/geochemical) proxies in Lake Walker support the absence of the paraglacial sediments (LS-O facies) in that Lake. However, in both lakes Pentecôte and Walker, transition from proglacial to paraglacial-postglacial sedimentation is characterized by increased clastic-organic input from their watersheds and diversity of palynomorphs.

4.7 Conclusion

Multi-proxy analyses including textural, geochemical (XRF) and palynological properties, as well as radiocarbon dating, allowed for detailed description of the lithostratigraphy and sediment facies at the transition from proglacial to paraglacial/postglacial sedimentary environments in fjord-lakes Pentecôte and Walker on the Québec North Shore (eastern Canada). The key results of this study are as follows:

- Two sediment facies were identified, namely: a rhythmically laminated clay (RLC) facies deposited in proglacial environments, and a laminated silty clay and clay facies deposited in paraglacial-postglacial environments. The latter comprises two sub-facies: laminated (organic-rich) silty clay and clay (LS-O) facies deposited in a paraglacial environment, and laminated to partially laminated sediments (LS) deposited in a postglacial environment. The RLC facies, previously described as proglacial laminated sediments (LLS facies) (Nzekwe et al. 2018) and as glaciomarine and/or glaciolacustrine sediments (Gagnon-Poiré et al. 2019) was renamed based on qualitative grain size analysis.
- The transition from proglacial (RLC facies) to paraglacial/postglacial sedimentation (LS-O/LS facies) reflects the following: 1) abrupt change from argillaceous low organic into clastic-organic sediments, respectively; 2) gradual and/or abrupt shifts in geochemical (μ -XRF) inputs; and 3) increase in palynomorph diversity.
- Based on radiocarbon dating, a hiatus is inferred between the depositional facies (RLC facies and LS-O/LS facies) found in the studied lakes. The hiatus in Lake Pentecôte is dated between 21904 ± 336 cal BP and 8075 ± 55 cal BP, while the hiatus in lake Walker is dated between 18264 ± 235 cal BP and 7904 ± 30 cal BP. This study thus provides new radiocarbon ages above and below the transition compared to that reported earlier (Gagnon-Poiré et al.

2019). More so, it has been demonstrated that rhythmic laminations in the lower sedimentary unit (RLC facies) are non-annual.

- Hydraulic potential modelling supports the hypothesis that a subglacial lake likely existed in the lakes Pentecôte and Walker basins during the LGM (21 ka cal BP). The potential for the ponding of subglacial meltwater is higher in Lake Walker compared to Lake Pentecôte, partly due to the different elevations, maximum depth and structural connectivity with the open coast. Despite challenges with radiocarbon dating of bulk sediments, integrated results from this study illustrate how successive depositional environments evolve in the studied fjord-lake basins upon deglaciation and rapid glacio-isostatic rebound.
- Finally, this paper demonstrates that fjord-lakes on the Québec North Shore, and by extension in other regions of the world have the potential (under favorable conditions) to preserve sediments during glacial periods.

4.8 Acknowledgement

This research was funded by the Natural Sciences and Engineering Research Council of Canada (NSERC) Discovery grants and Ship Time grant and by the Fonds de Recherche du Québec Nature et Technologies (FRQNT) – Recherche en équipe grant to P.F, G.S and P.L. Graduate scholarships from GEOTOP (2015) and NSERC CREATE EnviroNorth (2016) to O.P Nzekwe are acknowledged. We thank the following for their assistance in recovering the composite core (WA15-08-U) during the winter of 2015: Richard Niedereiter of UWITEC (Mondsee, Austria), Sylvain Boulianne of the Québec Ministères de Forêts, Faune et Parks and Thibault Labarre (INRS-ETE). We also thank the team that collected bathymetric/subbottom profiles from the lakes during prior field campaigns: Geneviève Philibert, Etienne Brouard, François-Xavier L'Heureux-Houde (Université Laval). Furthermore, we thank Anne de Vernal (GEOTOP-UQAM) for guidance on palynological analysis as well as David Fortin (Northern Arizona University), Arnaud De Coninck, François Lapointe, Jean-Philippe Jenny, Louis-Frédéric Daigle, Mathieu Des Roches and Léo Chassiot (INRS-ETE), Marie-Pierre St-Onge and Quentin Beauvais (UQAR-ISMER) and Valérie Béchu (Geological Survey of Canada – Québec) for their assistance in the laboratory. Finally, we thank the management and staff at La Réserve faunique de Port-Cartier-Sept-Îles for ease of access to the lakes and their assistance during fieldwork.

CHAPITRE 5

PRINCIPAUX RESULTATS ET CONTRIBUTION

5 PRINCIPAUX RÉSULTATS ET CONTRIBUTIONS

5.1 Résultats du premier article

Le premier article porte sur les sédiments récents des lacs Pentecôte, Walker et Pasteur. Le manuscrit montre comment les conditions environnementales et morphologiques ont influencé la distribution des sédiments laminés dans les trois lacs étudiés. L'utilisation de formules empiriques (Hutchinson 1957; Kinder et al. 2013; Larsen and MacDonald 1993; Larsen et al. 1998; Tylmann et al. 2013; Wetzel and Likens 1991) qui avaient déjà été appliquées à de petits lacs pourrait également servir pour les grands lacs. Les carottes à gravité échantillonnées en 2014 ont permis de définir quatre faciès sédimentaires : sédiments laminés, sédiments partiellement laminés, sédiments bioturbés et sédiments massifs. Une meilleure conservation des sédiments laminés est observée dans le lac Walker en comparaison aux lacs Pentecôte et Pasteur. Les facteurs favorisant les laminations au lac Walker incluent sa profondeur moyenne, sa profondeur maximale et son exposition topographique.

Les données de température du lac Walker acquises sur une période de deux ans ont montré qu'il existe une stratification thermique et que le mélange des eaux avait lieu deux fois par an. Donc, le lac Walker est interprété comme étant dimictique. Cette interprétation est également valable pour la plupart des autres lacs de la Côte-Nord situés à proximité (Pentecôte et Pasteur notamment) dont la géomorphologie est similaire à celle des lacs étudiés. En outre, sur la base d'une comparaison des profils de ^{210}Pb et du comptage des laminations de la carotte WA14-06-R du lac Walker, il a été proposé que les sédiments sont des varves.

5.2 Résultats du second article

Basé sur les résultats du premier article, le deuxième article établit un nouvel enregistrement varvé datant d'environ 900 ans pour le lac Walker. Ce nouvel enregistrement a été élaboré à partir d'une séquence composite WA15-08-U d'environ 4,0 m de long récupérée en 2015. L'enregistrement varvé s'étend d'environ 2340 à 3200 ± 20 cal BP, ce qui correspond à l'Holocène supérieur. Afin d'établir une chronologie varvée, deux méthodes de comptage manuel ont été comparées : le logiciel PeakCounter versus les images obtenues au MEB à même les lames minces. La comparaison des deux méthodes indique que la chronologie des varves établie à l'aide de lames minces montre une corrélation plus forte avec la datation au radiocarbone AMS et est donc plus fiable. La composition des sédiments varvés du lac Walker est clastique selon la définition de Zolitschka et al. (2015). L'épaisseur moyenne de la varve est de $0,86 \text{ mm a}^{-1}$. La nouvelle chronologie varvée du lac Walker est ancrée sur les datations radiocarbonées. Cependant, cette séquence offre des perspectives remarquables pour la reconstitution paléoclimatologique à haute résolution dans la région de la Côte-

Nord du Québec vers 2340 à 3200 ± 20 cal BP, où des enregistrements similaires sont relativement rares.

5.3 Résultats du troisième article

Cet article examine les changements paléoenvironnementaux survenus lors de la transition d'environnements glaciaires à paraglaciaux/postglaciaires dans le bassin versant des lacs Pentecôte et Walker. La méthodologie implique une combinaison de différents paramètres, notamment : granulométrie, géochimie (XRF), palynologie et paléomagnétisme. En utilisant ces méthodes, deux faciès sédimentaires ont été décrits le long de trois carottes: les carottes PC15-02C-P et PC15-04B-P du lac Pentecôte et la partie inférieure de la séquence composite de la carotte WA15-08-U (~480–729 cm cd) du lac Walker. Les faciès sédimentaires comprennent : les faciès argileux laminés rythmiquement (RLC) déposés dans un environnement proglaciaire et les sédiments laminés déposés dans un environnement paraglaciaire/postglaciaire. Ce dernier est divisé en deux sous-parties : les faciès d'argile silteuse laminée (riche en matière organique) et d'argile (LS-O) déposée dans un environnement paraglaciaire et les faciès à sédiments partiellement laminés (LS) déposés dans un environnement postglaciaire. Les principales caractéristiques de la transition de la sédimentation proglaciaire à la sédimentation paraglaciaire/postglaciaire sont les modifications abruptes des propriétés texturales, les modifications des signatures géochimiques, l'augmentation de la diversité des palynomorphes, ainsi que les anomalies négatives des inclinaisons paléomagnétiques. Selon la datation radiocarbone, un hiatus d'âge et/ou de sédimentation a été déduit entre ~ 22 et 8 ka cal BP dans le lac Pentecôte et entre ~18 et 8 ka cal BP dans le lac Walker. La modélisation du potentiel hydraulique indique que des lacs sous-glaciaires existaient probablement dans les bassins des lacs Pentecôte et Walker pendant le dernier maximum glaciaire (~ 21 ka cal BP) (Tarasov et al. 2012) avant la déglaciation, ce qui aurait favorisé la préservation des sédiments déposés dans les deux bassins.

5.4 Originalité et forces de la recherche

Cette recherche doctorale a révélé un potentiel élevé de nouveaux enregistrements paléoclimatiques sur la Côte-Nord du Québec, un domaine de forte pertinence sociétale pour les infrastructures régionales. L'utilisation de méthodologies novatrices dans le cadre d'une approche multidisciplinaire a permis de découvrir des archives sédimentologiques québécoises et de les caractériser de fond en comble. Les points forts de cette thèse sont les suivants :

5.4.1 Étude pionnière en limnologie des lacs étudiés

En ce qui a trait à la limnogéologie, les trois lacs étudiés (les lacs Pentecôte, Walker et Pasteur) étaient jusqu'alors inexplorés, car la littérature publiée sur eux était limitée, à l'exception de ceux

concernant la géomorphologie (Lajeunesse 2014). Par conséquent, cette recherche (Nzekwe et al. 2018) peut être considérée comme une étude pionnière pour ces lacs. L'étude sur les facteurs qui influencent la préservation des sédiments laminés dans ces lacs (chapitre 2) sera directement applicable aux études de reconnaissance dans d'autres lacs du Nord du Québec qui n'ont pas encore été étudiés (par exemple, le lac Yasinski, Baie-James; Figure 1.4). De plus, les informations sur la stratification thermique, le mélange des sédiments et les vitesses de sédimentation des bassins versants jusqu'aux lacs seront utiles aux communautés locales, comme la réserve faunique Port-Cartier-Sept-Îles. Avant cette recherche, les profondeurs des lacs étaient inconnues, la plupart des informations étant basées sur des observations faites par les pêcheurs locaux avec des appareils destinés au grand public. Cependant, cette étude (Nzekwe et al. 2018) et un article co-écrit (Gagnon-Poiré et al. 2019) sous la supervision de Patrick Lajeunesse ont répondu à ces questions de recherche.

5.4.2 Nouvel enregistrement varvé du lac Walker

L'application de l'analyse multi-échelles des sédiments laminés (scanner, photos numériques, logiciel PeakCounter et lames minces) a constitué un avantage majeur dans cette recherche. La découverte d'une nouvelle séquence varvée d'environ 900 ans dans le lac Walker (chapitre 3) constitue le premier enregistrement de varve dans la région de la Côte-Nord du Québec (d'après la littérature publiée). L'enregistrement varvé pourrait éventuellement être ajouté à la base de données globale des varves (Zolitschka et al. 2015). Cette étude contribuera à l'amélioration des modèles climatiques régionaux en fournissant une série chronologique de conditions climatiques environnementales basée sur les varves.

En outre, sur la base du nouvel enregistrement varvé du lac Walker, une recherche en cours montre que l'analyse spectrale de l'enregistrement varvé pourrait révéler des périodicités significatives pouvant être liées à des oscillations climatiques connues (Lapointe et al., en préparation; Annexe V). Éventuellement, on pourrait procéder à un étalonnage hydrologique des propriétés des sédiments laminés des lacs de la région. Ceci impliquera une comparaison statistique des propriétés des sédiments annuels avec les enregistrements instrumentaux (Lapointe et al. 2012) et potentiellement à l'aide des reconstitutions à partir des cernes d'arbres disponibles dans la zone d'étude. Ces données pourront servir à établir un modèle permettant de fournir des reconstitutions quantifiées du climat et de l'hydrologie dans la région. De telles reconstitutions, en particulier celles liées à des événements isolés (ex. turbidites, dépôts rapides et / ou inondations), pourraient permettre une meilleure gestion des risques liés à l'utilisation du territoire (ex. Plan-Nord du gouvernement du Québec) et des infrastructures régionales (ex. barrages hydroélectriques) gérées par Hydro-Québec.

5.4.3 Amélioration des modèles antérieurs portant sur la déglaciation sur la Côte-nord, Québec

En ce qui concerne les suggestions d'Occhietti et al. (2011) (voir section 1.12.2), cette thèse fournit des datations radiométriques et des preuves géologiques (sédiments laminés) qui s'étendent du dernier maximum glaciaire au récent. Plus précisément, cette thèse de doctorat (chapitre 4) propose une analyse multi-paramètres des sédiments déposés lors de la transition de l'environnement proglaciaire à l'environnement paraglaciaire/postglaciaire. En utilisant les paramètres physiques et géochimiques couplés à plusieurs datations radiocarbonées, il a été possible de corrélérer avec les modèles paléoenvironnementaux régionaux (Dietrich et al. 2017b; Gagnon-Poiré et al. 2019; Occhietti et al. 2011). L'étude récente (Gagnon-Poiré et al. 2019) est basée sur une seule date radiocarbone AMS échantillonnée à partir de sédiments déposés au cours de la transition glaciaire tardive à paraglaciaire/postglaciaire dans chaque lac. La présente étude se base sur trois nouvelles dates radiocarbonées à partir de sédiments déposés lors de la transition postglaciaire tardive dans les lacs Pentecôte et Walker, ce qui a permis de mieux caractériser cette transition importante.

5.5 Limites et défis de la recherche

5.5.1 Logistique et instrumentation

Dans le premier cas, les lacs Pentecôte, Walker et Pasteur sont situés dans une zone relativement isolée. Des problèmes de logistique ont donc été rencontrés au cours des travaux sur le terrain, malgré une planification minutieuse. Le lac Pasteur est le lac le moins accessible par la route ; seules des carottes courtes ont été récupérées dans ce lac en 2014. Les missions ultérieures pour ce lac ont été annulées en partie parce qu'il était peu probable que les sédiments soient des varves (chapitre 1) et également en raison de contraintes logistiques. Sur le lac Walker, l'utilisation d'un carottier à gravité à bord du ponton a posé des problèmes techniques, en partie à cause du bassin relativement profond du lac et de l'effet des vents forts ce qui a causé de fortes vagues. En fait, à l'automne 2014, la mesure des propriétés physicochimiques du lac Walker (chapitre 1) a été annulée à mi-parcours en raison d'une tempête et du risque de chavirement du bateau. Pour améliorer la sécurité, les sorties au lac ont ensuite été conduites à bord d'un autre bateau, le RV Louis-Hamelin, qui est mieux conçu pour le carottage et les conditions météorologiques défavorables.

5.5.2 Fabrication de lames minces

Le processus de fabrication des lames minces est relativement long et comporte plusieurs étapes qui pourraient introduire des erreurs dans le comptage des lamines. Lors de l'échantillonnage, il convient de veiller à ce que le sédiment soit parfaitement humide avant d'extraire les profilés de sédiment. Lors de l'échantillonnage de sédiments du lac Walker (carotte WA15-08-U), il serait recommandé d'extraire les sédiments le long des U « channels » collectés à des fins paléomagnétiques, car ce creux

au centre de la carotte facilite l'échantillonnage pour les lames minces.

Une étape essentielle est peut-être de s'assurer que les lames minces sont coupées avec un chevauchement adéquat (au moins 1 cm), ce qui permet la corrélation du nombre de varves d'une lame mince à l'autre. Une communication claire doit être établie avec la personne qui découpe les lames minces (une compagnie externe, Texas Petrographic Service, a été utilisée pour cette recherche). Ainsi, certaines lames minces de la séquence composite (WA15-08-U) ont été renvoyées, car il y avait de petits espaces sans sédiment (une erreur de la compagnie), ce qui a rendu le comptage des lamines et l'estimation des erreurs plus fastidieux. En conclusion, les lames minces doivent être inspectées immédiatement après leur retour.

5.5.3 Déploiement de pièges à sédiments

L'un des objectifs initiaux de la recherche visait à surveiller les transferts de sédiments et les processus limnologiques responsables de la formation de sédiments annuellement laminés dans la zone d'étude (par exemple, Cockburn et Lamoureux 2008; Fortin et al. 2015). En juin 2014, deux pièges à sédiments (SARL TECHNICAP, France) ont été déployés avec les capteurs de température et de pression (Chapitre 2) et l'acquisition de données s'est échelonnée sur une période de deux ans. Cependant, au printemps 2016, les pièges à sédiments avaient été déplacés de leur position fixe et ont été amenés dans le bassin profond, probablement à cause du fort courant d'eau observé lors de la fonte nivale printanière. Malheureusement, aucun sédiment n'a été recueilli dans les pièges à sédiments récupérés à l'automne 2016 (Nzekwe et al. 2015). Cet objectif a donc été supprimé et remplacé par un autre (Chapitre 4). Sur une note positive, les leçons tirées du déploiement infructueux des pièges à sédiments dans le lac Walker (annexe 4) ont été utiles pour le récent déploiement de pièges à sédiments à Grand Lac (un projet différent).

5.5.4 Datation radiocarbone sur sédiment total

Dans cette étude, la datation au radiocarbone était largement basée sur l'analyse de sédiment total en raison de la rareté de fragments de bois et autres fossiles datables. L'amélioration des datations dans les environnements étudiés ici passera par la datation de matériaux autres que les sédiments bruts. Il faudrait également trouver des fragments de bois au même niveau que les datations radiocarbonées obtenues sur du sédiment total pour estimer l'effet de réservoir possible, tout en améliorant les modèles d'âge. En plus, l'interruption d'âge pourrait être confirmé par l'analyse paléomagnétique de carotte PC15-04B-P (lac Pentecôte) et / ou par de nouveaux carottes de sédiment contenant des sédiments déposés au cours de la transition glaciaire-post-glaciaire / paraglaciaire (sous la direction de Guillaume St-Onge).

5.5.5 Contraintes de temps

Les contraintes de temps rencontrées au cours de la thèse étaient multiples. Du point de vue technique, le carottage et l'instrumentation dans les bassins profonds et isolés des trois lacs ont duré plusieurs mois. Cela était cependant nécessaire pour une planification et une logistique d'équipe soignées. Un retard important et imprévu s'est produit lorsque deux pièges à sédiments déployés au lac Walker en 2014-2016 n'ont pas été récupérés à la fin des deux premières années. Sur la base de l'objectif initial du projet, les pièges à sédiments étaient supposés fournir des données pour l'étalonnage des sédiments varvés du lac Walker (censé être le troisième chapitre de la thèse) et, entre autres, calculer les flux sédimentaires dans le lac. Un résumé du déploiement des pièges à sédiments sera fourni en annexe V. Malgré ce retard, de nouvelles hypothèses (hypothèses 3 et 4) ont été formulées et évaluées (chapitre 4).

Du point de vue des analyses de laboratoire, cette recherche a impliqué plusieurs analyses qui ont été effectuées dans plusieurs laboratoires. Il était donc nécessaire de déplacer les carottes et / ou les échantillons d'un endroit à un autre (par exemple, tomodensitogramme à l'INRS à Québec, le MSCL et paléomagnétisme à ISMER, à Rimouski, les datations aux radiocarbones à Université Laval, Québec et à UC Irvine, la palynologie au Geotop, à Montréal et les lames minces au Texas). Ceci est un avantage, cependant, il faut suffisamment de temps pour respecter le calendrier de chaque laboratoire et les parties prenantes, y compris les directeurs de recherche, les co-directeurs et les co-auteurs.

5.6 Discussion générale et conclusions

Cette thèse de doctorat a évalué les sédiments laminés de trois lacs profonds (les lacs Pentecôte, Walker et Pasteur) à l'aide d'analyses multidisciplinaires. En évaluant la première hypothèse (section 1.10.1), il a été démontré que, bien que les conditions préalables prises en compte pour les lacs étudiés (bassin relativement profond, climat boréal et apport sédimentaire saisonnier) soient favorables au dépôt de sédiments laminés, ces facteurs sont cependant insuffisants pour assurer la préservation des lamines, car d'autres facteurs sont en jeu (chapitre 2). Plus précisément, dans le bassin du lac Walker, des paramètres morphologiques tels que la profondeur relative, la profondeur maximale et certaines variables (profondeur moyenne, fetch moyen du vent, fetch maximal du vent et l'exposition topographique) favorisent la préservation des lamines par rapport aux lacs Pentecôte et Pasteur. En outre, dans les lacs dimictiques (tels que les lacs étudiés), lorsque les profondeurs auxquelles se déposent les sédiments laminés sont plus profondes que la profondeur du mélange des eaux et des débits/crues printaniers, la préservation des sédiments laminés est plus accentuée. La stratification thermique observée dans les lacs étudiés est similaire à celle observée dans les autres bassins. Par exemple, comme dans l'illustration du lac Suminko (Tylmann et al. 2012) (voir la figure 1.13), des sédiments laminés du lac Walker caractérisent l'hypolimnion; des sédiments partiellement laminés

marquent la thermocline et des sédiments bioturbés se déposent dans l'épilimnion (Figure 2.4). Notez que la différence de nomenclature des couches de stratification est basée sur le paramètre testé (composition chimique par rapport à la température, respectivement). Néanmoins, c'est la présence de stratification qui importe (Håkanson and Jansson 2002).

En évaluant la deuxième hypothèse (section 1.10.2), il a été démontré que (1) les sédiments de l'Holocène supérieur du lac Walker sont varvés, et (2) que le comptage par lames minces était plus approprié que le logiciel PeakCounter pour construire la chronologie des varves (Chapitre 3). Afin de comprendre les difficultés liées à l'utilisation du logiciel PeakCounter, une étude comparative du comptage manuel multi-paramètres de sédiments variés du lac Suigetsu (carotte SG06) au Japon (Marshall et al. 2012) montre que l'utilisation des données élémentaires XRF (60 µm) et les radiographies (résolution 60 µm) ont permis une délimitation optimale des sédiments de varves (épaisseur moyenne de 0,8–1 mm) dans ce lac. D'autre part, les analyses XRF faites au lac Walker possèdent une résolution maximale de 100 µm qui était insuffisante pour délimiter clairement les sédiments varvés de la carotte WA15-08-U (épaisseur moyenne de 0,86 mm). Par ailleurs, la méthode de comptage par lames minces reste une méthode efficace et fiable pour définir différentes chronologies, comme le montrent plusieurs études (Cuvet et al. 2010; Francus 1998, 2001; Francus and Asikainen 2001; Francus et al. 2002; Francus and Karabanov 2000; Jouve et al. 2013; Lapointe et al. 2012; Lapointe et al. 2019; Ojala and Alenius 2005; Tiljander et al. 2002; Zolitschka et al. 2015).

En ce qui a trait à la troisième hypothèse (section 1.10.3), l'existence d'un hiatus d'âge et/ou de sédimentation lors de la transition proglaciaire à para/postglaciaire dans les lacs Pentecôte et Walker (chapitre 4) doit être vérifiée de manière indépendante. Les contraintes chronologiques obtenues dans cette thèse ont principalement été la datation radiocarbone sur du sédiment total. À cet égard, de nouvelles carottes provenant d'une partie différente du bassin sédimentaire et plus susceptibles à contenir des microorganismes comme les diatomées ou les foraminifères ce qui permettrait de savoir si l'environnement sédimentaire était lacustre ou marin à la transition glaciaire postglaciaire et son âge associé. Nonobstant, le hiatus semble indiquer que des sédiments se sont déposés avant le Dryas Récent, et qu'une partie a été conservée, même avec l'érosion associée à la présence glaciaire. Les études à venir pourraient donc porter sur la datation des sédiments glaciomarins et glaciolacustres des lacs Pentecôte et Walker ou d'autres lacs de la Côte-Nord québécoise en utilisant des méthodes/matériaux autres que les échantillons de sédiment total (Vincent and Prest 1987).

En somme, les principaux résultats (chapitres 2 à 4) de cette thèse de doctorat indiquent ce qui suit : les lacs étudiés (lacs Pentecôte, Walker et Pasteur) ont le potentiel de préserver des sédiments laminés. Cependant, seul le lac Walker contient des sédiments récents (datant des 150 dernières années) qui sont varvés en raison de facteurs morphologiques plus favorables que les deux autres lacs. Le lac Walker contient des sédiments varvés de l'Holocène Supérieur, couvrant une période allant de

2340 à 3200 ± 20 cal BP, soit environ 900 ans. La transition de la sédimentation proglaciaire à la sédimentation paraglaciaire/postglaciaire dans les lacs étudiés est caractérisée par des changements abrupts de signatures texturales, géochimiques, palynologiques et paléomagnétiques. Les lacs Pentecôte et Walker contiennent des sédiments qui semblent avoir été préservés durant le dernier maximum glaciaire. Si cette hypothèse s'avère exacte, un lac sous-glaciaire aurait probablement existé dans les bassins des lacs Pentecôte et Walker pendant le dernier maximum glaciaire.

5.7 Bibliographie intégrée

- Andrews M, Knight J, Gray L. (2015) A simulated lagged response of the North Atlantic Oscillation to the solar cycle over the period 1960–2009. *Environmental Research Letters* 10:054022.
- Antevs E. (1922) The recession of the last ice sheet in New England. American Geographical Society.
- Antevs E. (1925) Retreat of the Last Ice Sheet in Eastern Canada. Geological Survey of Canada, , Ottawa
- Antevs E. (1928) The last glaciation, with special reference to the ice retreat in northeastern North America. New York American Geological Society
- Antevs E. (1931) Late-glacial correlations and ice recession in Manitoba. Geological Survey of Canada, Ottawa.
- Antoniades D. (2017) An Overview of Paleoenvironmental Techniques for the Reconstruction of Past Arctic Ice Shelf Dynamics. In: Copland L, Mueller D (eds), *Arctic Ice Shelves and Ice Islands*. Springer Netherlands, Dordrecht, pp. 207-226.
- Appleby P, Oldfield F. (1978) The calculation of lead-210 dates assuming a constant rate of supply of unsupported 210 Pb to the sediment. *Catena* 5:1-8.
- Appleby PG, Oldfield F, Thompson R, Huttunen P, Tolonen K. (1979) Pb-210 Dating of Annually Laminated Lake-Sediments from Finland. *Nature* 280:53-55.
- ARCHIVES.INRS. (2009) Le projet ARCHIVES : Analyse Rétrospectives des Conditions Hydroclimatiques à l'aide des Indicateurs de leur Variabilité à l'Echelle Séculaire.
- Arseneault D, Dy B, Gennaretti F, Autin J, Begin Y. (2013) Developing millennial tree ring chronologies in the fire - prone North American boreal forest. *Journal of Quaternary Science* 28:283-292.
- Bamber JL, Siegert MJ, Griggs JA, Marshall SJ, Spada G. (2013) Paleofluvial mega-canyon beneath the central Greenland ice sheet. *Science* 341:997-999.
- Barnekow L, Loader NJ, Hicks S, Froyd CA, Goslar T. (2007) Strong correlation between summer temperature and pollen accumulation rates for *Pinus sylvestris*, *Picea abies* and *Betula* spp. in a high-resolution record from northern Sweden. *Journal of Quaternary Science* 22:653-658.
- Bertrand S, Hughen AK, Sepulveda J, Pantoja S. (2012) Geochemistry of surface sediments from the fjords of Northern Chilean Patagonia (44–47°S): Spatial variability and implications for paleoclimate reconstructions. *Geochimica Et Cosmochimica Acta* 76:125-146.
- Besré F, Occhietti S. (1988) Les rhymites à laminations saisonnières de Leclercville, du Sangamonien s. l. (?) de la vallée du Saint-Laurent, Québec., Annales de l'ACFAS résumé, p. 111.
- Besré F, Occhietti S. (1990) Les varves de Deschaillons, les rythmites du Saint-Maurice et les rythmites de Leclercville, Pleistocene supérieur, vallée du Saint-Laurent, Québec. *Geographie Physique Et Quaternaire* 44:181-198.
- Blaauw M. (2010a) Methods and code for ‘classical’ age-modelling of radiocarbon sequences. *Quaternary Geochronology* 5:512-518.

Blaauw M. (2010b) R-Code for 'classical' age-modelling (CLAM V1.0) of radiocarbon sequences. Supplement to: Blaauw, M (2010): Methods and code for 'classical' age-modelling of radiocarbon sequences Quaternary Geochronology, 5(5), 512-518. PANGAEA.

Blatt H, Tracy RJ, Owens BE. (2006) Petrology, Igneous, Sedimentary, and Metamorphic. W.H Freeman & Company, New York.

Blott SJ, Pye K. (2001) GRADISTAT: a grain size distribution and statistics package for the analysis of unconsolidated sediments. Earth Surface Processes and Landforms 26:1237-1248.

Bluszczyk P, Luecke A, Ohlendorf C, Zolitschka B. (2009) Seasonal dynamics of stable isotopes and element ratios in authigenic calcites during their precipitation and dissolution, Sacrower See (northeastern Germany). Journal of Limnology 68:257-273.

Boespflug X, Long BFN, Occhietti S. (1995) Cat-Scan in Marine Stratigraphy - a Quantitative Approach. Marine Geology 122:281-301.

Boggs S. (1995) Principles of Sedimentology and Stratigraphy. Prentice-Hall, Inc., Upper Saddle River, New Jersey.

Bouchard F, Proulx V, Pienitz R, Antoniades D, Tremblay R, Vincent WF. (2017) Periphytic diatom community structure in thermokarst ecosystems of Nunavik (Québec, Canada). Arctic Science 4:110-129.

Boyd B, Anderson J, Wellner J, Fernandez R. (2008) The sedimentary record of glacial retreat, Marinelli Fjord, Patagonia: Regional correlations and climate ties. Marine Geology 255:165-178.

Bradley RS. (1999) Paleoclimatology: Reconstructing climates of the Quaternary. Academic Press, San Diego, 595 pp.

Breckenridge A, Lowell TV, Stroup JS, Evans G. (2012) A review and analysis of varve thickness records from glacial Lake Ojibway (Ontario and Quebec, Canada). Quaternary International 260:43-54.

Briner J, Axford Y, Forman S, Miller G, Wolfe A. (2007) Multiple generations of interglacial lake sediment preserved beneath the Laurentide Ice Sheet. Geology 35:887-890.

Brooks GR. (2020) Evidence of a strong paleoearthquake in ~9.1 ka cal BP interpreted from mass transport deposits, western Quebec – northeastern Ontario, Canada. Quaternary Science Reviews 234:106250.

Brouard E, Lajeunesse P, Cousineau PA, Govare É, Locat J. (2016) Late Wisconsinan deglaciation and proglacial lakes development in the Charlevoix region, southeastern Québec, Canada. Boreas 45:754-772.

Butler K, Prior CA, Flenley JR. (2004) Anomalous Radiocarbon Dates from Easter Island. Radiocarbon 46:395-405.

Campos C, Beck C, Crouzet C, Carrillo E, Van Welden A, Tripsanas E. (2014) Late Quaternary paleoseismic sedimentary archive from deep central Gulf of Corinth: time distribution of inferred earthquake-induced layers. Annals of Geophysics 56.

Casse M, Montero - Serrano JC, St - Onge G. (2017) Influence of the Laurentide Ice Sheet and relative sea - level changes on sediment dynamics in the Estuary and Gulf of St. Lawrence since the last deglaciation. Boreas 46:541-561.

Centre d'expertise hydrique. (2016) Historique des données de différentes stations hydrométriques. Ministère de l'Environnement et de la Lutte contre les changements climatiques https://wwwcehqgouvqcca/hydrometrie/historique_donnees/indexasp.

Channell J, Hodell D, Curtis J. (2012) ODP Site 1063 (Bermuda Rise) revisited: oxygen isotopes, excursions and paleointensity in the Brunhes Chron. *Geochemistry, Geophysics, Geosystems* 13.

Christoffersen P, Tulaczyk S, Wattrus NJ, Peterson J, Quintana-Krupinski N, Clark CD, Sjunneskog C. (2008) Large subglacial lake beneath the Laurentide Ice Sheet inferred from sedimentary sequences. *Geology* 36:563-566.

Clarke GKC. (2005) Subglacial processes. *Annual Review of Earth and Planetary Sciences* 33:247-276.

Cockburn JMH, Lamoureux SF. (2008) Inflow and lake controls on short-term mass accumulation and sedimentary particle size in a High Arctic lake: implications for interpreting varved lacustrine sedimentary records. *Journal of Paleolimnology* 40:923-942.

Cogné J. (2003) PaleoMac: a Macintosh™ application for treating paleomagnetic data and making plate reconstructions. *Geochemistry, Geophysics, Geosystems* 4.

Coleman AP. (1909) Lake Ojibway; last of the great glacial lakes. Ontario Bureau of Mines, pp. 284-293.

Cremer JF, Long B, Desrosiers G, de Montety L, Locat J. (2002) Application of scanography to sediment density analysis and sediment structure characterization: Case of sediments deposited in the Saguenay River (Quebec, Canada) after the July 1996 flood. *Canadian Geotechnical Journal* 39:440-450.

Croudace IW, Rindby A, Rothwell RG. (2006) ITRAX: description and evaluation of a new multi-function X-ray core scanner. *Special Publication: Geological Society of London* 267:51.

Cuven S, Francus P, Lamoureux SF. (2010) Estimation of grain size variability with micro X-ray fluorescence in laminated lacustrine sediments, Cape Bounty, Canadian High Arctic. *Journal of Paleolimnology* 44:803-817.

Davis RB, Hess CT, Norton SA, Hanson DW, Hoagland KD, Anderson DS. (1984) ^{137}Cs and ^{210}Pb dating of sediments from soft-water lakes in New England (U.S.A.) and Scandinavia, a failure of ^{137}Cs dating. *Chemical Geology* 44:151-185.

De Geer G. (1912) A geochronology of the last 12,000 years. *Proceedings of the 11th International Geological Congress*, 1910, Stockholm, pp. 241-258.

de Vernal A. (2009) Marine palynology and its use for studying nearshore environments. *IOP Conference Series: Earth and Environmental Science*.

de Vernal A, Bilodeau G, Henry M. (2010) Micropaleontological Preparation Techniques and Analyses. *Cahier du Geotop numero 3*.

Dearing JA. (1979) Application of Magnetic Measurements to Studies of Particulate Flux in Lake-watershed Ecosystems. Ph.D. Thesis, University of Liverpool, U.K.

Desloges JR, Gilbert R. (1994) Sediment source and hydroclimatic inferences from glacial lake sediments: the postglacial sedimentary record of Lillooet Lake, British Columbia. *Journal of Hydrology* 159:375-393.

Dietrich P, Ghienne J-F, Normandeau A, Lajeunesse P. (2016) Upslope-migrating bedforms in a proglacial sandur delta: cyclic steps from river-derived underflows? *Journal of Sedimentary Research* 86:113-123.

Dietrich P, Ghienne J-F, Normandeau A, Lajeunesse P. (2017a) Reconstructing ice-margin retreat using delta morphostratigraphy. *Scientific Reports* 7:16936.

Dietrich P, Ghienne J-F, Schuster M, Lajeunesse P, Nutz A, Deschamps R, Roquin C, Durner P. (2017b) From outwash to coastal systems in the Portneuf–Forestville deltaic complex (Québec North Shore): Anatomy of a forced regressive deglacial sequence. *Sedimentology* 64:1044-1078.

Dodge Y. (2003) *The oxford dictionary of statistical terms* Oxford University Press.

Dredge LA. (1983) Surficial geology of the Sept-Îles area, Quebec north shore. *Geological Survey of Canada*, Vol. 408, Ottawa, 1-40 pp.

Elson JA. (1969) Late Quaternary marine submergence of Quebec. *Revue de géographie de Montréal* 23:247-258.

ESRI. (2014) *ArcGIS Desktop: Release 10.3*. Environmental Systems Research Institute, Redlands, CA.

Evatt G, Fowler A, Clark C, Hulton N. (2006) Subglacial floods beneath ice sheets. *Philosophical Transactions of the Royal Society of London A: Mathematical, Physical and Engineering Sciences* 364:1769-1794.

Eyles N, Mullins HT, Hine AC. (1990) Thick and fast: sedimentation in a Pleistocene fiord lake of British Columbia, Canada. *Geology* 18:1153-1157.

Flowers GE. (2015) Modelling water flow under glaciers and ice sheets. *Proceedings Mathematical, physical and engineering sciences* 471:20140907.

Folk RL, Ward WC. (1957) Brazos River bar [Texas]; a study in the significance of grain size parameters. *Journal of Sedimentary Research* 27:3-26.

Fortin D, Francus P, ARCHIVES Team. (2012) Potentiel des sédiments lacustres annuellement laminés pour reconstruire les conditions hydroclimatiques au Québec-Labrador - Project ARCHIVES. Atelier du groupe ARCHIVES, Atelier Ouranos, Varennes, Québec.

Fortin D, Francus P, Gebhardt AC, Hahn A, Kliem P, Lise-Pronovost A, Roychowdhury R, Labrie J, St-Onge G, Team PS. (2013) Destructive and non-destructive density determination: method comparison and evaluation from the Laguna Potrok Aike sedimentary record. *Quaternary Science Reviews* 71:147-153.

Fortin D, Kaufman DS, Arnold M, Schiefer E, Hawley N. (2015) Late - Summer Peak in Sediment Accumulation in Two Lakes with Contrasting Watersheds, Alaska. *Geografiska Annaler: Series A, Physical Geography* 97:709-719.

Francus P. (1998) An image-analysis technique to measure grain-size variation in thin sections of soft elastic sediments. *Sedimentary Geology* 121:289-298.

Francus P. (2001) Quantification of bioturbation in hemipelagic sediments via thin-section image analysis. *Journal of Sedimentary Research* 71:501-507.

Francus P. (2006) Image Analysis, Sediments and Paleoenvironments. Developments in Paleoenvironmental Research, vol. 7. Springer, Dordrecht, 330 pp.

Francus P, Asikainen CA. (2001) Sub-sampling unconsolidated sediments: A solution for the preparation of undisturbed thin-sections from clay-rich sediments. *Journal of Paleolimnology* 26:323-326.

Francus P, Bradley RS, Abbott MB, Patridge W, Keimig F. (2002) Paleoclimate studies of minerogenic sediments using annually resolved textural parameters. *Geophysical Research Letters* 29.

Francus P, Bradley RS, Lewis T, Abbott M, Retelle M, Stoner JS. (2008) Limnological and sedimentary processes at Sawtooth Lake, Canadian High Arctic, and their influence on varve formation. *Journal of Paleolimnology* 40:963-985.

Francus P, Karabanov E. (2000) A computer-assisted thin-section study of Lake Baikal sediments: a tool for understanding sedimentary processes and deciphering their climatic signal. *International Journal of Earth Sciences* 89:260-267.

Francus P, Nobert P. (2007) An integrated computer system to acquire, process, measure and store images of laminated sediments., 4th International Limnogeology Congress, Barcelona, Spain (11–14th July).

Francus P, Ridge JC, Johnson MD. (2013a) The rise of varves. *Gff* 135:229-230.

Francus P, Von Suchodoletz H, Dietze M, Donner RV, Bouchard F, Roy AJ, Fagot M, Verschuren D, Kropelin S. (2013b) Varved sediments of Lake Yoá (Ounianga Kebir, Chad) reveal progressive drying of the Sahara during the last 6100 years. *Sedimentology* 60:911-934.

Fulton RJ. (1984) Quaternary Stratigraphy of Canada: A Canadian Contribution to IGCP Project 24. Ottawa, Canada: Canadian Government Publication Centre, Supply and Services Canada.

Gagnon-Poiré A. (2016) Sédimentation tardi-quaternaire glaciaire à postglaciaire dans trois fjords lacustres adjacents du sud-est du Bouclier canadien. (Mémoire de maîtrise non publiée) Centre d'études nordiques, Département de géographie. Université Laval, Québec.

Gagnon-Poiré A, Francus P, Fortin D, Lajeunesse P, Brigode P, Trottier A-P. (2018) The potential for reconstructing the hydroclimatic variability in the boreal forest of Québec-Labrador from Grand Lake varved sediments. 20th International Sedimentological Congress - ICS2018. Book of abstract, Québec, Canada, p. 893.

Gagnon-Poiré A, Francus P, Fortin D, Lajeunesse P, Trottier A-P. (2017) The potential of Grand Lake varved sediments to reconstruct the hydroclimatic variability of the boreal forest of Québec-Labrador. Colloque annuel du Centre d'Études Nordiques (CEN), Québec, Canada, 16-17 February.

Gagnon-Poiré A, Lajeunesse P, Normandeau A, Francus P, St-Onge G, Nzekwe OP. (2019) Corrigendum to “Late-Quaternary glacial to postglacial sedimentation in three adjacent fjord-lakes of the Québec North Shore (eastern Canadian Shield)”[Quat. Sci. Rev. 186 (2018) 91–110]. *Quaternary Science Reviews* 220:401-403.

Gilbert R. (1975) Sedimentation in Lillooet Lake, British Columbia. *Canadian Journal of Earth Sciences* 12:1697-1711.

Gorham E, Boyce FM. (1989) Influence of lake surface area and depth upon thermal stratification and the depth of the summer thermocline. *Journal of Great Lakes Research* 15:233-245.

Gouhier T, Grinsted A. (2012) Biwavelet: Conduct univariate and bivariate wavelet analyses, R package version 0.13. available at: <https://cran.r-project.org/web/packages/biwavelet/biwavelet.pdf>.

Gray LJ, Beer J, Geller M, Haigh JD, Lockwood M, Matthes K, Cubasch U, Fleitmann D, Harrison G, Hood L. (2010) Solar influences on climate. *Reviews of Geophysics* 48.

Grimm EC, Maher LJ, Nelson DM. (2009) The magnitude of error in conventional bulk-sediment radiocarbon dates from central North America. *Quaternary Research* 72:301-308.

Guyard H, Chapron E, St-Onge G, Labrie J. (2013) Late-Holocene NAO and oceanic forcing on high-altitude proglacial sedimentation (Lake Bramant, Western French Alps). *Holocene* 23:1163-1172.

Guyard H, St-Onge G, Pienitz R, Francus P, Zolitschka B, Clarke GKC, Hausmann S, Salonen VP, Lajeunesse P, Ledoux G, Lamothe M. (2011) New insights into Late Pleistocene glacial and postglacial history of northernmost Ungava (Canada) from Pingualuit Crater Lake sediments. *Quaternary Science Reviews* 30:3892-3907.

Hajdas I, Zolitschka B, Ivy-Ochs SD, Beer J, Bonani G, Leroy SA, Negendank JW, Ramrath M, Suter M. (1995) AMS radiocarbon dating of annually laminated sediments from Lake Holzmaar, Germany. *Quaternary Science Reviews* 14:137-143.

Håkanson L, Jansson M. (2002) *Principles of Lake Sedimentology*, 2nd ed. The Blackburn Press, New Jersey, 316 pp.

Hammer Ø, Harper DAT, Ryan PD. (2001) Past: Paleontological Statistics Software Package for education and data analysis *Paleontología Electrónica* 4::1-75.

Hardy L. (1977) La déglaciation et les épisodes lacustre et marin sur le versant québécois des basses terres de la baie de James. *Geographie Physique Et Quaternaire* 31:261-273.

Heiri O, Lotter AF, Lemcke G. (2001) Loss on ignition as a method for estimating organic and carbonate content in sediments: reproducibility and comparability of results. *Journal of Paleolimnology* 25:101-110.

Herman F, Beaud F, Champagnac J-D, Lemieux J-M, Sternai P. (2011) Glacial hydrology and erosion patterns: a mechanism for carving glacial valleys. *Earth and Planetary Science Letters* 310:498-508.

Hetu B. (1998) Deglaciation of the Rimouski area, Lower St. Lawrence (Quebec): stratigraphical evidences of a glacial readvance into the Goldthwait Sea between 12,400 and 12,000 yr BP. *Geographie Physique Et Quaternaire* 52:325-347.

Hughes OL. (1959) Surficial geology of Smooth rock and Iroquois Falls map areas, Cochrane District, Ontario. University of Kansas

Hughes TJ. (1998) *Ice sheets*. Oxford University Press.

Hutchinson G. (1957) *A treatise on limnology*. Vol. 1. Geography, physics, and chemistry. John Wiley&Sons. Inc New York:1015.

Hvorsley MJ, Stetson HC. (1946) Gravity coring instruments and mechanics of sediment coring. *Bull Geol Soc* 57:935.

Ineson S, Scaife AA, Knight JR, Manners JC, Dunstone NJ, Gray LJ, Haigh JD. (2011) Solar forcing of winter climate variability in the Northern Hemisphere. *Nature Geoscience* 4:753.

IPCC. (2007) Climate Change 2007: Synthesis Report. An Assessment of the Intergovernmental Panel on Climate Change. In: A. Allali RB, S. Diaz, I. Elgizouli, D. Griggs, D. Hawkins, O. Hohmeyer, B.P. Jallow, L. Kajfez-Bogataj, N. Leary, H. Lee, D. Wratt (ed). Intergovernmental Panel on Climate Change, Valencia, Spain, pp. 26-73.

IPCC. (2013) Climate Change 2013: The Physical Science Basis: Working Group I Contribution to the Fifth Assessment Report of the Intergovernmental Panel on Climate Change. In: Stocker TF, D. Qin, G.-K. Plattner, M. Tignor, S.K. Allen, J. Boschung, A. Nauels, Y.Xia, V. Bex and P.M. Midgley (ed). Cambridge University Press, Cambridge, United Kingdom and New York, NY, USA, p. 1535.

IPCC. (2014) Climate Change 2014: Impacts, Adaptation, and Vulnerability. Part A: Global and Sectional Aspects. Contribution of Working Group II to the Fifth Assessment Report of the Intergovernmental Panel on Climate Change. In: Field CB, V.R. Barros, D.J. Dokken, K.J. Mach, M.D. Mastrandrea, T.E. Bilir, M. Chatterjee, K.L. Ebo, Y.O Estrada, R.C. Genova, B. Girma, E.S. Kissel, A.N. Levy, S. MacCracken, P.R. Mastrandrea, and L.L. White (ed). Cambridge University Press, Cambridge, United Kingdom and New York, NY, USA, p. 1132.

Jenkins R. (1999) X-ray Fluorescence Spectrometry. Chemical Analysis: a Series of Monographs on Analytical Chemistry and Its Applications 152:12.

Jenny J-P, Arnaud F, Dorioz J-M, Giguet Covex C, Frossard V, Sabatier P, Millet L, Reyss J-L, Tachikawa K, Bard E. (2013) A spatiotemporal investigation of varved sediments highlights the dynamics of hypolimnetic hypoxia in a large hard-water lake over the last 150 years. *Limnology and Oceanography* 58:1395-1408.

Jenny J-P, Normandeau A, Francus P, Tararu ZE, Gregory-Eaves I, Lapointe F, Jautzy J, Ojala AEK, Dorioz J-M, Schimmelmann A, Zolitschka B. (2016) Urban point sources of nutrients were the leading cause for the historical spread of hypoxia across European lakes. *Proceedings of the National Academy of Sciences* 113:12655.

Johnsen SJ, Dahl-Jensen D, Gundestrup N, Steffensen JP, Clausen HB, Miller H, Masson-Delmotte V, Sveinbjörnsdóttir AE, White J. (2001) Oxygen isotope and palaeotemperature records from six Greenland ice-core stations: Camp Century, Dye-3, GRIP, GISP2, Renland and NorthGRIP. *Journal of Quaternary Science* 16:299-307.

Josenhans H, Lehman S. (1999) Late glacial stratigraphy and history of the Gulf of St. Lawrence, Canada. *Canadian Journal of Earth Sciences* 36:1327-1345.

Josenhans HW. (2001) Late-glacial stratigraphy and history of the Gulf of St. Lawrence: Reply. *Canadian Journal of Earth Sciences* 38:483.

Jouve G, Francus P, Lamoureux S, Provencher-Nolet L, Hahn A, Haberzettl T, Fortin D, Nuttin L, Team PS. (2013) Microsedimentological characterization using image analysis and mu-XRF as indicators of sedimentary processes and climate changes during Lateglacial at Laguna Potrok Aike, Santa Cruz, Argentina. *Quaternary Science Reviews* 71:191-204.

Juggins S. (2007) C2 Version 1.5 User guide. Software for ecological and palaeoecological data analysis and visualisation. Newcastle University, Newcastle upon Tyne, UK, p. 73.

Kinder M, Tylmann W, Bubak I, Fiłoc M, Gaśiorowski M, Kupryjanowicz M, Mayr C, Sauer L, Voellering U, Zolitschka B. (2019a) Holocene history of human impacts inferred from annually laminated sediments in Lake Szurpiły, northeast Poland. *Journal of Paleolimnology* 61:419-435.

Kinder M, Tylmann W, Enters D, Piotrowska N, Poręba G, Zolitschka B. (2013) Construction and validation of calendar-year time scale for annually laminated sediments—an example from Lake Szurpiły (NE Poland). *Gff* 135:248-257.

Kinder M, Tylmann W, Rzeszewski M, Zolitschka B. (2019b) Varves and mass-movement deposits record distinctly different sedimentation dynamics since the late glacial (Lake Szurpiły, northeastern Poland). *Quaternary Research*:1-15.

Kirschvink J. (1980) The least - squares line and plane and the analysis of palaeomagnetic data. *62:699-718.*

Knudsen MF, Riisager P, Jacobsen BH, Muscheler R, Snowball I, Seidenkrantz MS. (2009) Taking the pulse of the Sun during the Holocene by joint analysis of ^{14}C and ^{10}Be . *Geophysical Research Letters* 36.

Knudsen MF, Seidenkrantz M-S, Jacobsen BH, Kuijpers A. (2011) Tracking the Atlantic Multidecadal Oscillation through the last 8,000 years. *Nature Communications* 2:178.

Kobashi T, Box J, Vinther B, Goto - Azuma K, Blunier T, White J, Nakaegawa T, Andresen C. (2015) Modern solar maximum forced late twentieth century Greenland cooling. *Geophysical Research Letters* 42:5992-5999.

Lajeunesse P. (2014) Buried preglacial fluvial gorges and valleys preserved through Quaternary glaciations beneath the eastern Laurentide Ice Sheet. *Geological Society of America Bulletin* 126:447-458.

Lajeunesse P. (2016) Late Wisconsinan grounding-zone wedges, northwestern Gulf of St Lawrence, eastern Canada. *Geological Society, London, Memoirs* 46:227-228.

Lajeunesse P, Dietrich P, Ghienne J-F. (2019) Late Wisconsinan grounding zones of the Laurentide Ice Sheet margin off the Québec North Shore (NW Gulf of St Lawrence). *Geological Society, London, Special Publications* 475:241-259.

Lajeunesse P, Sinkunas B, Morissette A, Normandeau A, Joyal G, St-Onge G, Locat J. (2016) Large-scale seismically-induced mass-movements in a former glacial lake basin: Lake Témiscouata, northeastern Appalachians (eastern Canada). *Marine Geology* 384:120-130.

Lapointe F, Francus P, Lamoureux SF, Said M, Cuven S. (2012) 1750 years of large rainfall events inferred from particle size at East Lake, Cape Bounty, Melville Island, Canada. *Journal of Paleolimnology* 48:159-173.

Lapointe F, Francus P, Lamoureux SF, Vuille M, Jenny J-P, Bradley RS. (2017) Influence of North Pacific decadal variability on the western Canadian Arctic over the past 700 years. *Climate of the Past* 13:411-420.

Lapointe F, Francus P, Stoner JS, Abbott MB, Balascio NL, Cook TL, Bradley RS, Forman SL, Besonen M, St-Onge G. (2019) Chronology and sedimentology of a new 2.9 ka annually laminated record from South Sawtooth Lake, Ellesmere Island. *Quaternary Science Reviews* 222:105875.

Larsen CPS, MacDonald GM. (1993) Lake morphometry, sediment mixing and the selection of sites for fine resolution palaeoecological studies. *Quaternary Science Reviews* 12:781-792.

Larsen CPS, Pienitz R, Smol JP, Moser KA, Cumming BF, Blais JM, Macdonald GM, Hall RI. (1998) Relations between lake morphometry and the presence of laminated lake sediments: A re-examination of Larsen and Macdonald (1993). *Quaternary Science Reviews* 17:711-717.

Lean J. (1997) The Sun's variable radiation and its relevance for Earth. Annual Review of Astronomy and Astrophysics 35:33-67.

Lesemann J-E, Brennand TA. (2009) Regional reconstruction of subglacial hydrology and glaciodynamic behaviour along the southern margin of the Cordilleran Ice Sheet in British Columbia, Canada and northern Washington State, USA. Quaternary Science Reviews 28:2420-2444.

Livingstone SJ, Clark CD, Piotrowski JA, Tranter M, Bentley MJ, Hodson A, Swift DA, Woodward J. (2012) Theoretical framework and diagnostic criteria for the identification of palaeo-subglacial lakes. Quaternary Science Reviews 53:88-110.

Lüder B, Kirchner G, Lücke A, Zolitschka B. (2006) Palaeoenvironmental reconstructions based on geochemical parameters from annually laminated sediments of Sacrower See (northeastern Germany) since the 17th century. Journal of Paleolimnology 35:897-912.

Ludlam SD. (1969) Fayetteville Greenlake, New York. III: The laminated sediments 1. Limnology and Oceanography 14:848-857.

Lund S, Stoner JS, Channell JE, Acton G. (2006) A summary of Brunhes paleomagnetic field variability recorded in Ocean Drilling Program cores. Physics of the earth and planetary interiors 156:194-204.

Margold M, Stokes CR, Clark CD. (2015) Ice streams in the Laurentide Ice Sheet: Identification, characteristics and comparison to modern ice sheets. Earth-Science Reviews 143:117-146.

Marshall M, Schlolaut G, Nakagawa T, Lamb H, Brauer A, Staff R, Ramsey CB, Tarasov P, Gotanda K, Haraguchi T, Yokoyama Y, Yonenobu H, Tada R. (2012) A novel approach to varve counting using μ XRF and X-radiography in combination with thin-section microscopy, applied to the Late Glacial chronology from Lake Suigetsu, Japan. Quaternary Geochronology 13:70-80.

Marshall SJ, Clark PU. (2002) Basal temperature evolution of North American ice sheets and implications for the 100 - kyr cycle. Geophysical Research Letters 29.

Martin-Puertas C, Matthes K, Brauer A, Muscheler R, Hansen F, Petrick C, Aldahan A, Possnert G, Van Geel B. (2012) Regional atmospheric circulation shifts induced by a grand solar minimum. Nature Geoscience 5:397.

McDonald BC. (1969) Glacial and interglacial stratigraphy, Hudson Bay lowlands. Geological Survey of Canada Paper 68:78-99.

Menary MB, Scaife AA. (2014) Naturally forced multidecadal variability of the Atlantic meridional overturning circulation. Climate dynamics 42:1347-1362.

Ministère des ressources naturelles du Québec. (2002) Carte géologique du Québec. Ministère des ressources naturelles, Québec, DV 2002-06, Québec.

Moffa-Sánchez P, Born A, Hall IR, Thornalley DJ, Barker S. (2014) Solar forcing of North Atlantic surface temperature and salinity over the past millennium. Nature Geoscience 7:275.

Mouksil A, Nadeau J, Québec G. (2011) Géologie de la partie orientale de la région de Baie-Comeau (partie ouest de 22G). Ressources naturelles et Faune Québec.

Munro-Stasiuk MJ. (2003) Subglacial Lake McGregor, south-central Alberta, Canada. Sedimentary Geology 160:325-350.

Muscheler R, Adolphi F, Herbst K, Nilsson A. (2016) The revised sunspot record in comparison to cosmogenic radionuclide-based solar activity reconstructions. *Solar Physics* 291:3025-3043.

Myrbo A, Morrison A, McEwan R. (2011) Tool for Microscopic Identification (TMI). University of Minnesota.

Nakagawa T, Gotanda K, Haraguchi T, Danhara T, Yonenobu H, Brauer A, Yokoyama Y, Tada R, Takemura K, Staff RA, Payne R, Bronk Ramsey C, Bryant C, Brock F, Schlolaut G, Marshall M, Tarasov P, Lamb H. (2012) SG06, a fully continuous and varved sediment core from Lake Suigetsu, Japan: stratigraphy and potential for improving the radiocarbon calibration model and understanding of late Quaternary climate changes. *Quaternary Science Reviews* 36:164-176.

Nasmith H. (1962) Late glacial history and surficial deposits. British Columbia, Ministry of Energy, Mines and Petroleum Resources.

Naulier M, Savard MM, Begin C, Marion J, Arseneault D, Begin Y. (2014) Carbon and oxygen isotopes of lakeshore black spruce trees in northeastern Canada as proxies for climatic reconstruction. *Chemical Geology* 374:37-43.

Neil K, Gajewski K. (2018) An 11,000 - yr record of diatom assemblage responses to climate and terrestrial vegetation changes, southwestern Québec. *Ecosphere* 9:e02505.

Nicault A, Boucher E, Begin C, Guiot J, Marion J, Perreault L, Roy R, Savard MM, Begin Y. (2014) Hydrological reconstruction from tree-ring multi-proxies over the last two centuries at the Caniapiscau Reservoir, northern Quebec, Canada. *Journal of Hydrology* 513:435-445.

Normandeau A, Lajeunesse P, Poiré AG, Francus P. (2016) Morphological expression of bedforms formed by supercritical sediment density flows on four fjord - lake deltas of the south - eastern Canadian Shield (Eastern Canada). *Sedimentology* 63:2106-2129.

Nzekwe OP, Francus P, St-Onge G, Lajeunesse P, Fortin D, Gagnon-Poiré A, Philippe ÉGH, Normandeau A. (2018) Recent sedimentation in three adjacent fjord-lakes on the Québec North Shore (eastern Canada): facies analysis, laminae preservation, and potential for varve formation. *Canadian Journal of Earth Sciences* 55:138-153.

Nzekwe OP, Francus P, St-Onge G, Lajeunesse P, Jenny J-P, Labarre T. (2015) Les défis du déploiement et de la récupération des pièges à sédiments dans les lacs profonds: Une étude du lac Walker, Côte-Nord. Congrès des étudiants de l'INRS-ETE, Passé, Présent, Futur, 3 perspectives de l'Environnement, Québec.

O'Sullivan PE. (1983) Annually-laminated lake sediments and the study of Quaternary environmental changes — a review. *Quaternary Science Reviews* 1:245-313.

Occhietti S. (1980) Le Quartnaire de la région de Trois-Rivières-Shawinigan, Québec. Contribution à la paléo-géographie de la vallée moyenne du Saint-Laurent et correlations stratigraphiques. Paléo-Québec Université du Québec, p. 227.

Occhietti S. (1989) Quaternary geology of St. Lawrence Valley and adjacent Appalachian subregion. Chapter 4:350-389.

Occhietti S. (2007) The Saint-Narcisse morainic complex and early Younger Dryas events on the southeastern margin of the Laurentide Ice Sheet. *Geographie Physique Et Quaternaire* 61:89-117.

Occhietti S, Govare É, Klassen R, Parent M, Vincent J-S. (2004) Late Wisconsinan—Early holocene deglaciation of Québec-Labrador. In: Ehlers J, Gibbards PL (eds), Quaternary Glaciations—Extent and Chronology Part II: North America Elsevier, New York, pp. 243-273.

Occhietti S, Parent M, Lajeunesse P, Robert F, Govare É. (2011) Late Pleistocene—Early Holocene Decay of the Laurentide Ice Sheet in Québec—Labrador. In: Ehlers J, Gibbard PL, Hughes PD (eds), Quaternary Glaciations - Extents and Chronology. Elservier, Amsterdam.

Ojala AEK, Alenius T. (2005) 10000 years of interannual sedimentation recorded in the Lake Nautajarvi (Finland) clastic-organic varves. *Palaeogeography Palaeoclimatology Palaeoecology* 219:285-302.

Ojala AEK, Francus P, Zolitschka B, Besonen M, Lamoureux SF. (2012) Characteristics of sedimentary varve chronologies - A review. *Quaternary Science Reviews* 43:45-60.

Ojala AEK, Kosonen E, Weckstrom J, Korkonen S, Korhola A. (2013) Seasonal formation of clastic-biogenic varves: the potential for palaeoenvironmental interpretations. *Gff* 135:237-U212.

Ojala AEK, Saarinen T, Salonen V-P. (2000) Preconditions for the formation of annually laminated lake sediments in southern and central Finland. *Boreal Environment Research* 5:243-255.

Olsen J, Anderson NJ, Knudsen MF. (2012) Variability of the North Atlantic Oscillation over the past 5,200 years. *Nature Geoscience* 5:808.

PAGES 2k Network. (2013) Continental-Scale Temperature Variability during the Past Two Millennia: Supplementary Information. *Nature Geoscience* 6.

Paquette N, Gajewski K. (2013) Climatic change causes abrupt changes in forest composition, inferred from a high-resolution pollen record, southwestern Quebec, Canada. *Quaternary Science Reviews* 75:169-180.

Parent M. (1987) Late Pleistocene stratigraphy and event of the Asbestos - Valcourt region, Southeastern Quebec. University of Western Ontario, London, p. 295.

Paulen R. (2001) Quarternary geology of the Timmins area, northeastern Ontario University of Waterloo.

Philibert G. (2012) Évolution tardi-quaternaire du lac Jacques-Cartier, Réserve faunique des Laurentides, Québec. Département de Géographie, Faculté de Foresterie, de Géographie and Géomatique. Université Laval.

Philippe ÉG, Valet JP, St-Onge G, Thevarasan A. (2018) Are paleomagnetic records From U - Channels appropriate for studies of reversals and excursions? 19:4130-4142.

Piper DJW, Macdonald GM. (2001) Timing and position of Late Wisconsinan ice-margins on the upper slope seaward of Laurentian Channel. *Geographie Physique Et Quaternaire* 55:131-140.

Quigley RM. (1983) Glaciolacustrine and glaciomarine clay deposition: a North American perspective. In: Eyles N (ed), *Glacial Geology - An Introduction for Engineers and Earth Scientists*. Pergamon Press, New York, pp. 140-167.

R Core Development Team. (2008) A language and environment for statistical computing. R Foundation for Statistical Computing Vienna, Austria.

Reimer PJ, Bard E, Bayliss A, Beck JW, Blackwell PG, Ramsey CB, Buck CE, Cheng H, Edwards RL, Friedrich M. (2013) IntCal13 and Marine13 radiocarbon age calibration curves 0–50,000 years cal BP. *55*:1869-1887.

Renberg I. (1981) Improved methods for sampling, photographing and varve-counting of varved lake sediments. *Boreas* 10:255-258.

Ridge JC, Balco G, Bayless RL, Beck CC, Carter LB, Dean JL, Voytek EB, Wei JH. (2012) The new North American Varve Chronology: A precise record of southeastern Laurentide Ice Sheet deglaciation and climate, 18.2-12.5 kyr BP, and correlations with Greenland ice core records. *American Journal of Science* 312:685-722.

Ridge JC, Larsen FD. (1990) Re-evaluation of Antevs' New England varve chronology and new radiocarbon dates of sediments from glacial Lake Hitchcock. *GSA Bulletin* 102:889-899.

Robbins JA, Edgington DN. (1975) Determination of recent sedimentation rates in Lake Michigan using Pb-210 and Cs-137. *Geochimica Et Cosmochimica Acta* 39:285-304.

Rodrigues CG. (1992) Successions of invertebrate microfossils and the late Quaternary deglaciation of the central St Lawrence Lowland, Canada and United States. *Quaternary Science Reviews* 11:503-534.

Rolland N, Larocque I, Francus P, Pienitz R, Laperriere L. (2008) Holocene climate inferred from biological (Diptera : Chironomidae) analyses in a Southampton island (Nunavut, Canada) lake. *Holocene* 18:229-241.

Rothwell RG, Croudace IW. (2015) Twenty years of XRF core scanning marine sediments: What do geochemical proxies tell us? In: Croudace IW, Rothwell RG (eds), *Micro-XRF Studies of Sediment Cores, Developments in Paleoenvironmental Research* 17. Springer, Dordrecht, pp. 25-102.

Saarnisto M. (1986) Annually laminated lake sediments. In: B.E. B (ed), *Handbook of Holocene palaeoecology and palaeohydrology*. John Wiley and Sons Ltd, Chichester, pp. 343-370.

Saarnisto M, Huttunen P, Tolonen K. (1977) Annual lamination of sediments in Lake Lovojärvi, southern Finland, during the past 600 years. *Annales Botanici Fennici*. JSTOR, pp. 35-45.

Scaife AA, Ineson S, Knight JR, Gray L, Kodera K, Smith DM. (2013) A mechanism for lagged North Atlantic climate response to solar variability. *Geophysical Research Letters* 40:434-439.

Schimmelmann A, Lange CB, Schieber J, Francus P, Ojala AEK, Zolitschka B. (2016) Varves in marine sediments: A review. *Earth-Science Reviews* 159:215-246.

Schlolaut G, Marshall MH, Brauer A, Nakagawa T, Lamb HF, Staff RA, Bronk Ramsey C, Bryant CL, Brock F, Kossler A, Tarasov PE, Yokoyama Y, Tada R, Haraguchi T. (2012) An automated method for varve interpolation and its application to the Late Glacial chronology from Lake Suigetsu, Japan. *Quaternary Geochronology* 13:52-69.

Schneider CA, Rasband WS, Eliceiri KW. (2012) NIH Image to ImageJ: 25 years of image analysis. *Nature methods* 9:671.

Schnurrenberger D, Russell J, Kelts K. (2003) Classification of lacustrine sediments based on sedimentary components. *Journal of Paleolimnology* 29:141-154.

Schulz M, Mudelsee M. (2002) REDFIT: estimating red-noise spectra directly from unevenly spaced paleoclimatic time series. *Computers & Geosciences* 28:421-426.

Shaw J, Gareau P, Courtney R. (2002) Palaeogeography of Atlantic Canada 13–0 kyr. Quaternary Science Reviews 21:1861-1878.

Shaw J, Piper DJW, Fader GBJ, King EL, Todd BJ, Bell T, Batterson MJ, Liverman DGE. (2006) A conceptual model of the deglaciation of Atlantic Canada. Quaternary Science Reviews 25:2059-2081.

Shindell DT, Schmidt GA, Mann ME, Rind D, Waple A. (2001) Solar forcing of regional climate change during the Maunder Minimum. Science 294:2149-2152.

Sieger R, Grobe H. (2013) PanPlot 2-software to visualize profiles and time series. Alfred Wegener Institute.

Singer BS. (2014) A Quaternary geomagnetic instability time scale. Quaternary Geochronology 21:29-52.

Singer BS, Jicha BR, He H, Zhu R. (2014) Geomagnetic field excursion recorded 17 ka at Tianchi Volcano, China: New 40Ar/39Ar age and significance. Geophysical Research Letters 41:2794-2802.

Smith ND. (1978) Sedimentation processes and patterns in a glacier-fed lake with low sediment input. Canadian Journal of Earth Sciences 15:741-756.

Smith ND, Ashley GM. (1985) Proglacial lacustrine environment. In: Ashley GM, Shaw J, Smith JA (eds), Glacial Sedimentary Environments. Society of Economic Peleontologists and Mineralogists, Tulsa, Oklahoma.

Smith WT. (1962) Earthquakes of eastern Canada and adjacent areas, 1534-1927. R. Duhamel, Queen's Printer.

St-Onge G, Chapron E, Mulsow S, Salas M, Viel M, Debret M, Foucher A, Mulder T, Winiarski T, Desmet M. (2012) Comparison of earthquake-triggered turbidites from the Saguenay (Eastern Canada) and Reloncavi (Chilean margin) Fjords: Implications for paleoseismicity and sedimentology. Sedimentary Geology 243:63-107.

St-Onge G, Duchesne MJ, Lajeunesse P. (2011) Marine geology of the St. Lawrence Estuary. Iodp-Canada Summer School on Ocean and Climate Changes in Polar and Subpolar Environments.

St-Onge G, Long BF. (2009) CAT-scan analysis of sedimentary sequences: An ultrahigh-resolution paleoclimatic tool. Engineering Geology 103:127-133.

St-Onge G, Mulder T, Francus P, Long B. (2007) Continuous physical properties of cored marine sediments. Proxies in Late Cenozoic Paleoceanography Elsevier:63-98.

St-Onge G, Mulder T, Piper DJW, Hillaire-Marcel C, Stoner JS. (2004) Earthquake and flood-induced turbidites in the Saguenay Fjord (Quebec): a Holocene paleoseismicity record. Quaternary Science Reviews 23:283-294.

Stockmarr J. (1971) Tabletes with spores used in absolute pollen analysis. Pollen spores 13:615-621.

Stoner JS, St-Onge G. (2007) Chapter three Magnetic stratigraphy in paleoceanography: reversals, excursions, paleointensity, and secular variation. In: Hillaire-Marcel C, De Vernal A (eds), Developments in Marine Geology. Elsevier, pp. 99-138.

Stuiver M, Grootes P, Braziunas TF. (1995) The GISP2 $\delta^{18}\text{O}$ Climate Record of the Past 16,500 Years and the Role of the Sun, Ocean, and Volcanoes. Quaternary Research 44:341-354.

Stuiver M, Reimer PJ. (1993) Extended 14 C data base and revised CALIB 3.0 14 C age calibration program. *Radiocarbon* 35:215-230.

Stuiver M, Reimer PJ, Reimer RW. (2018) CALIB 7.1 [WWW program] at <http://calig.org>, accessed from 2018-01-01 to 2018-12-31.

Sturm M. (1979) Origin and composition of clastic varves Moraines and varves: origin, genesis, classification. Proceedings of an INQUA symposium on genesis and lithology of Quaternary deposits, Zurich, pp. 281-285.

Syvitski JP. (1991) Towards an understanding of sediment deposition on glaciated continental shelves. *Continental Shelf Research* 11:897-937.

Syvitski JP, Shaw J. (1995) Sedimentology and geomorphology of fjords. *Developments in sedimentology* 53:113-178.

Syvitski JPM, Praeg DB. (1987) *Sedimentology of Arctic Fjords Experiment: Data Report*.

Syvitski JPM, Praeg DB. (1989) Quaternary Sedimentation in the St-Lawrence Estuary and Adjoining Areas, Eastern Canada - an Overview Based on High-Resolution Seismostratigraphy. *Geographie Physique Et Quaternaire* 45:291-310.

Tarasov L, Dyke AS, Neal RM, Peltier WR. (2012) A data-calibrated distribution of deglacial chronologies for the North American ice complex from glaciological modeling. *Earth and Planetary Science Letters* 315:30-40.

Thiéblemont R, Matthes K, Omrani N-E, Kodera K, Hansen F. (2015) Solar forcing synchronizes decadal North Atlantic climate variability. *Nature Communications* 6:8268.

Thompson LG, Mosley-Thompson E, Davis ME, Lin P-N, Henderson K, Mashotta TA. (2003) Tropical Glacier and Ice Core Evidence of Climate Change on Annual to Millennial Time Scales. *Climatic Change* 59:137-155.

Thompson R, Kelts K. (1974) Holocene sediments and magnetic stratigraphy from Lakes Zug and Zurich, Switzerland. *Sedimentology* 21:577-596.

Thomson J, Croudace I, Rothwell R. (2006) A geochemical application of the ITRAX scanner to a sediment core containing eastern Mediterranean sapropel units. *Geological Society, London, Special Publications* 267:65-77.

Tiljander M, Ojala A, Saarinen T, Snowball I. (2002) Documentation of the physical properties of annually laminated (varved) sediments at a sub-annual to decadal resolution for environmental interpretation. *Quaternary International* 88:5-12.

Tian J, Brown TA, Hul FS. (2005) Comparison of varve and 14C chronologies from Steel Lake, Minnesota, USA. *The Holocene* 15:510-517.

Tourisme Québec. (2016) *Guide Touristique Officiel 2015-2016 Côte-Nord Tourisme Québec*.

Trottier A-P, Lajeunesse P, Normandeau A, Gagnon-Poiré A. (2018) Deglacial and postglacial paleoseismological archives in mass-movement deposits of lakes of south-central Québec. *Canadian Journal of Earth Sciences*.

Turner LJ, Delorme LD. (1996) Assessment of ^{210}Pb data from Canadian lakes using the CIC and CRS models. *Environmental Geology* 28:78-87.

Tylmann W, Szpakowska K, Ohlendorf C, Woszczyk M, Zolitschka B. (2012) Conditions for deposition of annually laminated sediments in small meromictic lakes: a case study of Lake Suminko (northern Poland). *Journal of Paleolimnology* 47:55-70.

Tylmann W, Zolitschka B, Enters D, Ohlendorf C. (2013) Laminated lake sediments in northeast Poland: distribution, preconditions for formation and potential for paleoenvironmental investigation. *Journal of Paleolimnology* 50:487-503.

Valpola SE, Ojala AE. (2006) Post-glacial sedimentation rate and patterns in six lakes of the Kokemäenjoki upper watercourse, Finland. *Boreal Environment Research* 11:195-211.

Veiga-Pires C, St-Onge G. (2008) 1st METECH workshop – From deep-sea to coastal zones: Methods and Techniques for studying Palaeoenvironments. IOP Conference Series: Earth and Environmental Science 5:011001.

Vincent J-S, Prest V. (1987) The early Wisconsinan history of the Laurentide ice sheet. *Geographie Physique Et Quaternaire* 41:199-213.

Vinther BM, Johnsen SJ, Andersen KK, Clausen HB, Hansen AW. (2003) NAO signal recorded in the stable isotopes of Greenland ice cores. *Geophysical Research Letters* 30.

Wang J, Yang B, Ljungqvist FC, Luterbacher J, Osborn TJ, Briffa KR, Zorita E. (2017) Internal and external forcing of multidecadal Atlantic climate variability over the past 1,200 years. *Nature Geoscience* 10:512.

Weeks R, Laj C, Endignoux L, Fuller M, Roberts A, Manganne R, Blanchard E, Goree W. (1993) Improvements in long - core measurement techniques: Applications in palaeomagnetism and palaeoceanography. *Geophysical Journal International* 114:651-662.

Wentworth CK. (1922) A scale of grade and class terms for clastic sediments. *The Journal of Geology* 30:377-392.

Wetzel RG, Likens GE. (1991) Limnological Analyses. Springer-Verlag, 391 pp.

Willis MJ, Herried BG, Bevis MG, Bell RE. (2015) Recharge of a subglacial lake by surface meltwater in northeast Greenland. *Nature* 518:223.

Wilson ME. (1918) Timiskaming Country, Quebec. Geological Survey of Canada, Ottawa

Zolitschka B. (2007) Varved lake sediments In: Elias SA (ed), Encyclopedia of quaternary science. Elsevier, Amsterdam, pp. 3105–3114

Zolitschka B, Brauer A, Negendank JrF, Stockhausen H, Lang A. (2000) Annually dated late Weichselian continental paleoclimate record from the Eifel, Germany. *Geology* 28:783-786.

Zolitschka B, Francus P, Ojala AEK, Schimmelmann A. (2015) Varves in lake sediments – a review. *Quaternary Science Reviews* 117:1-41.

6 ANNEXE I : INFORMATIONS COMPLEMENTAIRES CHAPITRE 1

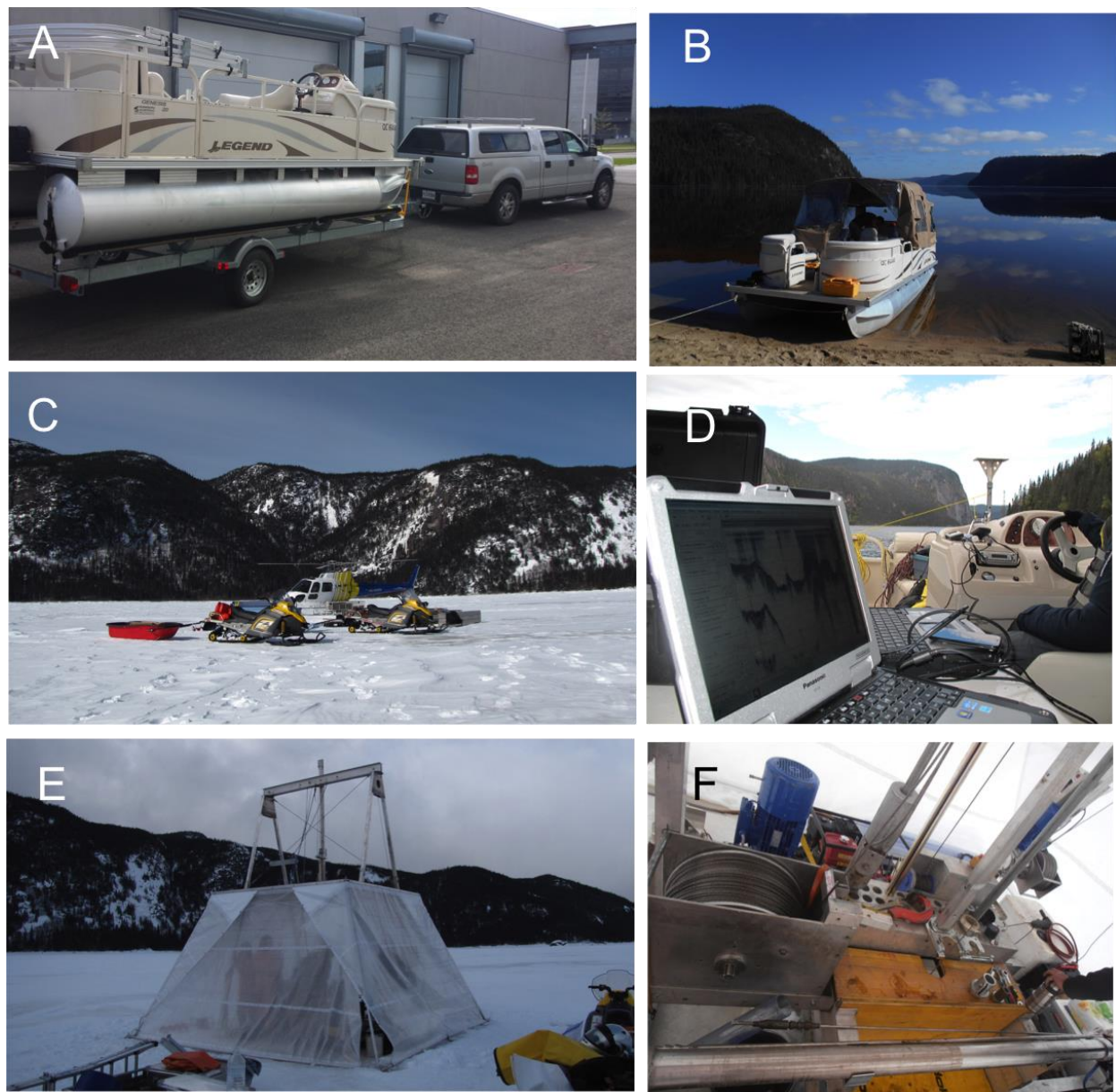


Figure S1 : Des photos montrant les travaux de terrain dans les lacs étudiés : A) Départ de l'Université Laval ; B) Le bateau ponton sur le lac Walker à l'été 2014 ; C) Préparation au carottage des sédiments en hiver 2015 ; D) Mesures souterraines sur le lac Walker ; E) Utilisation du carottier UWITEC sous une tente ; F) Vue rapprochée du carottier UWITEC.

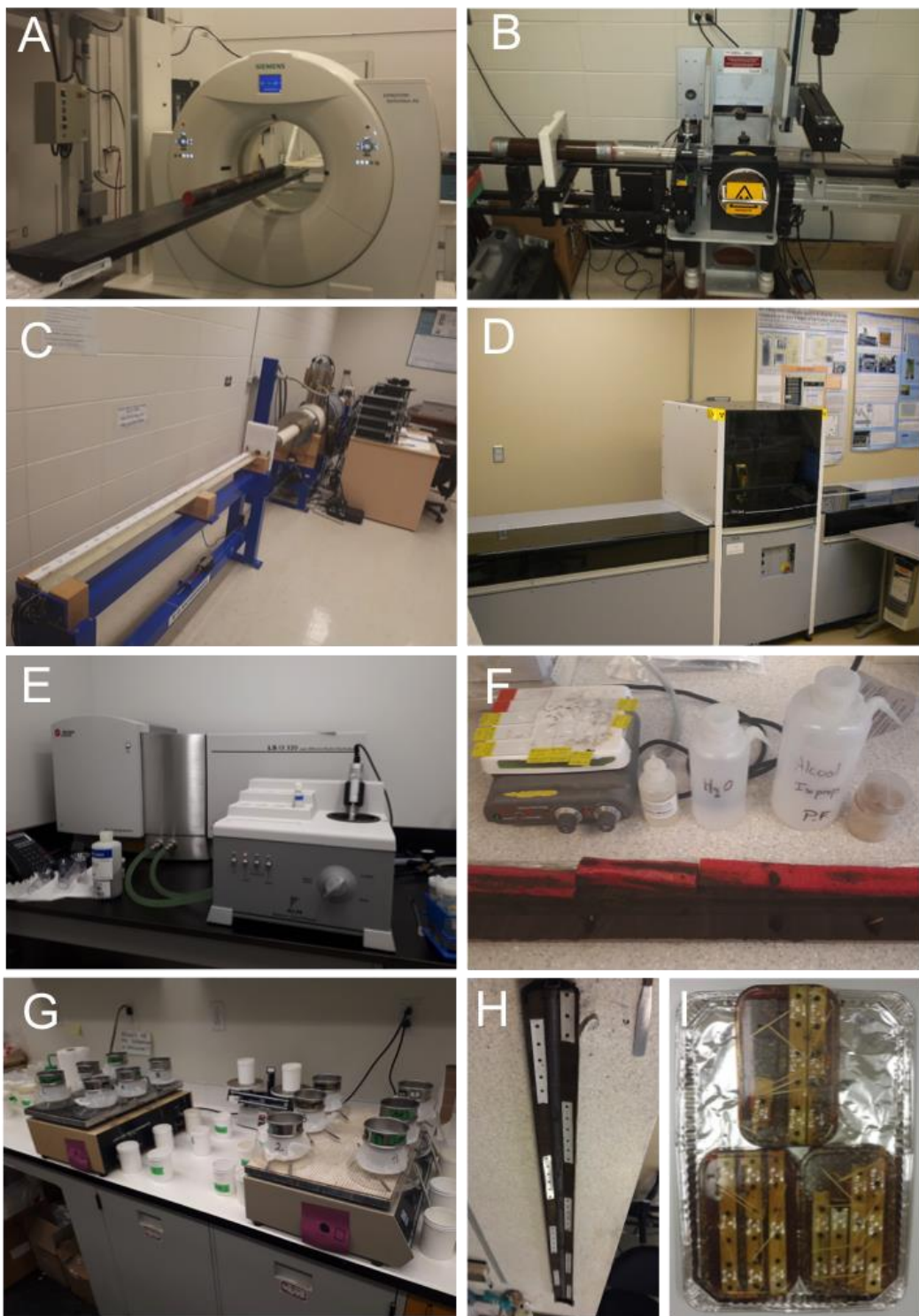


Figure S2 : Photos montrant quelques méthodes et matériaux utilisés dans la thèse de doctorat : A) la tomodensitogramme (CT-scan) (INRS-ETE) ; B) Le MSCL (UQAR-ISMER) ; C) Magnétomètre cryogénique 2G Enterprises modèle 755 SRM (UQAR-ISMER) ; D) L'ITRAX (INRS-ETE) ; E) L'analyseur de taille de particule par diffraction laser (INRS-ETE) ; F) La fabrication de lames de frottis ; G) L'analyse palynologique ; H et I) La fabrication des lames minces.

7 ANNEXE II : SUPPLEMENTARY INFORMATION CHAPTER 2 (ARTICLE 1)

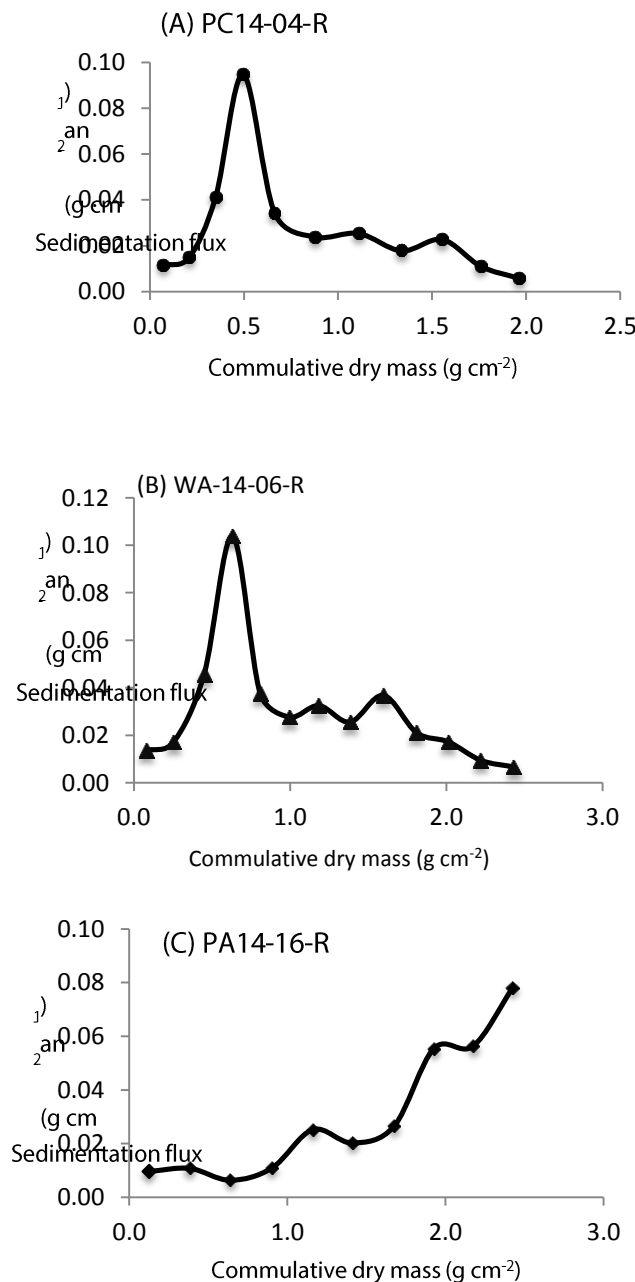


Figure S1: Plot of mass sedimentation rate ($\text{g cm}^{-2} \text{ a}^{-1}$) versus the cumulative dry weight (g cm^{-2}) of uppermost sediments from cores (A) PC14-04-R, Lake Pentecôte; (B) WA14-06-R, Lake Walker, and (C) PA14-16-R, Lake Pasteur, which suggest varying sedimentation rates in the dated cores.

WA11-W5-R (Lake Walker)

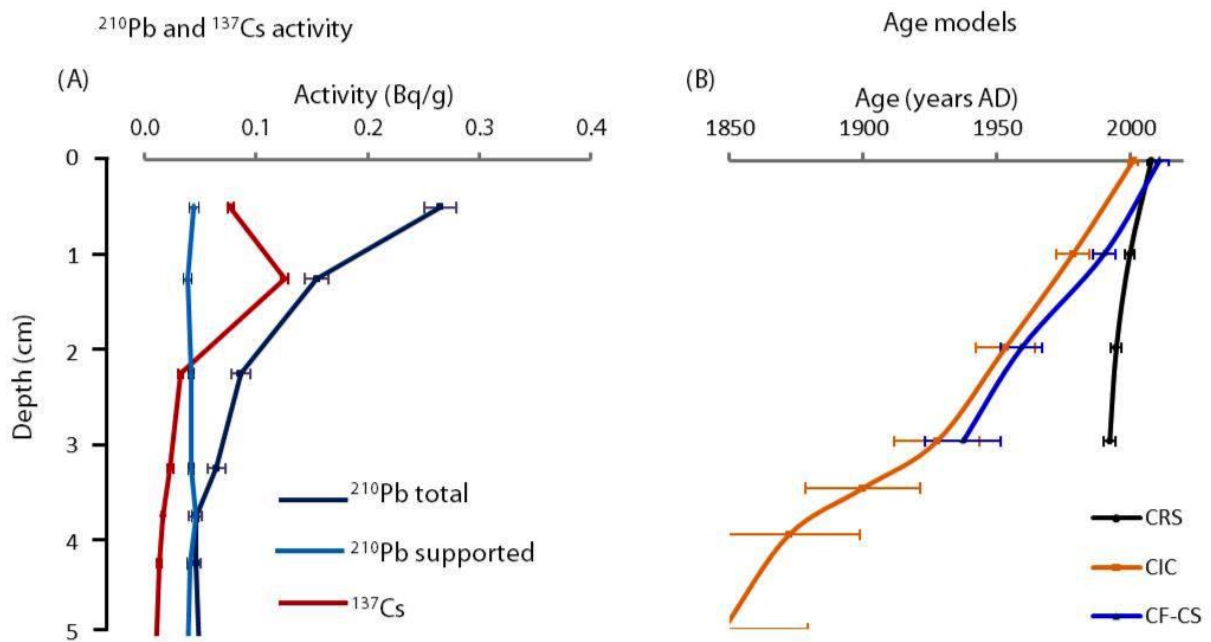


Figure S2: Recent chronology (^{210}Pb and ^{137}Cs) for the reconnaissance core, WA11-W5-R from Lake Walker. (A) Total (measured) and supported (from ^{226}Ra decay) ^{210}Pb activity and ^{137}Cs activity; (B) Chronology models based on the constant rate of supply (CRS), the constant initial concentration (CIC) and constant flux – constant sedimentation (CF-CS).

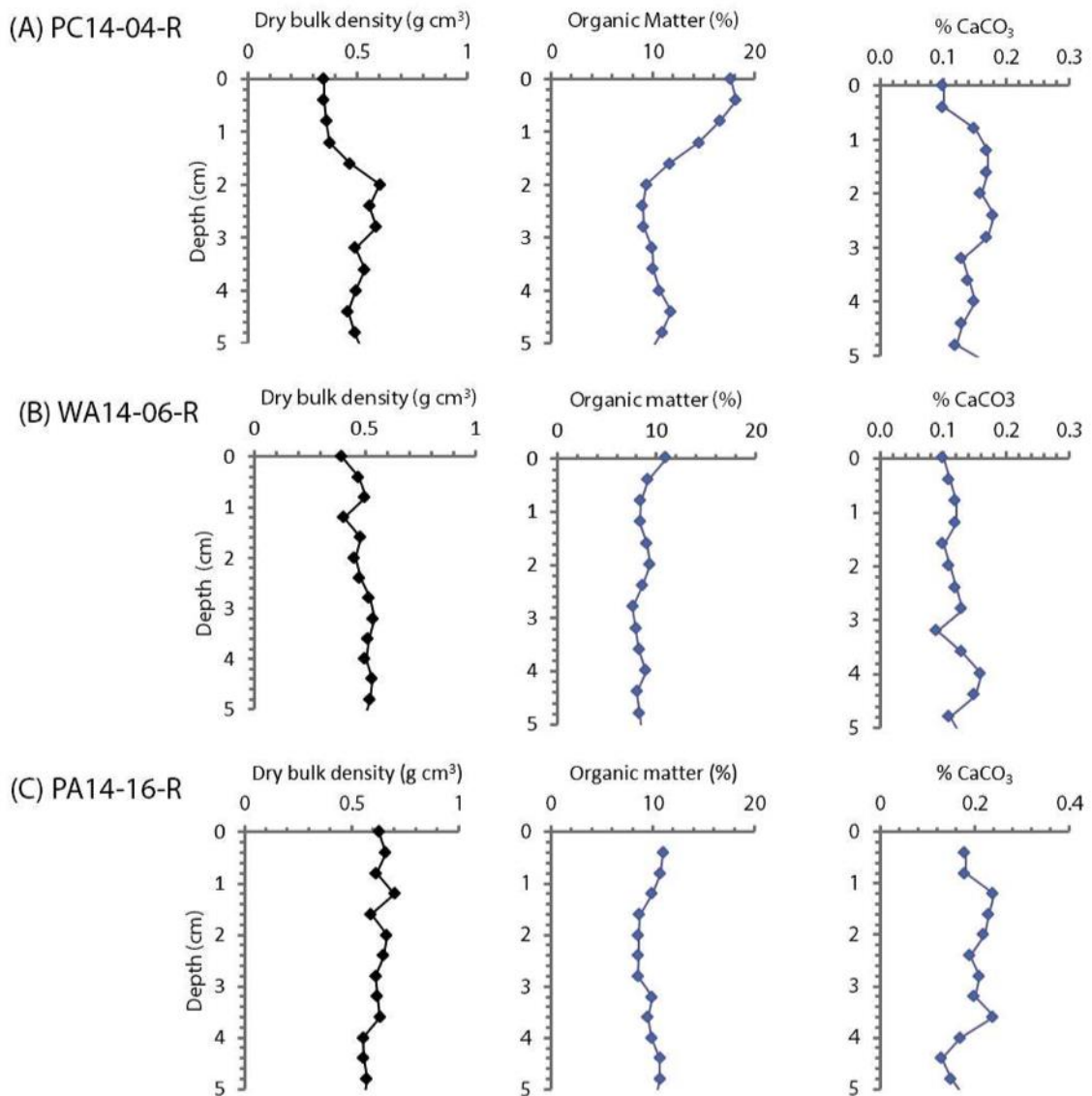


Figure S3: Dry bulk density, calculated from sediment wet/dry measurements; organic matter content calculated from loss of ignition (LOI) test at $550\text{ }^{\circ}\text{C}$ combustion, and carbonate content calculated from LOI at $1000\text{ }^{\circ}\text{C}$ combustion of uppermost sediments from cores (A) PC14-04-R, Lake Pentecôte, (B) WA14-06-R, Lake Walker; (C) PA14-16-R, Lake Pasteur.

8 ANNEXE III: SUPPLEMENTARY INFORMATION CHAPTER 3 (ARTICLE 2)

Table S1: List of markers (laminations) used to correlation cores to construct the composite sequence WA15-08-U (0-352 cm cd).

| Core section | Laminae label | Core section depth (cm) | Composite depth (cm cd) | Degree of confidence |
|-----------------|---------------|-------------------------|-------------------------|----------------------|
| WA15-08B-G | a | 9 | 9 | L |
| WA15-08B-G | b | 65 | 65 | L |
| WA15-08B-G | c | 118 | 118 | L |
| WA15-08B-G | d | 126 | 126 | L |
| WA15-08B-G | e | 130 | 130 | L |
| WA15-08B-G | f | 138 | 138 | L |
| WA15-08C-I-U-1 | g | 37 | 46 | M |
| WA15-08C-I-U-1 | h-b | 56 | 65 | M |
| WA15-08C-I-U-1 | i | 117 | 126 | M |
| WA15-08C-I-U-1 | j | 129 | 138 | M |
| WA15-08D-I-U-1 | k | 6 | 10 | L |
| WA15-08D-I-U-1 | l | 44 | 50 | M |
| WA15-08D-I-U-1 | m-h | 59 | 65 | H |
| WA15-08D-I-U-2 | n-d | 32 | 124 | L |
| WA15-08D-I-U-2 | o | 40 | 132 | L |
| WA15-08D-I-U-2 | p-j | 46 | 138 | L |
| WA15-08D-I-U-2 | q | 2 | 178 | L |
| WA15-08C-II-U-1 | r | 10 | 204 | L |
| WA15-08C-II-U-1 | s | 154 | 348 | H |
| WA15-08D-II-U-1 | t-q | 0 | 178 | L |
| WA15-08D-II-U-1 | u | 172 | 348 | H |
| WA15-08D-II-U-1 | v-s | 42 | 352 | H |

Degree of confidence: L – Low, M – Medium, H – High

Table S2: Showing test of normality of sample data of varve thickness (VT) and grain size parameters.

| | VT | Depth | mDo | sDo | Min Do | maxDo | 75Do | 90Do | 95Do | 98Do | 99Do |
|--------------------|--------------|--------------|--------------|--------------|-----------|--------------|--------------|--------------|--------------|--------------|--------------|
| N | 923 | 923 | 923 | 923 | 923 | 923 | 923 | 923 | 923 | 923 | 923 |
| Shapiro- Wilk W | 0.7127 | 0.9523 | 0.9326 | 0.9745 | 1 | 0.8618 | 0.9866 | 0.9735 | 0.9729 | 0.981 | 0.972 9 |
| p(normal) | 5.30E- 37 | 9.93E- 17 | 5.73E- 20 | 1.19E- 11 | 1 | 1.03E- 27 | 1.83E- 07 | 6.30E- 12 | 4.36E- 12 | 1.34E- 09 | 4.31E- 12 |

If p(normal) <0.05, sample data is not normally distributed

WA15-08-U (Lake Walker)

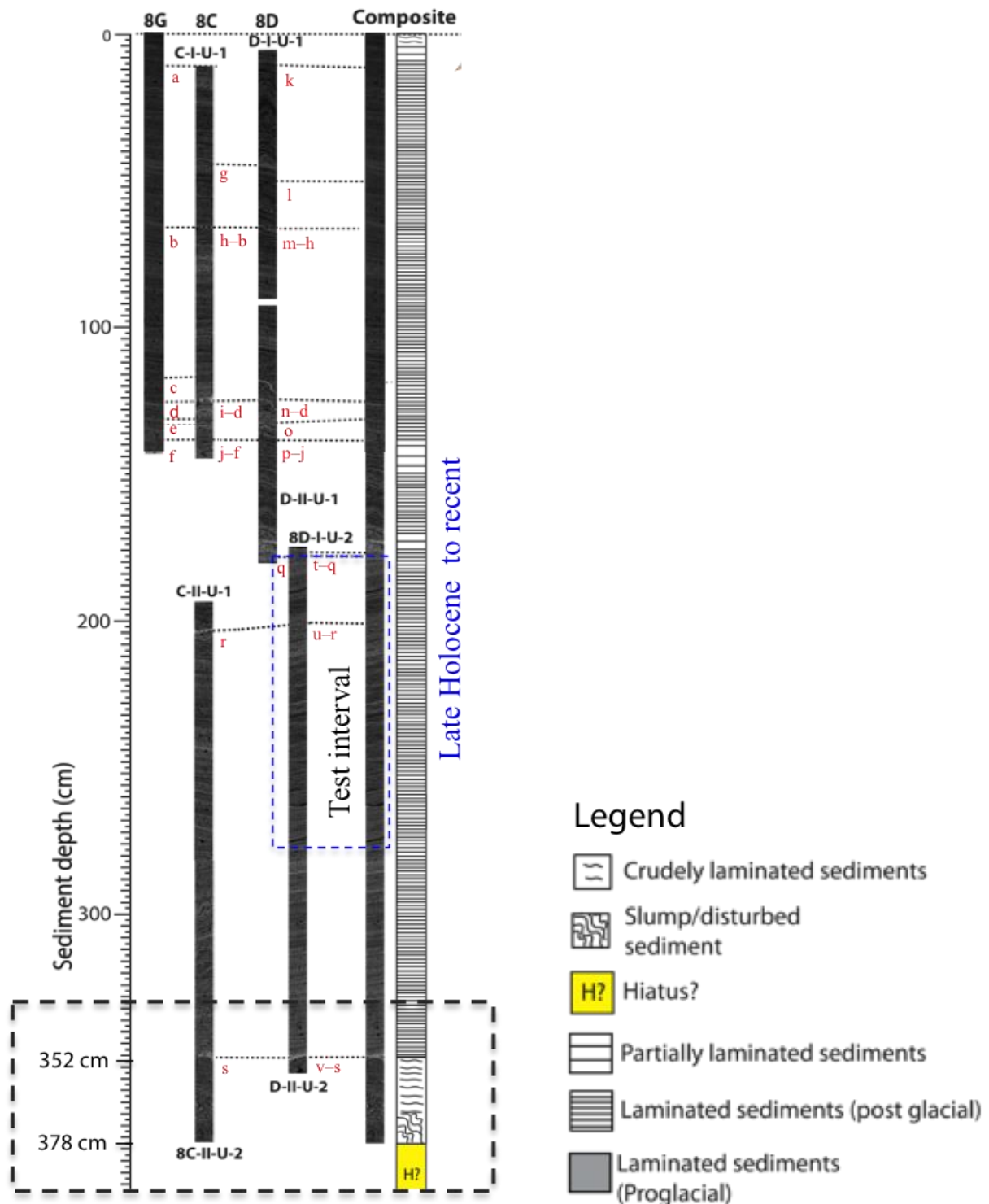
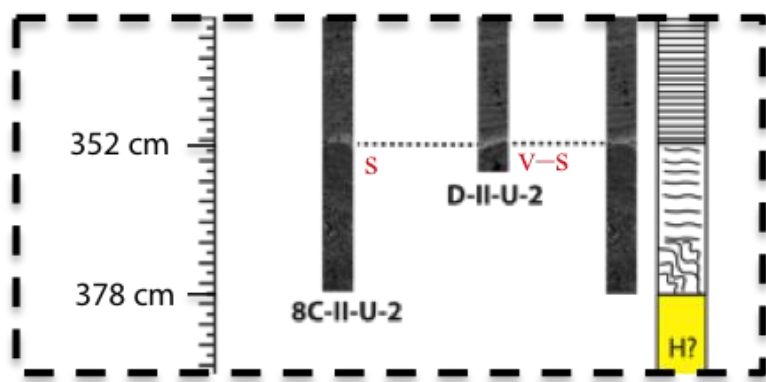


Figure S1: Correlation panel showing CT-scan images of core sections used to establish the composite sequence WA15-08-U (~0–352 cm cd; Table 3.1). The core comprises mainly partially laminated and laminated sediment, as shown in the legend. The uppermost (5 cm cd) part of the core was crudely laminated, while the lowermost part of the core (~352–378 cm cd) was disturbed, possibly due to pressure during coring. However, these two intervals are not discussed in detail because they are outside the test interval (~175–263 cm cd). Marker beds (laminations and rapidly deposited layers) that were used to correlate adjacent cores are shown. The degree of confidence of each marker is shown in Appendix III (Table S1). The insert (dashed line) shows an example of a marker with a high degree of reliability.



Legend

- Crudely laminated sediments
- Slump/disturbed sediment
- H? Hiatus?
- Partially laminated sediments
- Laminated sediments (post glacial)
- Laminated sediments (Proglacial)

Figure S2: (Insert from Figure S1, above) Showing an example of a marker with a high degree of reliability that was used to correlate adjacent cores to construct the composite sequence WA15-08-U.

| BC | BD | BE | BF | BG | BH | BI |
|--------|--------|-------|-----------|-------|--------|------|
| | | | | (VQI) | | |
| Mo inc | Mo coh | Dt | greyscale | year | lamina | note |
| 22886 | 5879 | 0.387 | 46 | --- | --- | --- |
| 23023 | 5937 | 0.387 | 36 | --- | --- | --- |
| 23082 | 6231 | 0.385 | 42 | --- | --- | --- |
| 23716 | 5950 | 0.386 | 41 | --- | --- | --- |
| 22893 | 6297 | 0.386 | 43 | --- | --- | --- |
| 22753 | 6347 | 0.388 | 43 | --- | --- | --- |
| 23008 | 5928 | 0.389 | 39 | --- | --- | --- |
| 22824 | 5630 | 0.389 | 41 | --- | --- | --- |
| 22914 | 5975 | 0.391 | 43 | 2 | --- | --- |
| 23233 | 5954 | 0.393 | 50 | --- | --- | --- |
| 23341 | 6117 | 0.39 | 54 | --- | --- | --- |
| 23496 | 6033 | 0.389 | 51 | --- | --- | --- |
| 22874 | 5939 | 0.388 | 56 | --- | --- | --- |
| 23446 | 5903 | 0.392 | 56 | --- | --- | --- |
| 23326 | 6038 | 0.392 | 54 | --- | --- | --- |
| 23594 | 5959 | 0.39 | 55 | 4 | --- | --- |
| 23194 | 5943 | 0.392 | 55 | --- | --- | --- |
| 23298 | 5698 | 0.391 | 54 | --- | --- | --- |
| 22571 | 5856 | 0.388 | 54 | --- | --- | --- |
| 22904 | 6094 | 0.387 | 51 | --- | --- | --- |

Figure S3: Screenshot of the output file from the PeakCounter software opened in Excel. It shows additional columns (that were added in the XRF data file) for grayscale value, year (indicates varve quality index, VQI; see column BG), lamina and note (for description of laminae where applicable, e.g. marking an RDL). Results show that a minimum of 6 to 8 XRF measurements were measured between each successively marked VQI, in column BG.

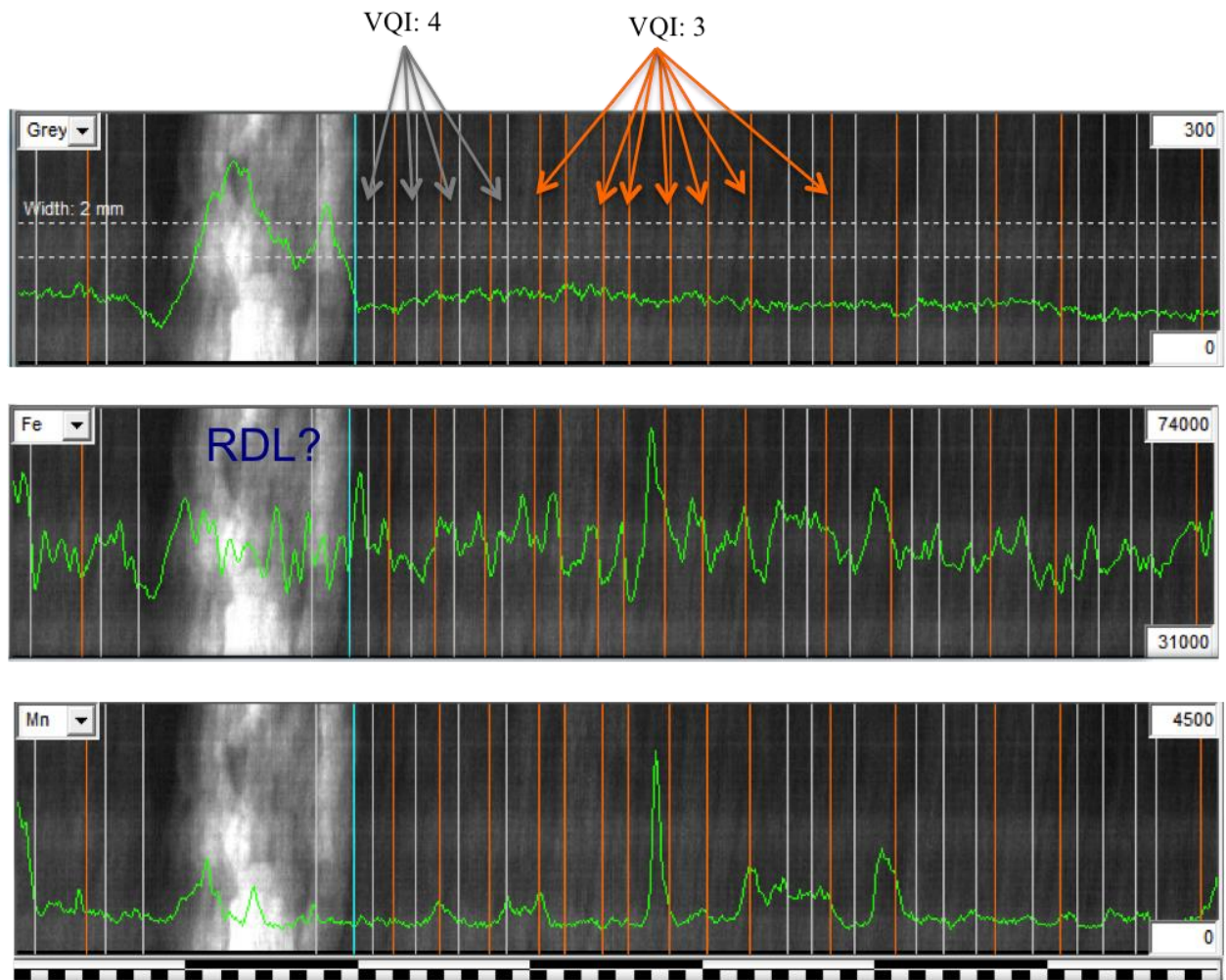


Figure S4: Close-up on multi-parameter counting of laminations/varves using PeakCounter 1.6.4 software showing varves according the varve quality index (VQI), Mainly VQI: 3 (red) and VQI: 4 (grey) were delineated. Also shown is a relatively “laminae” marked by relatively high grey scale value, high Fe, medium Mn and high Si and Ti (not shown). It is interpreted as a rapidly deposited layer (RDL?).

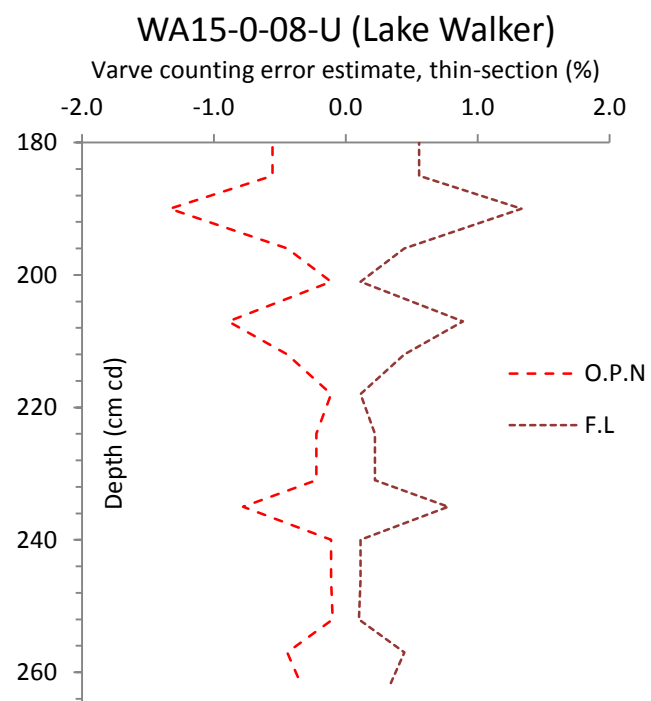


Figure S5: Varve counting error estimates (%) from thin-section based on variance between the values of two researchers (O.P.N and F.L) for varves from core WA15-08-U (~178–262 cm cd), Lake Walker, Québec North Shore.

Principal component analysis

The eigenvalue of the first five components are higher than the Joliffe cut-off (0.7) respectively, which indicates these components appear significant (Appendix III, Figure S4A). However, the broken stick line (Appendix III, Figure S4B) indicates that the first component (40% variance) is the principal component because only its eigenvalue % (40 %) plots above the broken stick line (red line) (Hammer et al. 2001). PCA loadings for the first principal component show two groups: Positive loadings (Si, K, Ca, Ti, Zn, Rb, Zr) and negative loadings (Mn, Fe, and inc/coh) (Appendix III, Figure S5A). The PCA scatter plot (Annexe III, Figure S6) reveals four associations: PC1 Si, Ti, K, Ca, and Zn; PC2: Mn and Fe; PC3: inc/coh, and PC4: Cl, Zr; PC1. PC1 indicates that the input is probably linked to silicates and carbonates, while Mn and Fe are likely linked to redox-sensitive elements (Rothwell and Croudace 2015). The inc/coh ratio relates organic matter content (Guyard et al. 2013), while Cl and Zr could be a proxy for marine environment. Together, the results probably suggest that the elementary geochemistry of the sediments is influenced by grain size and other factors (which were not analysed in this study, due to the focus on varved sediments).

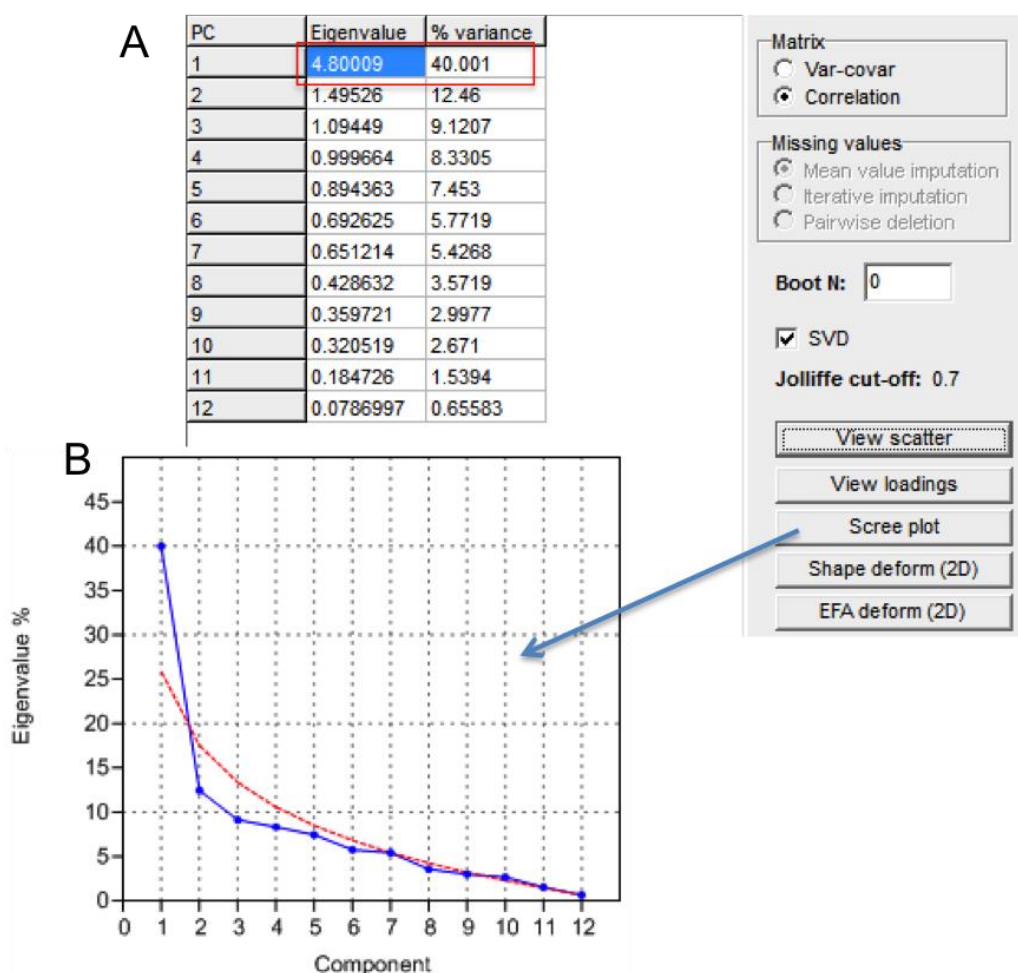


Figure S6: Principal component analysis of XRF elements from the composite core WA15-08-U (Lake Walker): A) eigenvalue of the components; B) Scree plot.

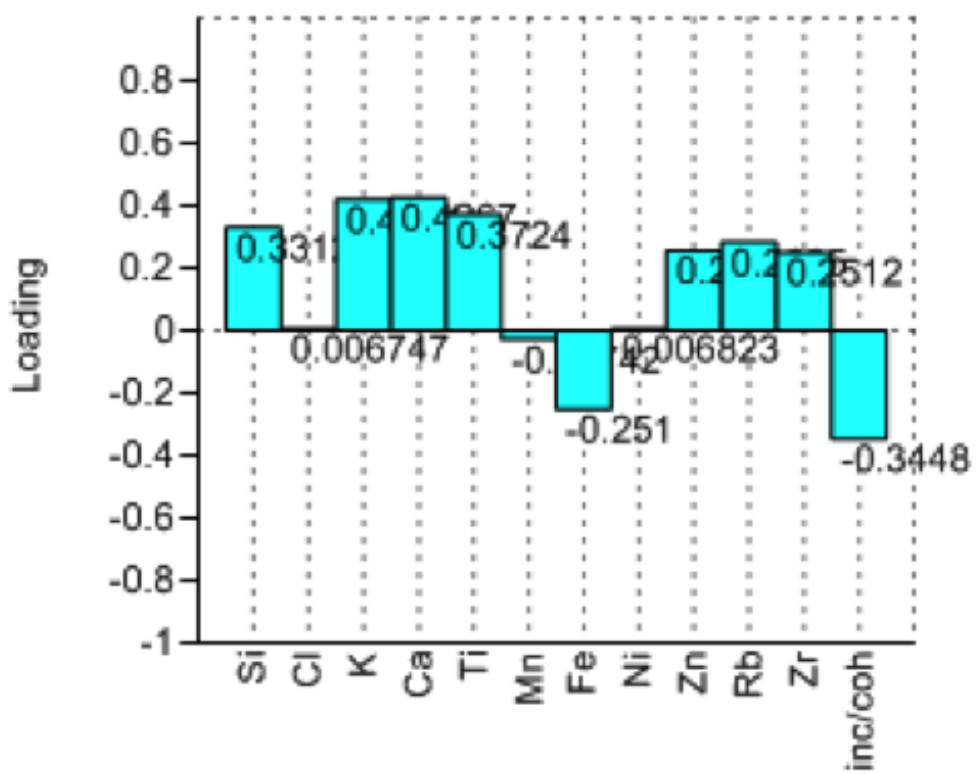


Figure S7: PCA loading from the first component (PC1, Figure S4).

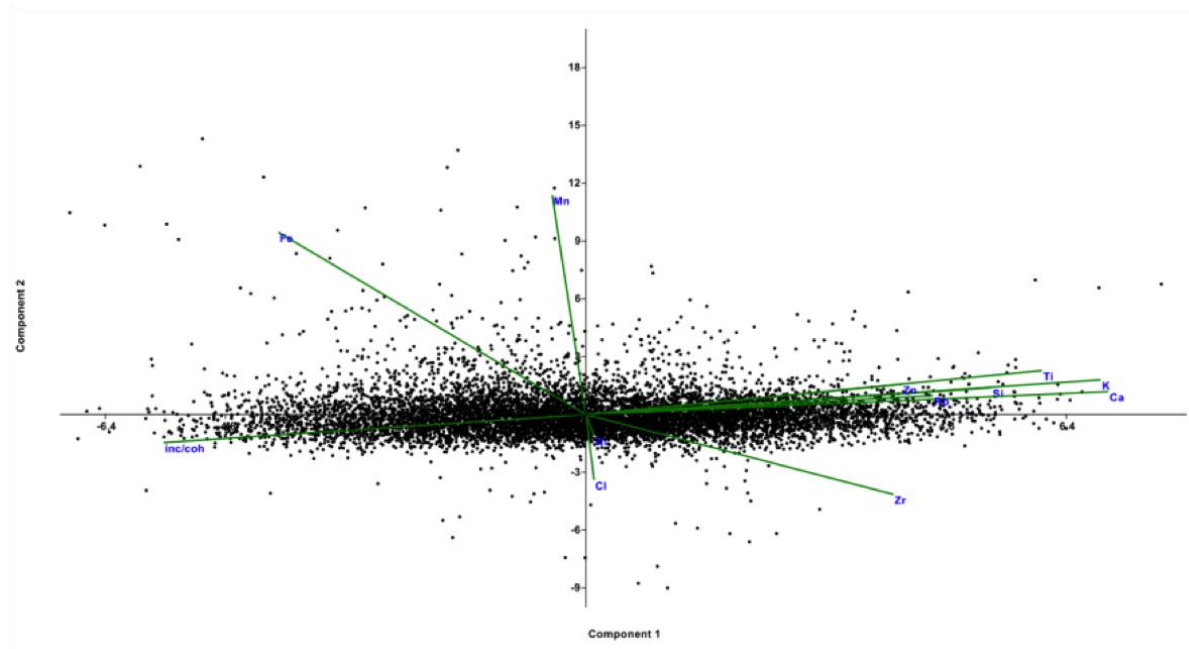


Figure S8: PCA scatter plots of the first component (PC1, Figure S4).

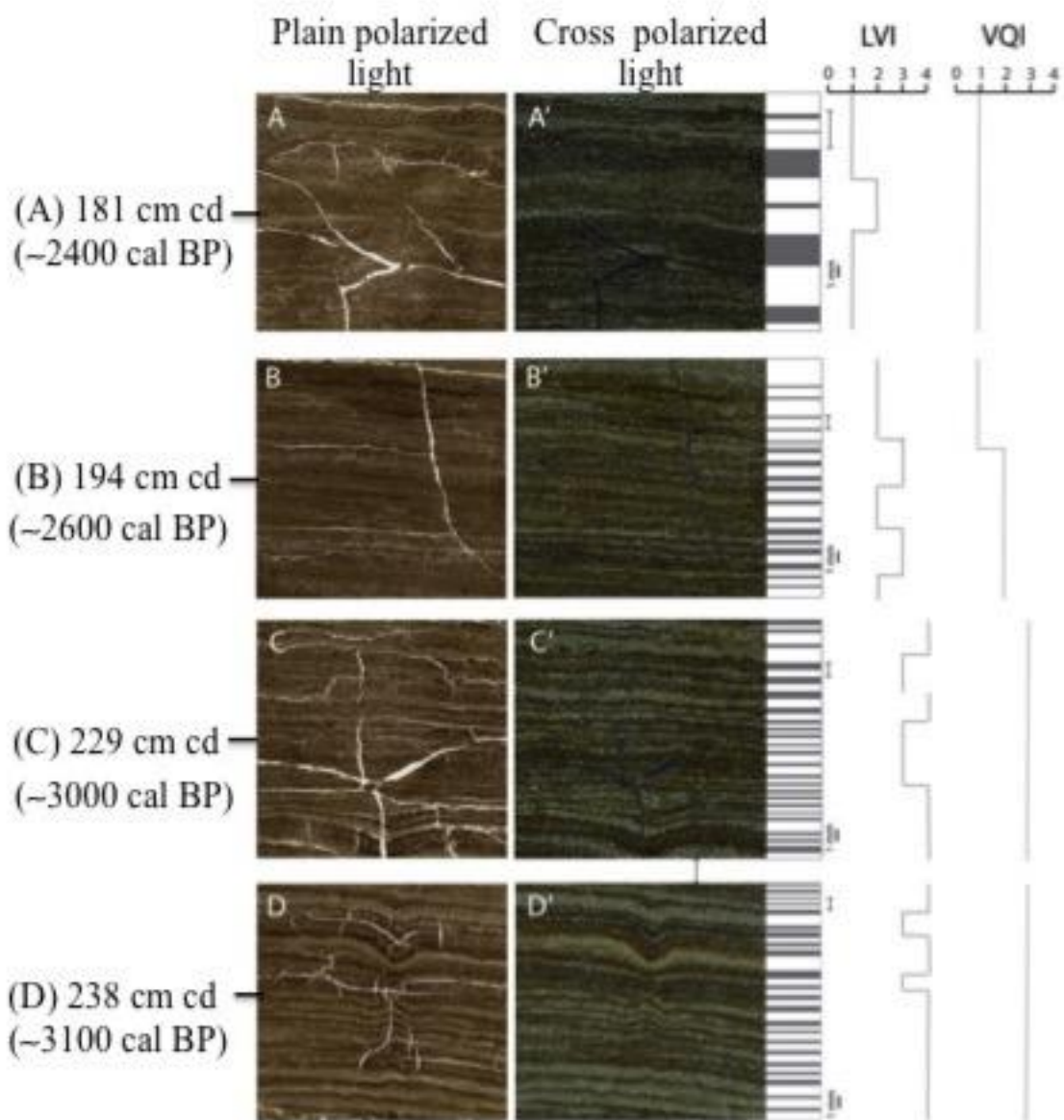


Figure S9: Illustration of varve structures at four different depths of the composite core WA15-08-U (~178–262 cm cd) from Lake Walker, which verifies the hypothesis that within the analyzed interval, laminae/varve quality index improves with increasing sediment depth.

9 ANNEXE IV : SUPPLEMENTARY INFORMATION CHAPTER 4 (ARTICLE 3)

Composite core WA15-08-U

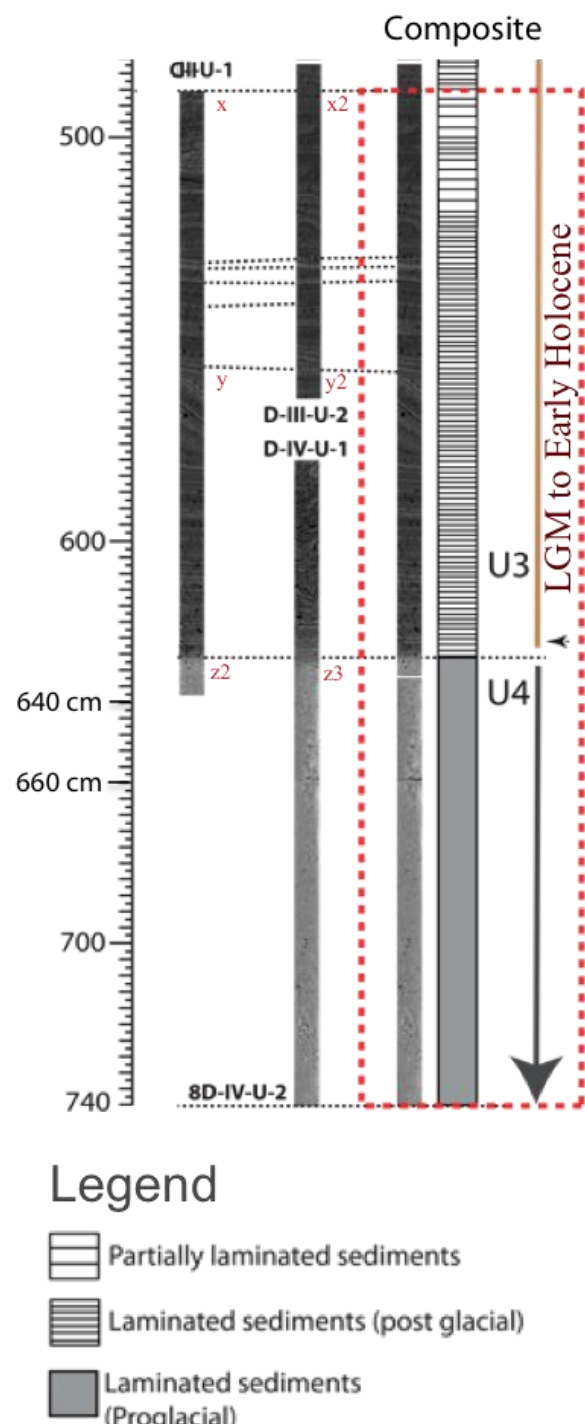


Figure S1: Correlation panel showing CT-scan images of core sections used to reconstruct the composite core WA15-08-U (~488–740 cm cd; Table 3.1). The core comprises mainly partially laminated and laminated sediment, as shown in the legend. Marker beds and/or laminations that were used to correlate adjacent cores are shown. This litholog is a revised version of the one previously reported (Gagnon-Poiré 2019).

PC15-04B-P

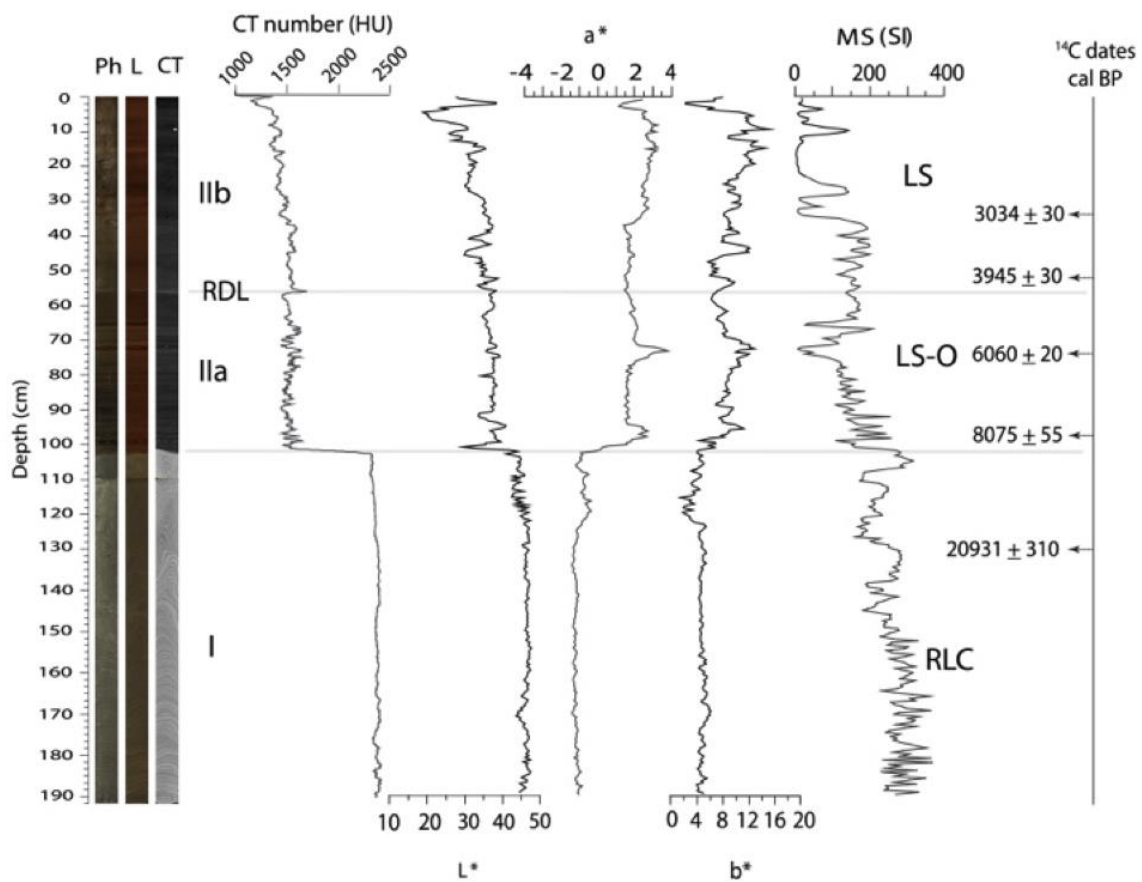


Figure S2: MSCL parameters of core PC15-04B-P (Lake Pentecôte). Sediment facies are RLC rhythmically laminated clay sediments; LS-O laminated organic-rich silty clay and clay sediments; and LS - laminated sediments.

WA15-08-U

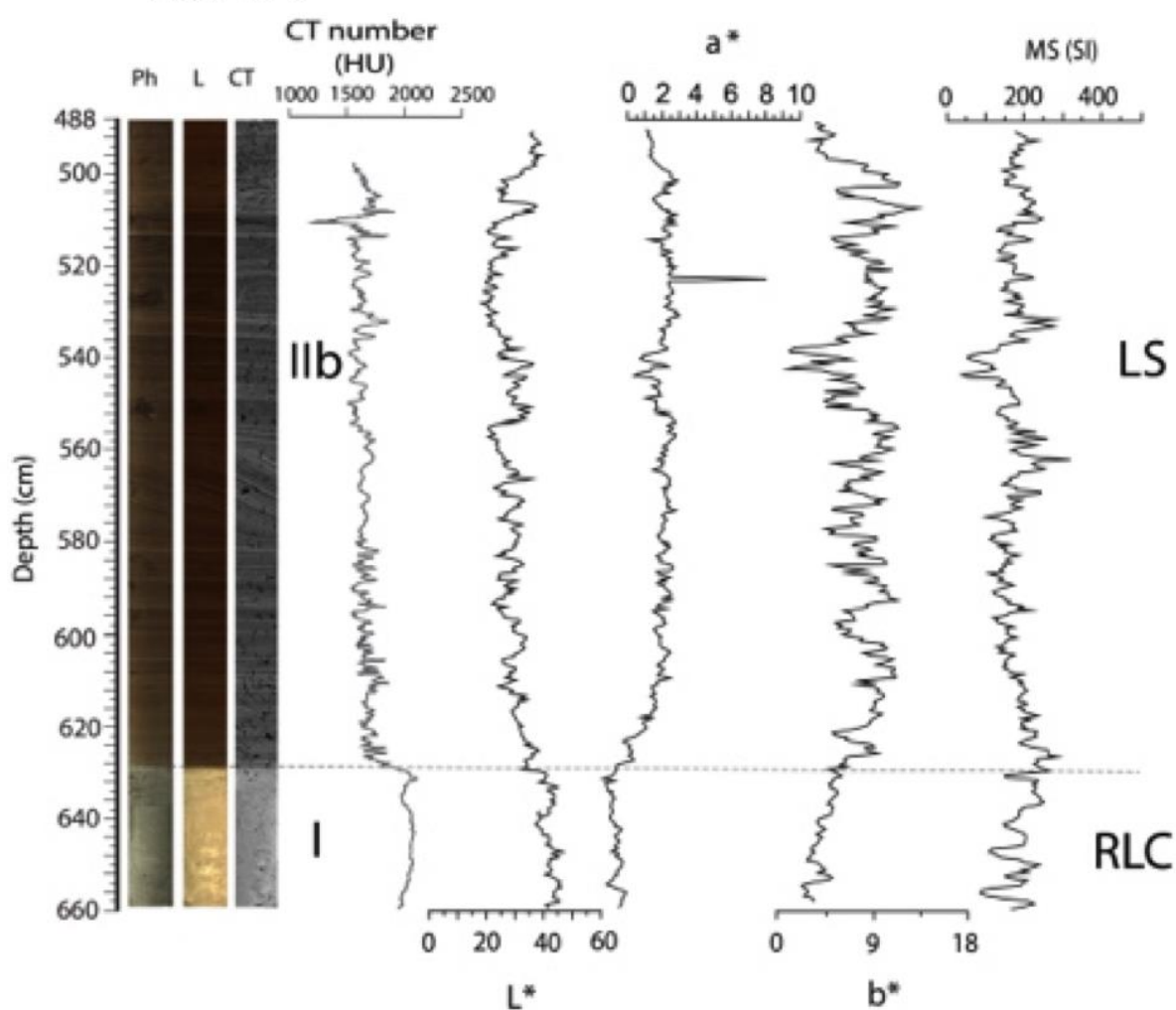


Figure S3: MSCL parameters of core WA15-08-U (Lake Walker). Sediment facies are RLC rhythmically laminated clay sediments, and LS - laminated sediments.

WA15-08-U

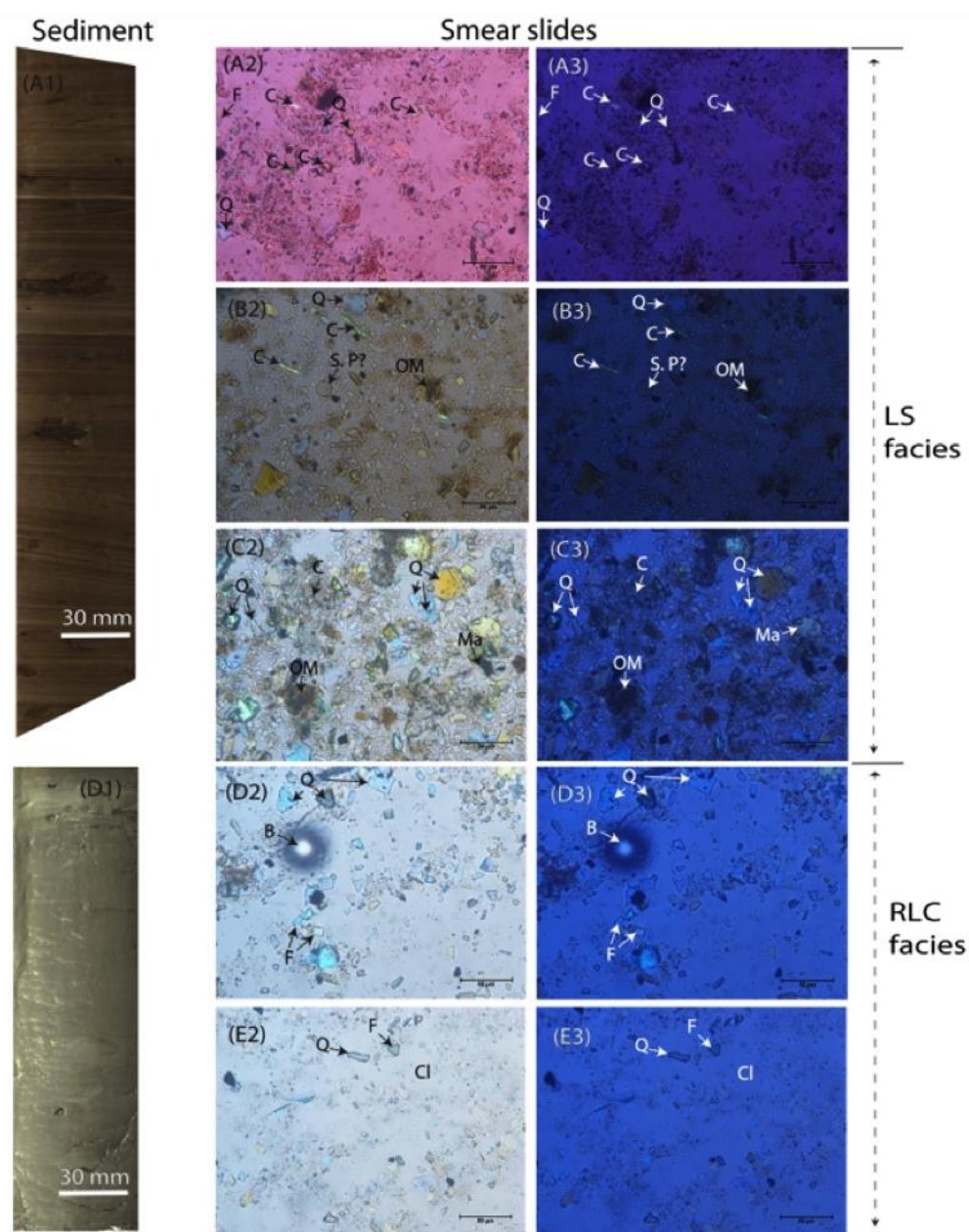


Figure S4: Smear slide images from core WA15-08-U-1 at selected depths, as seen in plane and crossed-polarized light: (A) RDL, 512 cm; (B) lamina couplet, 551 cm; (C) laminated section, 598 cm; (D) clayey silty lamina, 623 cm; (E) Gray clay, 628 cm. Identifiable minerals include: Q - quart, F - feldspar, C - carbonates (calcite), M - muscovite, Ma - mafics, V - vivianite, Cl - clay minerals, OM - organic matter, S.P? – structure of *S. Pteridophyte?*, B - bubble of air in mounting medium.

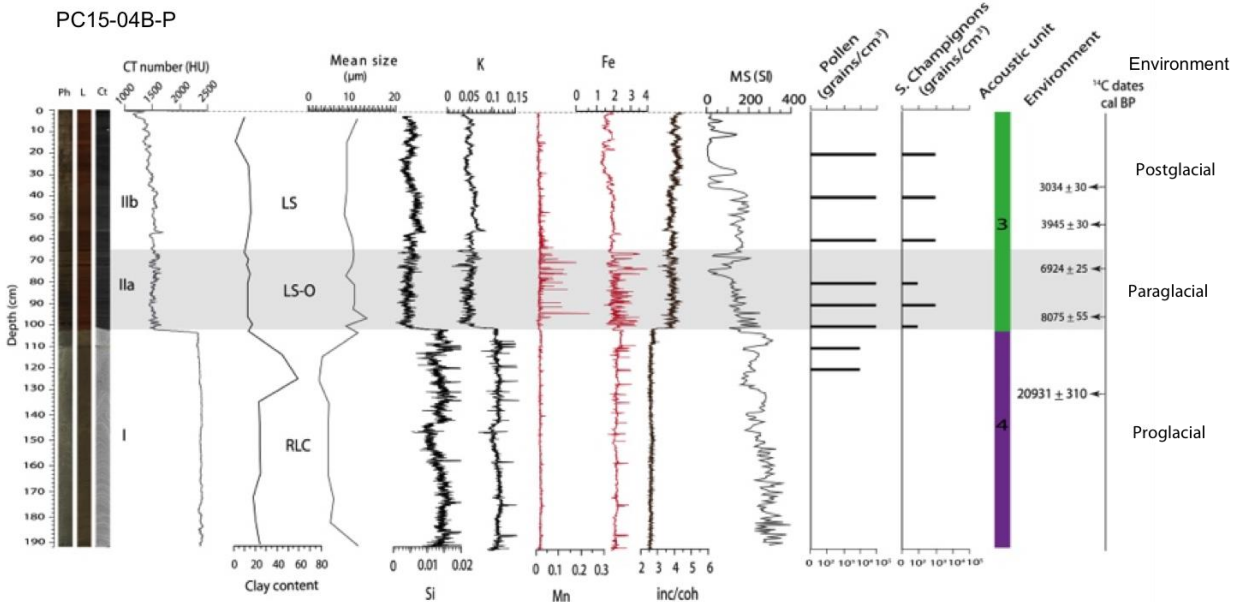


Figure S5: Correlation of multi-proxy analysis of core PC15-04B-P (Lake Pentecôte): digital photo (Ph), line scan image (L), CT-scan frontal view, CT number (HU) and vertical XRF profiles of selected elements, Magnetic susceptibility (MS), palynomorph counts (pollen and mushroom spores), acoustic stratigraphic units (Gagnon-Poiré et al. 2018) and radiocarbon dates. Sediment facies are RLC rhythmically laminated clay sediments; LS-O laminated organic-rich silty clay and clay sediments; and LS - laminated sediments.

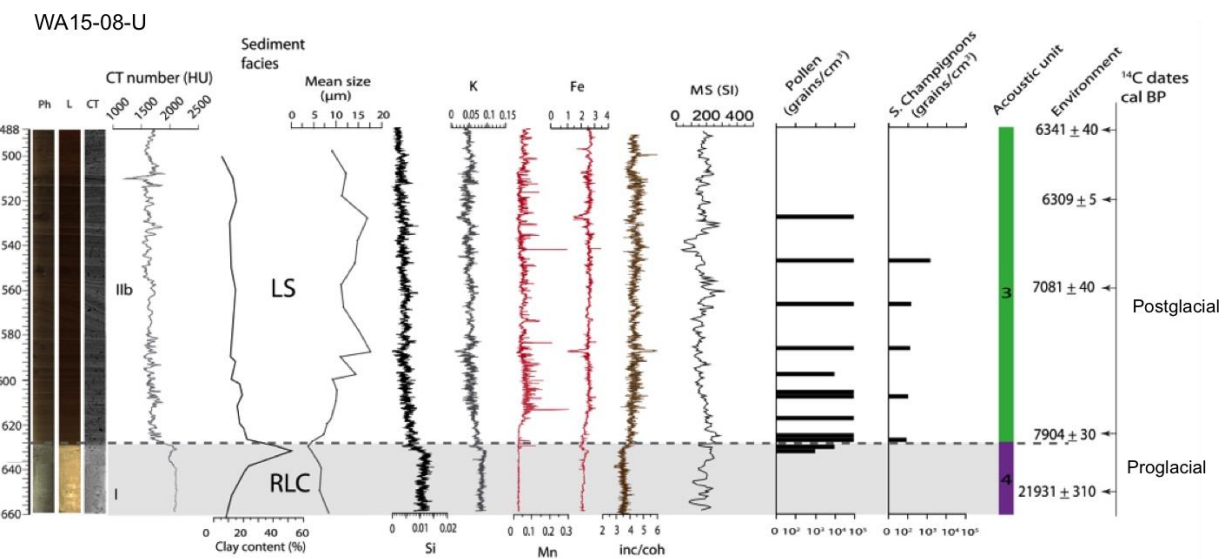


Figure S6: Correlation of multi-proxy analyses from core WA15-08-U (Lake Walker): digital photo (Ph), line scan image (L), CT-scan frontal view, CT number (HU), XRF profiles of selected elements, magnetic susceptibility (MS), palyynomorph counts (Pollen and Mushroom spores), acoustic stratigraphic units (Gagnon-Poiré et al. 2018) and radiocarbon dates. Sediment facies are RLC rhythmically laminated clay sediments, and LS - laminated sediments.

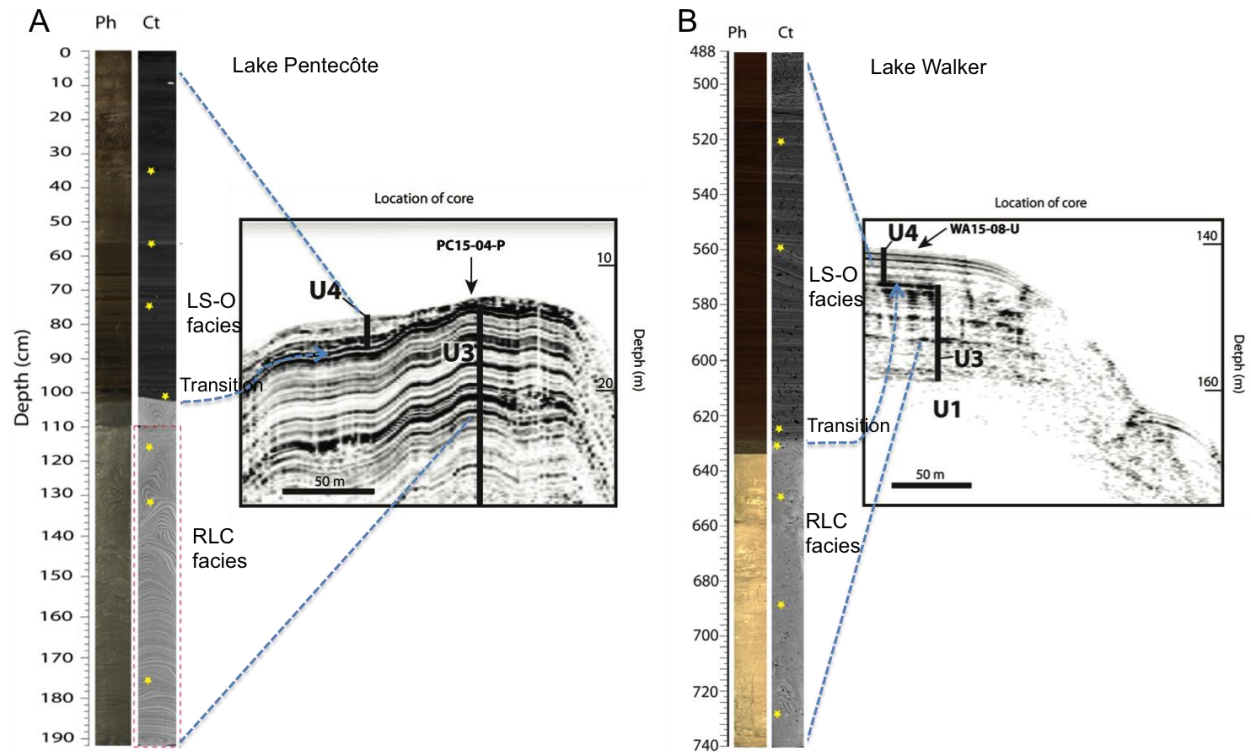


Figure S7: Schematic illustrations showing the location of cores (A) PC15-04B-P (Lake Pentecôte) and WA15-08-U described in the context of acoustic stratigraphy. The transition between the upper and lower units suggest a moderate to high-acoustic reflection, however, there are not strong evidence of large deformation in the immediate vicinity of the cores. Acoustic stratigraphic units described: U3 – Glaciomarine to glaciolacustrine deposits; U4 – Postglacial deposits (detailed in Gagnon-Poiré et al. 2019).

10 ANNEXE V: INFORMATIONS COMPLEMENTAIRES CHAPITRE 5

10.1 Insights on natural modes of climate variability during the Late Holocene inferred from particle size analysis of ~900-year varved record in Lake Walker, Québec North Shore (eastern Canada)

François Lapointe^{1, 2}, Obinna P. Nzekwe¹, Pierre Francus¹, Guillaume St-Onge³, Patrick Lajeunesse⁴, Jean-Philippe Jenny⁵

¹Institut National de la Recherche Scientifique, Centre - Eau Terre Environnement, Québec, QC G1K 9A9, Canada, & Canada Research Chair in Environmental Sedimentology & GEOTOP

²Climate Science Center, Department of Geosciences, University of Massachusetts, Amherst, MA 01003, USA

³Institut des sciences de la mer de Rimouski (ISMER), Université du Québec à Rimouski, Canada, & Canada Research Chair in Marine Geology & GEOTOP

⁴Centre d'études nordiques, Département de géographie, Université Laval, Québec, G1V 0A6, Canada

⁵Université Savoie Mont Blanc, INRA, CARRTEL, 74200 Thonon-les-Bains, France

¹Corresponding author: François Lapointe (flapointe@umass.edu)

Keywords: Laminations, varves, thin-section, Image analysis, spectral analysis, Québec North Shore

Article en préparation

Contribution des auteurs

Les corrélations spatiales ont été réalisées par François Lapointe. L'interprétation des résultats et l'écriture de l'article est en cours en collaboration de Obinna Nzekwe sous la supervision de Pierre Francus.

Methods and materials

Proxy data analyses

Linear detrending of varve thickness and grain-size data was done followed by normalization in order to allow for comparison with other time series. The Lake Walker (new varve) record was compared with time series such as the reconstructed NAO (Olsen et al. 2012) and Greenland temperature record (Kobashi et al. 2015). For spectral analysis, REDFIT (Schulz and Mudelsee 2002) was used (e.g.(Lapointe et al. 2017). Wavelet analysis was performed with the R software (R Core Development Team 2008) using the package bi-wavelet (Gouhier and Grinsted 2012).

Results

Spectral analysis of the Lake Walker varved record

The analysis reveals a significant periodicity (>95% confidence level (CL)) at ~230 year-cycle for all of the proxies, except the >30 µm (Figure S1). For each proxy, multidecadal cycles can be found and are located at 49 and 23 years for VT (Figure S1a), at 92, 58 and 18 years for D50 (Figure S1c), and 71, 58, and 15 years for D99 (Figure S1e). In the time series of the >30µm grain-size, spectral analysis reveals two strong multi-centennial periodicities at 462 and 308 years, a centennial-scale variability at 185 years and three multidecadal signals at 71, 65 and 54 years (Figure S1g).

Discussion

Spectral content of the Lake Walker varved record

The weak coefficient of correlation between varve thickness and most of the proxies from the Lake Walker record are relatively similar those highlighted in a high-artic Canadian lake, East Lake, Cape Bounty (Lapointe et al. 2012). The spectral peaks at 71–49 years (Figure S1g) are consistent to those found in the instrumental and reconstructed Atlantic Multidecadal Oscillation (AMO) (Knudsen et al. 2011). The cycles around ~230 and 185 years could be linked to solar activity (Knudsen et al. 2009) as suggested by spectral analyses of the 2300–3200 BP in the ^{14}C production rate. Spectral analysis was also made on the μ -XRF data of Lake Walker and this yielded similar result with grain-size. Continuous wavelet transforms (CWT) for each of the physical parameters at Lake Walker indicate strong multidecadal signal from ~2300 to 2750 BP (Figure S1dfh). On larger time scales, it appears that a ~250–180 year-cycle is present throughout most of the ~2300 to 3200 BP period (Figure S1bd),

except in the case of the coarse grain-size fractions where this mode of variability is absent after ~2900 BP (Figure S1fh). However, the varved record is relatively short to clearly determine if this long cycle was persistent, since most of this 250–180-year cycle is within the cone of influence of the CWT. Several spectral peaks (at 15, 18, 23, 50–70, 185, 300 years) in the Lake Walker record are compatible to those found in a reconstructed North Atlantic Oscillation (Olsen et al. 2012).

Comparison with reconstructed NAO and solar activity over the interval ~3220–2340 BP

Only one reconstructed NAO goes back enough in time to cover the time interval of the Lake Walker record, the 5,200 years NAO from Olsen et al. (2012). The overall comparison between the paleo-NAO and the Lake Walker record is good. Averaging the Lake Walker varved record to the resolution of the reconstructed NAO yields a strong correlation ($r = -0.68$, $p < 0.0001$). A clear shift from positive to negative values of the NAO is observed during 3220–2900 BP. This coincides with an increase in the coarse grain size fraction (D99) at Lake Walker, suggesting that negative NAO phase (NAO-) might have influenced hydroclimatic conditions in the Québec North Shore region, at least during the time interval ~3200–2300 BP.

The Lake Walker varved record is also inversely correlated with a temperature reconstruction at GISP2 (Figure S2a): $r = -0.44$, $p < 0.001$ (Kobashi et al. 2015). Cross-wavelet analysis between those two records depicts common variability at multidecadal timescales (40 to 70 years) between ~2800 and 2520 BP (Figure S2b). Interestingly, the varves are also inversely correlated with other Greenland temperature records, although at different time lags (Figure S3), which is expected since all of these proxy records (including Lake Walker) do contain age uncertainties during this period (Vinther et al. 2003). Altogether, these results suggest that a linkage between Greenland climate and the Québec North Shore is likely related to changes in the NAO (Figure S4).

Significant periodicities at Lake Walker are also compatible with those of solar variability. Record from this study were compared to the ^{14}C production rate (Muscheler et al. 2016) (Figure S5), a proxy of solar variability. In the relatively recent part of the Lake Walker period (~2600–2340 BP), no visual co-variability is observed, unlike with the reconstructed NAO and Greenland temperature (Figures S2 and S4). However, there is a good agreement with solar activity in the latter part, more specifically from ~3220 to 2600 BP, where correlation is significant $r = 0.44$, $p < 0.001$. This positive correlation would imply coarser sediment deposition during periods of lower solar activity.

The climatic anomaly around ~2700 BP has been detected in multiple sites around the world and has been suggested to have been triggered by a grand minimum in solar activity, namely the Homeric climate oscillation (e.g.(Martin-Puertas et al. 2012). Cross-wavelet analysis shows a common spectral power in the 250–185-year band between both records from ~2950 to 2500 BP. Also, a 100 to 80 year cycle around 2900–2700 BP and multidecadal signals at 3220–3150 BP and 2700–2600 BP can be noted.

Present-day teleconnexion

Spatial correlation suggests that the NAO, in its negative phase, increases the likelihood of precipitations in the region around Lake Walker during the months of July to October (Figure S6a). This is further supported by a significant negative correlation between total rainfall (sum) recorded at the Sept-Îles weather station, located ~70 km east of Lake Walker, and the NAO (Figure S6b). Although relatively farther from the study area, flow discharge of the Des Outardes River in Québec (Centre d'expertise hydrique 2016) is negatively correlated to the NAO (Figure S6c). In general, most of the St-Lawrence Valley receives precipitation during the NAO- (Figure S6a).

These significant correlations are strongly indicative that the climate of the Québec North Shore region is influenced by the NAO, which may point to similar climatic conditions ~3300 years ago (Figure S4). The present-day teleconnexion of the NAO influence on precipitation on Greenland has also been investigated. An increase in precipitation during NAO+ in summer time (JJA) for the region of Lake SS1220, where the reconstructed NAO (Olsen et al. 2012) is located (Figure S7). This period (JJA) is close in time with the maximum correlation reached from the NAO using the meteorological and reanalysis dataset and the Lake Walker region (JASO; Figure S4a). This could explain the negative correlation observed in today's teleconnexion (Figure S6), but also back in time (Figure S7), if boundary conditions of climate did not change in that time.

Solar influence on climate variability

Although satellite-based measurements of total solar irradiance indicate weak difference between the solar maximum versus minimum (0.1% of the total solar energy), large variations of the ultraviolet spectrum have been detected (Lean 1997). These significant changes at the 200–300 nm of the solar emission spectrum can have large impacts on heating upon the stratosphere. During stronger (weaker) solar activity, stratospheric temperatures increase (decrease) as more UV sunlight is being absorbed by ozone, and this results in an increase in the temperature gradients between stratospheric high and low latitudes. This ultimately leads to a positive phase of the NAO atmospheric pattern, maximizing ~2–4 years following the 11-year solar cycle peak due to ocean feedbacks (Andrews et al. 2015; Gray et al. 2010; Ineson et al. 2011; Menary and Scaife 2014; Scaife et al. 2013; Thiéblemont et al. 2015). Using paleo-records, other studies have shown that weaker solar activity induce a NAO- pattern of atmospheric circulation during the Homeric Minimum (Martin-Puertas et al. 2012) and other more recent solar minima (Moffa-Sánchez et al. 2014; Shindell et al. 2001). Strong common power at multi-decadal scales is seen between the Lake Walker record, the reconstructed NAO and the GISP2 (Kobashi et al. 2015) during the 2700BP event (and after) suggesting a linkage between low solar activity and multi-decadal variability presumably linked to the AMO (Wang et al. 2017).

Summary and Conclusion

Spectral analysis revealed significant periodicities that can be linked to the NAO and solar activity. The Lake Walker varved record is inversely correlated to the reconstructed NAO and suggests that the Québec North Shore region was influenced by this climate mode of variability ~2300 years ago. Present-day correlation revealed that rain events in the Lake Walker region increased during the NAO-, and this could explain the link between our record and the paleo-NAO. This would thus suggest that present-day NAO influence on the region was similar ~2300 years ago.

All grain size proxies at Lake Walker show increasing values during the period ~2700–2800 BP, coincident with a Grand Solar Minimum, and significant correlation between reconstructed solar activity and the Lake Walker record during the period ~2300–3200 BP is strongly suggestive that solar forcing played a role in climate change during this time interval.

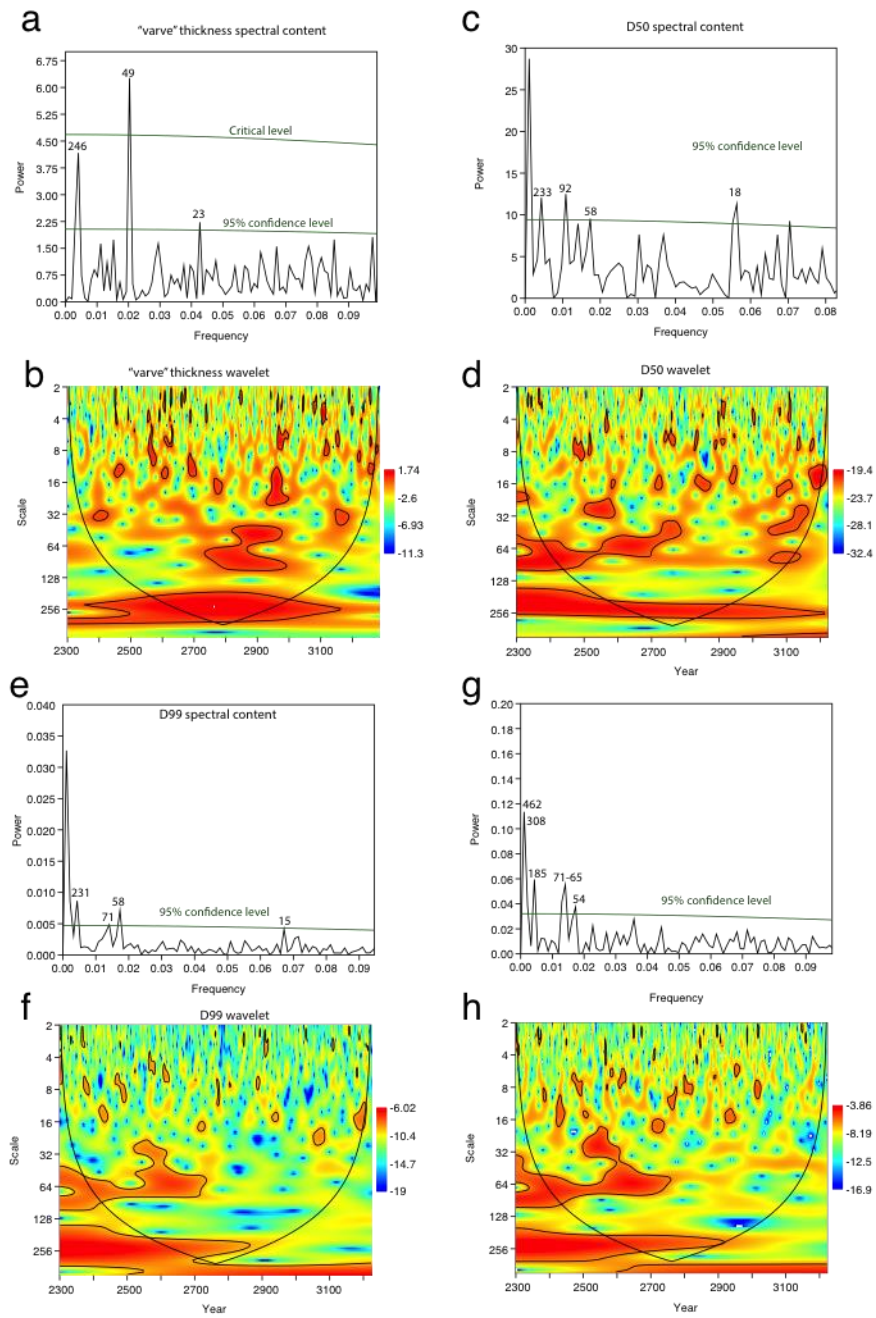


Figure S1: Spectral analysis of the Lake Walker varved record: a) Spectral analysis of the varve thickness series, and b its wavelet spectrum. c, d and e, f and g, h same as a, b but for the median grain-size (D50), the 99th percentile (D99) and the fraction >30µm, respectively.

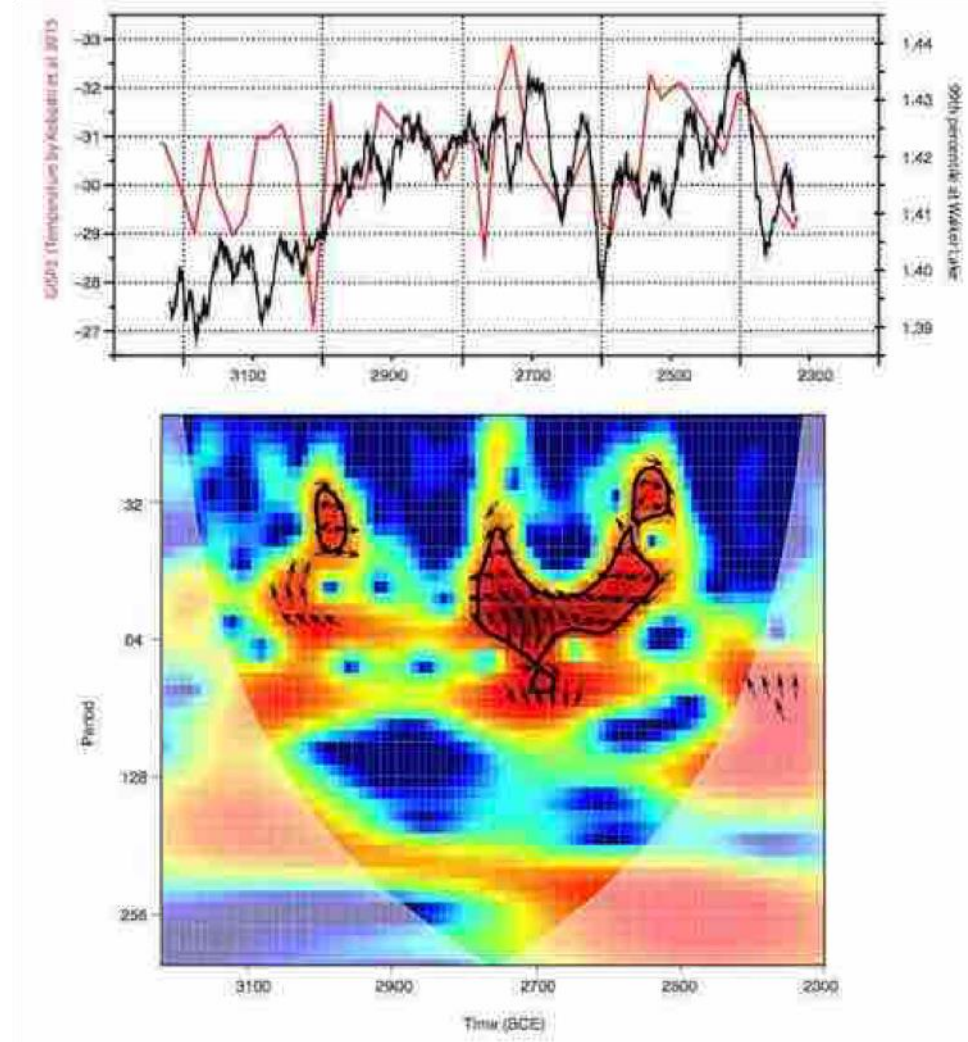


Figure S2: Same as Figure S1 but using the Greenland temperature record (Kobashi et al., 2015). Below: cross-wavelet analysis between both time series using the resolution of the lower resolved record to avoid interpolation.

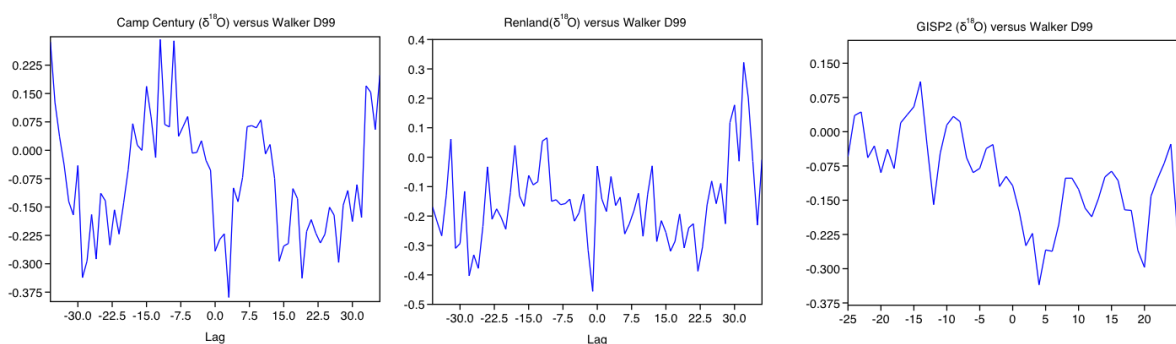


Figure S3: Cross-correlation between Greenland $\delta^{18}\text{O}$ records and the 99th percentile at Lake Walker.

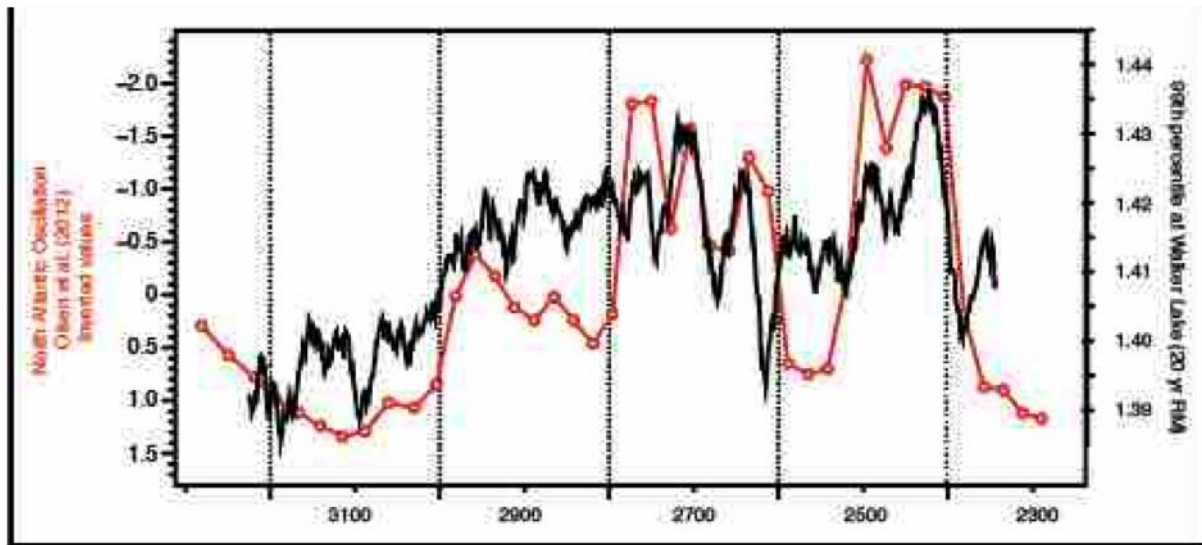


Figure S4: Comparison between the reconstructed NAO (Olsen et al., 2012) and the 99th percentile at Lake Walker.

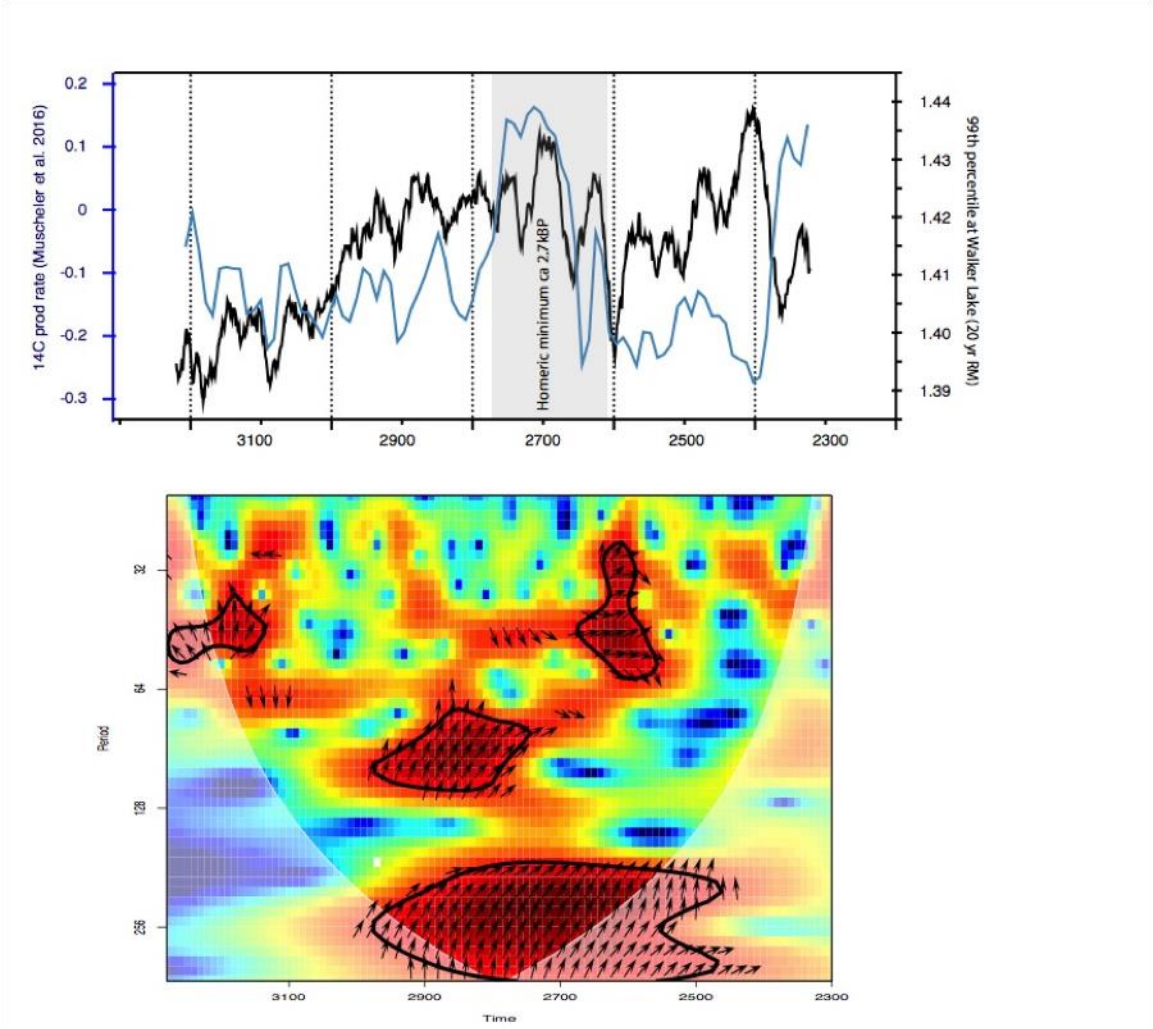


Figure S5: Comparison between reconstructed solar activity (^{14}C production rate) and the 99th percentile at Lake Walker.

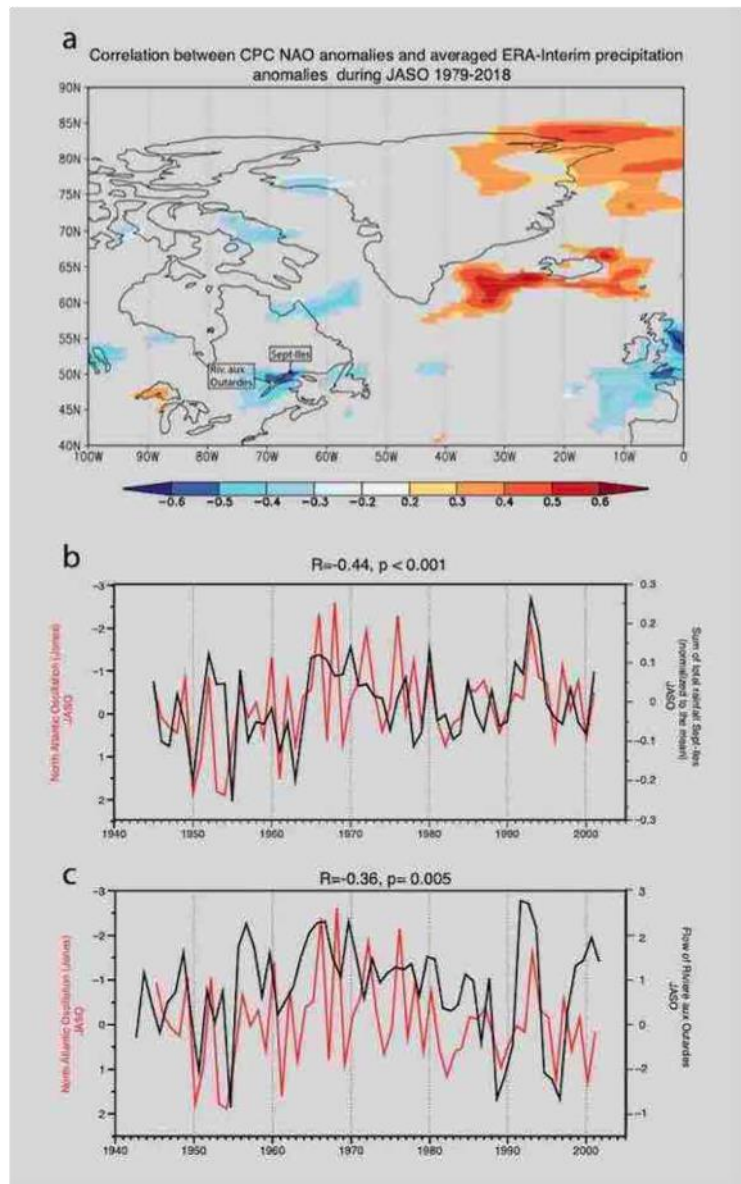


Figure S6: Correlation between North Atlantic Oscillation (Climate Prediction Center; CPC) and precipitations anomalies (Dee et al. 2011). b) Comparison between the time series at Sept-Iles total rainfall (log-transformed and normalized to the mean) and NAO during July-October. c) Same as b) but compared with the discharge time series of the Rivière Aux-Outardes, Québec during JASO. Note that Sept-Îles weather station stopped operating in 2002.

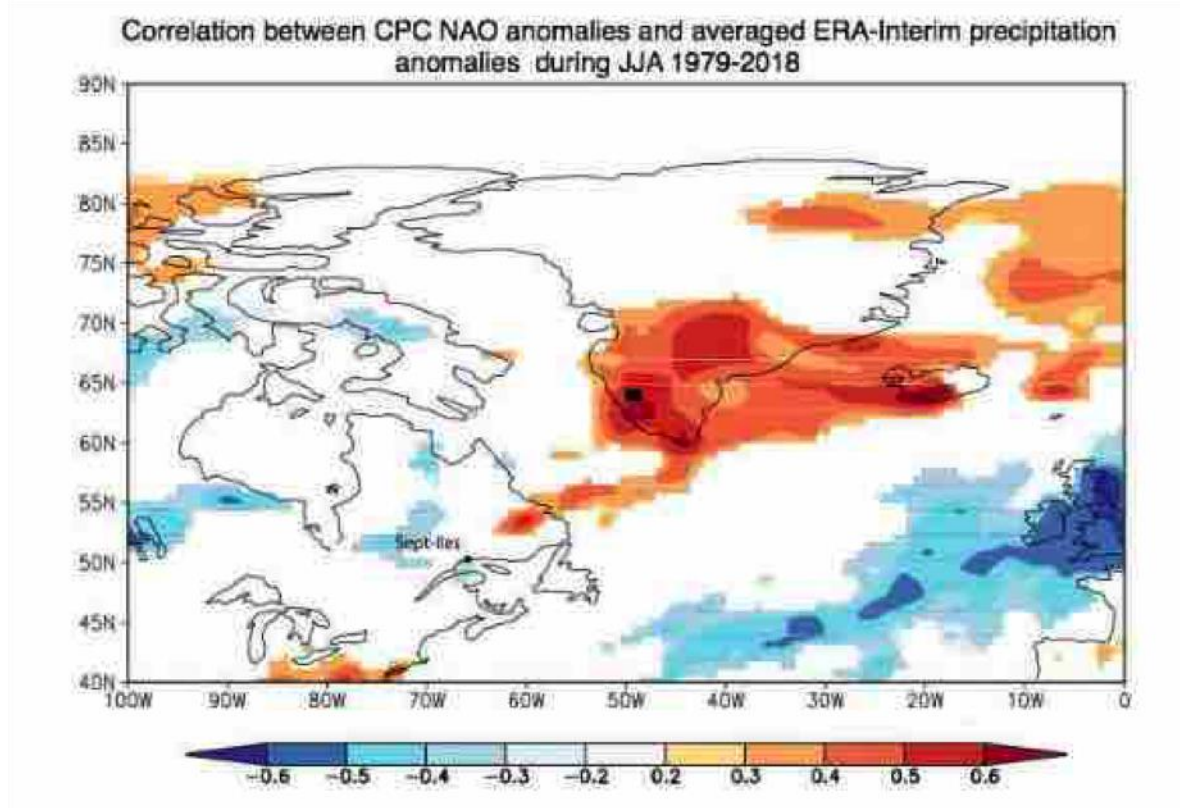


Figure S7: Correlation between NAO and precipitations (Dee et al., 2011).

10.2 Deployment of sediment traps in Lake Walker, Québec North Shore, eastern Canada

Objective

To monitor sediment transfers and limnological processes responsible for the formation of annually laminated sediments in Lake Walker (e.g. Cockburn and Lamoureux 2008; Fortin et al. 2015).

Methodology

Two programmable sequencing sediment traps (model PPS 4/3, SARL TECHNICAP, France) were deployed (alongside temperature and pressure sensors, Onset HOBO Data Loggers, USA) in Lake Walker on 5th June 2014. The deployment location (50°23'17.2" N, 67°10'23.4" W) was chosen due to its proximity to the area of core sampling and its relative closeness to the inflow of two rivers in the northern part of the lake (Figure 1). Each sediment trap unit consists of a 131 cm long cylindro-conical tube (made of glass reinforced polyester) with a funnel-shaped sieved collecting area of 0.05 m² at the top, and a 12-volt AA alkaline battery-powered motor unit close to its base. A rotary disk connects the motor unit to a tray that houses a carousel with attachment for twelve 250 ml polypropylene sampling bottles. The motor unit was programmed to suit the selected sampling plan, that is, to rotate twice a month from June to September, once a month from October to November (summer to spring), once a month between December and April (winter), and once in May (all within a 1-year period). The monitoring period lasted for two years, from June 2014 to July 2016.

The sediment traps were positioned vertically, approximately 155 m apart along a polypropylene rope. An acoustic releaser was attached ~3 m above the lower end of the rope, and was expected to aid recovery of the trap. Ten temperature sensors were placed 15 m apart from each other along the same rope (and set to take readings every hour). Similarly, two pressure sensors were attached to the rope, one at the same position as the acoustic releaser (~165 m depth) and another at a depth of ~35 m, estimated to be within the photic zone of the lake. In order to ensure an upright suspension of the equipment line-up, a load (two concrete blocks) of ~100 kg was tied to the base of the rope while two buoys located 20 m apart were attached at the upper end of the rope. An illustration of this arrangement is shown in Figure 2.

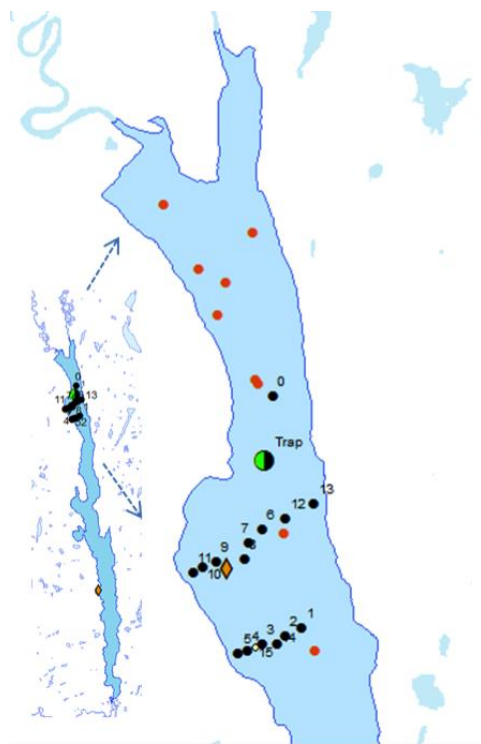


Figure S8: Simplified illustration showing the deployment location of sediment traps and the S4 current meter (map visualised with ArcGIS 10.2 software; map layout unfinished).

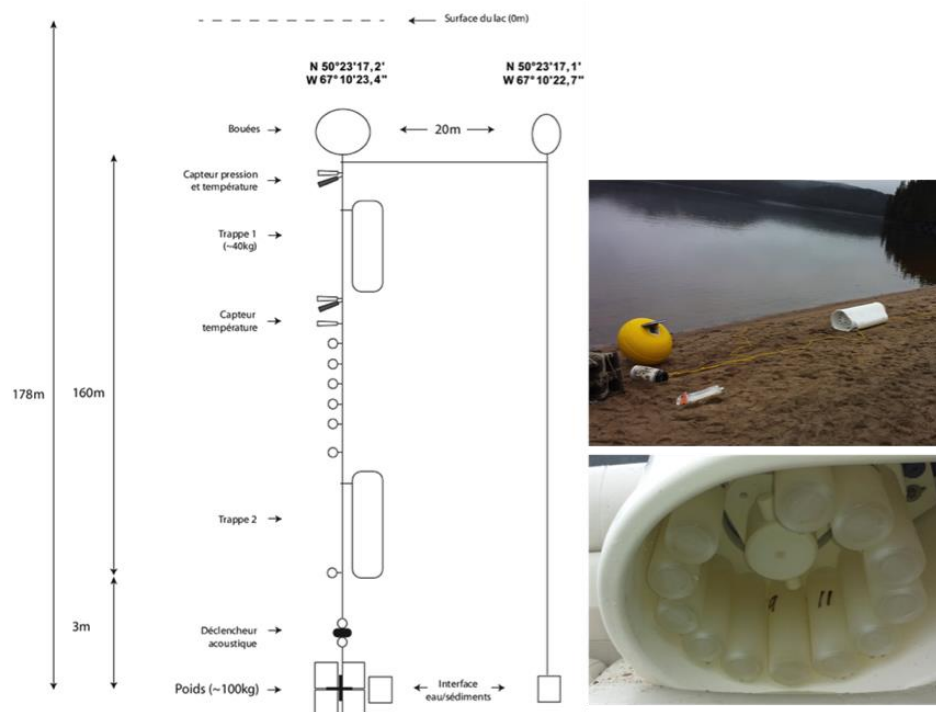


Figure S9: Diagram showing the deployment of sediment traps in Lake Walker (left). Photo shows a carousel with attachment for sampling bottles (below), and (above) a load and buoy, which were attached to the rope to maintain suspension in water.

Observations during monitoring

During fieldwork in the spring of 2016, the following were observed: 1) The sediment traps had been moved from their fixed position into the deep basin of the lake probably due to strong currents associated with the spring snowmelt period; 2) The battery of the acoustic releaser was “dead”, consequently the sediment traps could not be released from the load in order to float on the lake surface, and 3) no sediment was collected in the sediment traps (Nzekwe et al. 2015).

Lessons learned

In the first instance, the sediment traps were deployed before clear information about the limnology and potential for laminae formation/preservation (Nzekwe et al. 2018) as well as basin bathymetry (Gagnon-Poiré et al. 2019) of Lake Walker were fully understood. Consequently, the deployment strategy and/or location were possibly not ideal. A better float mechanism would have been achieved by: 1) deploying the sediment traps in a part of the lake basin where topographic exposure but relatively stable water currents were prevalent, as opposed to near the inflow of the Schmon and Gravel Rivers in the northern part of the lake; 2) using three to four buoys would have provided a more stable float and/or displacement, as opposed to two buoys; and 3) the battery life of the acoustic releaser should have been guaranteed to last longer than the planned monitoring period. These recommendations were considered in the successful deployment of the sediment traps in Grand Lake, Labrador (a different project).